1241359
[0073923H]

SGW-59365
Revision 0

Model Package Report: 100-BC Scale-Appropriate Fate and Transport Model

Version 1.0

Prepared for the U.S. Department of Energy
Assistant Secretary for Environmental Management

Contractor for the U.S. Department of Energy
under Contract DE-AC06-08RL14788

ch2m SM

P.O. Box 1600
Richland, Washington 99352

RECEIVED
NOV 16 2016
EDMC

Approved for Public Release;
Further Dissemination Unlimited

SGW-59365
Revision 0

Model Package Report: 100-BC Scale-Appropriate Fate and Transport Model

Version 1.0

Document Type: ENV Program/Project: EP&SP

G. Ruskauff
INTERA, Inc.

J. Ewing
INTERA, Inc.

T. Jones
INTERA, Inc.

H. Rashid
INTERA, Inc.

T. J. Hammond
INTERA, Inc.

Date Published
November 2016

Prepared for the U.S. Department of Energy
Assistant Secretary for Environmental Management

Contractor for the U.S. Department of Energy
under Contract DE-AC06-08RL14788

ch2m

P.O. Box 1600
Richland, Washington 99352

APPROVED
By Julia Raymer at 2:24 pm, Nov 03, 2016

Release Approval Date

Approved for Public Release;
Further Dissemination Unlimited

TRADEMARK DISCLAIMER

Reference herein to any specific commercial product, process, or service by tradename, trademark, manufacturer, or otherwise, does not necessarily constitute or imply its endorsement, recommendation, or favoring by the United States Government or any agency thereof or its contractors or subcontractors.

This report has been reproduced from the best available copy.

Printed in the United States of America

Executive Summary

This model package report (MPR) describes the numerical groundwater flow and transport model of the 100-BC-5 OU area (100-BC Model) developed for use by CH2M Hill Plateau Remediation Company in support of remediation activities at the Hanford Site, Washington. This MPR describes model objectives, conceptual model basis of the numerical model, model construction, flow calibration and sensitivity analysis, transport parameters, and basic testing of the model's flow and transport functions for fitness of purpose via simple representative, but not necessarily site-specific remediation actions.

The primary purposes of this model include the following:

- Computing groundwater head, hydraulic gradients, and flows to the Columbia River for use in general flow system understanding as well as potential remediation system (e.g. pump and treat) design/evaluation.
- Estimating future groundwater concentrations of hexavalent chromium and strontium-90 to support risk screening and evaluation of remediation options.
- Estimating contaminant discharge to the Columbia River and potential influent concentrations for extracted groundwater.

Contaminated groundwater in the 100-BC-5 OU flows northward and discharges into the Columbia River. The Hanford formation becomes unsaturated a few hundred meters before the chromium plume discharges to the river, and it is in this area that a pronounced increase in hydraulic gradient occurs due to loss of transmissivity. The hydraulic gradient is typically on the order of or less than 10^{-4} in the saturated Hanford and Ringold sediments. Wells in the AWLN away from the river show time delays from river stage changes as a function of distance. Wells proximal to the river respond immediately to daily stage fluctuations, and on the order of 10's of days several hundred meters away from the river. Current interpretation is that there is flow from the west (upriver) and possibly leakage from the 182-B pond directing plume migration to the north-northeast into the river.

The model domain encompasses the sediments above Ringold Upper Mud (RUM) and basalt in the vicinity of the 100-BC-5 OU including the Ringold E and Hanford

Formations–the Ringold Upper Mud (RUM) and basalt are considered impermeable relative to the Ringold E and Hanford sediments. Division of the HSUs was accomplished using data collected during the pause in the RI/FS since 2009 including borehole geophysics and lithology logs. This data was incorporated into the Hanford North geologic framework model (GFM) used as the geologic basis for the groundwater flow and transport numerical model.

In 2012 PNNL performed a series of characterization activities during excavation of the 100-C-7:1 pit for chromium-contaminated soil remediation. These activities included single-well pumping and short-duration tracer tests, and AWLN analysis as documented in PNNL-21845 *Investigation of Hexavalent Chromium Flux to Groundwater at the 100-C-7:1 Excavation Site*. Slug tests were also conducted in 12 wells completed in the Ringold E and Hanford formations as documented in ECF-100BC-11-0145 REV 0. The PNNL data showed that the Hanford formation in the area interpreted to be part of a cataclysmic flood channel has hydraulic conductivity on the order of 6,000 m/d. Slug test results in 3 wells completed in the Hanford did not give a quantitative result because the test ended too rapidly for analysis – it can only be concluded that the Hanford formation is generally much more permeable than the Ringold E, which had hydraulic conductivities ranging from 0.8 to 15 m/d. This data, along with calibration to AWLN data was used to estimate model hydraulic properties at the scale of the chromium plume – the most extensive groundwater contamination - by exploiting the correlation between river stage fluctuation and aquifer head changes occurring over about 10 to 40 days. A spatially-distributed parameter estimation technique was used to estimate hydraulic conductivity; specific storage, specific yield, and anisotropy were represented by areas of constant properties. This resulted in aquifer properties conditioned to large-scale hydraulic responses that are also representative of the plume migration scale.

Flow model calibration emphasized 2012 through July 2014 because this period had the most comprehensive data set and included the PNNL data – for maximum consistency and to eliminate potential inconsistency due to the highly transient nature of groundwater flow in the OU the 2012 PNNL data was not used separately from the corresponding river hydrologic and hydrogeologic conditions. Calibration data included AWLN and manual water-level measurements, groundwater flow direction and gradient from wells 199-B4-14, 199-B5-8, and 199-B8-6 (used in PNNL-21845) as well as water-level changes (in order to emphasize the influence of river-induced changes).

Data more directly useful for transport predictions was also used in flow model calibration including groundwater velocity estimates (ranging from about 3 to 5 m/d) from PNNL tracer tests. Monitoring of the chromium plume between 2012 and 2014 showed mass– some released from 100-C-7:1 excavation - moving through the Hanford part of the unconfined aquifer at about 1 m/d; this interpretation was used to constrain the groundwater flow velocities over a distance of about 800 m.

In the revised CSM average linear groundwater velocity is on the order of 1 to 7 m/d, which is supported by field observations. Under these conditions the chromium plume in the upper unconfined aquifer is reduced to less than 10 μg/L in about 8 years without a continuing source. The chromium plume in the deep unconfined aquifer (Ringold E) does not dissipate until after about 80 years because groundwater velocity is so much lower than in the upper unconfined aquifer. The rapidity of the plume response implies that responses to remediation activities also should be noticeable quickly.

Estimated residual chromium soil concentration and leaching coefficients from PNNL column experiments were used to qualitatively match chromium plume evolution between 2011 and 2015. The broad trends of interpreted plume migration were captured, including the increase in groundwater chromium concentrations in early 2012 thought to be from dust control water applied to contaminated soil that made its way into the aquifer when the excavation was close to groundwater between about November 2011 and February 2012. Additionally, persistent chromium concentrations at well 199-B3-47 were interpreted as due a source which was implemented for waste site 116-B-11. Even this qualitative transport calibration increases confidence that the fate and transport model is representative of actual conditions. Significant uncertainty, judged irreducible, still exists over the long-term chromium source.

The estimated residual chromium soil concentration was used as the source for long-term (125 year) forecasts under a no further action scenario.

The following results were observed in the Cr(VI) no further action scenario:

1. Aquifer concentrations drop below 48 μg/L in about 15 years.
2. At no time are there any shoreline concentrations greater than the MCL.
3. Concentrations are everywhere below 10 μg/L after about 110 years.

Conceptual and parameter uncertainties include the following:

- The configuration of the Hanford/Ringold contact in the western portion of the OU is not well constrained by well data, but is of minor importance because it is not in an area that will affect future plume migration.
- Hydraulic conductivity (and hence transmissivity and groundwater flow rate) uncertainty grows away from AWLN wells. Because the AWLN wells bracket the Cr(VI) plume southern extent and discharge flow path to the river this uncertainty is qualitatively judged of modest importance.
- Broad hydrogeologic heterogeneity is inferred from calibration to the AWLN data, and is also reported by PNNL-21845.
- The Hanford and Ringold formations can be difficult to distinguish. Thus, small discrepancies in contact horizons can result in conceptual inconsistency in hydraulic properties manifesting themselves in groundwater (plume) velocities.
- The long-term behavior of the chromium source cannot be known with high certainty because chromium exists in several chemical states in the aquifer with greatly differing release characteristics.
- Laboratory data suggests that over the long-term Cr(VI) leachability of contaminated sediments declines. Coefficients were estimated from laboratory-scale data and applied to field-scale computations. This scale change is judged to have significant, but unresolvable uncertainty.

- Due to reactor operations chromium is a ubiquitous soil contaminant that, despite extensive soil remediation, may still linger in the PRZ in some locations that are not well understood.

Contents

1 Purpose 1-1

1.1 Need 1-1

1.2 Background 1-1

1.3 Document Organization 1-4

1.4 Model Objectives 1-5

2 Model Conceptualization 2-1

2.1 Hydrogeologic Overview 2-1

2.1.1 Hanford Formation 2-2

2.1.2 Ringold Formation Units 2-5

2.1.3 Hanford and Ringold Hydraulic Conductivity, Specific Storage, and Specific Yield 2-6

2.2 Features, Events, and Processes (FEPs) 2-9

2.2.1 FEP: Anthropogenic Recharge 2-9

2.2.2 FEP: Natural Recharge 2-10

2.2.3 FEP: Columbia River Interaction 2-14

2.2.4 FEP: Groundwater Flow 2-17

2.2.5 FEP: Potential Hexavalent Chromium Sources 2-22

2.2.6 FEP: Potential Strontium-90 Sources 2-22

2.3 Nature and Extent of Contamination 2-22

2.4 Conceptual Model Summary 2-28

3 Model Implementation 3-1

3.1 Software 3-1

3.2 Discretization 3-3

3.2.1 Temporal Discretization 3-3

3.2.2 Spatial Discretization 3-5

3.3 Parameterization 3-8

3.3.1 Recharge Boundary Condition 3-8

3.3.2 West, South, and East Landward Boundary Conditions 3-9

3.3.3 River Boundary Conditions 3-10

3.3.4 Initial Head Condition 3-11

3.3.5 Initial Cr(VI) and Sr-90 Concentration 3-11

3.3.6 Aquifer Hydraulic Property Parameterization 3-11

3.3.7 Effective Porosity 3-16

3.3.8 Dispersivity 3-16

3.3.9 Adsorption 3-20

3.4 Flow Model Calibration 3-20

3.4.1 General Approach 3-20
3.4.2 Parameter Estimation Framework 3-23
3.4.3 Flow Model Calibration Results 3-24
3.4.4 Qualitative Flow Model Evaluation 3-25
3.4.5 Calibrated Flow Model Properties 3-28
3.5 Chromium Transport Model Calibration 3-28
3.5.1 Transport Calibration Approach and Data 3-28
3.5.2 Transport Calibration Results 3-32
3.6 No Further Action Cr(VI) Forecasts 3-35
4 Model Sensitivity and Uncertainty Analysis 4-1
4.1 Sensitivity Analysis 4-1
4.2 Uncertainty Analysis 4-2
5 Model Limitations 5-1
6 Model Configuration Management 6-1
6.1 Version History 6-1
7 Model Recommendations 7-1
8 References 8-1

Appendices

A Priest Rapids to B-Gauge CorrelationA-i
B Observed Data and Simulated Hydrographs ..... B-i

Figures

Figure 1-1. Hanford Site Map 1-2
Figure 1-2. 100-BC Topography 1-3
Figure 1-3. 100-BC Reactors and Operable Units 1-4
Figure 2-1. Stratigraphy and Hydrogeologic Units of 100-BC 2-2
Figure 2-2. Geologic Cross Section A-A' 2-3
Figure 2-3. Saturated Hanford Formation Thickness with 2013 Cr(VI) Plume 2-4
Figure 2-4. Elevation of Top of Ringold Unit E, 100-BC (Hanford/Ringold Contact) 2-5
Figure 2-5. Top of Ringold Mud (RUM) and 2013 Cr(VI) Plume 2-6
Figure 2-6. Ringold Hydraulic Conductivity ECDF from SGW-44022 2-7
Figure 2-7. Hanford Hydraulic Conductivity ECDF from SGW-44022 2-8
Figure 2-8. Natural Vegetation Recharge Scenario applied for Preliminary Remediation Goal Calculation in 100-Area Waste Sites subject to Historic Irrigation 2-13

Figure 2-9. Aerial Imagery of 100-BC Model Domain Showing Spatial Variability of Surface Conditions that are Reflected in Natural Recharge Rates that Depend on Surface Soil Type and Vegetation Density 2-15
Figure 2-10. Conceptualization of Spatially and Temporally Variable Natural Recharge Rate Boundary Condition 2-16
Figure 2-11. Pore-water Samples from the Columbia River Bed 2-18
Figure 2-12. 100-BC 2013 Water Table (DOE/RL-2014-32, Rev. 0) 2-19
Figure 2-13. Hydraulic head data for wells 199-B4-14, 199-B5-8, and 199-B8-6 along with computed flow direction (PNNL-21845) 2-20
Figure 2-14. Groundwater Flow Direction (Azimuth) and Hydraulic Gradient Computed from Hydraulic Head Data from Wells 199-B8-6, B4-14, and 199-B5-8 (PNNL-21845) 2-20
Figure 2-15. Estimated Groundwater Velocity in the Hanford Formation Near 100-C-7 and 100-C-7:1 Based on Calculated Hydraulic Gradients (PNNL-21845) 2-21
Figure 2-16. Selected AWLN Well Hydrographs 2-21
Figure 2-17. Hanford Site and Outlying Areas Water-Table Map, April/May 2006 (PNNL-16346) 2-23
Figure 2-18. Well 199-B3-47 Cr(VI) Concentrations over Time 2-24
Figure 2-19. 100-BC 2013 Hexavalent Chromium Plume (DOE/RL-2014-32, Rev. 0) 2-25
Figure 2-20. 100-BC Hexavalent Chromium in the Lower Part of the Unconfined Aquifer (Ringold) 2013 (DOE/RL-2014-32, Rev.0) 2-26
Figure 2-21. 100-BC Cross Section Showing Hexavalent Chromium Distribution, Southwest to Northeast 2013 (DOE/RL-2014-32, Rev.0) 2-27
Figure 2-22. Western 100-BC Cross Section Showing Chromium Distribution 2013 (DOE/RL-2014-32, Rev.0) 2-27
Figure 2-23. 100-BC Wells Screened in Ringold E 2-28
Figure 2-24. 100-BC 2013 Strontium Plume (DOE/RL-2014-32) 2-29
Figure 2-25. 100-BC 2013 Tritium Plume (DOE/RL-2014-32) 2-30
Figure 3-1. Comparison Between Daily River Stage and Average River Stage Based on Stress Period Length at B-River Gauge for January, 2012 to July, 2014 3-4
Figure 3-2. Comparison Between Daily River Stage and Average River Stage Based on Stress Period Length at B-River Gauge for January, 2006 to July, 2014 3-4
Figure 3-3. Comparison between Daily River Stage and Average River Stage Based on Stress Period Length at B-River Gauge for the Predictive Model 3-5
Figure 3-4. 100-BC Groundwater Flow and Transport Model Plan View Grid 3-6
Figure 3-5. 100-Area GFM with Columbia River, MODFLOW Model Layers and 2013 Cr(VI) Plume at Easting = 565000.5 m 3-7
Figure 3-6. 100-Area GFM with Columbia River, MODFLOW Model Layers and 2013 Cr(VI) Plume at Easting = 565277.5 m 3-8
Figure 3-7. 100-Area GFM with Columbia River, MODFLOW Model Layers and 2013 Cr(VI) Plume at Easting = 565000.5 m 3-8
Figure 3-8. 2011 Recharge 3-9

Figure 3-9. GHB head vs. distance considering stage, gradient, prior levels, and distance correction for the first 8 stress periods 3-10
Figure 3-10. Pilot point locations in Layer 1 3-13
Figure 3-11. Pilot point locations in Layer 2 3-13
Figure 3-12. Pilot point locations in Layer 3 3-14
Figure 3-13. Pilot point locations in Layer 4 3-14
Figure 3-14. Pilot point locations in Layer 5 3-15
Figure 3-15. Pilot point locations in Layer 6 3-15
Figure 3-16. Longitudinal Dispersivity by Rock Type 3-17
Figure 3-17. Longitudinal Dispersivity by Reliability Level for all Rock Types with Linear and Log Fits 3-18
Figure 3-18. Longitudinal Dispersivity by Reliability Level for Alluvial Sediments only with Linear and Log Fits 3-19
Figure 3-19. Calibration Features 3-22
Figure 3-20. Observed versus Simulated AWLN Heads 3-24
Figure 3-21. Observed versus Simulated Manually Measured Heads 3-25
Figure 3-22. Observed and Simulated Flow Direction over time computed from wells 199-B4-14, B8-6, and B5-8 3-26
Figure 3-23. Observed versus Simulated Hydraulic Gradient Magnitude computed from wells 199-B4-14, B8-6, and B5-8 3-26
Figure 3-24 February 2013 Annual Report and Model Simulated Maps 3-27
Figure 3-25. February 2014 Annual Report and Model Simulated Maps 3-27
Figure 3-26. Layer 1 Hydraulic Conductivity 3-29
Figure 3-27. Layer 2 Hydraulic Conductivity 3-29
Figure 3-28. Layer 3 Hydraulic Conductivity 3-30
Figure 3-29. Layer 4 Hydraulic Conductivity 3-30
Figure 3-30. Layer 5 Hydraulic Conductivity 3-31
Figure 3-31. Layer 6 Hydraulic Conductivity 3-31
Figure 3-32. Simulated (left) and Mapped (right) Chromium Plume at the top of the unconfined aquifer, Fall 2011 (DOE/RL-2010-96, Draft A) 3-33
Figure 3-33. Simulated (left) and Mapped (right) Chromium Plume at the top of the Unconfined Aquifer, Fall 2012 (DOE/RL-2013-22, Rev. 0) 3-33
Figure 3-34. Simulated (left) and Mapped (right) Chromium Plume at the top of the unconfined aquifer, Fall 2013 (DOE/RL-2014-32, Rev. 0) 3-34
Figure 3-35. Simulated (left) and Mapped (right) Chromium Plume at the top of the unconfined aquifer, Fall 2014 (DOE/RL-2015-07, Rev. 0) 3-34
Figure 3-36. Simulated (left) and Mapped (right) Chromium Plume at the top of the unconfined aquifer, Fall 2015 (Mary Hartmann, personal communication, November 5, 2015) 3-35
Figure 3-37. Simulated 2025 Cr(VI) Upper Unconfined Aquifer Plume and WCH-380 Porewater Data 3-36

Figure 3-38. Leach rate constant multiplier to quantify the declining source strength for release of Cr(VI) 3-37
Figure 3-39. Maximum Simulated Cr(VI) Concentration by Model Layer over 125 Years - No Further Action Case 3-37
Figure 3-40. Shoreline Length above Selected Thresholds - No Further Action Case 3-38
Figure 3-41. Simulated 2020 Cr(VI) Plume Extents in Model Layers 1 and 6 - No Further Action Case 3-39
Figure 3-42. Simulated 2025 Cr(VI) Plume Extents in Model Layers 1 and 6 - No Further Action Case 3-40
Figure 3-43. Simulated 2040 Cr(VI) Plume Extents in Model Layers 1 and 6 - No Further Action Case 3-41
Figure 3-44. Simulated 2065 Cr(VI) Plume Extents in Model Layers 1 and 6 - No Further Action Case 3-42
Figure 4-1. Flow Model Parameter Identifiability 4-1
Figure 4-2. CDF of Calibrated Hanford and Ringold E Hydraulic Conductivity Pilot Points 4-2

Tables

Table 2-1. Horizontal Hydraulic Conductivity Estimates for 100-BC Sediments 2-8
Table 2-2. Native Vegetation Recharge Scenario Phases and Recharge Rates (mm/yr) 2-13
Table 3-1. Dispersivity-scale relationships 3-19
Table 3-2. Recommended Dispersivity Values for 100-BC 3-20
Table 3-3. Single-Value Parameter Estimates 3-28
Table 6-1. Version History of the 100-BC GWFTM 6-1

Terms

AWLN	Automated Water Level Network
CHPRC	CH2M HILL Plateau Remediation Company
COPC	Contaminant of Potential Concern
Cr(VI)	Hexavalent Chromium
DOE	U.S. Department of Energy
DWS	Drinking Water Standard
ECF	Environmental Calculation File
EMMA	Environmental Model Management Archive
FEP	Feature, Event, or Process
FY	fiscal year
GFM	Geologic Framework Model
GHB	General Head Boundary (MODFLOW term for mixed boundary condition)
GWFTM	Groundwater Flow and Transport Model
HEIS	Hanford Environmental Information System (environmental database)
HSU	Hydro-Stratigraphic Unit
MODFLOW	MODular groundwater FLOW code (software)
MT3DMS	Modular 3-Dimensional Multiple Species transport code (software)
OU	Operable Unit
PNNL	Pacific Northwest National Laboratory
PRZ	Periodically Rewetted Zone
RI/FS	Remedial Investigation and Feasibility Study

1 Purpose

The groundwater flow and transport model for the 100-BC-5 OU of the U.S. Department of Energy's (DOE) Hanford Site was developed to provide the computational basis for simulation of fate and transport of groundwater contaminants. This model focuses on the hexavalent chromium and strontium-90 plumes, which are currently (2015) present at or above drinking water standards.

1.1 Need

The 100-BC groundwater flow and transport model provides a consistent, mass conservative hydrogeologic framework for comparing and contrasting potential remediation actions as required for the RI/FS. Model output used for this purpose could include groundwater potentials, hydraulic gradients, flow rates, future groundwater contamination concentrations, and likely influent concentrations for remedies that extract contaminated groundwater. A model that included most of the 100 Area was previously used for these computations before additional data collection began in 2012.

1.2 Background

The U.S. government took possession of the land now known as the Hanford Site in 1943 to produce weapons-grade plutonium as a part of the Manhattan Project. The Hanford Site is divided into numerically designated areas. These areas served as the location for reactor, chemical separation, and related activities for the production and purification of special nuclear materials and other nuclear activities. The reactors and their ancillary/support facilities were located along the south shore of the Columbia River in the 100 Area, because of the need for large quantities of water to cool the reactors. The 100-BC area is located in the northern portion of the Hanford Site adjacent to the Columbia River. It is the western-most reactor area and is adjacent to the 100-K Area to the east. It covers more than 11.54 km^2 (4.45 mi^2) of land along the southern shore of the Columbia River. The 100-BC boundary at the river is the ordinary low water mark, which is characterized by the presence of the "green line" of algae delineating the permanently inundated portion of the river channel. The 100-BC area is shown in Figure 1-1; the B and C reactors were located in this area.

100-BC is located on the south bank of the Columbia River, upstream from the other Hanford Site reactor areas. The topography of 100-BC is relatively flat inland (Figure 1-2) from the Columbia River. The area has been disturbed and graded extensively by human activity from reactor construction in the 1940s through current waste site remediation activities. Surface elevations in this region range from approximately 150 m (490 ft) above mean sea level (AMSL) at the southern border to 130 m (430 ft) in the north. The riverbank slopes steeply (10:1 grade) to the river shoreline where the elevation is approximately 122 m (400 ft) AMSL.

Significant topographic features near 100-BC include Gable Butte to the south as well as an extensive gravel beach that is exposed along the Columbia River during periods of low river stage. On the upstream end of the area, the bank is less steep and broadens into a gently sloping shoreline (50:1 grade) that is approximately 150 m (492 ft) wide (*Fiscal Year 1991 Report on Archaeological Surveys of the 100 Areas, Hanford Site, Washington* [PNL-8143]).

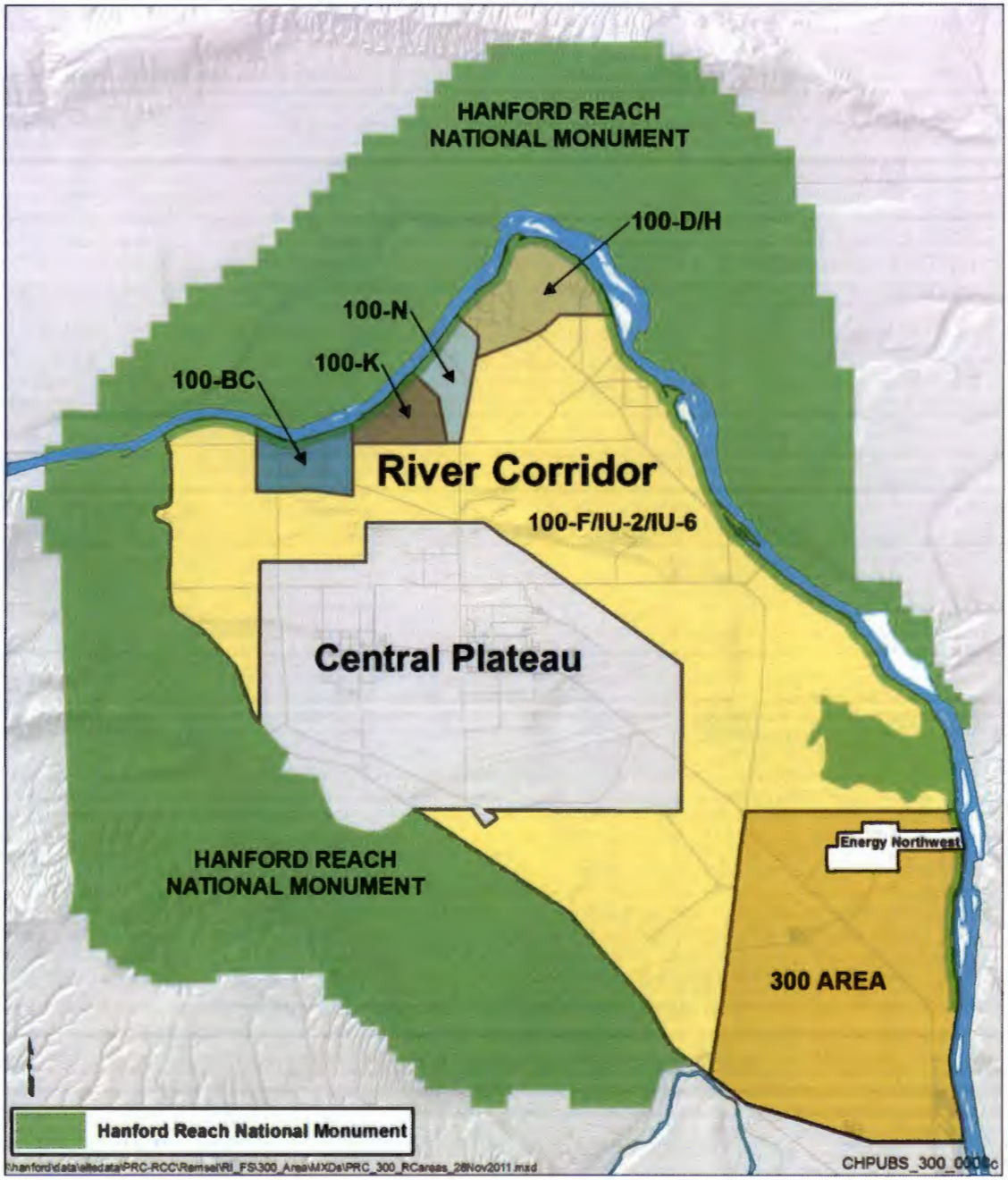

Figure 1-1. Hanford Site Map

In 100-BC, soil in the vadose zone comprises unconsolidated gravel and sand of the Hanford formation. The water table is at a depth of up to 30 m (98 ft).

The Hanford Site is characterized by a semi-arid climate, and is the driest and warmest portion of the Columbia Basin. The Cascade Range, to the west, creates a rain shadow effect on the Hanford Site climate, while the Rocky Mountains and mountain ranges in southern British Columbia protect it from the more severe polar air masses from the north (*Hanford Site Climatological Summary 2004 with Historical Data* [PNNL-15160]).

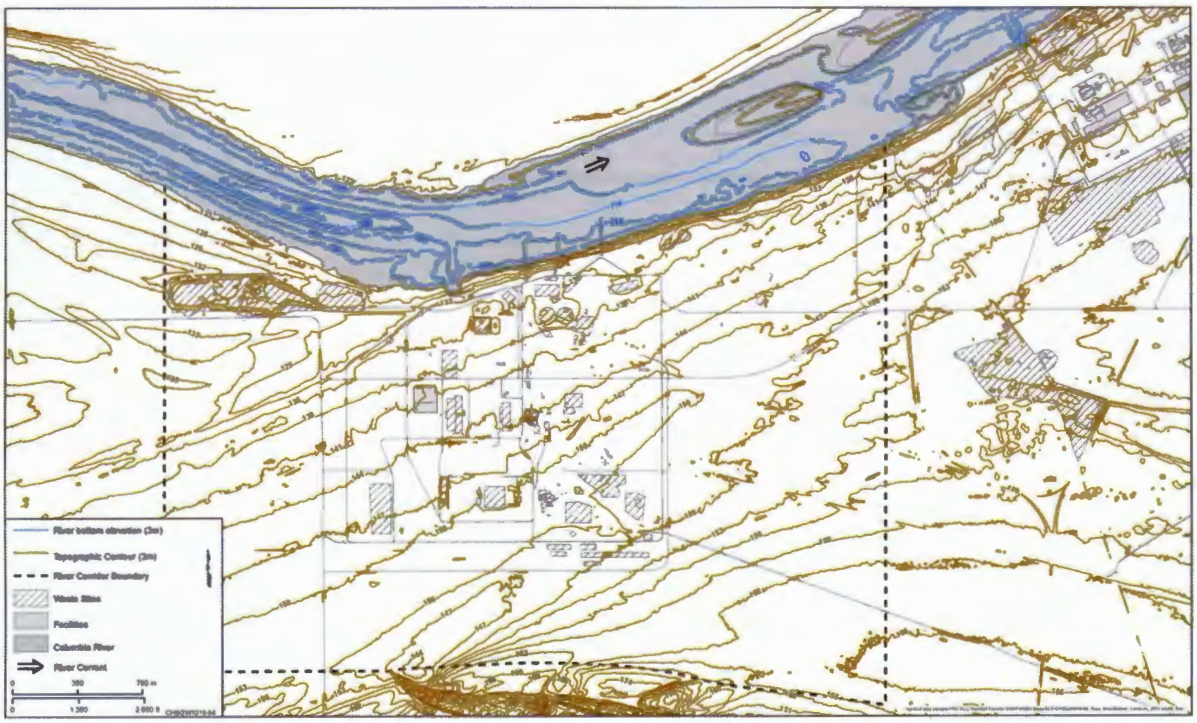

Figure 1-2 100-BC Topography

The Columbia River is the only natural surface water feature near 100-BC and forms the northern boundary of the model area. The Columbia River has played a major role in the depositional and erosional processes that produced the sedimentary and geologic features across the Hanford Site.

The stretch of the river that extends from Priest Rapids Dam, approximately 21 km (13 mi) upstream of 100-BC, to the headwaters of Lake Wallula, is the only free flowing portion of the Columbia River in the United States. This stretch of river, the Hanford Reach, is part of the Hanford Reach National Monument, established in June 2000 through Presidential Proclamation.

Figure 1-3 shows the operable unit (OU) boundaries, facilities, and reactors. B reactor was shut down in 1968. C reactor was shut down in 1969.

Producing plutonium for national defense was the primary mission of the Hanford Site reactors. Materials that passed through the reactors for manufacture, or materials contacting items that passed through the reactors, were considered radiologically contaminated. These materials represent the majority of the wastes that were produced. Active physical barriers and strong administrative measures were in place to minimize radiological hazards throughout the Hanford Site production areas to protect plant personnel. These measures affected the placement of disposal locations and waste management procedures for various waste streams.

Waste streams from the reactor production process include the following:

- Process inputs:

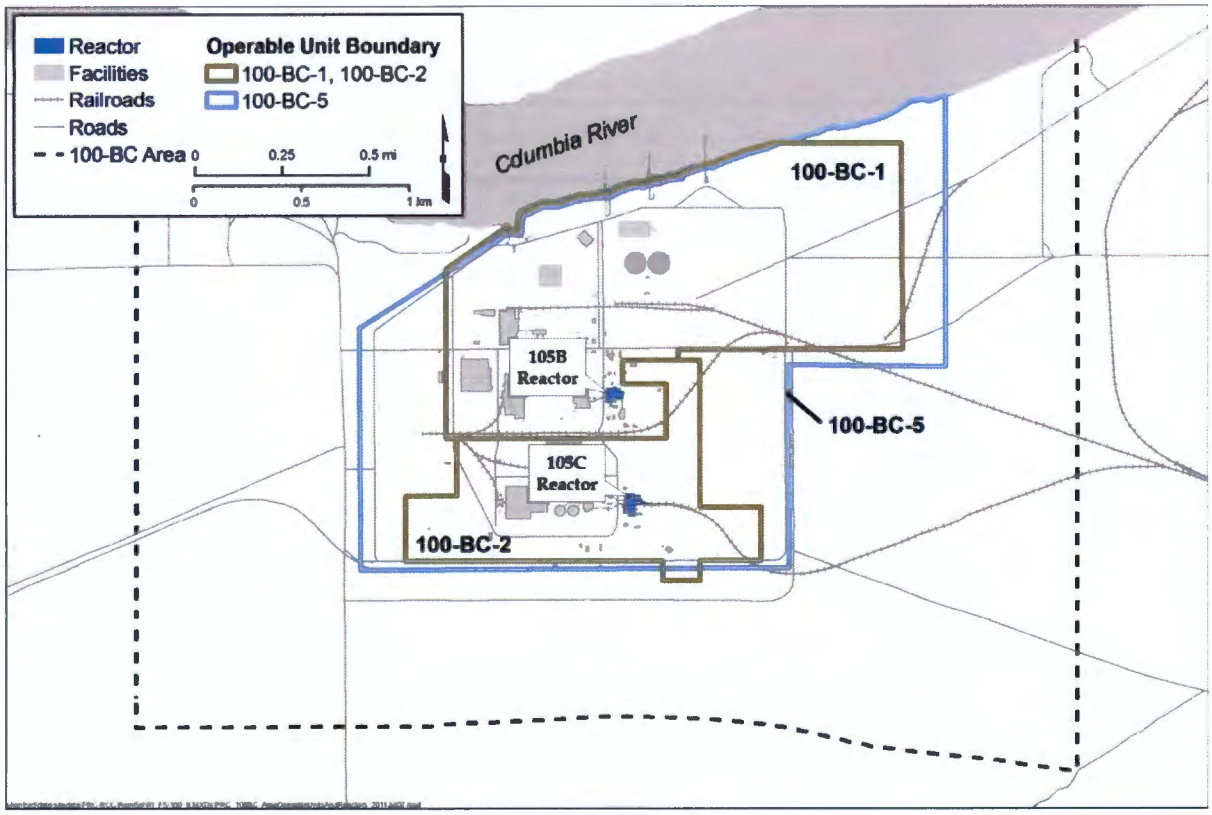

Figure 1-3 100-BC Reactors and Operable Units

  - Raw materials to be processed through the reactor
  - Process chemicals for water conditioning and inhibiting corrosion (for example, sodium dichromate) because water management was crucial to the operation of the reactors and represented a major input subsystem
  - Materials used for reactor maintenance, such as acids, solvents, and solid metal components

- Process outputs:
  - Product and waste isotopes, such as plutonium-239 and strontium-90, respectively
  - Radioactively and chemically contaminated materials (solid and liquid wastes)
  - Radioactively and chemically contaminated cooling water

Liquid wastes from reactor operations and associated facilities were released to the vadose zone and the Columbia River. Solid wastes were disposed in burial grounds associated with the facilities.

1.3 Document Organization

The organization of this model package report follows guidance set forth in CHPRC-00189, Rev. 9, Appendix G, *Quality Assurance Project Plan for Modeling* as follows:

- Chapter 1 sets forth the objectives that the 100-BC Model is constructed to meet.

- Chapter 2 describes the conceptualization of the system to be simulated with the numerical model, including identification of the relevant features, events, and processes (FEPs).
- Chapter 3 describes the implementation of the conceptual model as a numerical computer simulation model.
- Chapter 4 provides an overview of the sensitivity and describes sources of uncertainty for the predictions made with this model. There is some intentional redundancy in Chapters 3 to 5 to allow the report to be used as a reference document as well as a descriptive document.
- Chapter 5 enumerates the limitations of this model that result from the conceptualization, selection, and exclusion of relevant FEPs, assumptions, and numerical implementation.
- Chapter 6 describes how this model is uniquely identified, tracked, and preserved as a configuration management item.
- Chapter 7 lists recommended improvements to the model that could be made for future versions.
- Chapter 8 provides references cited in this model package report.
- Appendix A describes an assessment of the relationship between Priest Rapids dam and B-gauge stage data.
- Appendix B shows the observed head data and simulated hydrographs for the evaluation model.

1.4 Model Objectives

The overall objectives of the modeling effort is to provide a basis to assist in making informed remediation action decisions based on descriptions of current and expected future groundwater contaminant concentrations at decision points within the OU boundaries.

Problem-specific analyses will be described for each use of the model in separate environmental calculation files.

This page intentionally left blank.

2 Model Conceptualization

The conceptual site model (CSM) is a framework for interpreting data from 100-BC characterization efforts. The CSM synthesizes what is known into a framework that is pertinent for decision making. The American Society for Testing and Materials Standard Guide for Conceptualization and Characterization of Ground-Water Systems (ASTM D5979) defines the CSM as a written, pictorial, and diagrammatic information and interpretations. The CSM results from a blending of information and expert opinion on topics that range from small-scale processes to large-scale regional constraints, honors existing data, addresses how well interpretations and parameters are known, and integrates the parts into a whole-system view of the regulatory problem that can be translated into a quantitative representation. The following section describe the data and components of the CSM. **Key conceptual points are emphasized by bold text.**

2.1 Hydrogeologic Overview

The 100-BC Area lies on the northern flank of the Wahluke Syncline and is located adjacent the Columbia River.

Figure 2-1 shows the generalized stratigraphy of 100-BC. The area is underlain by Miocene (approximately 17 to 8.5 million years before present) basalt of the Columbia River Basalt Group and late Miocene to Pleistocene (approximately 10.5 million to 12,000 years before present) suprabasalt sediments.

Sediments overlying the basalts are approximately 200 m (660 ft) thick at 100-BC. Most of this sedimentary sequence can be divided into two main units: the Ringold Formation of late Miocene to middle Pliocene age (approximately 10.5 to 3 million years before present) and the Hanford formation of Pleistocene to Recent age (approximately 1 million to 12,000 years before present). Holocene surficial deposits of silt, sand, and gravel form the veneer at the surface.

The sediments that overlie the basalt are divided into two primary units: the Ringold Formation of late Miocene to middle Pliocene age (approximately 10.5 to 3 million years [m.y.] before present [B.P.]) (*Sedimentology and Stratigraphy of the Miocene-Pliocene Ringold Formation, Hanford Site, South-Central Washington* [WHC-SA-0740-FP]) and the informally named Hanford formation of Pleistocene age (approximately 1 million to 12,000 B.P.) (*Geology and Ground-Water Characteristics of the Hanford Reservation of the U.S. Atomic Energy Commission, Washington* [Newcomb et al., 1972]). Holocene surficial deposits of silt, sand, and gravel form a relatively thin veneer at the surface (*Geology and Hydrology of the Hanford Site: A Standardized Text for Use in Westinghouse Hanford Company Documents and Reports* [WHC-SD-ER-TI-003]; "Long History of Pre-Wisconsin, Ice Age Cataclysmic Floods: Evidence from Southeastern Washington State" [Bjornstad et al., 2001]).

The 100-BC Area is underlain by Miocene-aged (approximately 17 to 8.5 m.y. B.P.) basalt of the Columbia River Basalt Group and late Miocene- to Pleistocene-aged sediments (Ellensburg Formation, approximately 10.5 million to 12,000 B.P.) that are interbedded with basalt flows. The basalt may exceed 3,050 m (10,000 ft) in thickness, including the interbedded sediments of the Ellensburg Formation.

The physical properties of these formations influence the distribution of contamination in the subsurface. The Hanford formation, two upper units of the Ringold Formation (Ringold unit E and RUM) have been contacted by contaminated fluids. The rest of the Ringold Formation consists of a lower mud unit and Ringold units A, B, and C. **Contaminant migration units below the RUM is very unlikely in most locations because the low hydraulic conductivity of the RUM makes it an effective aquitard where it underlies the overlying Ringold unit E throughout 100-BC.**

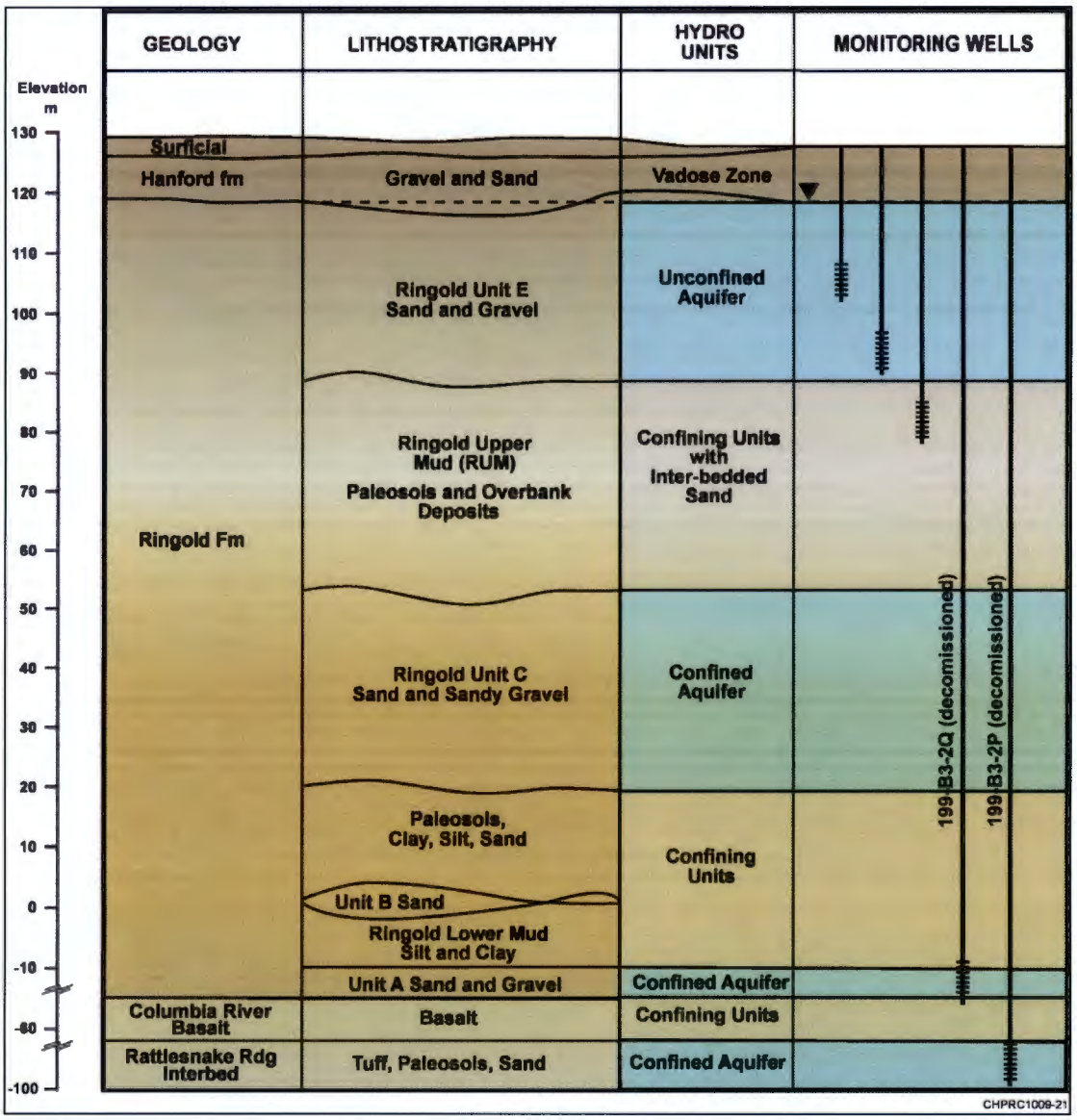

Figure 2-1 Stratigraphy and Hydrogeologic Units of 100-BC

2.1.1 Hanford Formation

The Hanford formation is an unofficial designation for a geologic unit that consists of gravel, sand, and silt deposited by cataclysmic floodwaters that drained out of glacial Lake Missoula during the Pleistocene age (*Draft Environmental Assessment: Reference Repository Location Hanford Site, Washington* [DOE/RW-0017]). The Hanford formation ranges in thickness from more than 60 m (200 ft) southeast of 100-BC to less than 15 m (50 ft) near the Columbia River (Figure 1-1Figure 2-2 and Figure 2-3). **The Hanford formation saturated thickness decreases towards the Columbia River as the Hanford/Ringold contact elevation rises, and the Hanford is unsaturated in the area where the chromium groundwater plume is interpreted to discharge to the river (see Section 2.3). This implies the transmissivity, assuming hydraulic conductivity is unchanged, of the Hanford must drop towards the river.**

The Hanford formation is divided into three facies: gravel-dominated, sand-dominated, and silt-dominated (*Standardized Stratigraphic Nomenclature for Post-Ringold-Formation Sediments Within the Central Pasco Basin* [DOE/RL-2002-39]). While the gravel-dominated facies are observed throughout 100-BC, the sand-dominated facies were observed locally and cannot be correlated between boreholes. **Silt-dominated Hanford formation facies are not significant in 100-BC**.

The Hanford formation in 100-BC is characterized by large to very large, cobble- to boulder-size clasts in open framework gravels. The formation includes discrete sand lenses with minor to no silt and clay material. The clasts typically are sub-round to round gravel and sub-angular to round in the sand grain fraction. The gravel-dominated facies typically are well stratified and contain little cementation (*Geologic Setting of the 100-HR-3 Operable Unit, Hanford Site, South-Central Washington* [WHC-SD-EN-TI-132]). **Boulder gravel in the upper 6 to 15 m (20 to 50 ft) demonstrates the high-energy depositional environment created during the Missoula Floods. This is interpreted to be due to 100-BC's location proximal to the main paleo-flood pathway into the upper Pasco Basin from the northwest (SGW-44022). This channel is thought to exist between 100-BC and Gable Butte.**

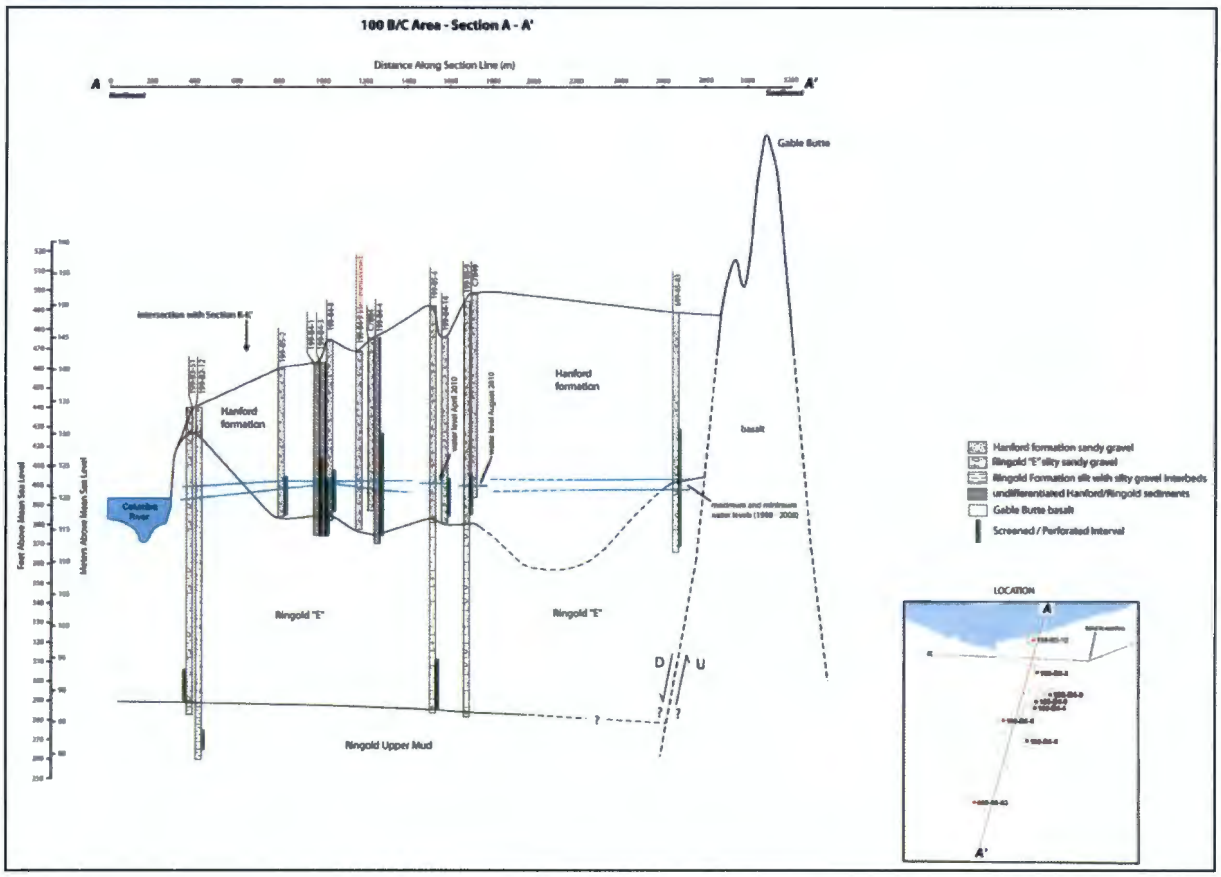

Figure 2-2 Geologic Cross Section A-A'

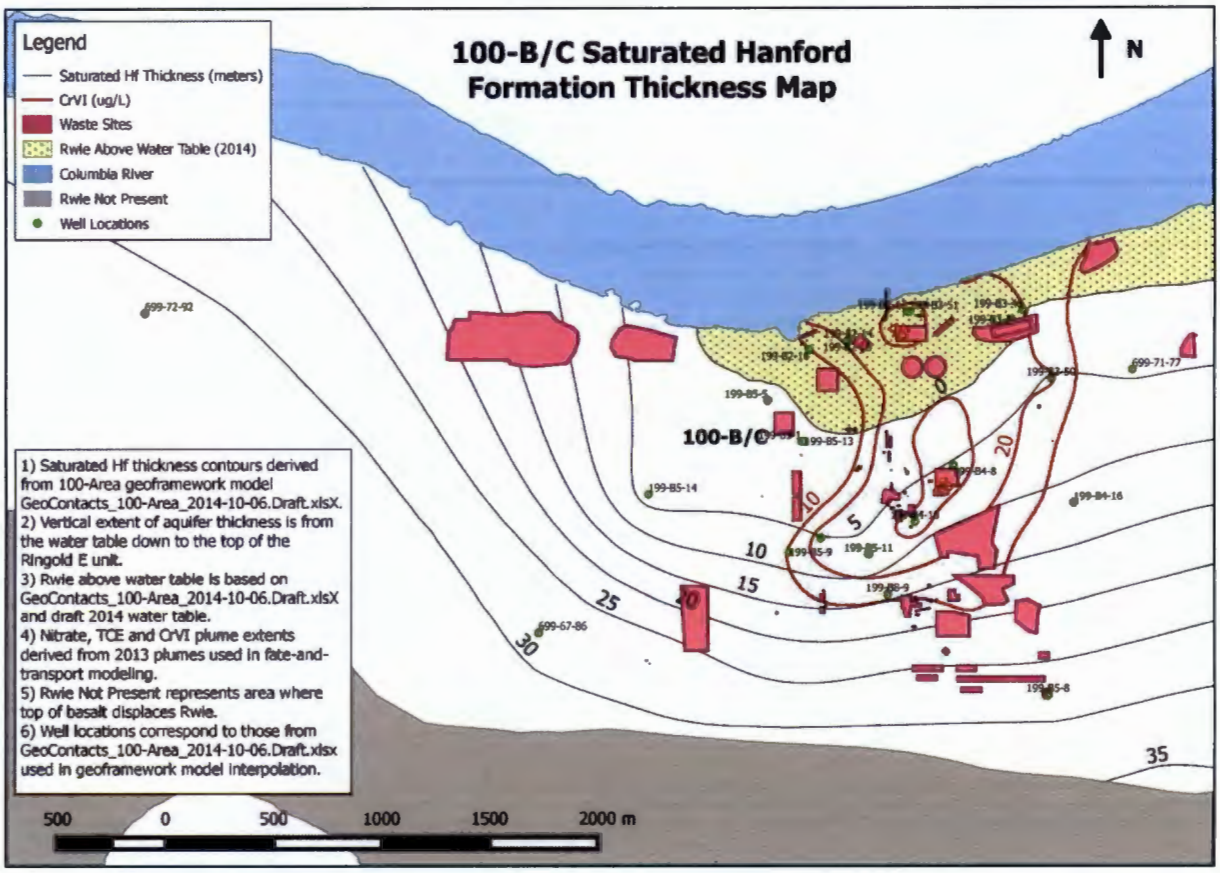

Figure 2-3 Saturated Hanford Formation Thickness with 2013 Cr(VI) Plume

The Hanford formation in 100-BC was deposited on an erosional surface of Ringold unit E. Geologists identify the contact between the Hanford formation and Ringold Formation based on characteristics such as basalt clast content, gravel content, coloration, and cementation. The Hanford formation typically is less cemented than the Ringold Formation and has greater gravel content. **The Hanford formation/Ringold Formation contact can be difficult to identify at 100-BC. Therefore, the Hanford formation/Ringold Formation contact has not been determined in all boreholes.**

The contact between Ringold unit E and the Hanford formation is important because the saturated hydraulic conductivity for the gravel-dominated sequence of the Hanford formation is potentially orders of magnitude higher than that of the more compacted and locally cemented Ringold unit E. Because hydraulic conductivity varies with the formation, different groundwater responses may occur where channels now filled with the Hanford formation have been scoured into the Ringold unit E. These buried channels could become preferential pathways for groundwater during high river stages (*Vadose Zone Hydrogeology Data Package for Hanford Assessments* (hereinafter called Vadose Zone Hydrogeology Package [PNNL-14702]), carrying contaminants where they are present. **The contact is highest in wells near the river and dips to the south.** The contact is much deeper farther southeast in new Well 199-B5-8, at approximately 94 m (308 ft) AMSL (Figure 2-4).

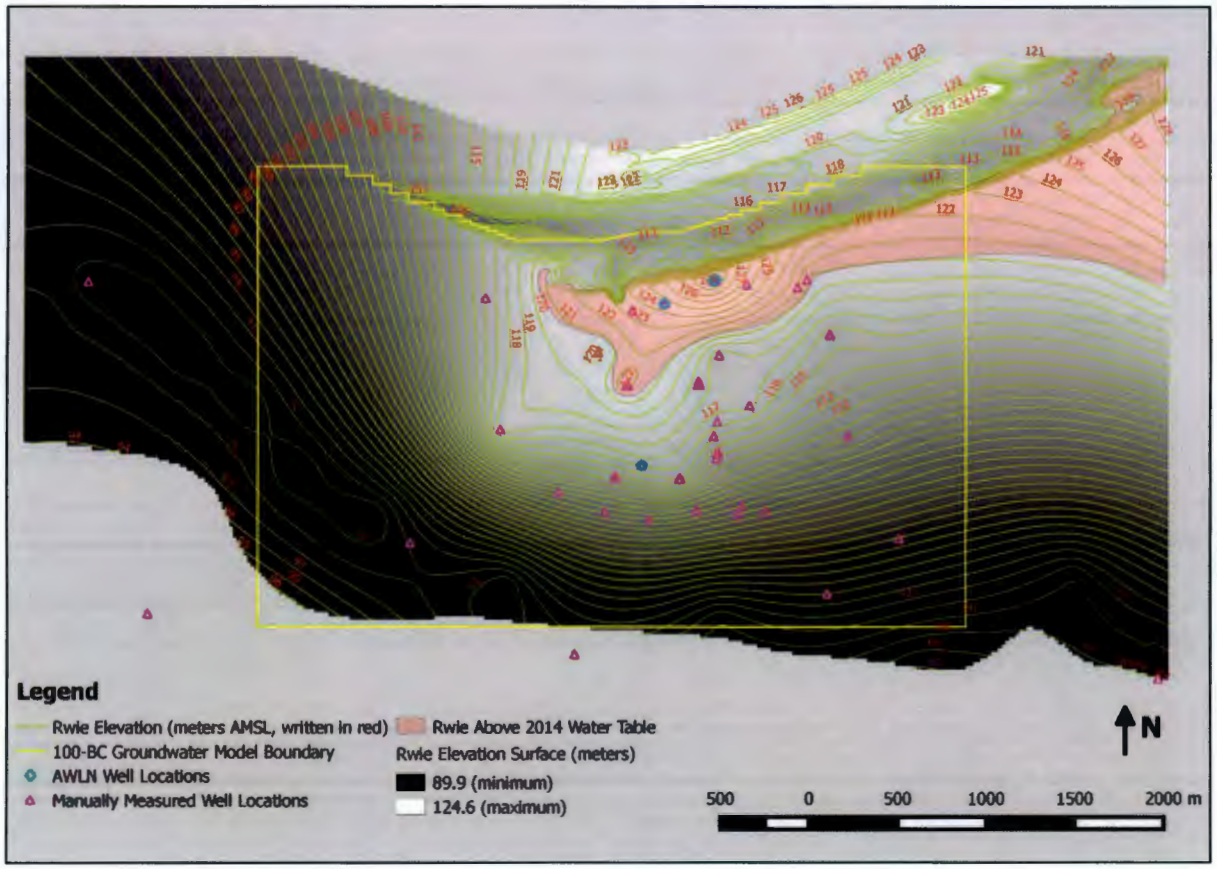

Figure 2-4 Elevation of Top of Ringold Unit E, 100-BC (Hanford/Ringold Contact)

2.1.2 Ringold Formation Units

The Ringold Formation beneath 100-BC contains most of the units commonly encountered elsewhere at the Hanford Site. The fluvial gravel and sand units A, B, C, and E (in ascending order) are present and interbedded with fine grained lacustrine and fluvial over bank deposits and paleosols. The uppermost unit of the Ringold Formation in 100-BC is Ringold unit E, which comprises predominantly sandy gravel. This unit ranges from 29 to 47 m (95 to 154 ft) thick beneath the main portion of 100-BC.

In the 100 Area, the uppermost fine grained Ringold sediments are informally termed the RUM unit. Distinguishing sandy, gravelly beds within the RUM unit from Ringold units C and B is not always possible. Similarly, silts and clays of the RUM unit may grade into deeper silt and clay units, making correlation of the units between boreholes difficult. In 100-BC, only Well 199-B3-2 penetrated the entire Ringold Formation. In that well, the RUM unit is interpreted to be approximately 34 m (110 ft) thick. The upper 0.5 to 4 m (2 to 13 ft) of the RUM unit in 100-BC comprises clay and silt and deeper sediments range from silty clayey gravel to silty sand. The RUM is interpreted to be the bottom of the unconfined aquifer flow system. The top elevation of the RUM is shown in Figure 2-5.

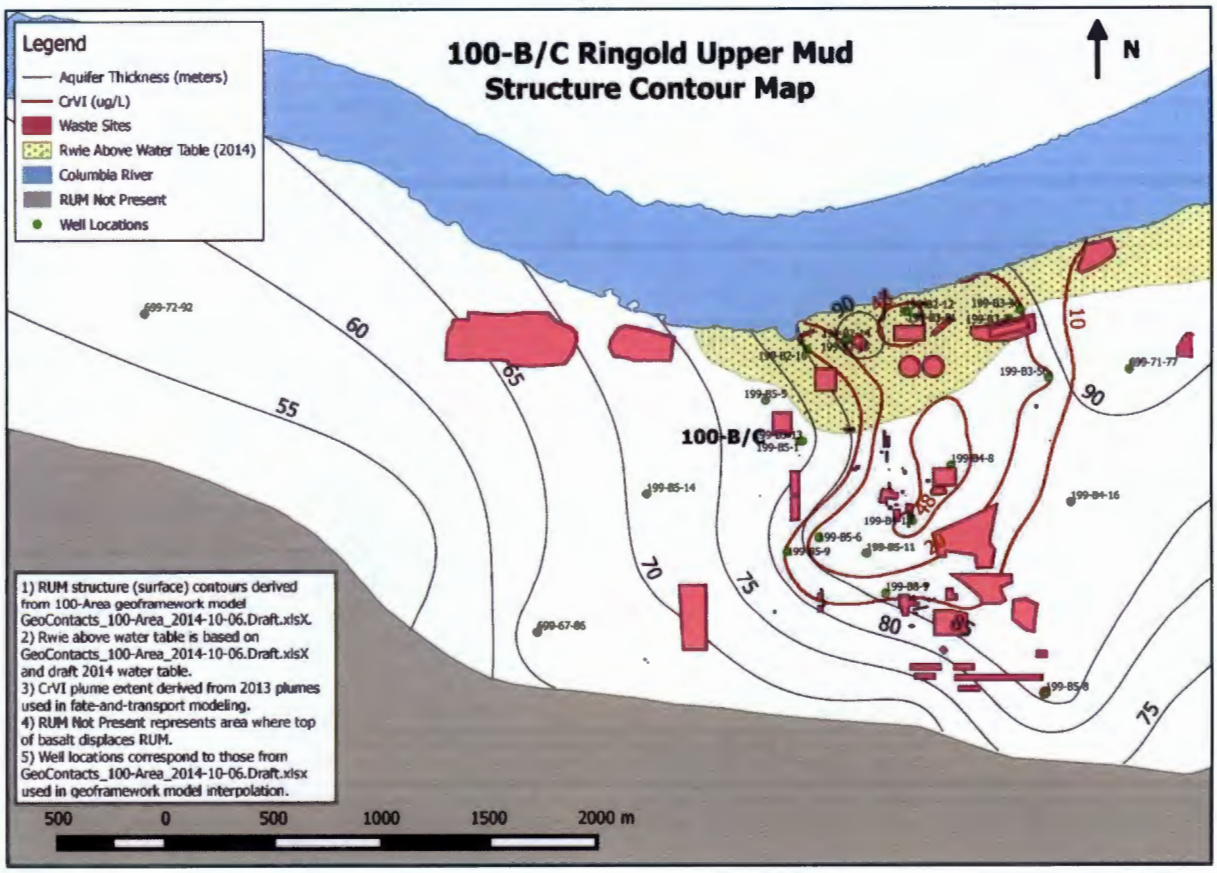

Figure 2-5 Top of Ringold Mud (RUM) and 2013 Cr(VI) Plume

2.1.3 Hanford and Ringold Hydraulic Conductivity, Specific Storage, and Specific Yield

SGW-44022 summarizes 100 Area hydraulic conductivity estimates from slug and pumping tests. No 100-BC data was available when SGW-44022 was written. Cumulative distribution plots of hydraulic conductivity by formation and test type (slug vs. pumping) are shown in Figure 2-7 and Figure 2-7. Note there is a systematic bias to higher values from pumping tests. This is because pumping tests are much less influenced by any near well residual effects from drilling compared to slug tests (Butler and Healey, 1998). Only one well – 199-B2-15 completed in a sandy gravel in the RUM – had both pumping and slug tests; the pumping test hydraulic conductivity was about 3 times the slug test value. Thus, the general trend of higher pumping test hydraulic conductivity holds, but cannot be more precisely identified for the Hanford or Ringold E. The 100 Area values reported in SGW-44022 for Hanford and Ringold range over more than 2 orders of magnitude, and thus add little to 100-BC site-specific understanding. However, it is clear that **the Hanford formation has systematically higher hydraulic conductivity than the Ringold E**.

Slug tests were performed in 100-BC wells in 2010 and 2011 to estimate horizontal hydraulic conductivity (Table 2-1). The two wells screened in the RUM had the lowest hydraulic conductivity, approximately 1 m/d (3 ft/d). Wells screened in Ringold unit E had hydraulic conductivity ranging from 2.5 to 16 m/d (8.2 to 52 ft/d). The lowest Ringold E hydraulic conductivity (2.5 m/d or 8.2 ft/d) was in a well screened at the bottom of the aquifer.

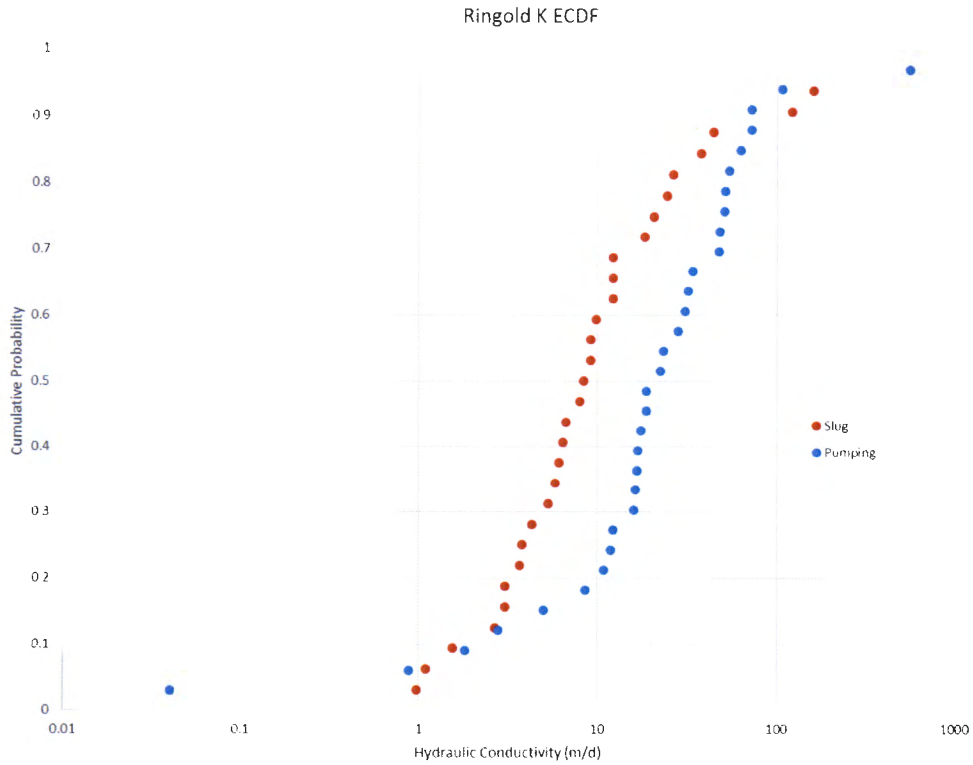

Figure 2-6 Ringold Hydraulic Conductivity ECDF from SGW-44022

Note that the pumping test at 199-B2-15 gave a value about 3 times higher than the slug test. This result confirms the general pattern seen in the SGW-44022 data of higher values in the Hanford; actual formation hydraulic conductivity should be considered to be higher than shown by the slug tests.

During excavation of 100-C-7:1 in 2012 PNNL conducted characterization activities on the Hanford formation. This included 3 constant-rate injection tests which gave hydraulic conductivity ranging from 5,200 to 7,300 m/d with an average of 6,000 m/d based on a saturated thickness of 9 ft; PNNL-21845. However, because the distance between pumping and observation wells is small (5 to 10 ft) considerable uncertainty still exists about effective larger-scale properties.

Bierschenk (1959) used the Ferris analytic approach to estimate hydraulic conductivity for Hanford "glaciofluviatile" deposits in the 100 Area between 200 and 700 m/d. These wells ranged from about 1 to 5 km inland from the river; thus, these values represent bulk effective Hanford properties.

Slug and single-well tests do not provide reliable estimates of storativity even though the analytic test solutions incorporate the parameter (Lohman, 1972; Horne, 1990).

PNNL-21845 assumed a specific storage of 1 x 10^{-5} 1/m in its analyses. Estimated specific yield ranged from 0.01 to 0.16; PNNL stated the lower value should not be considered representative.

PNNL-18732 reports aquifer characterization in the 200-ZP-1 OU located in the 200 West area. The Ringold E was the tested formation. Storativity of 9.7 x 10^{-4} was reported for a saturated thickness of 55.4 m giving a specific storage of 1.7 x 10^{-5} 1/m. Specific yield was estimated at 0.097; similar type-curve matches could be generated with specific yield ranging from 0.08 to 0.13.

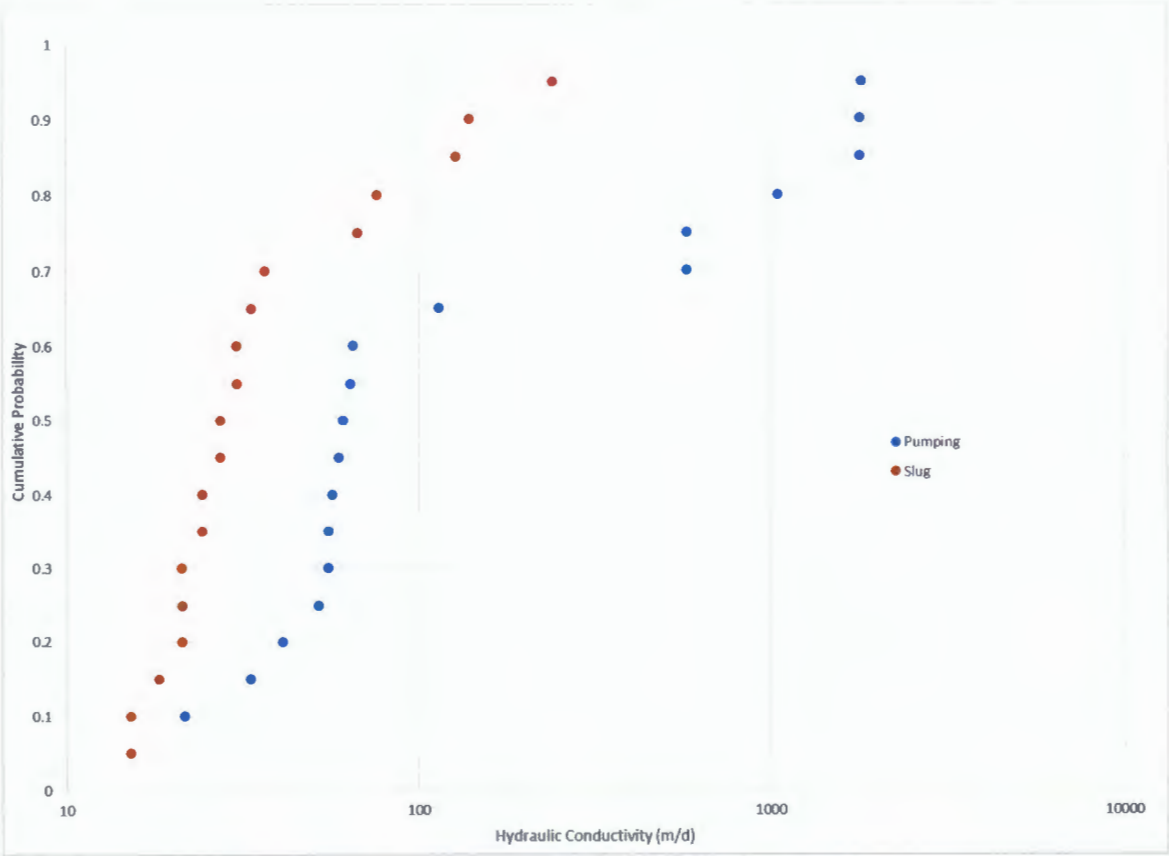

Figure 2-7 Hanford Hydraulic Conductivity ECDF from SGW-44022

Table 2-1 Horizontal Hydraulic Conductivity Estimates for 100-BC Sediments

Well	Hydrogeologic Unit	Type of Test	Hydraulic Conductivity	
			(m/d)	(ft/d)
199-B2-12	Silty sandy gravel in RUM	Slug	0.8	3
199-B2-14	Top of Ringold unit E	Slug	12	39
199-B2-15	Silty sandy gravel in RUM	Slug	1.1	4
		Pumping	3.0	9.8
199-B2-16	Lower part Ringold unit E (long screen)	Slug	6.4	21
199-B3-47	Top of Ringold unit E	Slug	16	52
199-B3-51	Bottom of Ringold unit E	Slug	2.5	8
199-B4-14	Hanford formation	Slug	NC	NC
199-B5-5	Lower part Ringold unit E (long screen)	Slug	15	49
199-B5-6	Bottom of Ringold unit E	Slug	9.1	30

Table 2-1 Horizontal Hydraulic Conductivity Estimates for 100-BC Sediments

Well	Hydrogeologic Unit	Type of Test	Hydraulic Conductivity	
			(m/d)	(ft/d)
199-B5-8	Hanford formation	Slug	NC	NC
199-B8-6	Hanford formation*	Slug	NC	NC
199-B8-9	Hanford formation	Slug	NC	NC

* Well 199-B8-6 was previously thought to be screened in Ringold unit E. Re-evaluation of the borehole log indicates it is screened in the Hanford formation. Its response to slug testing supports the new interpretation.

Source: Analysis of Slug Test Data at the 100-BC-5 Operable Unit (ECF-100BC5-11-0145) for slug tests; Aquifer Test Analyses for Wells 199-B2-15 and 199-F5-53 (ECF-HANFORD-11-0149) for pumping test.

NC = Not calculated. The slug test suggests that the materials are highly permeable. A pumping test would be a better alternative to estimating the accurate value of the hydraulic conductivity at this location.

Bierschenk (1959) cites an S value of 0.06 from a multiple-well test at 699-62-43; the magnitude indicates this should be interpreted as S_y.

A pumping test in the alluvium at the USGS Idaho Water Science Center (http://nevada.usgs.gov/water/AquiferTests/idaho.cfm?studyname=idaho) was conducted in 2010, and a specific storage of 1.5 x 10^{-6} 1/ft (5 x 10^{-6} 1/m) was estimated.

2.2 Features, Events, and Processes (FEPs)

2.2.1 FEP: Anthropogenic Recharge

During reactor operations groundwater heating was noticed from hot cooling water leaking from pipelines and retention basins, and hot-water mounds and river-bank thermal springs were formed (HW-77710). With the B and C reactor shutdown in the late 1960's the driving force ceased and the water drained from the vadose zone.

Leaks from existing underground water pipes are a potential source of anthropogenic recharge. For example, a leak from a fire hydrant affected water quality in 199-B5-1 from 2003 to 2006 (*Hanford Site Groundwater Monitoring for Fiscal Year 2006* [PNNL-16346]). Groundwater in that well became dilute, as evidenced by low specific conductance and low concentrations of contaminants and natural chemical parameters. The leak has been repaired, and water quality has returned to that of ambient groundwater.

The 182-B reservoir (constructed in the 1940's) is a concrete structure (147 by 94 m and 5.5 m deep) that is part of the Export Water System. The reservoir has a storage capacity of 9,500,000 L (2, 500,000 gal). This system supplies process, fire control, dust suppression and other nonpotable water. No data are available to document the state of the reservoir, but it is suspected of leaking at an unknown rate. SGW-44022 states "...the 182-B had chronic leaks from cracks and construction joints, which resulted in a persistent groundwater mound beneath the reservoir." No such mound is evident in recent water-table maps. Additionally, well 199-B5-1, the closest well to the reservoir, does not show any changes in specific conductance since the pipeline leak was repaired. It is also possible the well is not on a flow path from the reservoir to the river. In tension with this interpretation is the possibility that the reservoir leakage is not great enough to be detected at 199-B5-1.

Untreated (that is, raw) Columbia River water is used in 100-BC to control fugitive dust from remedial action processes. Typical remedial action processes and site features that contribute to fugitive dust include digging, open excavations, soil stock piles, and vehicle use on dirt roads. During remedial action, it has been important to control fugitive dust primarily for contamination control, worker inhalation concerns, and offsite perceptions. Control is maintained by applying water and by halting remediation activities when fugitive dust cannot be controlled because of wind conditions. According to the 100 Area RDR/RAWP (DOE/RL-96-17), "...use of water for dust control is minimized." This means that the quantity of water used is sufficient to control airborne emissions but excessive quantities of dust control water are not applied to minimize potential adverse impacts on groundwater. In the future, remedial actions will have less impact within 100-BC because most of the waste sites have been remediated and revegetated.

The typical quantity of dust suppression water used in 100-BC during periods of active remediation, including the water used on haul roads, is 908,000 L/week (240,000 gal/week). Dust control water is largely removed from the soil column during waste site excavation.

2.2.2 FEP: Natural Recharge

Recharge is the result of net infiltration through the vadose zone reaching the aquifer, and is driven by the partition of precipitation (meteoric water, including snow) into potential evaporation, transpiration, run-off, run-on, and net recharge. In an arid or semi-arid climate such as at the Hanford Site, the net downward recharge flux that results from the partition of these fluxes is episodic and usually infrequent. However, this effect is typically damped towards a nearly constant rate with increasing depth as soil moisture variability with depth measured at Hanford Site lysimeters shows (PNNL-17841, *Compendium of Data for the Hanford Site (Fiscal Years 2004 to 2008) Applicable to Estimation of Recharge Rates*). This is the basis for representing recharge in the vadose zone model using a constant rate applicable to a given soil type and vegetation cover (DOE/RL-2011-50, *Regulatory Basis and Implementation of a Graded Approach to Evaluation of Groundwater Protection*).

Direct measurement of recharge at the water table is typically impractical due to inaccessibility, especially for many areas of the Hanford Site where the water table is commonly located at depths below ground surface (bgs) of 80 m or more. Other aquifer-influencing operations, such as artificial discharges (from anthropogenic discharges such as those associated with past waste management operations at the Hanford Site) or perturbations to the aquifer system from remedial action pump and treat systems, where present, complicate efforts at making a direct measurement of natural recharge for a deep water table. Instead, measurements and analyses in the unsaturated zone at shallow depths are used to characterize deep drainage. Deep drainage here is defined here as the water flux leaving the depth below which the processes of evapotranspiration can return water from the unsaturated soil to the atmosphere (PNNL-17841). This deep drainage, with sufficient time, will be manifest as the natural recharge flux. The time required for this to happen will depend on the thickness and hydraulic properties of the vadose zone and the deep drainage rate itself. Changes in the deep drainage rate, such as would result from changes in surface vegetative conditions that increase or decrease the evapotranspiration rate, can take many years to be reflected in the recharge rate for a thick vadose zone in arid conditions such as at the Hanford Site and can be an important consideration in characterizing recharge as well (PNNL-17841).

Important physical properties and processes that influence recharge include climate, soil hydraulic properties and stratigraphy, vegetative cover, land use, and topography (PNNL-17841). Climate determines the driving forces for recharge, namely the quantity of precipitation available for the land-surface water balance, and the energy fluxes that are determinant in the partitioning of precipitation into evaporation, transpiration, and recharge. Soil hydraulic properties and stratigraphy determine the rate at which water is transmitted through the vadose zone, and hence the effective time for processes of

evaporation and transpiration to influence the net downward flux. Vegetative cover determines the strength of the transpiration portion of the land-surface water balance. Land use will change the influencing factors including the vegetative cover and surface soils, and hence the hydraulic properties and soil stratigraphy of a site, and hence transpiration rates. Topography is the primary determinant for the portion of precipitation that is subject to overland flow, either "run-on" or "run-off," for a given site. Knowledge of all of the influences is important to the estimation of recharge at a given location.

Natural recharge from precipitation at the Hanford Site is highly variable both spatially and temporally, ranging from near-zero to more than 100 mm/yr depending on climate, vegetation, and soil texture ("Variations in Recharge at the Hanford Site" [Gee et al., 1992] and PNL-10285, *Estimated Recharge Rates at the Hanford Site*). Vegetative areas and fine-textured soil, like silt loams, tend to have lower recharge rates, while areas with little vegetation and coarse-textured soil, such as dune sands, tend to have higher recharge rates. PNL-10285 developed estimates of natural recharge for 1992 conditions using a systematic procedure. First, distributions of soil and vegetation types were mapped. Then, a recharge rate was assigned to each combination of soil/vegetation type based on data from lysimeters, tracer studies, neutron probe measurements, and computer modeling. The data used for these estimates derive from a number of sources, such as distribution of recharge estimated using the 1992 climate, a 1966 soil map (*Soil Survey Hanford Project in Benton County, Washington* [Hajek, 1966]), and 1979 vegetation/land-use patterns. Estimated recharge rates for 1992 ranged from 2.6 to 127 mm/yr, and the total volume of natural recharge from precipitation over the Hanford Site was estimated to be 2.35×10^4 m^3/d.

For numerical simulation, two general approaches are available with regard to addressing recharge. In the first, the surface energy and fluid balance can be explicitly simulated as part of the larger vadose model numerical implementation. In this approach, meteorological data (precipitation, wind speed, humidity, solar radiation, air temperature), surface soil parameters, and vegetation parameters (root density and depth with time, leaf area index with time, growth cycle dates, etc.) would be used to directly simulate the surface water balance and thereby estimate net deep recharge. Under this approach, the processes simulated for the upper boundary would dominate time step control of the simulation, particularly as this approach would require high-temporal-resolution meteorological data (e.g., hourly) to support a reasonably accurate simulation of the processes in question. A second approach is to segregate the simulation of the surface balance processes to arrive at a net recharge rate used for deeper vadose zone simulations. In this approach the full process-based simulation described for the surface soil is still performed, but only for the near surface. This has been done, and the effective net recharge rates are available in references such as PNNL-14702, *Vadose Zone Hydrogeology Data Package for Hanford Assessments*, for application to deeper vadose zone simulations. The second approach is clearly more efficient and is preferred. It is noted that the recharge rates from the second approach are strongly a function of vegetation cover and surface soil type, and that due to land-surface condition changes in time, these rates will change over time. A typical progression might be from a pre-operational natural vegetation cover (low recharge due to vegetation efficiently returning a high proportion of meteoric water to the atmosphere through transpiration) to an operational cover (such as gravel maintained vegetation-free with high recharge) to a transitional period following remediation with declining recharge rates, and finally a return to a mature native plant community with low recharge once again. Thus, the historic and projected land cover condition is the determining factor for selecting recharge rates to apply with time.

There has been considerable study devoted to estimation of recharge rates at the Hanford Site to support flow and transport modeling needs. PNL-10285 produced a defensible map of estimated recharge rates across the Hanford Site for current climate and 1991 vegetation/and use patterns. Various recharge data packages have been prepared to support performance assessments (e.g., PNNL-13033, *Recharge Data*

Package for the Immobilized Low-Activity Waste 2001 Performance Assessment, PNNL-14744, *Recharge Data Package for the 2005 Integrated Disposal Facility Performance Assessment*; PNNL-16688, *Recharge Data Package for Hanford Single-Shell Tank Waste Management Areas*) and site-wide assessments (e.g., PNNL-14702). These studies, in turn, have been supported by a significant field research program (e.g., PNL-6403, *Recharge at the Hanford Site: Status Report*; PNL-6810, *The Field Lysimeter Test Facility (FLTF) at the Hanford Site: Installation and Initial Tests*; PNL-7209, *Field Lysimeter Test Facility: Second Year (FY 1989) Test Results*; Gee et al. [2005], "Measurement and Prediction of Deep Drainage from Bare Sediments at a Semiarid Site"; Gee et al. [2007], "Hanford Site Vadose Zone Studies: An Overview"; PNNL-17841).

The 100 Area specific recharge rates reported in PNNL-14702 vary with surface soil type, providing an estimate of the range of possible recharge rates for various land uses. The three surface soil types were the Ephrata sandy loam or stony loam, Burbank sandy loam and Rupert sand. Additionally, PNNL-14702 also provides recharge rates for disturbed soil conditions: the disturbed soil rates were selected for use in calculation of soil screening levels (SSLs) and preliminary remediation goals (PRGs) for the 100 Area source operable units using vadose zone models.

For the groundwater model of the 100-BC area that is the subject of this report, an important improvement in this model is the treatment of the natural recharge for this model as spatially-and temporally-variable, using recharge rates that vary by surface soil type and vegetation cover type, and that are fully consistent with the rates used for vadose zone models used to derive SSL and PRG values. Rates of net recharge from precipitation were acquired from DOE/RL-2011-50, which summarized net natural recharge rates compiled in PNNL-14702. These are the same sources of recharge rates used for vadose zone modeling. An example of temporal variability, already applied in vadose zone models, is the natural vegetation recharge scenario illustrated in Figure 2-8 using values tabulated in Table 2-2. Note the higher recharge rates during the operation period, when a waste site was cleared and maintained in gravel-covered, vegetation-free state. In contrast, revegetation following remedial activities vastly reduces the recharge rates expected in the future as the surface condition changes within the expectations of this scenario. The purpose of such a recharge scenario is to define the upper boundary condition for a vadose zone model of a waste site in terms of a recharge rate that changes in time as a function of the surface soil and vegetation present during the history and expected future condition of that site.

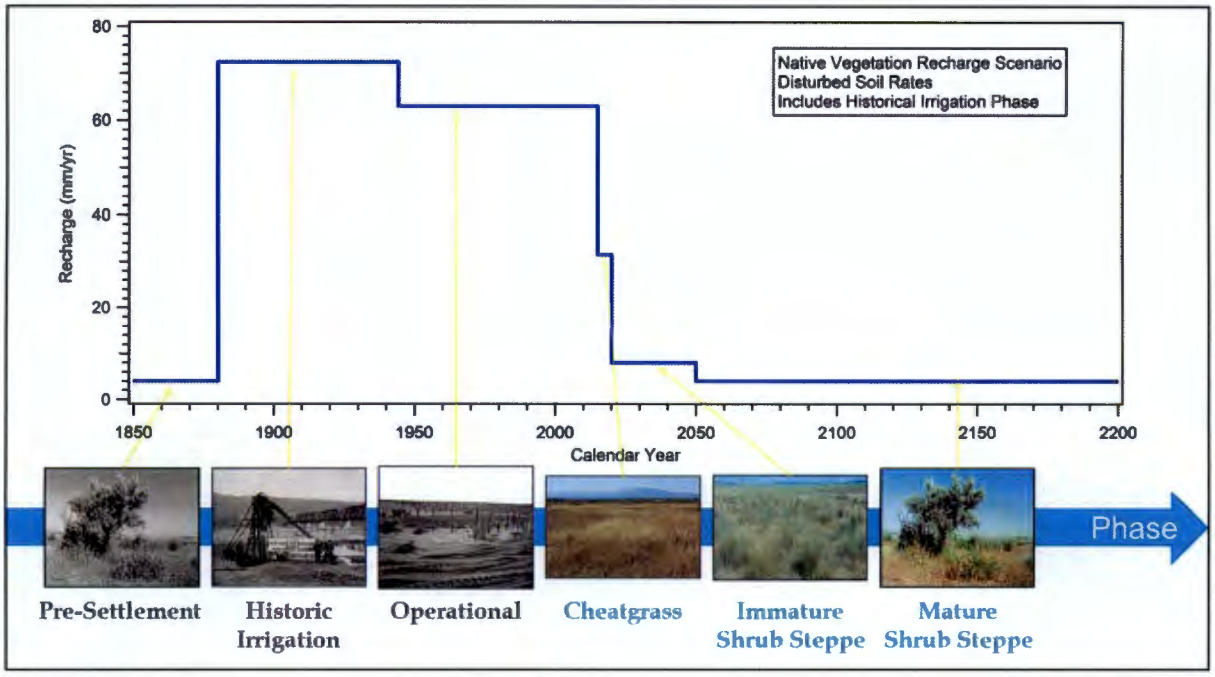

Figure 2-8 Natural Vegetation Recharge Scenario applied for Preliminary Remediation Goal Calculation in 100-Area Waste Sites subject to Historic Irrigation

Table 2-2. Native Vegetation Recharge Scenario Phases and Recharge Rates (mm/yr)

	Historic Simulation (pre-2010) (calculation of initial hydraulic conditions)			Predictive Simulation (post-2010) (calculation of peak groundwater concentration)			
Surface Soil Type	Pre-Settlement (< 1880)	Historic Irrigation [a] (1880-1944)	Hanford Operations (1944-2010)	Bare Soil (2010-2015)	Cheatgrass (2015-2020)	Developing Shrub-Steppe (2020-2050)	Mature Shrub-Steppe (2050 >)
Hanford sand, disturbed	4.0[b]	72.4[c]	63.0[d]	63.0[d]	31.5[e]	8.0[f]	[g]

a. Irrigated agriculture was prevalent in some 100-Area sites prior to Hanford Site construction; irrigation therefore was conservatively assumed applicable throughout any operational units with historic irrigation, applied from calendar years 1880 through 1944.

b. Source: PNNL-14702 Rev. 1, Table 4-15, all areas with soils disturbed by excavations; shrub steppe.

c. Recharge rates for historic irrigation phase is that from the long-term irrigation rate (Irrigation II) under the irrigation recharge scenario.

d. Source: PNNL-14702 Rev. 1, Table 4-15, all areas with soils disturbed by excavations; no vegetation.

e. Source: PNNL-14702 Rev. 1, Table 4-15, all areas with soils disturbed by excavations; cheatgrass.

f. Source: PNNL-14702 Rev. 1, Table 4-15, all areas with soils disturbed by excavations; young shrub steppe.

g. Source: PNNL-14702 Rev. 1, Table 4-15, all areas with soils disturbed by excavations; shrub steppe.

Applying the recharge scenario concept to a groundwater model, it is acknowledged that spatial variability needs to be included in the representation of this process. Figure 2-9 shows aerial imagery that illustrates the variability in surface conditions present in calendar year 2011; some portions of the model domain are highly disturbed and vegetation free, associated with higher recharge rates, while other portions show undisturbed natural vegetation cover that will have commensurately lower recharge rates.

The extent of the groundwater model incorporates a variety of surface soil types and vegetation types that evolve over different portions of the model domain in different ways. This makes the management of this boundary condition, varying in both time and space, a process that can best be addressed using a geographic information system (GIS) approach. The GIS representation of natural recharge with spatial and temporal variability is conceptualized as shown in Figure 2-10. In this concept, waste sites follow the same temporally-variable recharge scenario developed for vadose zone models used to calculate PRGs and reflect disturbed soil conditions. Other land areas outside of the waste sites follow different evolutions; some may remain in pre-Hanford mature shrub-steppe with native surface soil types throughout the historic and project future periods. Other areas may currently be covered in the invasive cheatgrass species and will remain this way.

Using aerial imagery, National Land Cover Database (NLCD 2011), BRMP Vegetation Class (2011), and other spatial data sources, a GIS approach is implemented to provide spatially-variable recharge rate maps that are a function of surface soil type and vegetation cover present throughout the 100-BC groundwater model domain at selected time periods. Use of multiple time-period maps to represent the natural recharge process in this groundwater model provides temporal variability, reflecting changing conditions during the simulation time.

The described approach to specify spatially and temporally variable representation of the natural recharge process as a boundary condition of the groundwater model provides the following advantages:

- Full consistency of natural recharge rates for waste sites as simulated in vadose zone models for PRG development to the recharge rates applied to the spatial extent of those waste sites within the larger groundwater model
- Increased model fidelity by prescribing higher recharge rates in waste site areas of the groundwater (maintained vegetation free with disturbed soil) and lower recharge rates in other areas, ensures that the higher driving force of increased recharge focused over contaminant plume source areas is represented in the model (in contrast to approaches that apply a using spatially-averaged natural recharge rate across the model domain)
- Increased model fidelity by prescribing recharge rates that vary in time, ensuring that the impact of reducing recharge through re-vegetation activities is factored into groundwater model (in contrast to applying a temporally-constant recharge rate that assumes present conditions persist in the future)

2.2.3 FEP: Columbia River Interaction

The flow of the Columbia River at 100-BC is to the east and is controlled mainly by Priest Rapids Dam. The flow rate at Priest Rapids from 1992 through 2011 averaged approximately 3,240 m^3/sec (114,500 ft^3/sec). Flow volumes are highest from April through early July because of runoff from regional and high elevation snowmelt. Flows are lowest from September through October. The width of the Columbia River through the Hanford Reach at 100-BC can vary from approximately 300 to 1,000 m (1,000 to 3,300 ft), depending on the flow rate. The elevation of the river also changes with the flow rate, resulting in wetting and drying of the shoreline area (NEPA Characterization Report [PNNL-6415]).

Source: NAIP 4 Band Imagery (7/15/2011); image courtesy of University of Washington.

Figure 2-9. Aerial Imagery of 100-BC Model Domain Showing Spatial Variability of Surface Conditions that are Reflected in Natural Recharge Rates that Depend on Surface Soil Type and Vegetation Density

High river stage can be greater than 123 m (404 ft) AMSL and generally occurs in May or June. Low river stage, approximately 118.5 m (389 ft), typically occurs in September or October. Diurnal fluctuations in 100-BC river stage range up to 1.5 m (5 ft). Seasonal fluctuations average 4.0 m (13 ft) over a year, and have ranged up to 5.6 m (18 ft).

Contaminant flow paths from 100-BC to the Columbia River are related to the locations of geologic units both on shore and within the Columbia River. **The evaluation of the near-river well geology indicates that the top of the aquitard (RUM) lies more than 15 m (49 ft) beneath the bottom of the Columbia River - the RUM does not intersect the bottom of the Columbia River at 100-BC**. Therefore, the river partially penetrates the unconfined aquifer system.

Groundwater discharges to the Columbia River via seeps and upwelling to the riverbed. This groundwater flow provides a pathway for contaminant transport to the Columbia River. Rapid, periodic, or cyclic elevation fluctuations of the river occur in controlled response to flood conditions, hydroelectric production, and salmon spawning programs at a series of dams and reservoirs upriver of the site. These rapid elevation changes in the river cause periodic influences on flow conditions within the aquifer. Daily fluctuations of more than 2 m (6 ft) are common. Even greater changes (more than 4.5 m [15 ft]) are observed seasonally, with a period of high river stage in the spring or early summer and low river stage in the fall. Periods of high or low river flow affect the unconfined aquifer flow the most.

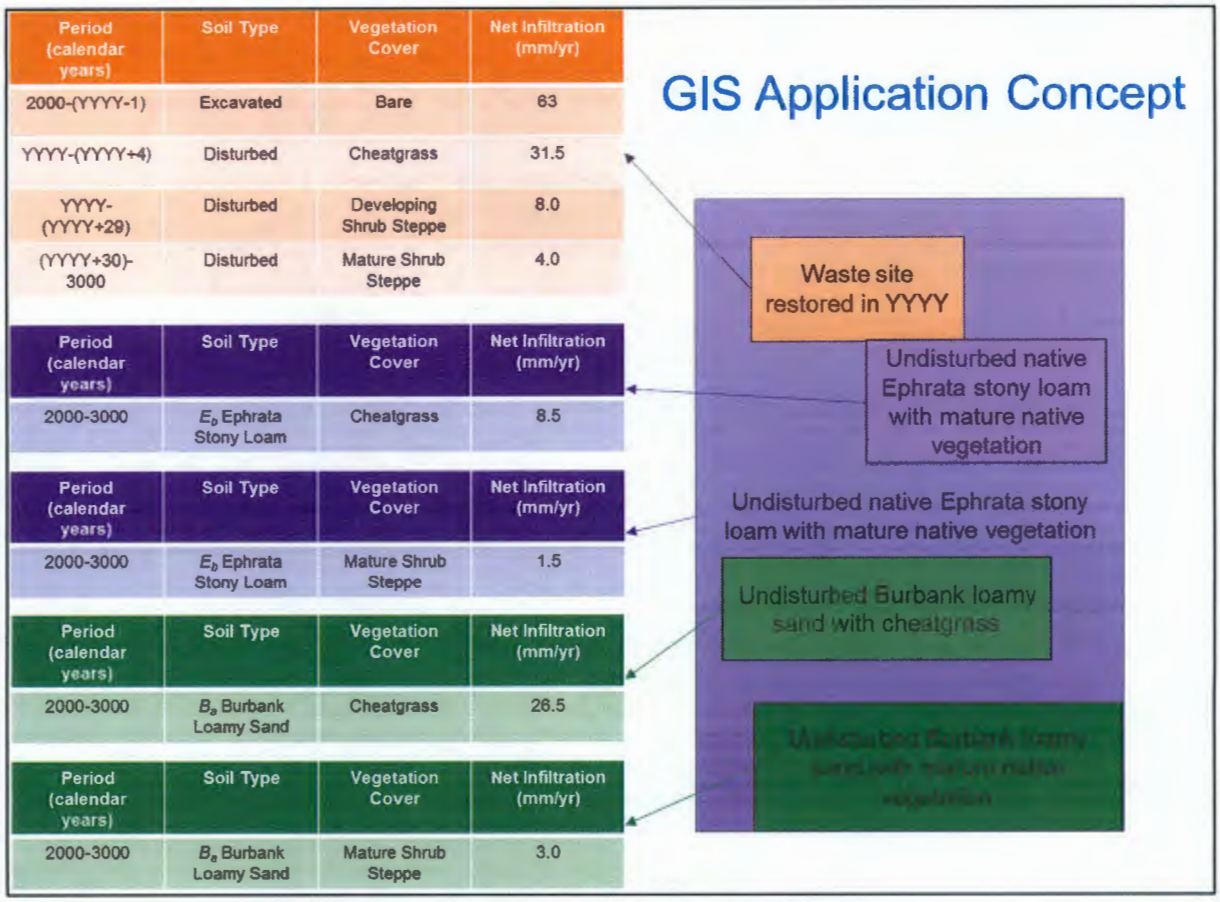

Figure 2-10. Conceptualization of Spatially and Temporally Variable Natural Recharge Rate Boundary Condition

The nature and extent of groundwater contaminants entering the Columbia River is of great interest, especially with regard to how it may affect water quality and aquatic plants and animals. Groundwater seeps (small water streams flowing across shoreline areas during low river stage periods) have been identified and studied in the 100 Areas (*Sampling and Analysis of 100 Area Springs* [DOE/RL-92-12]) and 300 Area. Pore water or groundwater upwelling (groundwater entering into the space between rocks and sediment of the riverbed) have also been studied in the 100 and 300 Areas. These upwelling areas have been identified using specific conductivity and/or water temperature data (riverbed locations with higher conductivities and/or warmer temperatures than the Columbia River water column are indicative of groundwater entering the bottom of the river), then subsequently characterized to determine contaminant concentrations in surface water, sediment, and pore water at those locations. Specific conductance of groundwater in 100-BC ranges from 300 to 550 µS/cm, while that of river water averages 150 µS/cm. Figure 2-11 shows electrical conductivity and temperature of pore-water samples collected from the riverbed near 100-BC (WCH-380). Groundwater upwelling from both sides of the river can be seen.

The nearshore groundwater conditions are directly affected by river stage. A wide range of mixing ratios has been observed between upwelling water at the bottom of the river and groundwater at nearshore locations (*Technical Evaluation of the Interaction of Groundwater with the Columbia River at the Department of Energy Hanford Site, 100-D Area* [SGW-39305]). This mixing ratio represents a continuum from pure groundwater to pure river water, depending on where in the groundwater pathway the measurement is taken. Water from the zone of interaction is a mixture of groundwater and river water.

Geologic control on the connection between river and aquifer can occur from the presence of altered river-bed properties. For instance, PNNL-17708 identified a preferential aquifer-river connection from Hanford/Ringold contacts in the 300 Area.

2.2.4 FEP: Groundwater Flow

The water-table depth at 100-BC ranges from approximately 12 m (40 ft) beneath the northern bluff near the Columbia River, to approximately 30 m (100 ft) at the southern margins. Water table elevation is approximately 120 to 122 m (395 to 401 ft) AMSL, as illustrated in Figure 2-12. Groundwater flows perpendicular to the water-table contours (that is, toward the Columbia River). In some locations, groundwater discharges to the river through riverbank seeps (springs). Most discharge occurs as upwelling through the riverbed. West of 100-BC, the river stage is approximately equal to the water table elevation, and groundwater flow is often from the river into the aquifer. Elsewhere, average flow is from the aquifer into the river.

In addition to water movement in and out of the riverbank (i.e., one dimensional flow perpendicular to the shoreline), there is a component of flow in the downstream direction (Newcomb and Brown, 1961). Because the river flows downstream in response to an elevation gradient, groundwater and bank storage also tend to travel downstream, although at a considerably slower rate than the river flow. Finally, vertical components of flow are induced by the river that does not fully penetrate the aquifer.
As discussed in Section 2.1 the Hanford/Ringold contact rises to the north toward the river resulting in a progressive loss of Hanford transmissivity until it is above the water table. Conservation of mass requires that the volume of water carried by the Hanford must be transmitted through the lower-hydraulic conductivity Ringold to the river. This effect can be seen in Figure 2-12 in the increased hydraulic gradient in about the last 600 m of the unconfined aquifer where only the Ringold is present. **This implies that the Ringold acts as the controlling factor for contaminated groundwater discharge to the river.**

Groundwater flows into 100-BC from the west and south, in the gaps between Umtanum Ridge, Gable Butte, and Gable Mountain. **Under current flow conditions, more groundwater appears to be flowing in from the west and southwest than from the southeast.** Wells west of 100-BC have slightly higher water level elevations than do 100-BC wells. West of 100-BC, the river stage is approximately equal to the water table elevation, and groundwater flow is often from the river into the aquifer. Elsewhere, average flow is from the aquifer into the river.

A water-level network with transducers has been in place in selected wells since 2010. Wells 199-B8-6, B4-1, and B5-8 were monitored during excavation of 100-C-7:1, and the data analyzed by PNNL. Figure 2-13 shows the head data and computed flow direction for the period analyzed by PNNL-21845.
The major seasonal effects of the Columbia River are shown in the water-level rise in spring 2011 and 2012. Groundwater flow direction varies on the order of 50^0 during these changes. Figure 2-14 illustrates the direction and magnitude of the hydraulic gradient from PNNL-21845. The gradient magnitude is highest during summer, when the river stage is lowest. Figure 2-15 shows the computed groundwater velocity from estimated hydraulic gradient, hydraulic conductivity, and effective porosity. These values are similar in range to the velocities estimated from two tracer tests of about 5 and 3 m/d.

Source: Field Summary Report for Remedial Investigation of Hanford Site Releases to the Columbia River, Hanford Site, Washington: Collection of Surface Water, Pore Water, and Sediment Samples for Characterization of Groundwater Upwelling (WCH-380)

Figure 2-11 Pore-water Samples from the Columbia River Bed

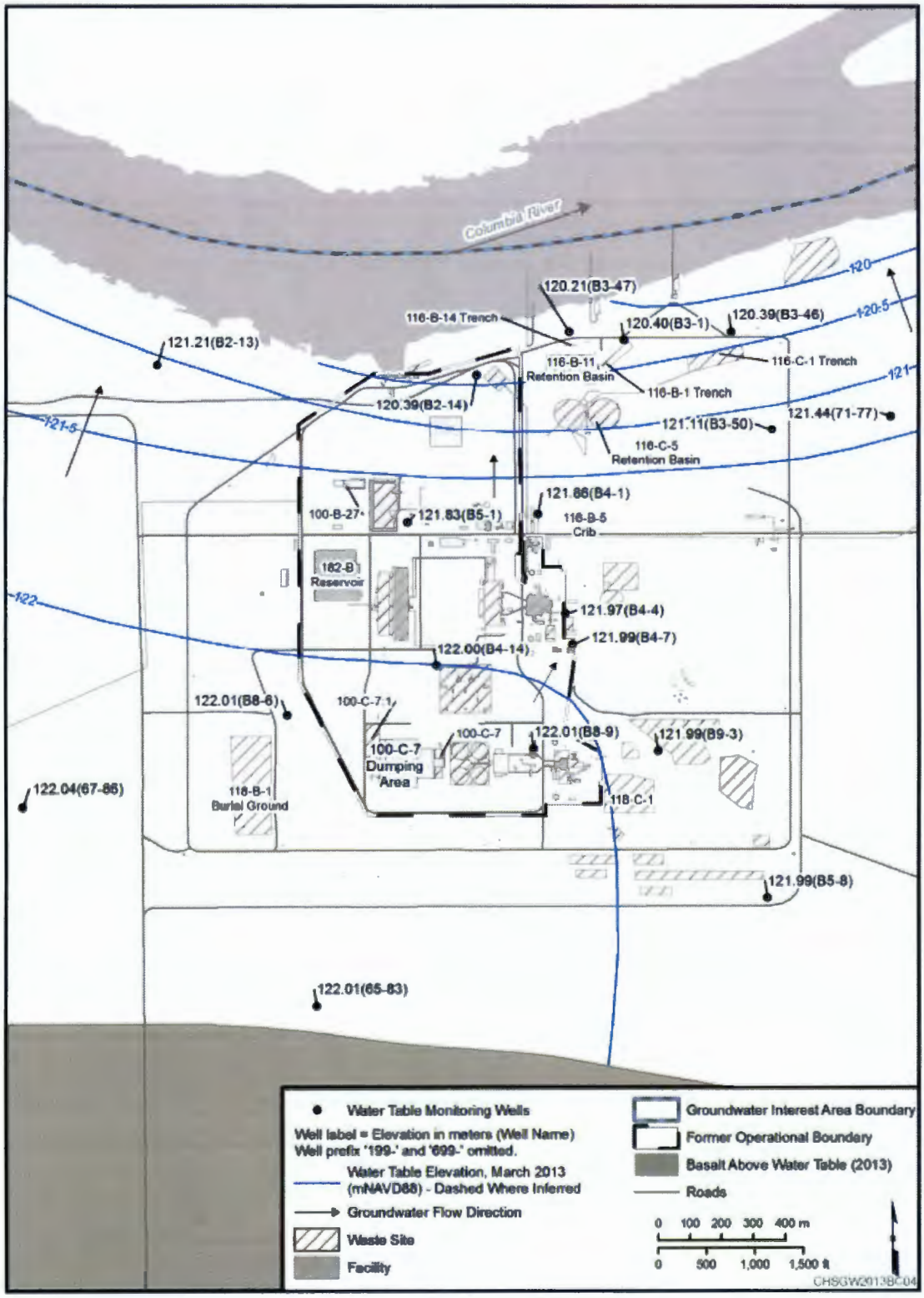

Figure 2-12 100-BC 2013 Water Table (DOE/RL-2014-32, Rev. 0)

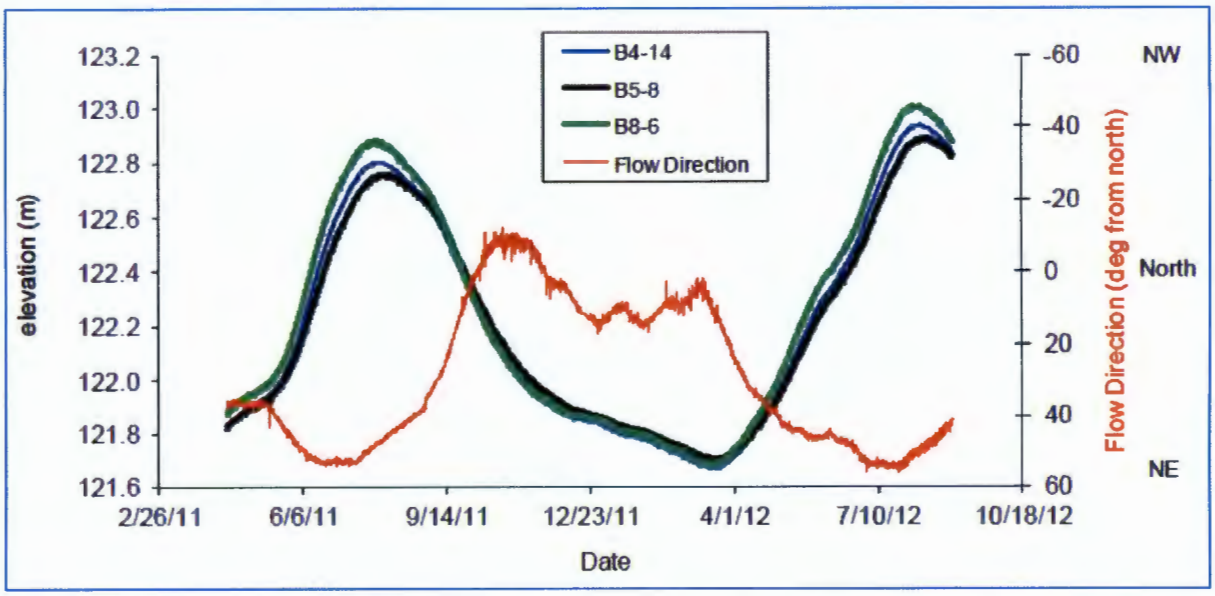

Figure 2-13. Hydraulic Head Data for Wells 199-B4-14, 199-B5-8, and 199-B8-6 along with Computed Flow Direction (PNNL-21845)

The effect of distance from the river is illustrated in Figure 2-16 with hydrographs (generated from the 2013 groundwater annual report webpage; http://www.hanford.gov/c.cfm/sgrp/GWRep13/start.htm) from wells 199-B3-47, 199-B2-14, 199-B4-14, and 199-B5-8 which are about 145, 220; 1,400; and 2,800 m from the Columbia River, respectively. The well closest to the river, 199-B3-47, has the highest water levels and largest fluctuation. The water-level fluctuation in the next distant well (199-B2-14) is not a large, but is qualitatively similar to 199-B3-47. Wells 199-B4-14 and 199-B5-8 show very smooth and lagged responses; 199-B5-8 slightly more so than 199-B4-14.

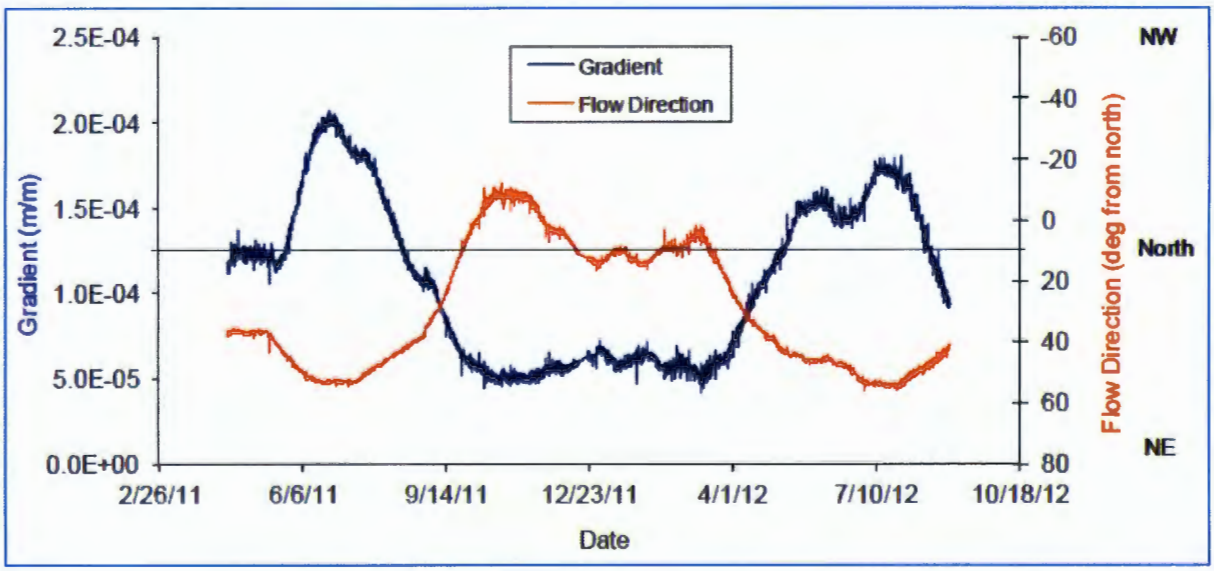

Figure 2-14 Groundwater Flow Direction (Azimuth) and Hydraulic Gradient Computed from Hydraulic Head Data from Wells 199-B8-6, B4-14, and 199-B5-8 (PNNL-21845)

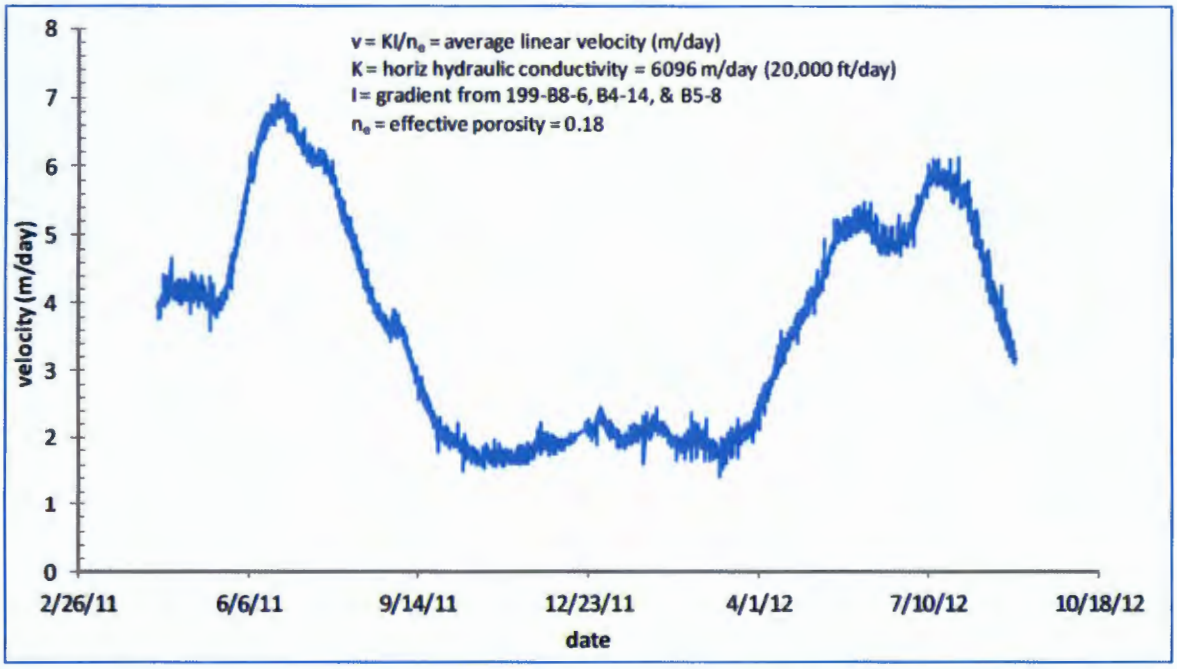

Figure 2-15. Estimated Groundwater Velocity in the Hanford Formation Near 100-C-7 and 100-C-7:1 Based on Calculated Hydraulic Gradients (PNNL-21845)

The water table on the north side of the Columbia River in Grant County is much higher than in 100-BC (150 to 300 m [490 to 980 ft] AMSL; *Hanford Site Groundwater Monitoring for Fiscal Year 2006* [PNNL-16346]; Figure 2-17). **Groundwater from Grant County north of the river and 100-BC south of the river discharges to the Columbia River.**

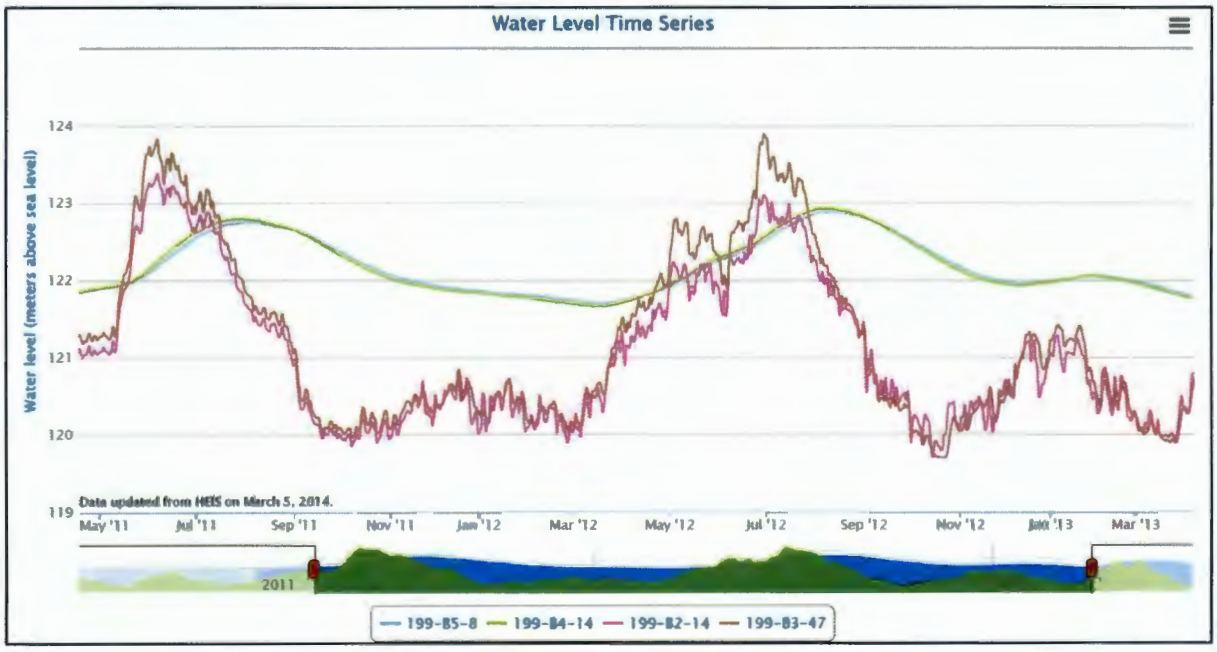

Figure 2-16. Selected AWLN Well Hydrographs

2.2.5 FEP: Potential Hexavalent Chromium Sources

Soil in 100-BC has been extensively remediated via RTD to varying depths. The largest and deepest excavation occurred at waste sites 100-C-7 and 100-C-7:1, which were excavated almost to the water table. Soil remediation goals were met, but some Cr(VI) soil contamination (ranging from 10 to 40 mg/kg) remained near the bottom of the excavation (PNNL-21845). Downgradient monitoring well 199-B4-14 showed a rise in Cr(VI) concentrations beginning in April 2012 likely from infiltrating dust control water when the excavation was close to the water table between November 2011 and February 2012. Concentrations have continued to decline since 2012, but it is not yet clear what, if any, impacts Cr(VI) residual may be having.

Relatively stable concentrations at some wells, especially in the shallow unconfined aquifer, are suggestive of continuing sources. One well that shows this pattern is 199-B3-47 as shown in Figure 2-18. Waste site 116-B-11 (retention basins) is up gradient along the flow path leading to the well, and pothole sampling after excavation revealed concentrations on the order of 2 mg/kg of residual Cr(VI) (CVP-99-00001, Rev.0). Other possible waste sites that could be contributing based on flow direction include the 116-C-5 retention basins and the 116-B-14 trench–any or all of these sites could be sources because all that is known is the concentration at 199-B3-47.

2.2.6 FEP: Potential Strontium-90 Sources

Strontium-90 concentration in some wells is steady or decaying slower than radioactive decay. This suggests potential residual sources. This FEP is further documented in ECF-100BC5-16-0051.

2.3 Nature and Extent of Contamination

Hexavalent chromium [Cr(VI)], strontium-90, and tritium have been identified as groundwater COPCs in the 100-BC-5 OU. **Generally, chromium concentrations are highest near the top of the unconfined aquifer and decline with depth.** Given that the Hanford formation forms the upper part of the unconfined aquifer over much of the site and carries the bulk of groundwater flow this suggest some residual source may be present. In recent years chromium concentrations in wells 199-B5-1 and 199-B8-6 have declined indicating clean groundwater moving into 100-BC-5 from the west and south. Figure 2-19 shows the fall 2013 chromium plume in the unconfined aquifer (Hanford and Ringold sediments).

However, at some locations there is chromium contamination deeper in the lower Ringold E as shown in Figure 2-20. This contamination is illustrated in cross section in Figure 2-21 and Figure 2-22. **Concentrations in the lower Ringold are changing slowly in wells 199-B5-5 and B5-6** (Figure 2-23) **because of the lower hydraulic conductivity (lower velocity)** not because there is a source nearby–the well is too deep.

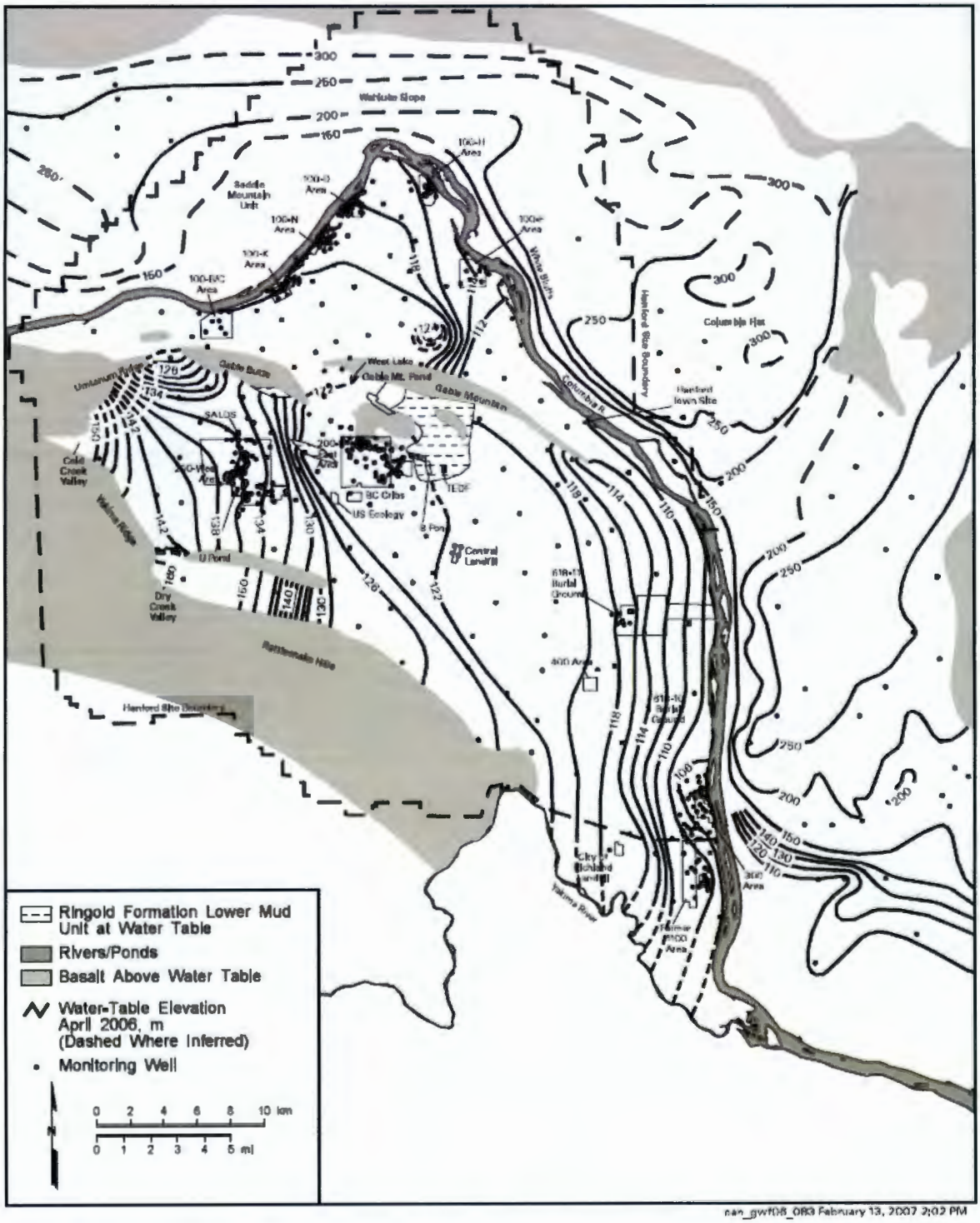

Figure 2-17. Hanford Site and Outlying Areas Water-Table Map, April/May 2006 (PNNL-16346)

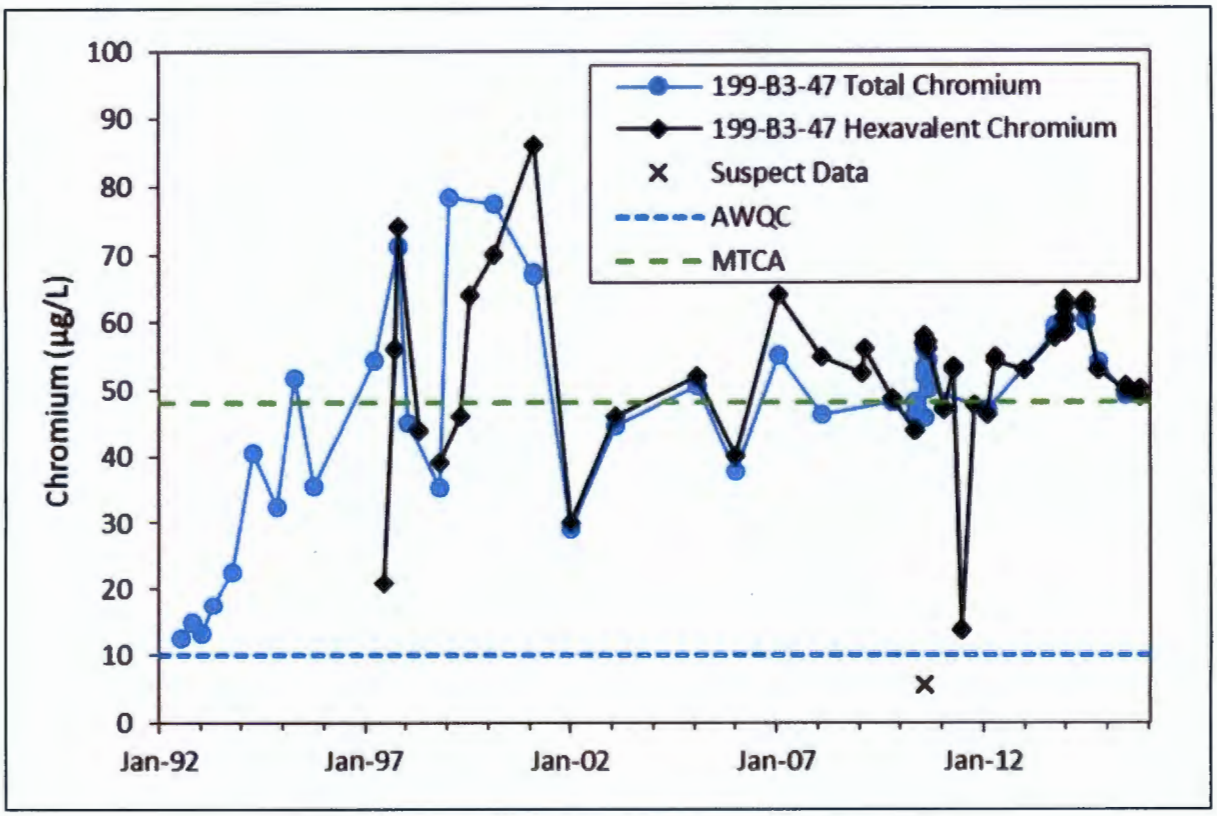

Figure 2-18. Well 199-B3-47 Cr(VI) Concentrations over Time

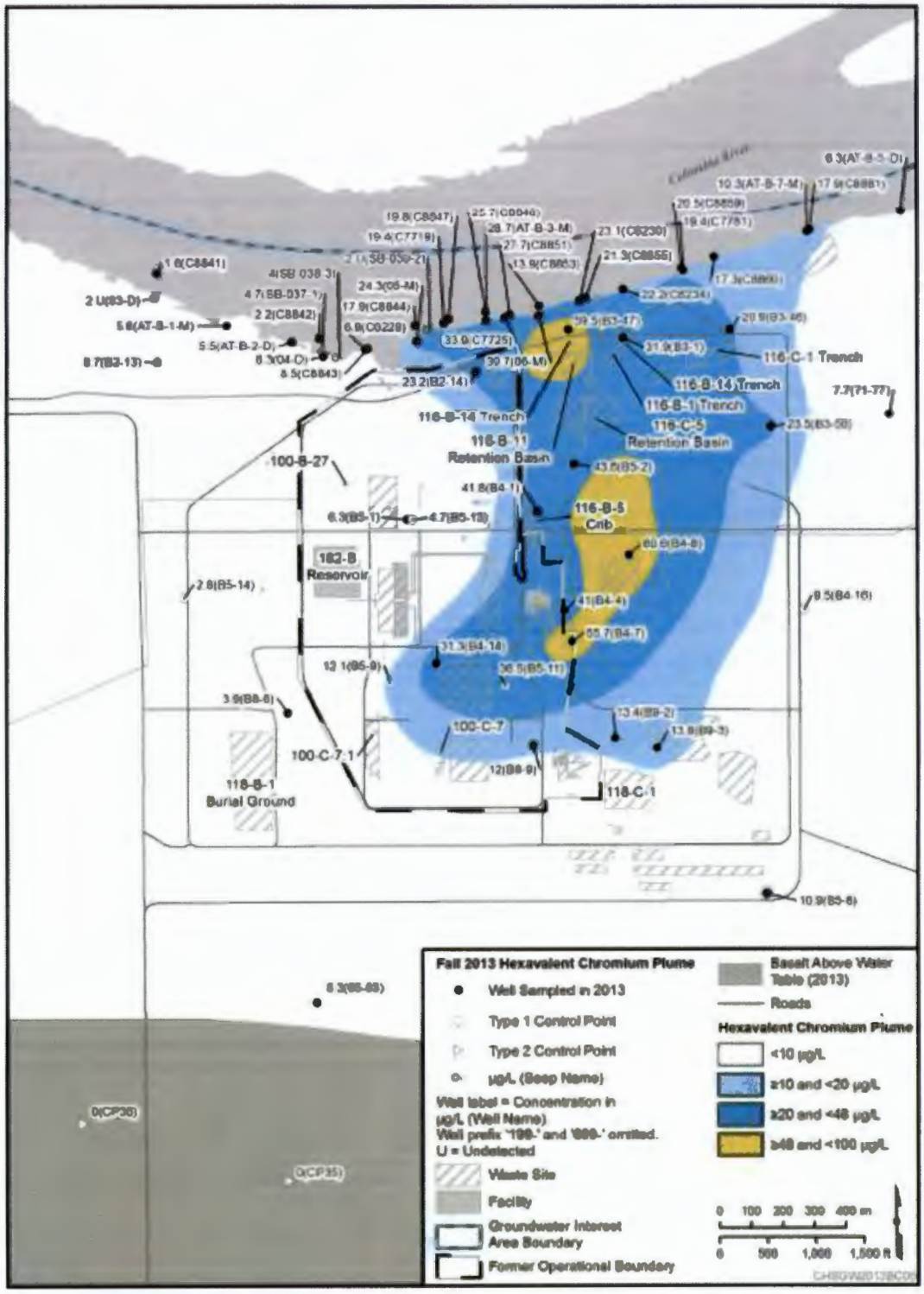

Figure 2-19. 100-BC 2013 Hexavalent Chromium Plume (DOE/RL-2014-32, Rev. 0)

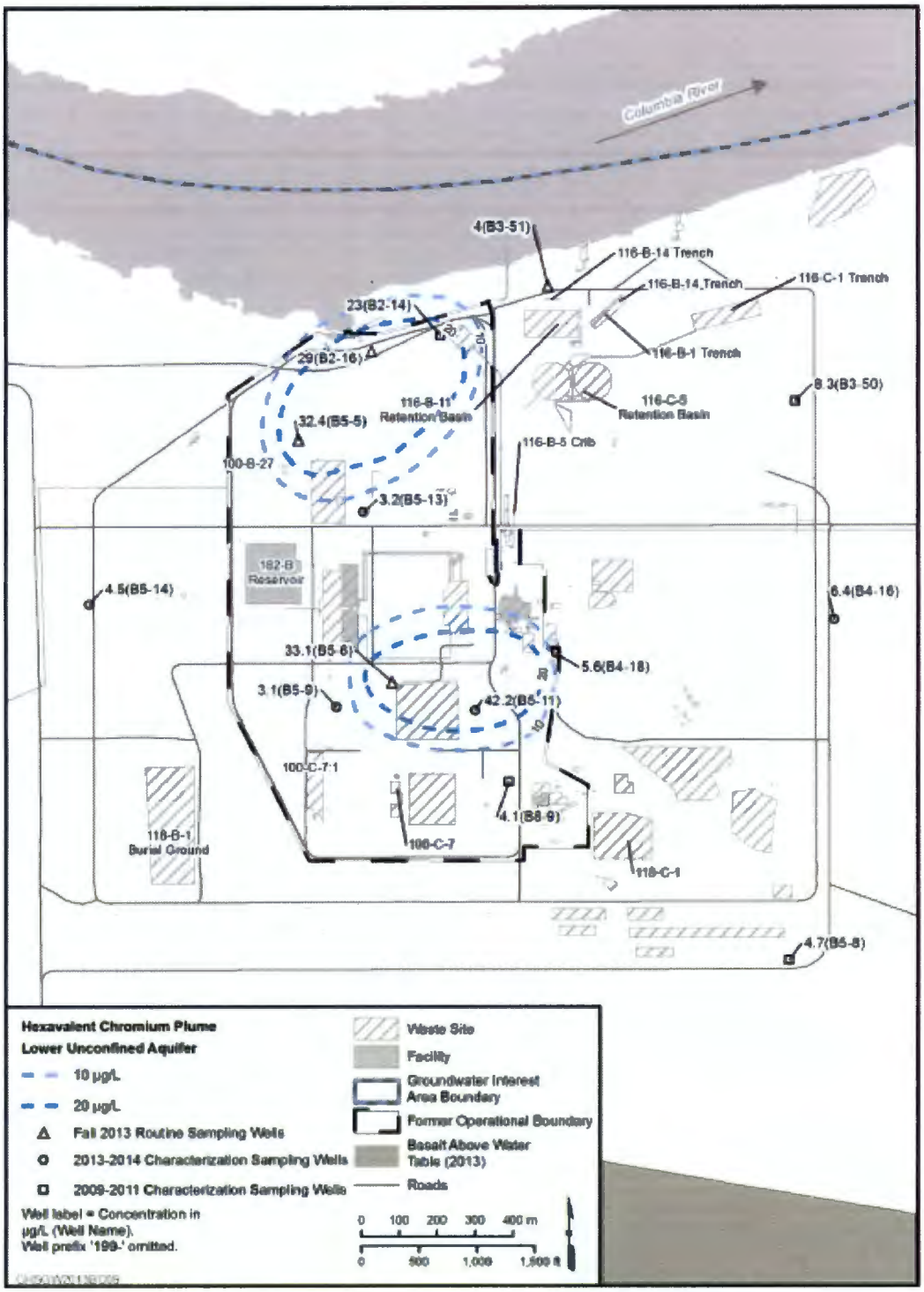

Figure 2-20. 100-BC Hexavalent Chromium in the Lower Part of the Unconfined Aquifer (Ringold) 2013 (DOE/RL-2014-32, Rev.0)

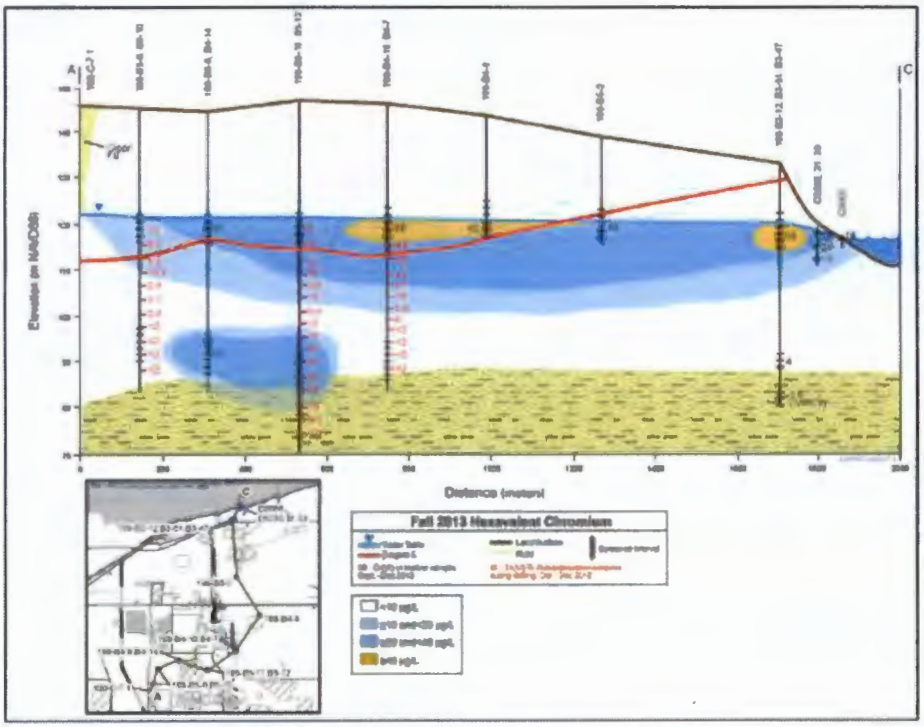

Figure 2-21. 100-BC Cross Section Showing Hexavalent Chromium Distribution, Southwest to Northeast 2013 (DOE/RL-2014-32, Rev.0)

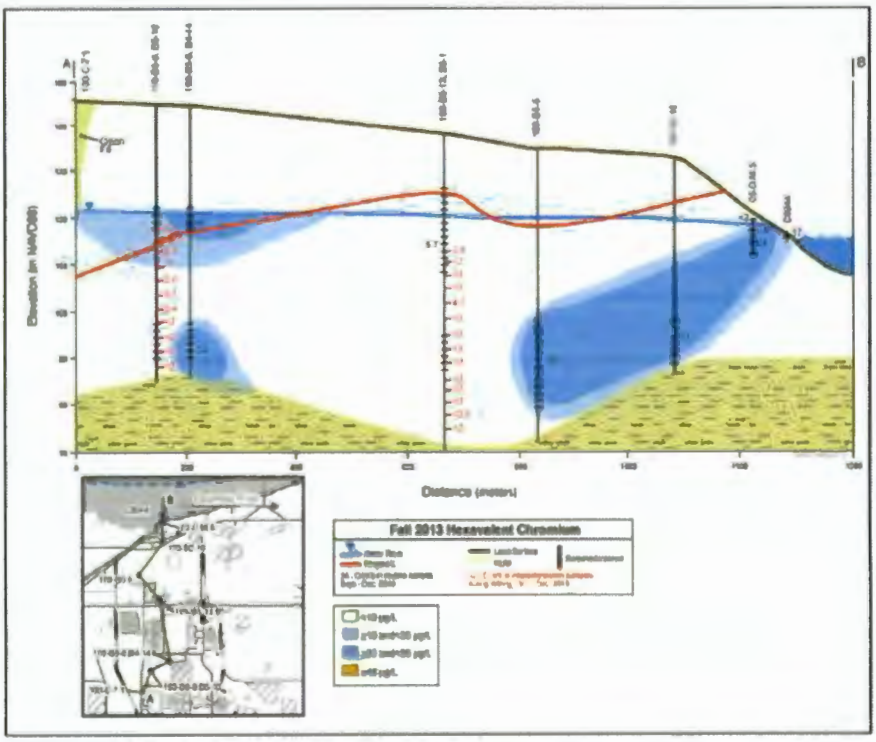

Figure 2-22. Western 100-BC Cross Section Showing Chromium Distribution 2013 (DOE/RL-2014-32, Rev.0)

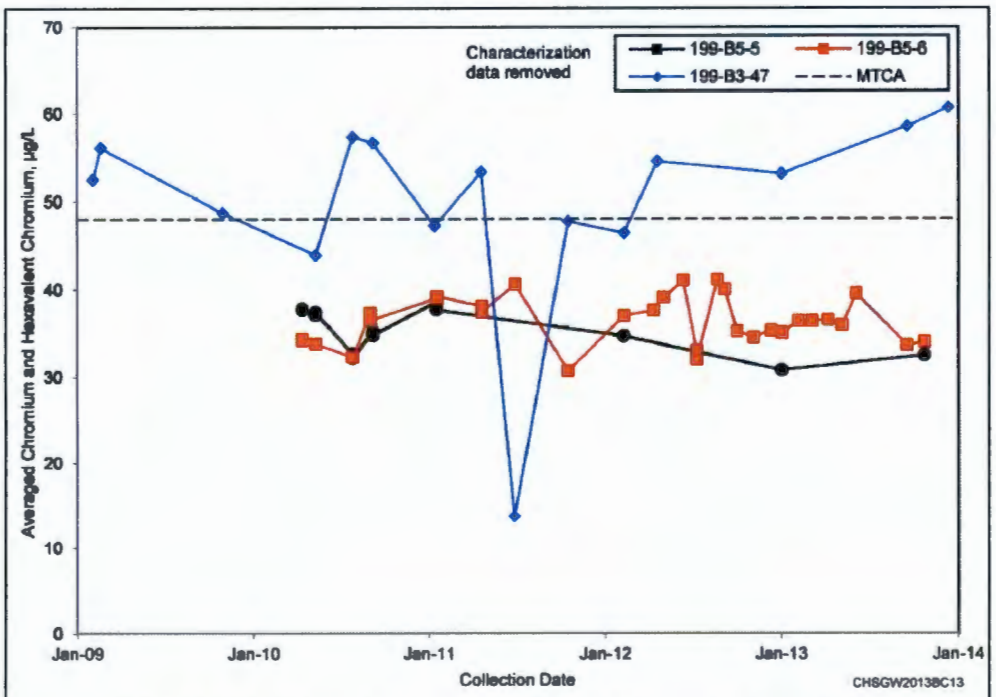

Figure BC.9 100-BC Hexavalent Chromium Data in Wells Screened in Ringold Unit E

Figure 2-23. 100-BC Wells Screened in Ringold E

Strontium-90 contamination is limited to the upper portion of the unconfined aquifer. Figure 2-24 shows the fall 2013 Sr-90 plume.

Tritium concentrations are highest near the top or middle of the unconfined aquifer, and lower at the bottom. As of 2013 no concentrations exceeded the drinking water standard (Figure 2-25).

2.4 Conceptual Model Summary

Key elements (FEPs and their components) include the following:

1. Contaminant migration in units below the RUM is very unlikely because the low hydraulic conductivity of the RUM makes it an effective aquitard where it underlies the overlying Ringold unit E throughout 100-BC.

2. The Hanford formation saturated thickness decreases towards the Columbia River as the Hanford/Ringold contact elevation rises, and the Hanford is unsaturated in the area where the chromium groundwater plume is interpreted to discharge to the river.

3. As Hanford saturated thickness decreases towards the river the transmissivity, assuming hydraulic conductivity is unchanged, of the Hanford declines and groundwater hydraulic gradient increase.

4. The Hanford formation in 100-BC is characterized by large to very large, cobble- to boulder-size clasts in open framework gravels. The formation includes discrete sand lenses with minor to no silt and clay material.

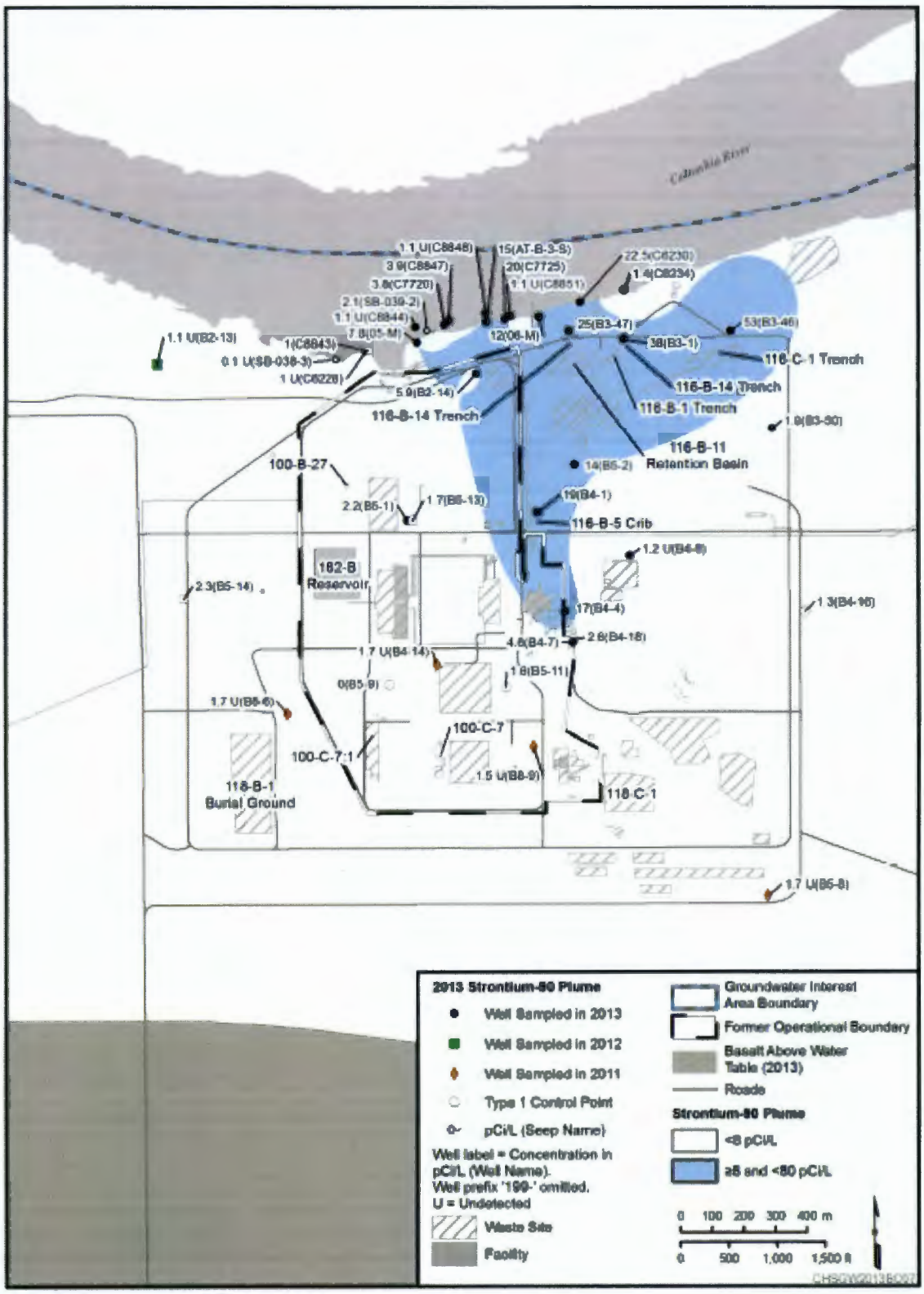

Figure 2-24 100-BC 2013 Strontium Plume (DOE/RL-2014-32)

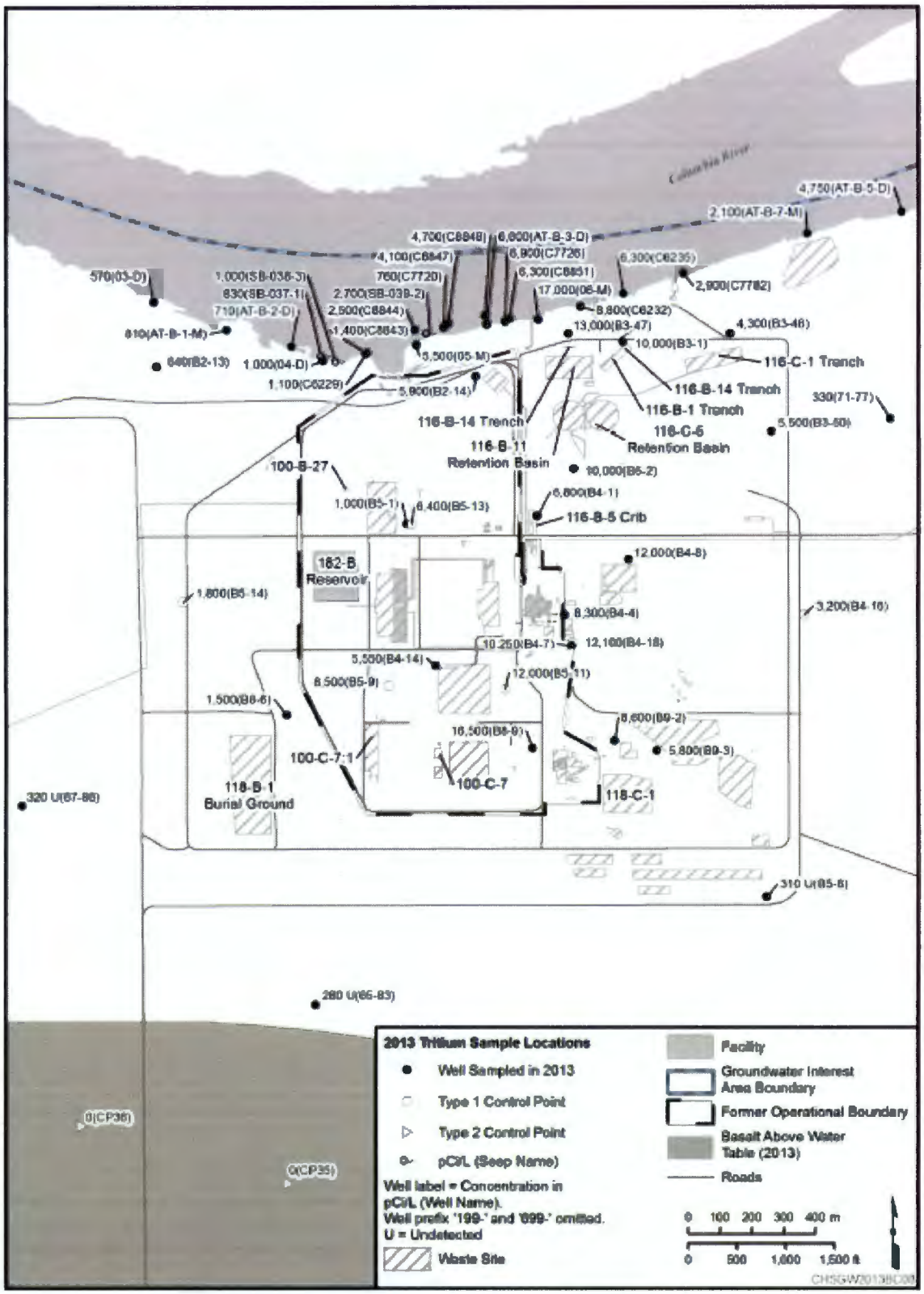

Figure 2-25 100-BC 2013 Tritium Plume (DOE/RL-2014-32)

5. Boulder gravel in the upper 6 to 15 m (20 to 50 ft) demonstrates the high-energy depositional environment created during the Missoula Floods. This is interpreted to be due to 100-BC's location proximal to the main paleo-flood pathway into the upper Pasco Basin from the northwest (SGW-44022). This channel is thought to exist between 100-BC and Gable Butte.
6. The Hanford formation/Ringold Formation contact can be difficult to identify at 100-BC. Therefore, the Hanford formation/Ringold Formation contact has not been determined in all boreholes. The contact is highest in wells near the river and dips to the south.
7. The Hanford formation has systematically higher hydraulic conductivity than the Ringold.
8. The flow of the Columbia River at 100-BC is to the east and is controlled mainly by Priest Rapids Dam.
9. The evaluation of the near-river well geology indicates that the top of the aquitard (RUM) lies more than 15 m (49 ft) beneath the bottom of the Columbia River-the RUM does not intersect the bottom of the Columbia River at 100-BC.
10. Groundwater discharges to the Columbia River via seeps and upwelling to the riverbed.
11. Because of the progressive loss of Hanford transmissivity as it rises above the water table the Ringold formation controls groundwater discharge to the river.
12. Under current flow conditions, more groundwater appears to be flowing in from the west and southwest than from the southeast.
13. Groundwater from Grant County north of the river and 100-BC south of the river discharges to the Columbia River implying that a groundwater divide exists under the Columbia River.
14. Chromium contamination is highest near the top of the unconfined aquifer and decline with depth.
15. Chromium concentrations are changing slowly in the lower Ringold E because of the Ringold's lower hydraulic conductivity and velocity.
16. Strontium-90 contamination is limited to the upper portion of the unconfined aquifer.
17. Tritium concentrations are highest near the top or middle of the unconfined aquifer and lower at the bottom.

This page intentionally left blank.

3 Model Implementation

3.1 Software

MODFLOW (Harbaugh et al., 2000) and MT3DMS (SERDP-99-1) were selected for implementation of the 100-BC Model because they fulfill the following specifications:

- Among the more versatile and widely used software packages for models of this type.
- Are freely available and distributed with the source code.
- It is fully documented and has been verified in applications similar to those at the Hanford Site.
- There is wide expertise in use of these software packages.
- Together, these software packages are capable of directly simulating the principal FEPs that are relevant to the 100-BC simulation requirements.
- For those FEPs that they do not directly simulate, the needs can be met through links to other codes, such as linking to Subsurface Transport Over Multiple Phases (STOMP) for vadose calculations as described in the FEP section on recharge.

Use of MODFLOW is in keeping with DOE direction for simulation of groundwater at the Hanford Site (Hanford Groundwater Modeling Integration [Klein, 2006]). DOE has not specified a groundwater transport simulator for use with MODFLOW; however, MT3DMS is the most commonly applied transport simulator used with MODFLOW. All software for implementation of this model was used in accordance with PRC-PRO-IRM-309, *Controlled Software Management*.

The software used to implement this model and perform calculations and was approved under the requirements of, and use was compliant with, PRC-PRO-IRM-309. This software is managed under the following software quality assurance documents consistent with PRC-PRO-IRM-309:

- CHPRC-00257, Rev. 1, MODFLOW and Related Codes Functional Requirements Document
- CHPRC-00258, Rev. 2, MODFLOW and Related Codes Software Management Plan
- CHPRC-00259, Rev. 1, MODFLOW and Related Codes Software Test Plan
- CHPRC-00260, Rev. 2, MODFLOW and Related Codes Acceptance Test Report
- CHPRC-00261, Rev. 2, MODFLOW and Related Codes Requirements Traceability Matrix

CHPRC-00259, Rev. 1, distinguishes between safety software and support software based on whether the software managed calculates reportable results or provides run support, visualization, or other similar functions.

The following describes the MODFLOW Controlled Calculation software.

- Software Title: MODFLOW-2000 (MODFLOW-2000, the U.S. Geological Survey Modular Ground-water Model - User Guide to Modularization Concepts and the Ground-Water Flow [Open File Report 00-92])—solves transient groundwater flow equations using the finite difference discretization technique.
- Software Version: MODFLOW-2000-SSPA Version 1.19.01 modified by S.S. Papadopalous and Associates for minimum saturated thickness and to use the ORTHOMIN Solver—approved as

CHPRC Build 0008 using executable mf2k-mst-chprc08dpv.exe (compiled to default double precision for real variables).

- Software Version: Standard MODFLOW-2000 Version 1.19.01 approved as build 7 using executables mf2k-chprc07dpl.exe and mf2k-chprc07spl.exe for single and double precision real variables, respectively.
- Hanford Information System Inventory (HISI) Identification Number: 2517 (Safety Software S3 graded Level C).

The following describes the MT3DMS Controlled Calculation Software:

- Software Title: MT3DMS (SERDP-99-1, MT3DMS: A Modular Three-Dimensional Multispecies Transport Model for Simulation of Advection, Dispersion, and Chemical Reactions of Contaminants in Groundwater Systems; Documentation and User's Guide)
- Software Version: MT3DMS-SSPA Version 5.30 approved as CHPRC Build 8 using executables mt3d-mst-chprc08dpv.exe compiled for double precision real variables.
- Software Version: Standard MT3DMS Version 5.30 approved as CHPRC Build 7 using executables mt3d-chprc07dpl.exe and mt3d-chprc07spl.exe for single and double precision real variables, respectively.
- Hanford Information System Inventory (HISI) Identification Number: 2518 (Safety Software graded Level C).

Support software is used that has been identified in CHPRC-00258, Rev. 1, or is scheduled by the software owner to be included as support software in the next revision to that document. Software with a trademark designation is commercial software. Software listed without a trademark has been developed internally.

- **Groundwater Vistas™:** (*Guide to Using Groundwater Vistas* [Rumbaugh and Rumbaugh, 2007].) Translated well pumping data from spreadsheet HistroricWells.csv to WEL file. It also provided graphical tools used for model quality assurance.
- **ArcGIS™:** (*The ESRI Guide to GIS Analysis, Volume 1: Geographic Patterns and Relationships* [Mitchell, 1999].) Provided visualization tool for assessing validity of interpolated HSU surfaces and HSU extents.
- **PEST™:** ([Doherty, 2007]) Used for automated calibration and run coordination.
- **LEAPFROG Hydro™:** (Version 1.2.0.62.) Used for translated the Hanford North GFM into a MODFLOW computational grid.

Safety Software (MODFLOW and MT3DMS) is checked out in accordance with procedures specified in CHPRC-00258, Rev. 2. Executable files are obtained from the CHPRC software owner who maintains the configuration-managed copies in MKS Integrity™, installation tests identified in CHPRC-00259, Rev. 1, are performed and successful installation confirmed, and software installation and checkout forms are required and must be approved for installations used to perform model runs.
Approved users are registered in HISI for safety software.

Use of the software previously identified must be consistent with intended use for CHPRC as identified in CHPRC-00257, Rev. 1, and be a valid use of this software for the problem addressed in this application. The software must be used within its limitations as identified in CHPRC-00257, Rev. 1.

3.2 Discretization

3.2.1 Temporal Discretization

B-river gauge has data starting from January, 2004 through July, 2014. Generally, Columbia River stage is relatively steady from October to March and fluctuates from April to September. AWLN wells used for calibration show a time delay from river stage changes from between about 10 to 40 days, and started collecting data in 2011, with all the wells available from 2012 on. Manual water-level data collected during sampling is also available at a much lower frequency. Additionally, simulation of the no further action scenario for 125 years requires a different time discretization for efficiency. These factors dictated multiple temporal discretizations.

The 100-BC groundwater flow model was implemented four different ways for distinct purposes as follows:

1. **Calibration** to river induced changes to establish aquifer hydraulic properties emphasizing the most recent and extensive data. This period was from January 2012 through July 2014 with stress periods ranging from 5 to 30 days. Particular care was taken to increase temporal discretization during periods of rapid river stage change to accurately capture the transient effects that provide information on hydraulic properties. Thus, a 5-day stress period length was used for April to September (i.e., rising limb to the peak river stage and falling limb from the peak river stage) of each year to capture this response, and a 30-day stress period length was used for October to March of each year. Figure 3-1 shows the comparison between daily river stage and average river stage based on stress period length at B-River gauge for January, 2012 to July, 2014.

2. **Evaluation** of hydraulic conditions from 2006 through July 2014. This version was built on the first in order to test the overall consistency with a longer, but not as comprehensive dataset. A 30-day/31-day stress period length was used for years between 2006 and 2011, with 2012 through 2014 stress period unchanged from the calibration model. No parameter adjustments were made on the basis of this model. Figure 3-2 shows the comparison between daily river stage and average river stage based on stress period length at B-River gauge for January, 2006 to July, 2014.

3. **Calibration** of interpreted chromium plume migration from 2004 through 2015. With the much higher estimated groundwater velocity plume migration in the upper unconfined aquifer it was possible to approximately generate the interpreted 2011 conditions and subsequent migration of high concentrations from dust control water applied at 100-C-7:1 from 2012 through 2015. This model used the same temporal configuration as the evaluation version.

4. Long-term **forecast** of solute concentrations. Based on a detailed flow budget analysis of aquifer discharge to the river longer stress periods could be used for solute transport analysis. A 30-day/31-day stress period length was used for 50 years beginning January 2015. For the last 75 years March 2013 was selected as an average condition and applied for 75 one-year stress periods. Figure 3-3 shows the comparison between daily river stage and average river stage based on stress period length at B-River gauge for the 10-year predictive model.

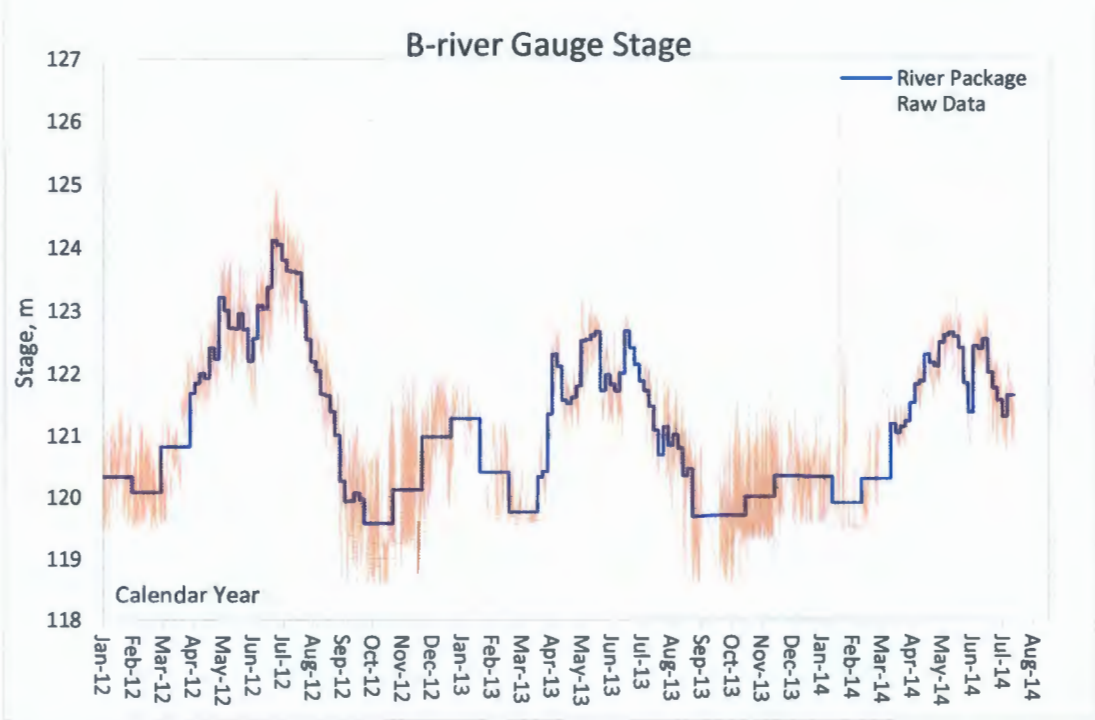

Figure 3-1. Comparison Between Daily River Stage and Average River Stage Based on Stress Period Length at B-River Gauge for January, 2012 to July, 2014

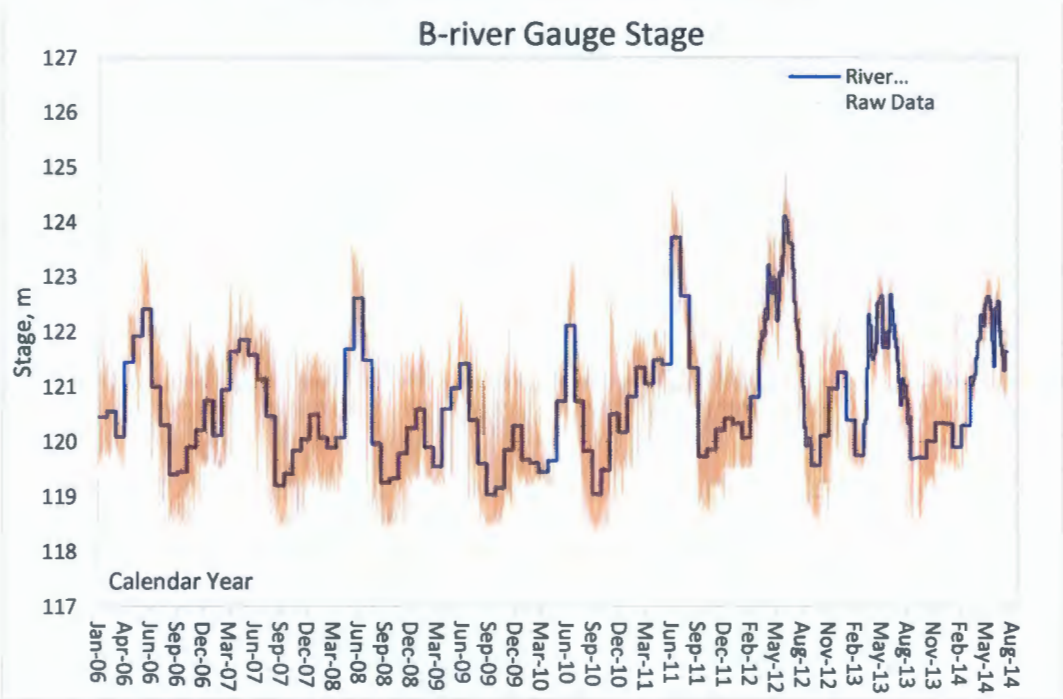

Figure 3-2. Comparison Between Daily River Stage and Average River Stage Based on Stress Period Length at B-River Gauge for January, 2006 to July, 2014

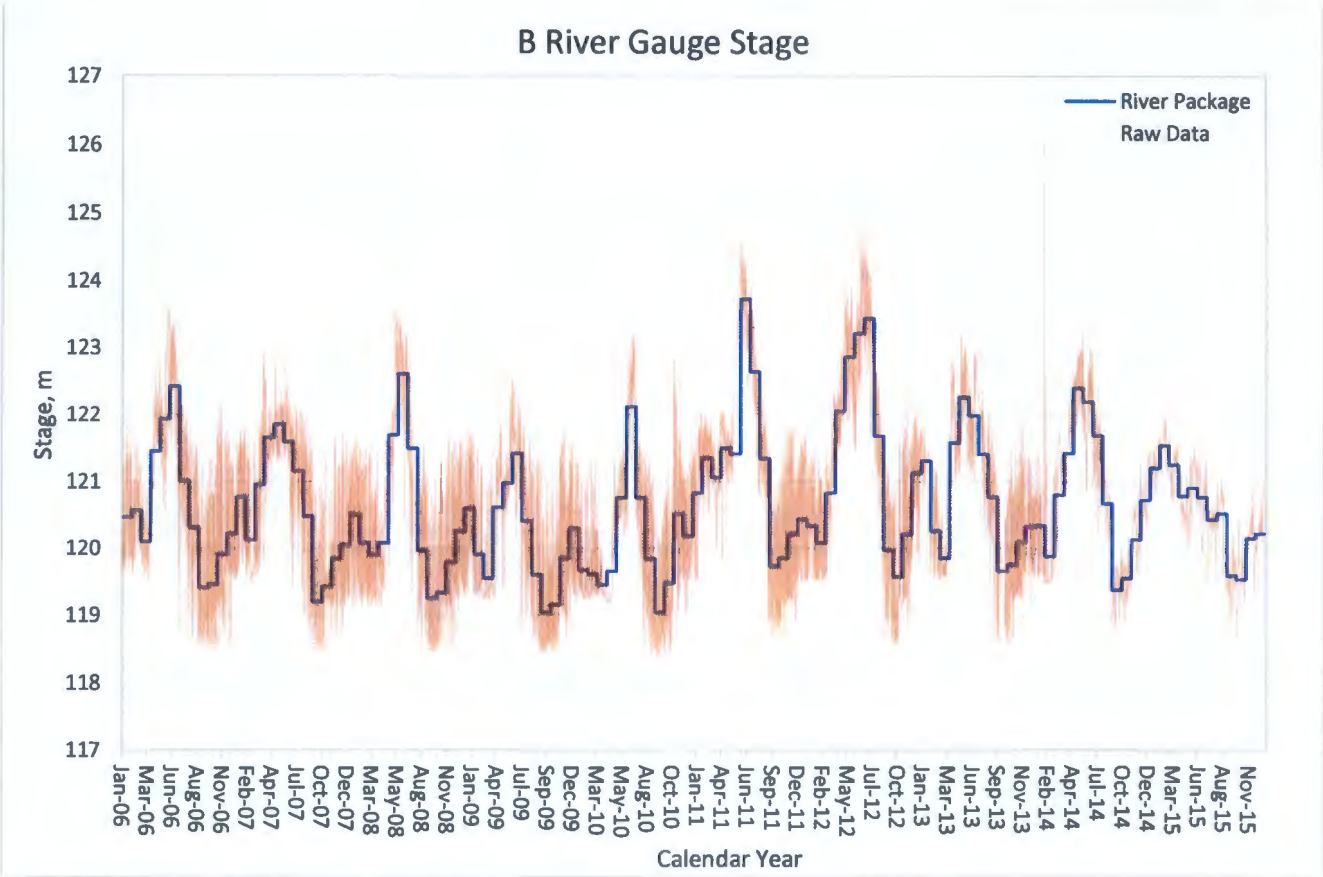

Figure 3-3. Comparison between Daily River Stage and Average River Stage Based on Stress Period Length at B-River Gauge for the Predictive Model

3.2.2 Spatial Discretization

Spatial discretization is the same for all models. The finest grid spacing of 5 m was used where chromium and strontium plumes are currently interpreted to exist. The largest row and column spacing was 50 m. A total of 799,296 cells are in the model, of which 775,020 are active. The model origin is at 562,800 m easting and 143,400 m northing in Washington South NAD83 HARN.

The 100-BC GWFTM extends to the Columbia River on the north side of the model, basalt above water table (no flow boundary) to the south, and uses a general head boundary on the east and west sides of the model. Land surface is the top of the model and the bottom of Ringold formation Unit E comprises the lower model boundary. The 100-BC GFM is restricted to approximately center of the width of the Columbia River by a polyline lateral extent so that Leapfrog Hydro's MODFLOW building tool assigns no flow for the cells beyond the center line of the river. Features of the 100-BC GWFTM are shown in Figure 3-4.

Columbia River bathymetry (PNNL-19878) comprises the upper boundary surface of the broader 100-Area GFM along the Hanford Reach within the model domain. This also applies to the 100-BC model since it lies completely within the domain of the 100-Area GFM. To create the original 100-Area GFM upper boundary surface, high-resolution land surface LiDAR (Aero-Metric LiDAR) was mosaicked with the river bathymetry using GIS (ECF-Hanford-13-0020).

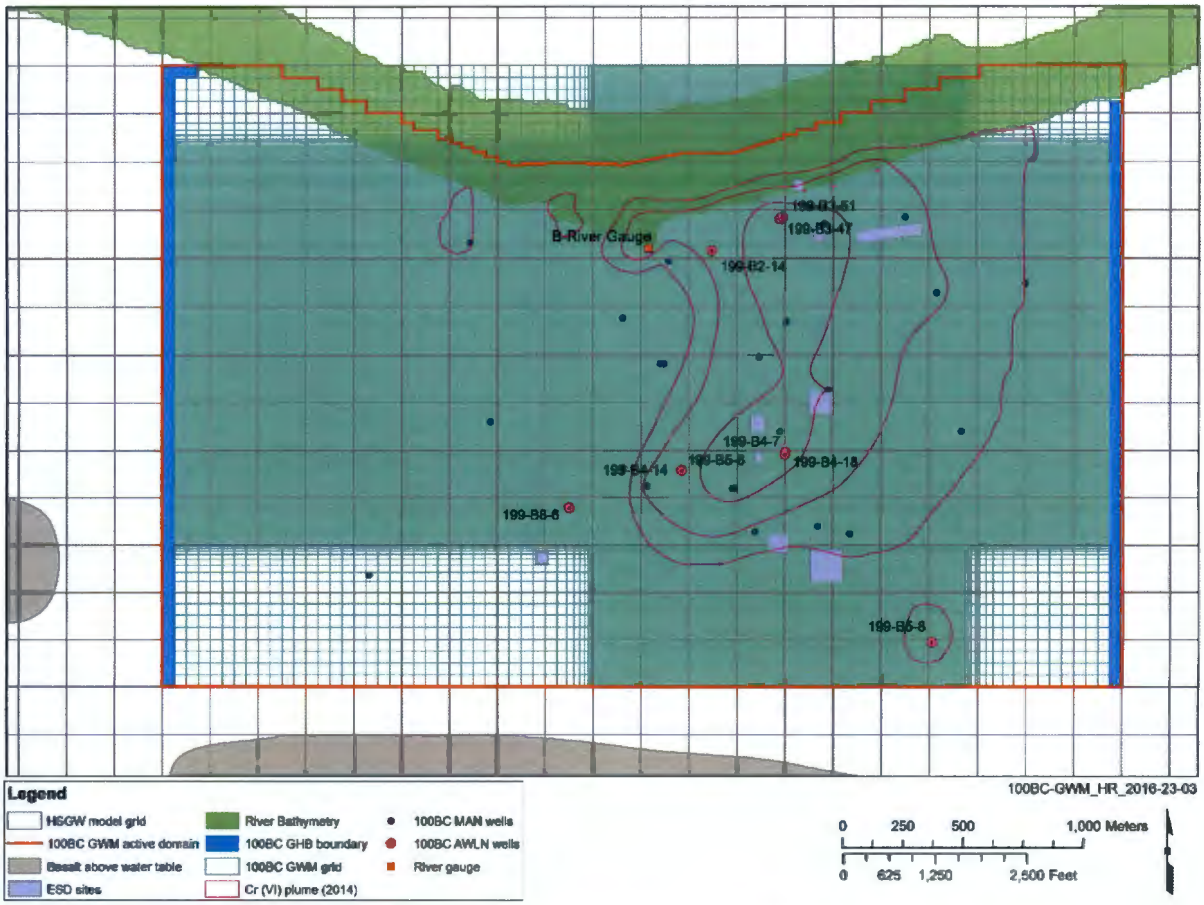

Figure 3-4. 100-BC Groundwater Flow and Transport Model Plan View Grid

The model boundary was selected to contain two key natural boundaries (e.g., river, no-flow), well locations with extensive data, and plume extents for CrVI and Sr-90 within the 100-BC operable unit. The 100-Area and 100-BC GFMs use top of basalt as their lower boundary surfaces and are comprised (from land surface down) of the Hanford formation (HF), Ringold E (Rwie) and Ringold Upper Mud (RUM) hydro-stratigraphic units. Since the RUM is assumed to be a no flow boundary, only Hf and Rwie are utilized in the 100-BC GWFTM.

The MODFLOW model building tool in Leapfrog Hydro requires model origin (lower left corner), number of layers within a hydro-stratigraphic unit, model grid spacing and minimum layer thickness as initial input. The tool then creates a MODFLOW grid and assigns a hydro- stratigraphic unit to each cell based on the radial basis function interpolation technique. It was required to discretize the model grid as finely as possible so that all the flow and transport properties can be well-represented by the model cells. However, model cells need to be limited to lower a number of total model cells to avoid longer runtimes and other numerical issues. 100-BC GWFTM was created with 362 rows, 368 columns, and 6 layers so that the model satisfies these criteria. Hanford unit is split into 2 layers and Rwie unit is split into 4 layers. The following procedures were performed to generate model grid and hydro-stratigraphic unit assignment at each cell of 100-BC GWFTM:

a. 100-Area GFM was re-generated with water table and Columbia River bathymetry as the upper boundary surface (i.e., topography in Leapfrog Hydro). The resultant contact surfaces are slightly

different than the original 100-Area GFM due to different upper boundary surfaces (i.e., land surface vs water table)

b. The model layer thicknesses are dictated by the overall thickness of the 100-Area GFM which serves as the environment for the 100-BC GWFTM. For example, Leapfrog Hydro was only able to generate MODFLOW model grid when a minimum layer thickness of 1.8 m was selected with 2 layers in Hanford formation and 4 layers in Ringold E formation. This is because a minimum saturated thickness of 10.8 m (which is the minimum thickness of the 100-Area GFM, 1.8 x 6 layers) is required. Since the combined thickness of Hanford and Ringold E formation is approximately 11 m in its thinnest area (i.e., the south-west side of the model), a minimum thickness more than 1.8 m would result in more than 11 m total thickness which is conceptually unrealistic.

c. The MODFLOW grid setup has at least 1.8 m thick saturated zone for all the model cells which is important in preventing wet-dry issues during MODFLOW model simulation. MODFLOW model files are created and exported.

d. 100-Area GFM is developed using pre-defined contact surfaces. Therefore, changing the upper boundary from land surface to water table resulted in different geologic units in few areas of Layer 1 compared to the original model. This was fixed by evaluating the previously created MODFLOW grid in the original 100-Area GFM. The updated MODFLOW files are saved and exported for use.

e. The model is then imported to Groundwater Vistas software and the top elevation of the model is changed to land surface outside Columbia River bathymetry. Now, the upper boundary of the model uses the land surface topography and Columbia River bathymetry which is identical to the upper boundary surface of the 100-Area GFM. This allows for the attributes of original 100-Area GFM to be represented in the MODFLOW model and for assignment of a reasonable saturated thickness for each layer

Figure 3-5 through Figure 3-7 show cross-sectional view of the 100-Area GFM along with 2013 Cr(VI) shallow and deep plumes, Columbia River, and MODFLOW model layering.

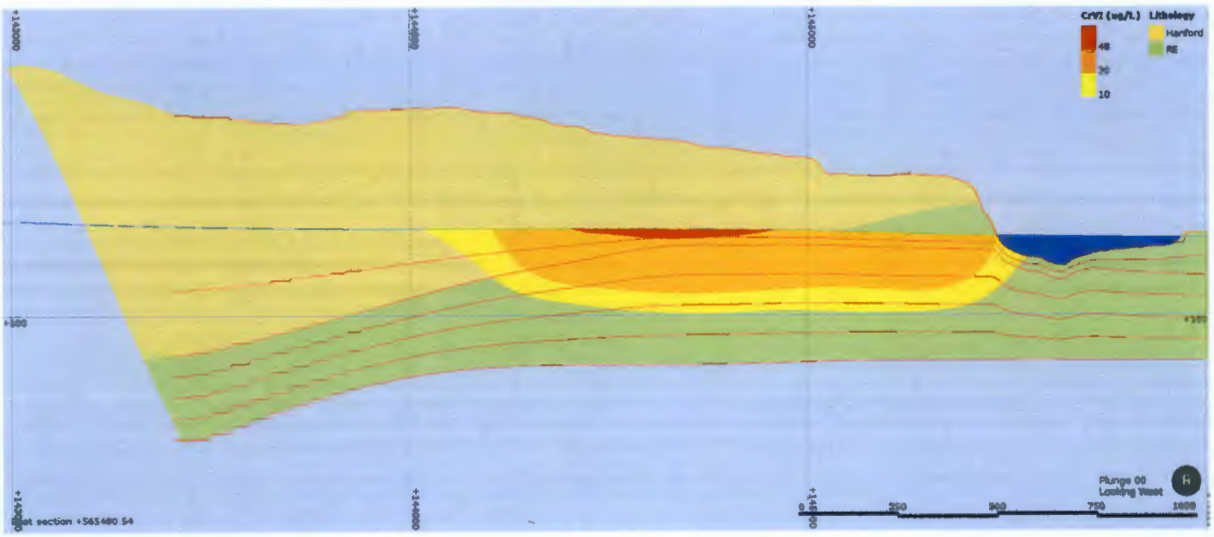

Figure 3-5. 100-Area GFM with Columbia River, MODFLOW Model Layers and 2013 Cr(VI) Plume at Easting = 565000.5 m

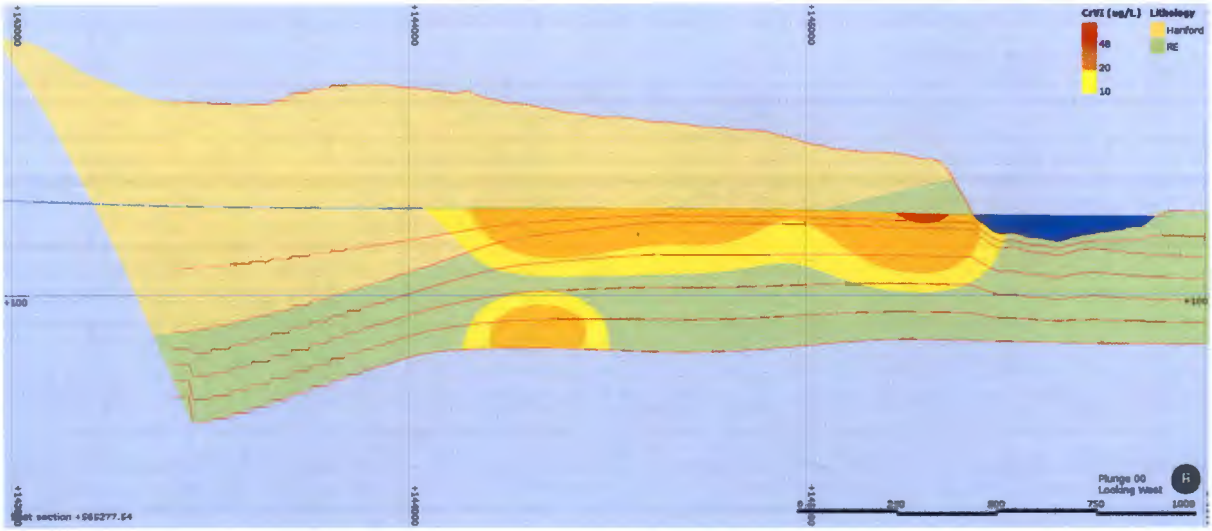

Figure 3-6. 100-Area GFM with Columbia River, MODFLOW Model Layers and 2013 Cr(VI) Plume at Easting = 565277.5 m

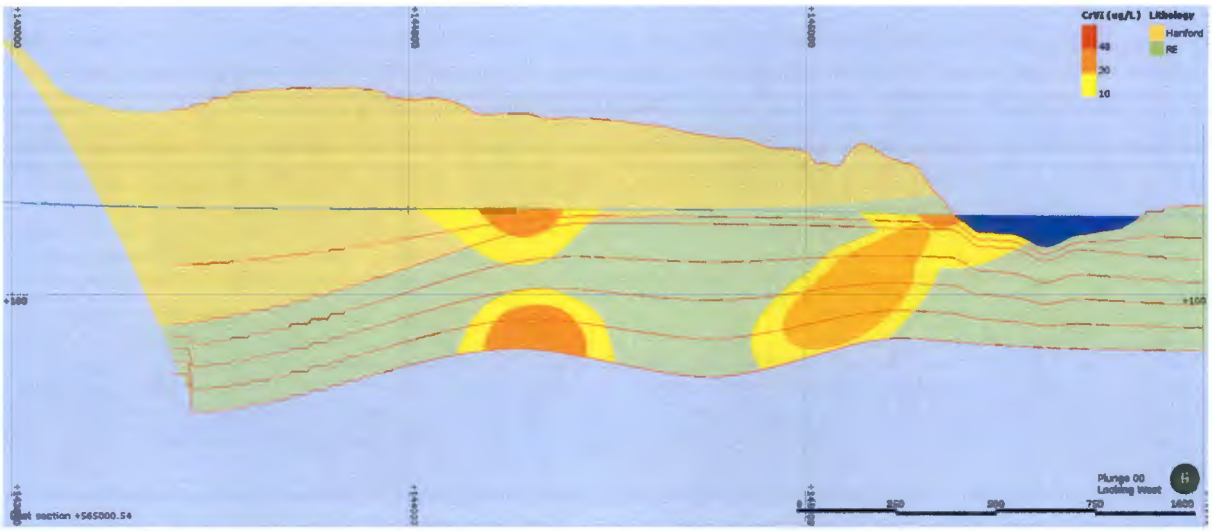

Figure 3-7. 100-Area GFM with Columbia River, MODFLOW Model Layers and 2013 Cr(VI) Plume at Easting = 565000.5 m

3.3 Parameterization

3.3.1 Recharge Boundary Condition

Recharge was computed as described in EMDT-BC-0007-r0 for 2011, 2021, and 2051. The 2011 shape file (Figure 3-8) was imported into Groundwater Vistas, and units adjusted from mm/yr to m/d using the matrix calculator. Recharge changes in 2021 and 2051.

Additionally, the footprint of the 182-B reservoir was assigned a recharge zone in MODFLOW, and was implemented as an adjustable parameter for calibration.

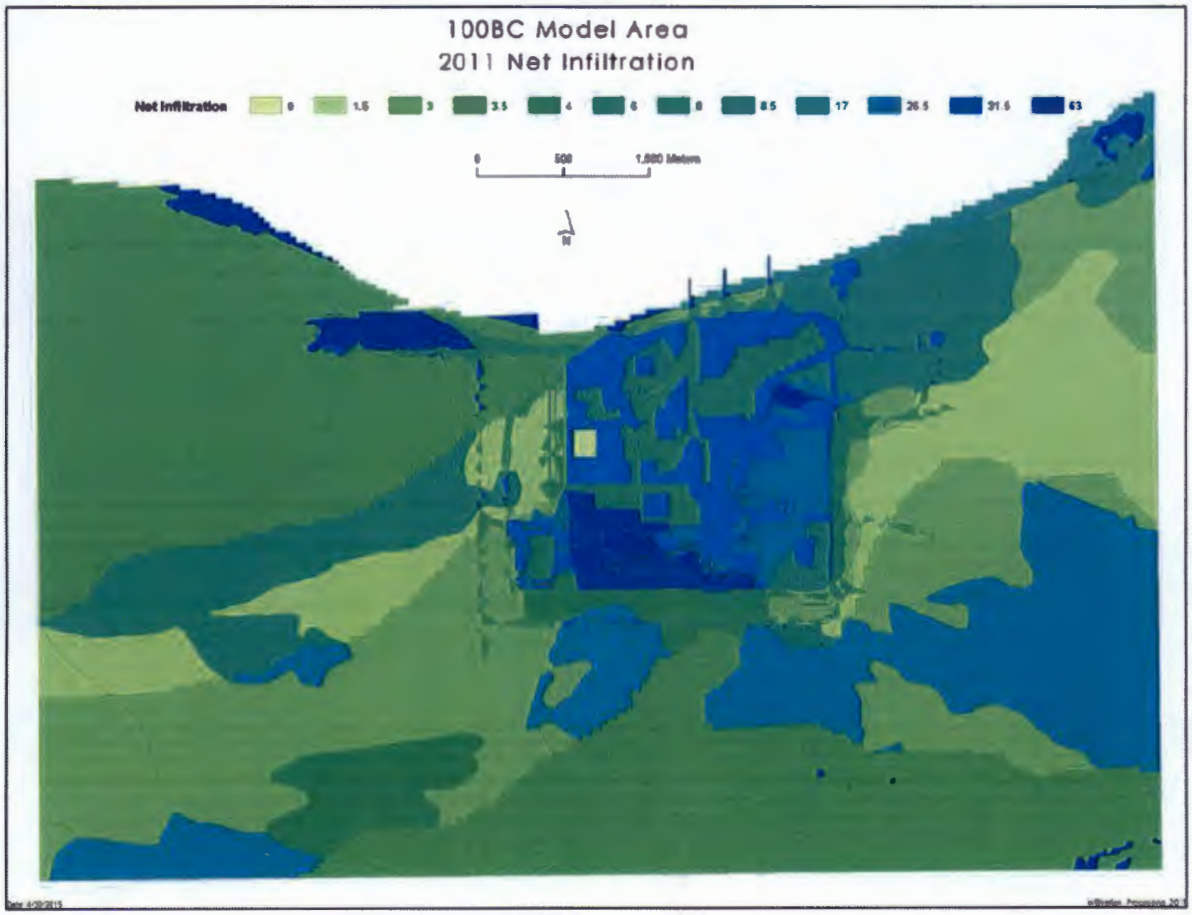

Figure 3-8. 2011 Recharge

3.3.2 West, South, and East Landward Boundary Conditions

General-head boundary conditions are used at western and eastern boundaries of the 100-BC GWFTM to represent the influence of the unconfined aquifer not included in the model domain. While these boundaries may approximately be no-flow as defined by streamlines (Figure 2-12) it is more correct to allow for external influences to propagate through the boundaries (such as the Columbia River upstream from 100-BC). The fluctuations in the Columbia River stage are conceptualized to impact the head at these lateral boundaries with the impact of the river being largest near the river and lessening with increasing distance from the river. The observed water levels at several wells within the 100-BC area were compared to the B-gage stage data and a synthetic formula was developed to incorporate both the B-gage stage and the prior groundwater level at those locations through the use of a damping parameter. The synthetic formula also allowed for a systematic increase in the groundwater levels at those locations to account for the regional groundwater gradient toward the river and a time lag to account for the time required for river fluctuations to propagate through the aquifer. The formula was fit to the observed water levels as a function of distance of the wells from the river. In this way, the effect of the Columbia River fluctuations as well as the aquifer between points along the boundaries was accounted for in generating the heads and conductance along the western and eastern boundaries. The GHB head over distance along the boundary is illustrated for the first 8 calibration stress periods in Figure 3-9. The boundary shows the effects of ow river stage beginning in January (sp1) and then rising and becoming more variable in April. Note that at about 1,500 m from the river the fluctuations are strongly damped, broadly consistent with

the well water-levels illustrated in Figure 2-16. The quality assurance checking performed for this algorithm is not shown here, but is preserved in the Environmental Model Management Archive (EMMA) under this model name and version.

A no-flow boundary was used to represent the southern edge of the model where the basalt outcrops.

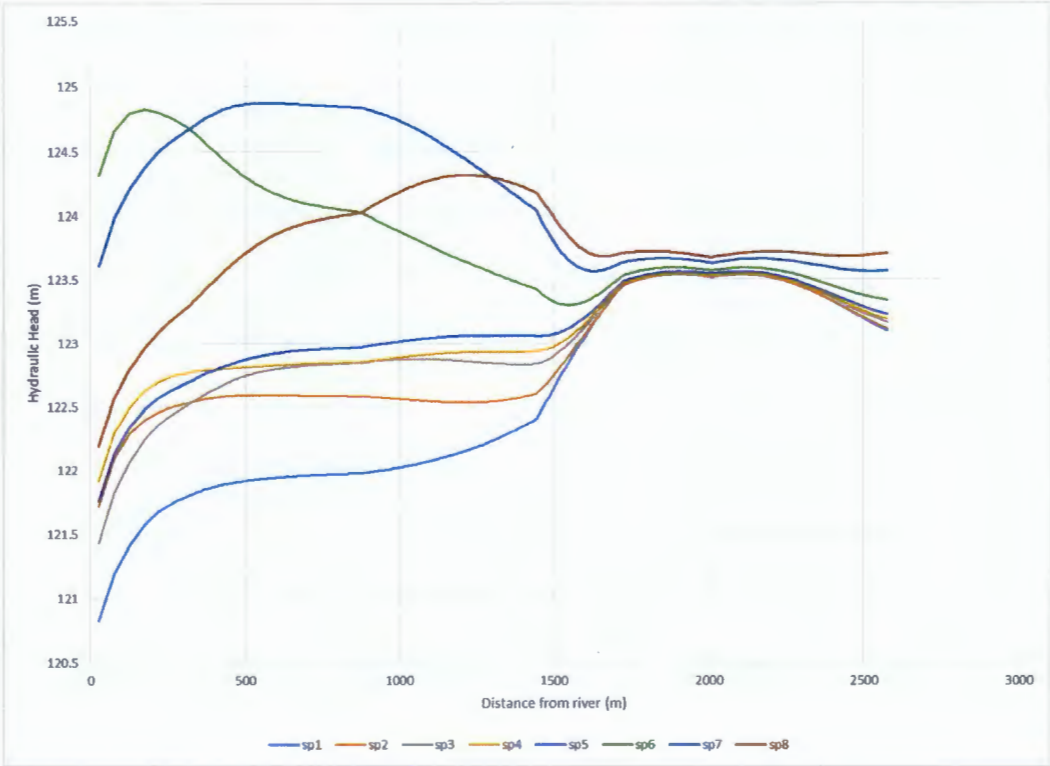

Figure 3-9 GHB Head vs. Distance Considering Stage, Gradient, Prior Levels, and Distance Correction for the First 8 Stress Periods

3.3.3 River Boundary Conditions

PNNL-14753 rev. 1 documents the steady-state water-surface of the Columbia River from the MASS1 surface-water model. This data is assumed to adequately represent the variation in the slope of the river over all times of interest. Practically, this assumption may be violated during sharp increases in stage as the flood wave propagates downstream. The MASS1 simulated stages were interpolated onto the PNNL groundwater model river nodes; in turn this data was interpolated and sampled at grid centers underlying the river. The relative stage at each location was then used with the B-gauge data to compute the river stage. The B-gauge transducer data was averaged over each stress period.

As stage changes over time the area of the riverbed that is submerged also changes–this phenomena is noted as seeps along the river. To account for this a river boundary is only assigned to cell when the stress period average stage is above the cells bathymetry- only cells within the river are included in the computation. For grid cells where the stage is below the bathymetry a drain boundary condition is substituted and the elevation set to the land (bathymetric) surface to emulate riverbank seeps that occur when the river drops.

The 100-Area GFM shows that Columbia River contains both Hanford and Ringold E formation in its riverbed within 100-BC GWFTM area. Riverbed hydraulic conductivity (with an assumed riverbed

thickness of 1 m) for both Hanford and Ringold E formation were made PEST adjustable but not spatially variable. The quality assurance checking performed for this algorithm is not shown here, but is preserved in the Environmental Model Management Archive under this model name and version.

3.3.4 Initial Head Condition

The initial hydraulic head everywhere in the model was assigned from 2013 water-table conditions as published in the 2014 annual groundwater report (DOE/RL-2014-32, Rev. 0). This was done by importing the shape files into Groundwater Vistas and having it perform interpolation. Because this is a transient solution that uses an iterative solver the primary effect is to speed up the solution.

3.3.5 Initial Cr(VI) and Sr-90 Concentration

The three-dimensional (3D) plumes for hexavalent chromium and strontium-90 were built in Leapfrog Geo (ECF-100BC5-15-0039, Rev.0). Both three-dimensional (3D) plumes were interpolated to 100-BC GWFTM grid. The following steps were followed to form the initial concentration condition:

1. 2013 water level elevation for layer 1 and cell center elevations for layer 2 through 6 were imported to Leapfrog Geo
2. The 3D plume is then sampled at all the grid points for each layer
3. The interpolated concentrations were exported as a .csv file
4. Concentrations under the DWS (10 ug/L for Cr(VI) and 8 pCi/L for strontium-90) were removed from the .csv file
5. An R script was used to process the .csv file in MODFLOW readable matrix format.

This data was prepared for maps published in the fall 2013 and 2014 annual groundwater reports (DOE/RL-2015-07, Rev. 0; DOE/RL-2014-32, Rev. 0), and for a revised 2014 plume based on maximum chromium concentrations.

3.3.6 Aquifer Hydraulic Property Parameterization

Simulation of transient groundwater flow under unconfined conditions requires the following input data:

- Horizontal hydraulic conductivity in each model layer of the Hanford and/or Ringold
- The ratio of vertical to horizontal hydraulic conductivity (KvKh) used to compute vertical hydraulic conductivity
- Specific storage (S_s)
- Specific yield (S_y)

These properties were specified using the MODFLOW LPF (Layer Property Flow) package. The first model layer is unconfined (type 1) where transmissivity is a function of saturated thickness, and the remained are convertible (type 3) where transmissivity is computed from layer thickness when simulated head is above the layer or as saturated thickness when head is below the top of the layer.

Uniform values of KvKh for the Hanford and Ringold were specified, and used to multiply horizontal hydraulic conductivity to yield vertical hydraulic conductivity for model input, S_s and S_y were input as constant values for all layers and formations. Upper and lower bounds on KvKh were set at 0.01 and 0.5, respectively. Specific storage upper and lower bounds were set at 1×10^{-4} and 5×10^{-6} 1/m, respectively.

Two hydrostratigraphic units (HSUs) are present in the model:

1. Hanford formation, mostly in layer 1 and layer 2
2. Ringold E formation, mostly in layer 3 thru layer 6 and a portion in the north-east side of layer 1 and layer 2 where the chromium plume discharges to the river

Hydraulic conductivity from slug tests in the Ringold E formation varies from 2.5 m/d to 15 m/d (Table 4-2, ECF-100BC5-11-0145, Rev.0). In the 100 Area hydraulic conductivity in the Hanford formation varies from 10 m/d to over 1,000 m/d (Section 2.1.3). The apparent channel scour in the top of the RUM suggests a cataclysmically deposited Hanford channel may exist in the southern side of 100-BC. However, the extent of the channel is not known.

Horizontal hydraulic conductivity was parameterized by points interpolated over the model grid via ordinary kriging. This approach is termed the "pilot point" method of parameterization (Doherty, 2003). Pilot points at each layer are placed based on the following criteria:

1. Uniform distribution of the pilot points over the entire model domain so that at least 2-3 points are available for interpolation within the correlation scale (range)
2. High density of pilot points in vicinity of calibration targets (e.g., AWLN wells, manual measurement wells)
3. Non-adjustable pilot points at slug test well locations (Table 4.2, ECF-100BC5-11-0145, Rev. 0)

In the context of this application the correlation scale (range) of the semivariogram represents an influence distance for interpolation, not the actual correlation scale of hydraulic conductivity; insufficient data exists to determine the correlation scale of hydraulic conductivity. The PEST groundwater utility PPK2FAC was used to generate kriging factors from the pilot points at each layer for all the model cells. A spherical variogram with a correlation range of 1,500 m was used to interpolate hydraulic conductivity. Pilot points were applied to two layers at a time in order to reduce the chance of inconsistent parameterization. That is, layers 1 and 2 had one set of pilot points, layers 3 and 4 another, and 5 and 6 yet another. A total of 82 pilot points was used. The PEST groundwater utility FAC2REAL was used to calculate hydraulic conductivity at each model cell based on the pilot point values and kriging factors generated by PPK2FAC program. PEST was run with regularization constraints computed from the PPKREG utility so that FAC2REAL program always generates hydraulic conductivity values based on smoothness constraints. Figure 3-10 through Figure 3-15 show the location of the pilot points with respect to hydro-stratigraphic units (HSUs), calibration wells, and Cr(VI) 2014 plume outline in layers 1 through 6, respectively.

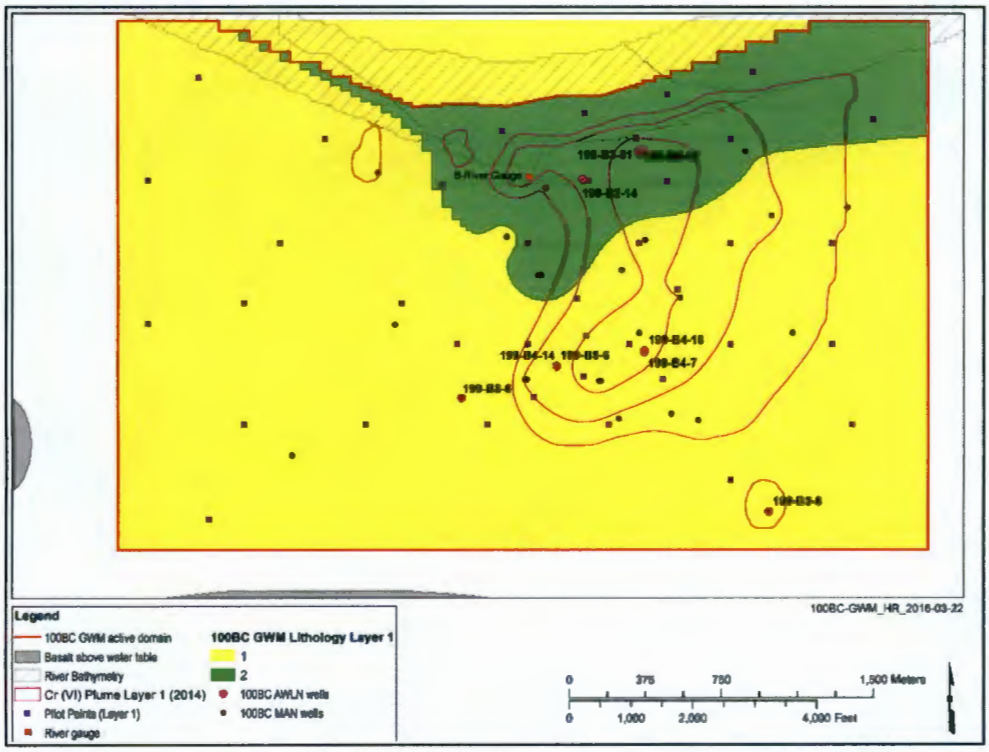

Figure 3-10. Pilot point locations in Layer 1

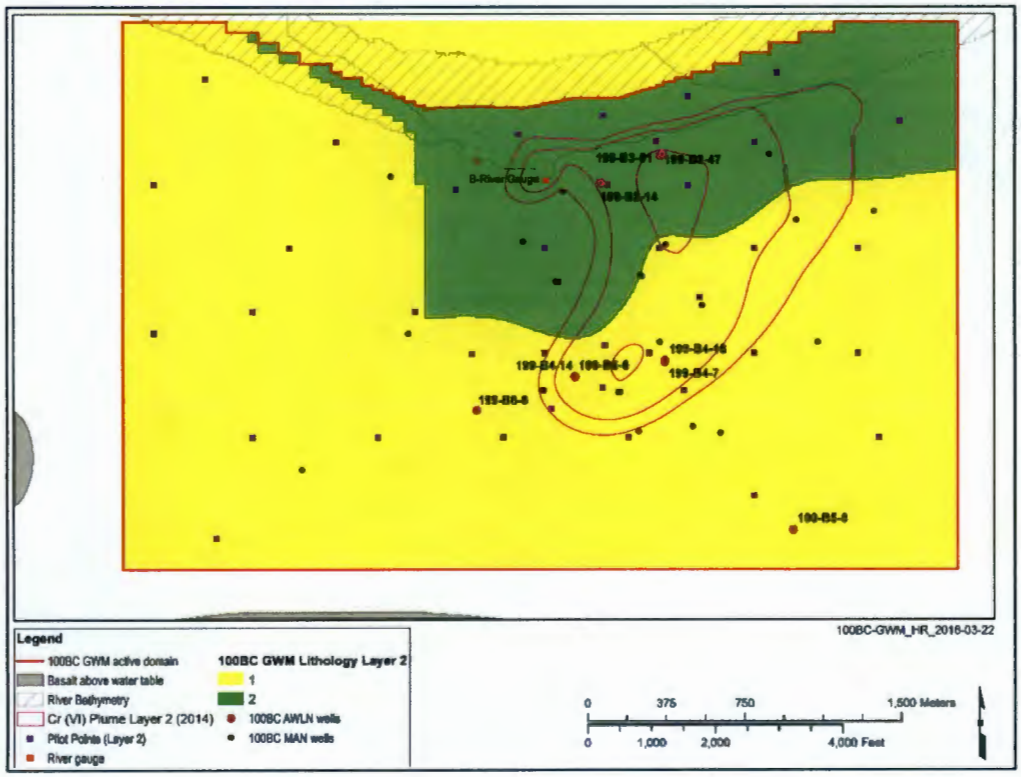

Figure 3-11. Pilot Point Locations in Layer 2

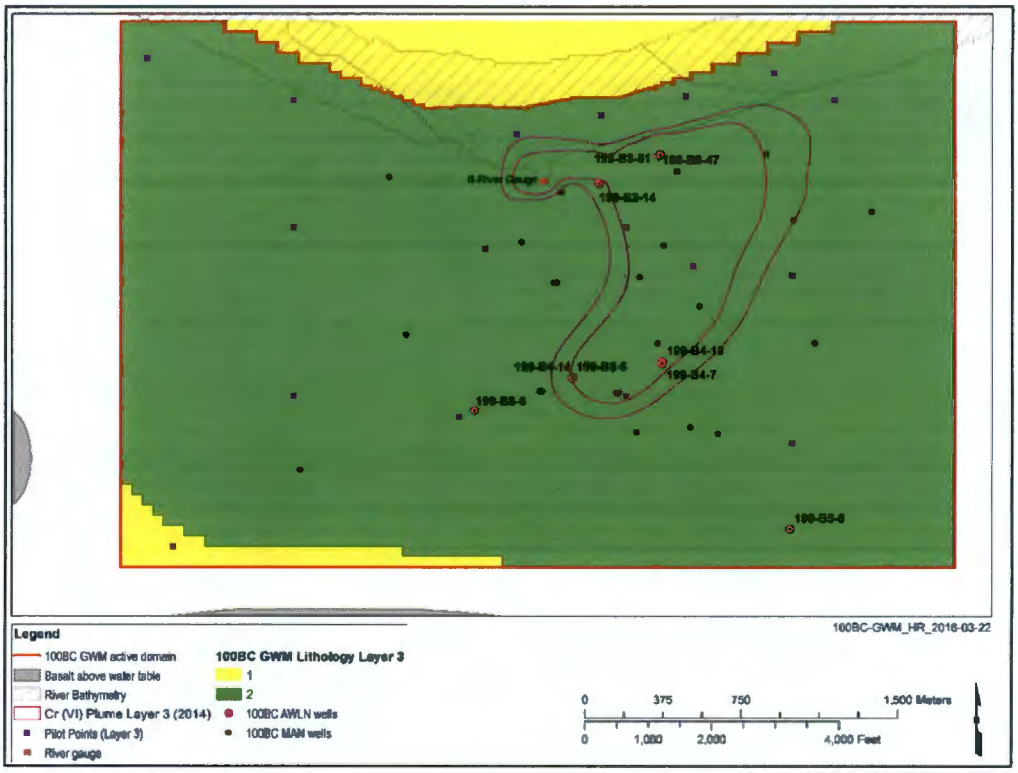

Figure 3-12. Pilot Point Locations in Layer 3

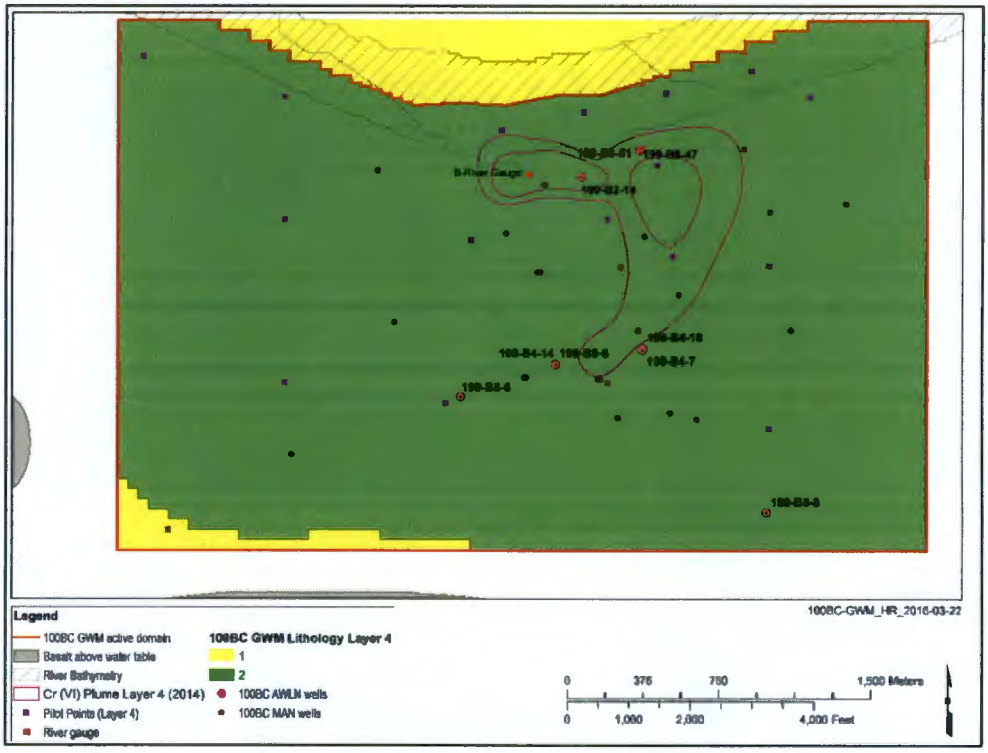

Figure 3-13. Pilot Point locations in Layer 4

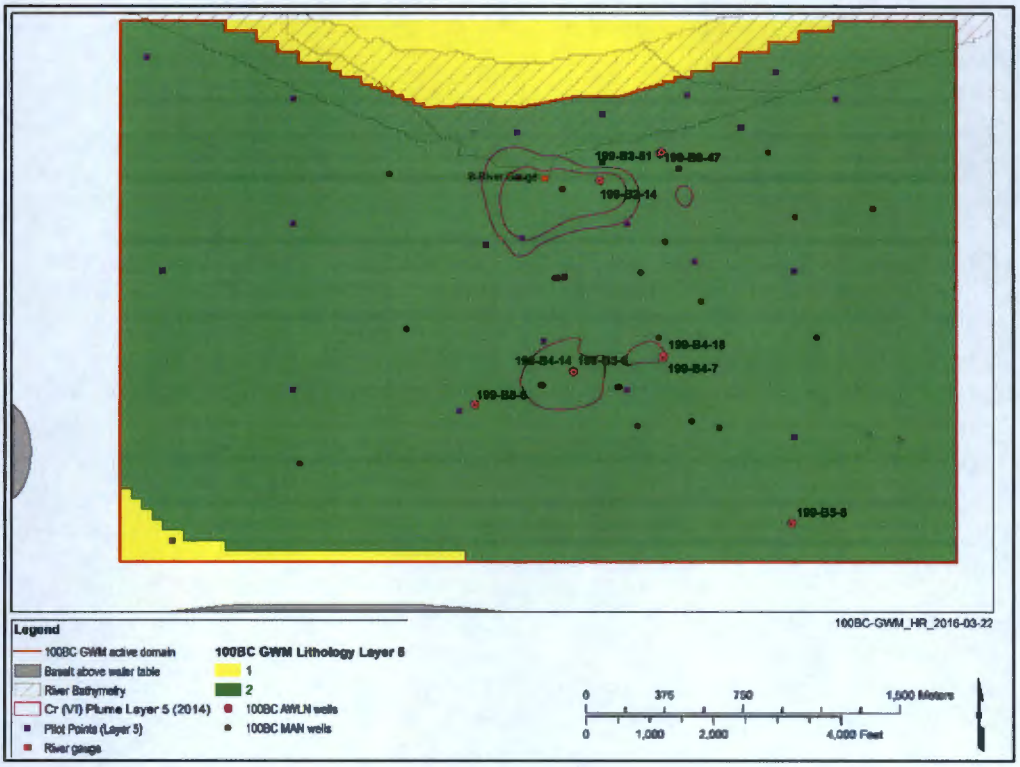

Figure 3-14. Pilot Point Locations in Layer 5

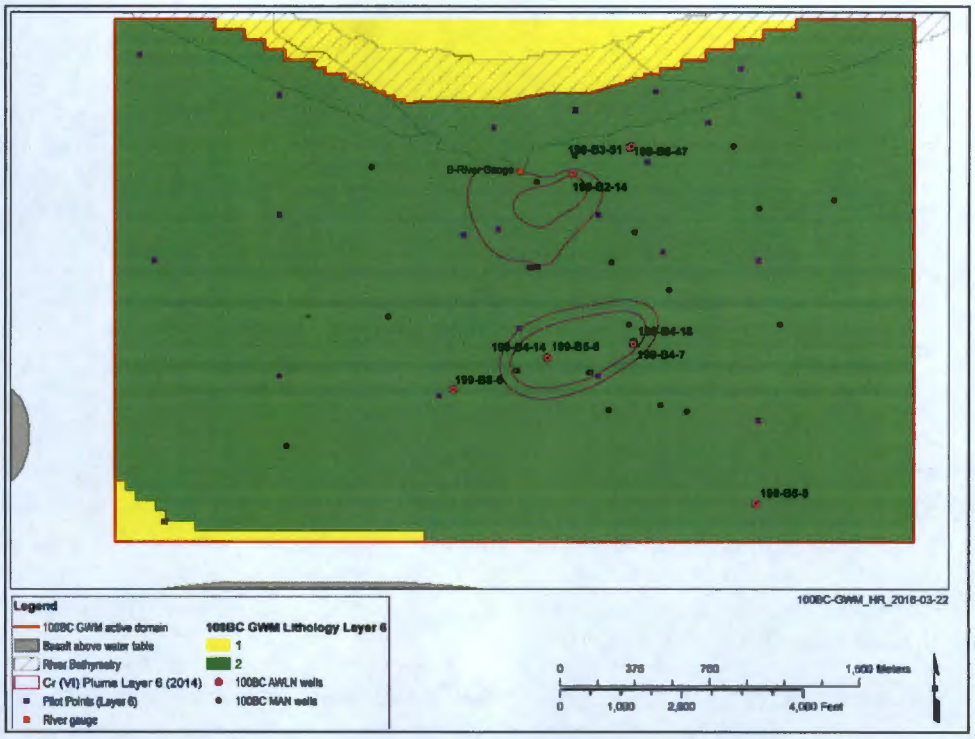

Figure 3-15. Pilot Point Locations in Layer 6

Uniform values of KvKh for the Hanford and Ringold were specified, and used to multiply horizontal hydraulic conductivity to yield vertical hydraulic conductivity for model input. S_s and S_y were input as constant values for all layers and formations. Upper and lower bounds on KvKh were set at 0.01 and 0.1, respectively. Specific storage upper and lower bounds were set at $1x10^{-4}$ and 5×10^{-6} 1/m, respectively. Specific yield upper and lower bounds were set at 0.4 and 0.1, respectively.

3.3.7 Effective Porosity

PNNL-21845 estimates Hanford effective porosity from tracer tests at 0.18 with a range from 0.24 to 0.14. The uncertainty was due to the simplified methodology. A uniform value of 0.18 was used.

3.3.8 Dispersivity

Dispersivity is a characteristic property of the geologic system, often found to be scale-dependent (e.g., a function of mean travel distance of solutes). Representative dispersivity values are typically determined from examination of values at similar transport scales from tracer tests and modeling of contaminant plumes. Dispersivity data from the scientific literation was evaluated and appropriate dispersivity values for use in the 100-BC transport model selected. This analysis supersedes that in SGW-44022.

Schulze-Makuch (2005) gathered data from additional sources and added this data to the data presented by Gelhar et al. (1992). Schulze-Makuch (2005) presents 184 additional dispersivity values from 39 authors in a similar fashion to that of Gelhar et al. (1992). An evaluation of some of the data summarized by Schulze-Makuch (2005) revealed a number of discrepancies such as: (1) incorrect reporting of dispersivity [e.g., average dispersivity value referenced from Rivett et al. (1994) should be 49 cm, not 49 m; and transverse horizontal dispersivities from Lavenue and Domenico (1986) were reported as longitudinal dispersivities], (2) from two to five dispersivity values were tabulated for identical flow paths from some reference sources which could lead to over representation and bias if multiple values are included in the dataset for the same tested flow path [e.g., Ptak and Teutsch (1994); D'Alessandro et al. (1997); Himmelsbach et al. (1998)], (3) inappropriate selection of transport scale [e.g., use of the total model grid length rather than the mean travel distance for regional plumes presented in Avon and Bredehoeft (1989) and Chapelle (1986)], and (4) omitting dispersivities reported in sources [e.g., Chiang et al. (1989); Engesgaard et al. (1996); Mas-Pla et al. (1992); D'Alessandro et al. (1997)] . Since direct inclusion of all of the data reported in Schulze-Makuch (2005) could lead to undesirable uncertainty in the combined dataset constructed to support development of a dispersivity-scale relation, it was decided to only use data from those original sources that could be readily obtained and verified with emphasis on field studies with scales of interest (i.e., greater than 1 m). Where multiple dispersivity values where reported for the same flow path (e.g., from multiple tests and/or multiple analysis methods) in the original data sources, a geometric mean value was calculated for inclusion in the dataset. Schulze-Makuch (2005) adopted the reliability classification system above defined by Gelhar et al. (1992).

Literature data other than that cited in Gelhar et al. (1992) and Schulze-Makuch (2005) for tracer tests conducted at the Nevada National Security Site (IT Corp, 1998; Reimus et al., 1999; SNJV, 2006, 2007) and analysis of a long plume in Canada (van der Kamp et al., 1994) are also included in the dataset. Reliability codes were assigned to these date based on the criteria in Gelhar et al. (1992). For these data, a geometric mean value was calculated for inclusion in the dataset where multiple dispersivity values where reported for the same flow path.

Plots of the longitudinal dispersivity versus scale in log-log space are shown in Figure 3-16 and Figure 3-17 by rock type and reliability level, respectively. The data show a systematic increase in longitudinal dispersivity with increasing transport scale, which is consistent with findings by previous authors (e.g., Gelhar et al., 1992). The equations for these fits are given in Table 3-1. At 100-BC, the unconfined

aquifer is located within the alluvial sediments of the Hanford and Ringold formations. Therefore, linear and log fits were obtained for the data from only alluvial sediments (Figure 3-18). The equations for these fits, which are very similar to those for the fits to all of the data, are also given in Table 3-1.
Recommended values as a function of transport distance are given in Table 3-2. Transverse horizontal and vertical dispersivities were selected based on a ratio of longitudinal to transverse horizontal dispersivity of about 10 and a ratio of longitudinal to transverse vertical dispersivity of about 100, respectively. Because groundwater contamination from sources at greatly different transport distances from the river intermingle it was not possible to implement scale-dependent dispersivity. Lower-end values of 10, 1, and 0.1 m were used for horizontal longitudinal, horizontal transverse, and vertical transverse dispersivity to minimize plume spreading but still account for the dispersion process.

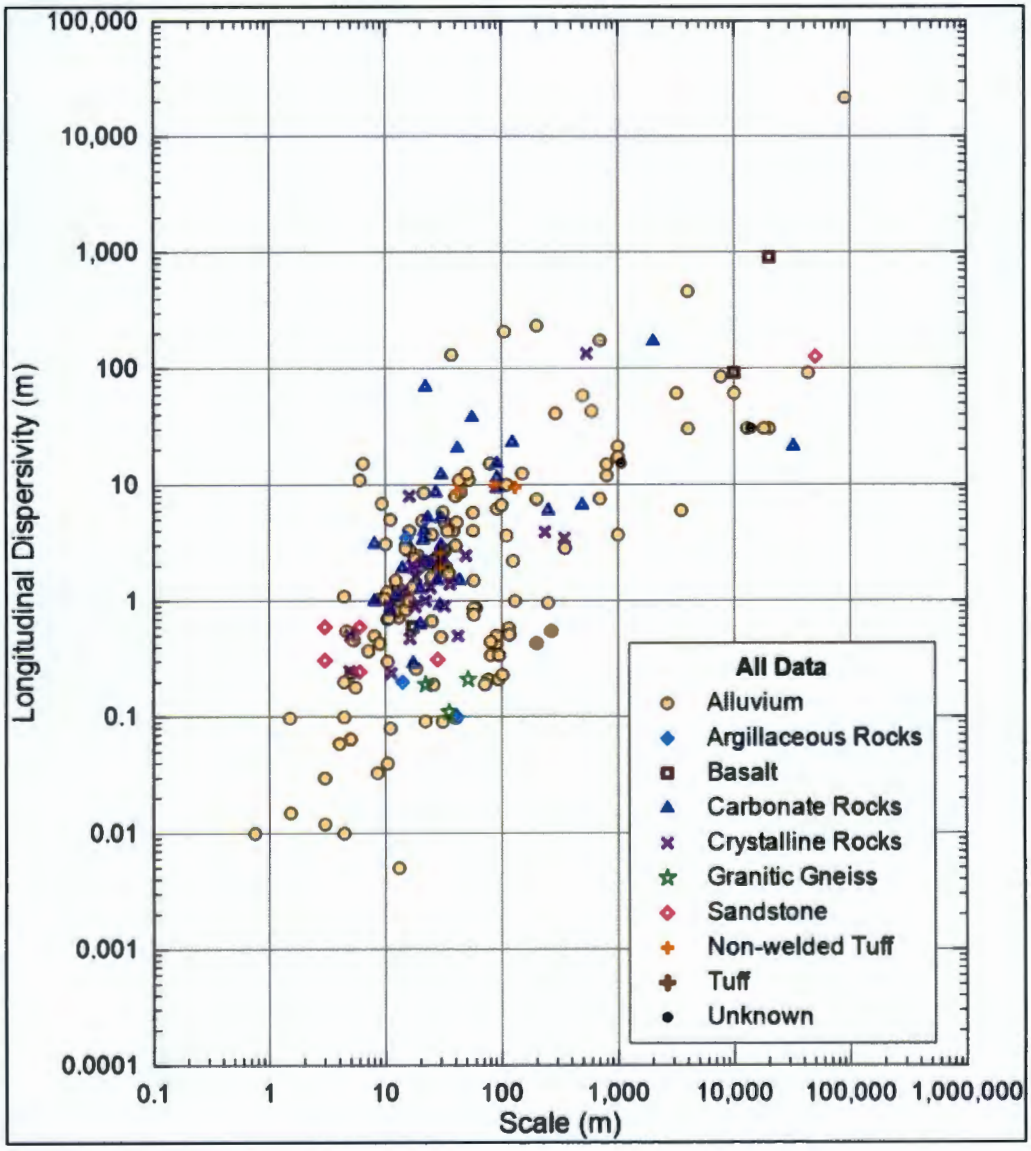

Figure 3-16. Longitudinal Dispersivity by Rock Type

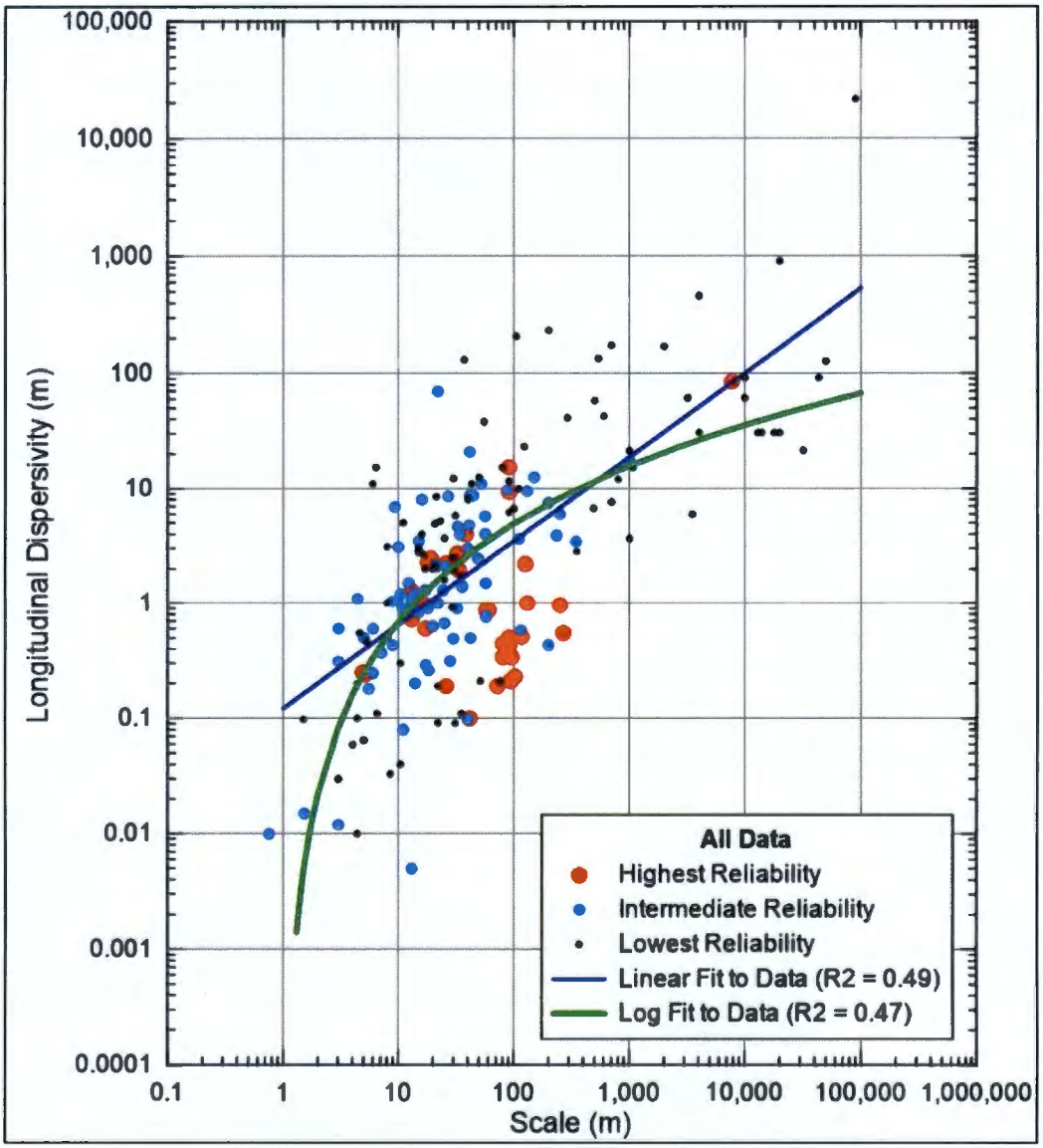

Figure 3-17. Longitudinal Dispersivity by Reliability Level for all Rock Types with Linear and Log Fits

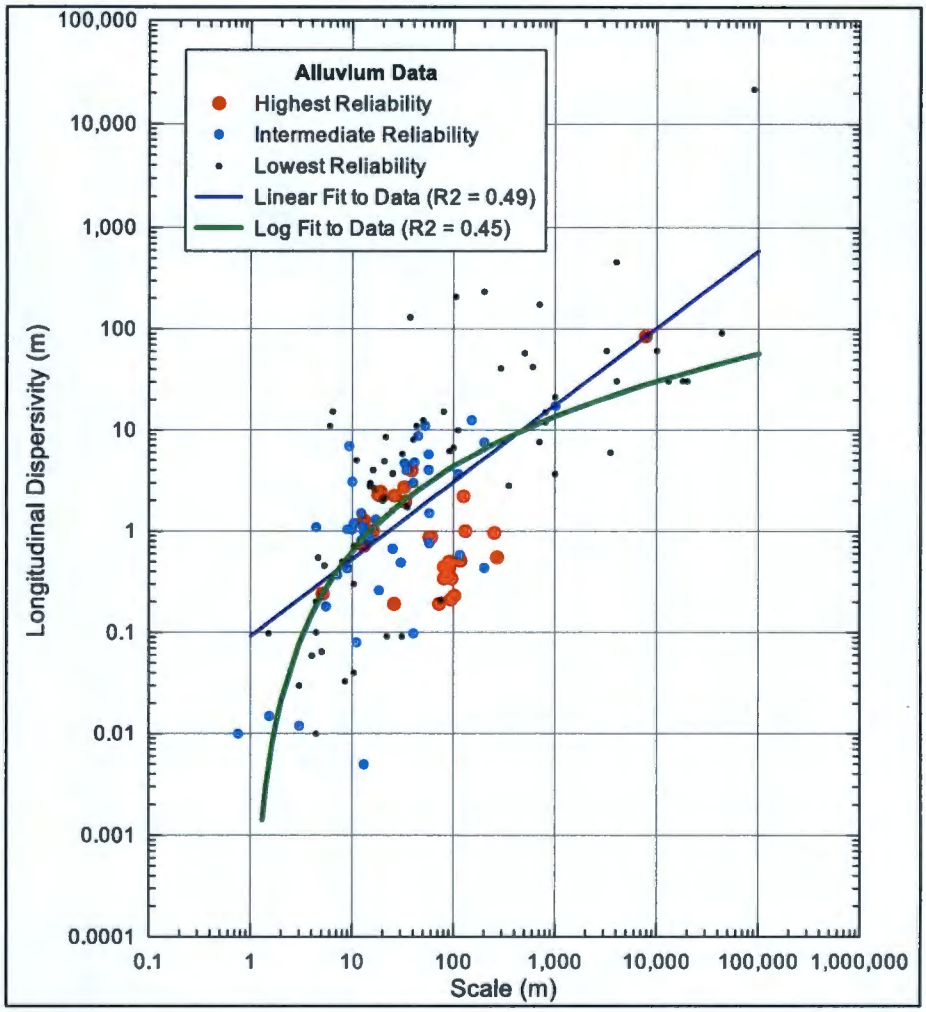

Figure 3-18. Longitudinal Dispersivity by Reliability Level for Alluvial Sediments only with Linear and Log Fits

Table 3-1 Dispersivity-scale relationships

Relationship Type	Relationship*	Coefficient of Determination (R^2)
	All Data	
linear	$\log(\alpha) = 0.7282 * \log(x) - 0.9141$	0.49
log	$\log(\alpha) = 1.2367 * \log(x) - 0.1658$	0.47
	Alluvium Data	
linear	$\log(\alpha) = 0.7615 * \log(x) - 1.0369$	0.49
log	$\log(\alpha) = 1.2176 * \log(x) - 0.2050$	0.45

* α= longitudinal dispersivity x = transport distance

Table 3-2 Recommended Dispersivity Values for 100-BC

Transport Distance	Calculated Longitudinal Dispersivity (m)[a]				Recommended Longitudinal Dispersivity (m)[b]	Recommended Horizontal Transverse Dispersivity (m)[c]	Recommended Vertical Transverse Dispersivity (m)[d]
	All Data - Linear	All Data - Log	Alluvium Data - Linear	Alluvium Data - Log			
500	11	12	10	12	10	1	0.1
1000	19	16	18	14	18	1.8	0.18
5000	60	28	60	24	60	6	0.6
7000	77	32	82	27	82	8.2	0.82

a. Calculated using the equations in Table 1.
b. Based on the linear fit to the alluvial sediment data only.
c. An order of magnitude lower than the longitudinal dispersivity.
d. Two orders of magnitude lower than the longitudinal dispersivity.

Dispersivity is not an intrinsic property of the medium. In order to have a basis for predicting dispersivity from statistical distributions, its dependence on the scale of the measurement and on the type of test and method of analysis must be known. Such data are not available for the Hanford Site. The trends in dispersivity with travel distance are compiled from data obtained from locations around the world. As a result, the appropriate longitudinal dispersivity to apply at large scales for Hanford Site models has uncertainty associated with the range and distribution of data.

3.3.9 Adsorption

PNL-10899, *Strontium-90 Adsorption-Desorption Properties and Sediment Characterization at the 100 N-Area,* characterized the adsorption and desorption of strontium-90 for the 100-NR2-OU area. Results showed a range of K_d values from 7 to 59 mL/g, and K_d decreases as the particle size of the sediment increases. In addition, K_d of 15 mL/g was estimated for bulk sediments more representative of actual field conditions.

PNNL-17674 investigated the mobility of chromium in 100 Area sediments, and found that K_d was close to zero (retardation near 1). Therefore, Cr(VI) is considered not to sorb in this analysis.

3.4 Flow Model Calibration

3.4.1 General Approach

MODFLOW solves the following mathematical-conceptual model:

$$\frac{\partial}{\partial x}\left(K_{xx}\frac{\partial h}{\partial x}\right)+\frac{\partial}{\partial y}\left(K_{yy}\frac{\partial h}{\partial y}\right)+\frac{\partial}{\partial z}\left(K_{zz}\frac{\partial h}{\partial z}\right)+W=S_s\frac{\partial h}{\partial t}$$

Where x, y, and z are Cartesian coordinate axes, K is the hydraulic conductivity coincident with each axis, W is water source or sink rate, S_s is specific storage, t is time, and h is hydraulic head (the state variable).

MT3DMS solves the following mathematical-conceptual model:

$$\frac{\partial(\theta C^k)}{\partial t} = \frac{\partial}{\partial x_i}\left(\theta D_{ij}\frac{\partial C^k}{\partial x_j}\right) - \frac{\partial}{\partial x_i}\left(\theta v_i C^k\right) + q_s C_s^k + \sum R_n$$

Where R is retardation, θ is effective porosity, t is time, x is Cartesian coordinate, C is concentration, k is transport component, D is dispersion tensor, v is groundwater velocity, q_s is water source/sink volume, C_s is source/sink concentration, and R_n is the chemical reaction term.

The transport equation is related to the flow equation by velocity determined from the hydraulic head computed by the flow model and Darcy's Law:

$$v_i = \frac{q_i}{\theta} = -\frac{K_i}{\theta}\frac{\partial h}{\partial x_i}$$

Transport model predictive power can be improved by:

1. Refining estimates of hydraulic conductivity by calibration to hydraulic head responses to river stage fluctuations.
2. Acquiring site-specific knowledge of effective porosity.
3. Incorporating hydraulic gradient estimates ($\partial h/\partial x_i$) and improving their model representation.
4. Incorporating independent estimates of velocity to act as an additional constraint on K, θ, and hydraulic gradient.

The ultimate use of the model is as a tool to evaluate potential groundwater remediation times and strategies. In order to improve the representation of the groundwater system for transport model development included the following approaches to address the items above.

6. Ferris (1963) presents a conceptual model and analytic solution that allows estimation of hydraulic diffusivity (T/S), which could be used to independently estimate T assuming S to supply a flow model constraint. Idealized assumptions include uniform aquifer thickness, completely penetrating river, great inland aquifer extent from its subcrop in the river, observation wells are far enough from the river to be unaffected by vertical flow, and that the range in fluctuations is a small fraction of the saturated thickness. As seen in Section 2 many of these assumptions are violated at 100-BC. However, the conceptual approach is still useful when implemented within the framework of a numerical model that overcomes Ferris' simplifying assumptions. To this end AWLN data from 199-B2-14, 199-B3-47, 199-B3-51, 199-B4-7, 199-B4-14, 199-B4-18, 199-B5-6, 199-B5-8, and 199-B8-6 was used for flow model calibration because it provides a multiyear record of detailed aquifer water-level changes responding to the Columbia River.
7. PNNL-21845 estimated site-specific effective porosity of the Hanford at 0.18.
8. PNNL-21845 computed the magnitude and direction of hydraulic gradient from wells 199-B4-14, 199-B5-8, and 199-B8-6 near 100-C-7. This approach was expanded to include 2012 through July 2014 AWLN data and associated gradient components as part of flow model calibration.

9. PNNL-21845 conducted several drift and pump back tracer tests to estimate ambient groundwater velocity and effective porosity. This data was incorporated into the flow model by evaluating the hydraulic gradient in the same network (wells 199-B4-14, 199-B5-8, and 199-B8-6), hydraulic conductivity at the wells, and computing with the PNNL effective porosity. The velocity estimated from Cr VI plume migration was evaluated similarly using wells 199-B4-14, 199-B4-1, and 199-B4-8. Additional computations (ECF-100BC5-15-0123, Draft, November, 2015) based on estimated Cr(VI) peak concentration migration from 199-B4-14 to other wells was also included.

10. The depicted annual groundwater plume for Cr(VI) in 2013 and 2014 show a eastward convex shape. Four control networks were established to force the groundwater flow direction so that simulated Cr(VI) plume maintained a similar shape.

Figure 3-19 shows the location of the AWLN wells, manual measurement wells, 100-C-7 and 100-C-7:1 waste sites, and three-point/four-point networks.

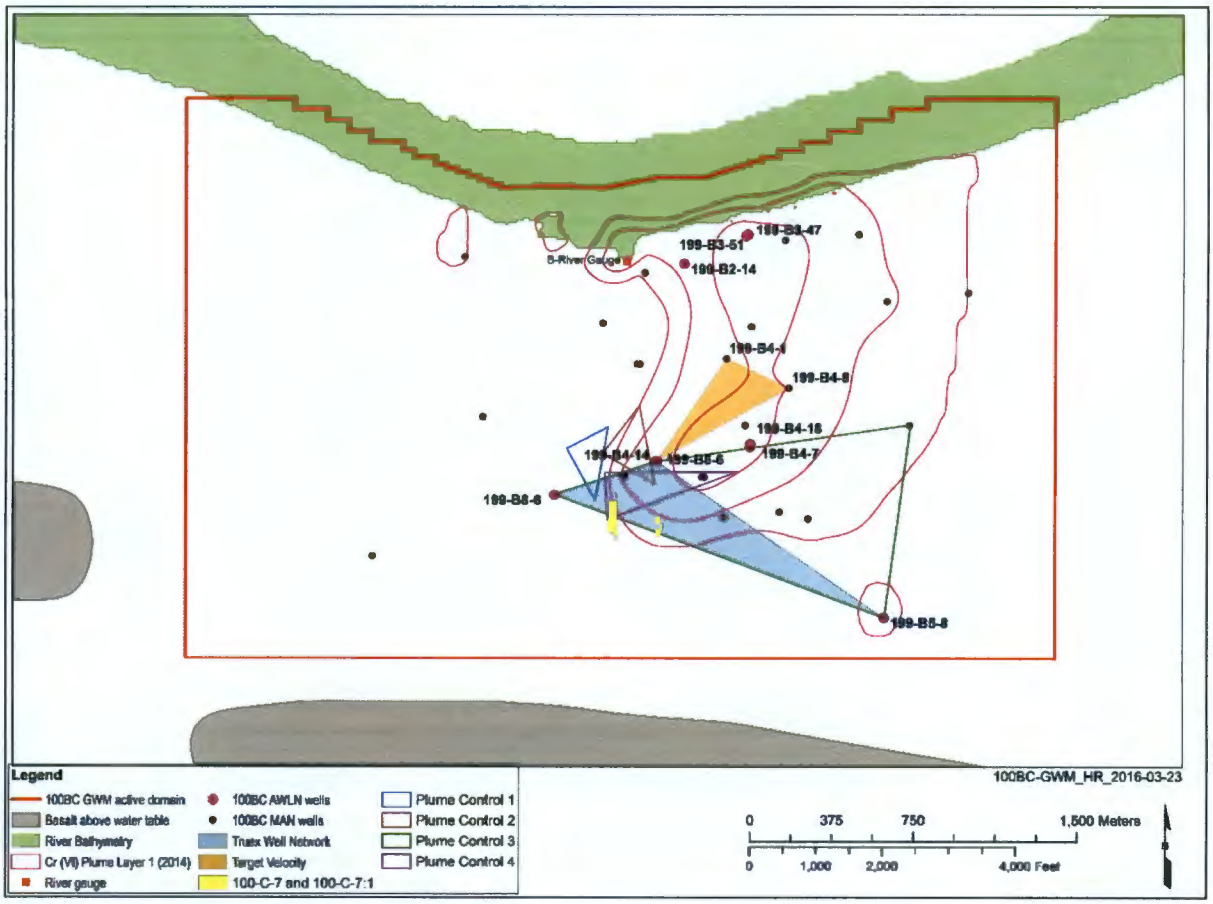

Figure 3-19 Calibration Features

The use of the AWLN data provides constraint on the bulk aquifer properties that affect plume migration. It also can help identify different hydraulic diffusivity (T/S) paths that can be a surrogate for transport paths (Knudby and Carrera, 2006).

3.4.2 Parameter Estimation Framework

The PEST (Doherty, 2007) parameter estimation software was used to facilitate model calibration in concert with manual adjustments. The 2012 through July 2014 calibration dataset incorporated the following elements:

1. Stress-period averaged AWLN water levels from wells 199-B2-14, 199-B3-47, 199-B3-51, 199-B4-7, 199-B4-14, 199-B4-18, 199-B5-6, 199-B5-8, and 199-B8-6 (781 total data points). AWLN water level at well 199-B4-16 has measurements for calendar year 2015 which is outside the calibration period. However, measurements show similar water levels as well 199-B5-8. Therefore, AWLN water levels from well 199-B4-16 was also monitored over the calibration period so that it can be compared to 199-B5-8.
2. Hydraulic gradient magnitude and direction from AWLN wells 199-B4-14, 199-B5-8, and 199-B8-6 (204 total data points).
3. Manual water-level measurements (241 data points).
4. Change from initial observed water level for wells 199-B4-14, 199-B5-8, and 199-B8-6 in order to emphasize the details of the water-level changes (325 total data points).
5. The two PNNL-21845 tracer-test estimated velocities.
6. A constraint of average velocity (1 m/d) between 199-B4-14, 199-B4-1, and 199-B4-8 (derived from ECF-100BC5-15-0123), with a direction of N45E.
7. Four constraints of groundwater flow direction near southern side of the Cr(VI) plume footprint were used to force the groundwater flow in the direction of depicted Cr(VI) plume in annual groundwater report.

The deviation between observed and simulated values (objective function) is mathematically minimized using singular value decomposition with regularization as described by Doherty (2007). The above data ranges in magnitude from $1x10^{-5}$ to nearly 360 because of the difference in units and data type. Weights were assigned to account for magnitude and contribution to the objective function.

The evaluation flow model, from 2006 through July 2014, was implemented in PEST although not used in formal parameter estimation. The model included all the calibration model data, plus additional manual water-level measurements.

The overall calibration process was as follows:

- Run the PEST software
- Review estimated model parameters and model fit to data for reasonableness and agreement
- Identify potential conceptual or parameter issues to be resolved and an approach
- Implement parameter, model setup, or other change
- Repeat

PEST provides several outputs of the process, including a file listing the residual (.res) between simulated and observed. This data was used to review goodness of fit. No absolute value of goodness of fit was set as a stopping criteria; an overall weight of evidence was considered including goodness of fit and plausibility of estimated parameters.

A qualitative transport evaluation was also conducted as part of this cycle with the criteria of matching interpreted chromium plume migration between 2011 and 2015 as documented by maps produced every fall as part of annual groundwater or other reports. Flow models were adjusted to preserve the interpreted chromium plume trajectory and velocity even at the expense of better fitting hydraulic data. The ultimate model use is for transport and this is judged to be an acceptable compromise.

3.4.3 Flow Model Calibration Results

A plot of observed versus simulated hydraulic head from the AWLN network is shown in Figure 3-20. The wells nearest the river (199-B2-14, B3-47, and B3-51) show the largest range and most scatter. The balance of the wells are several hundred meters inland and reflect the dampened signal from the river. The same data for manual water-levels is shown in Figure 3-21. The single high value was down weighted. The simulated values show more scatter at lower heads because longer stress periods were used during winter months when lower values occur.

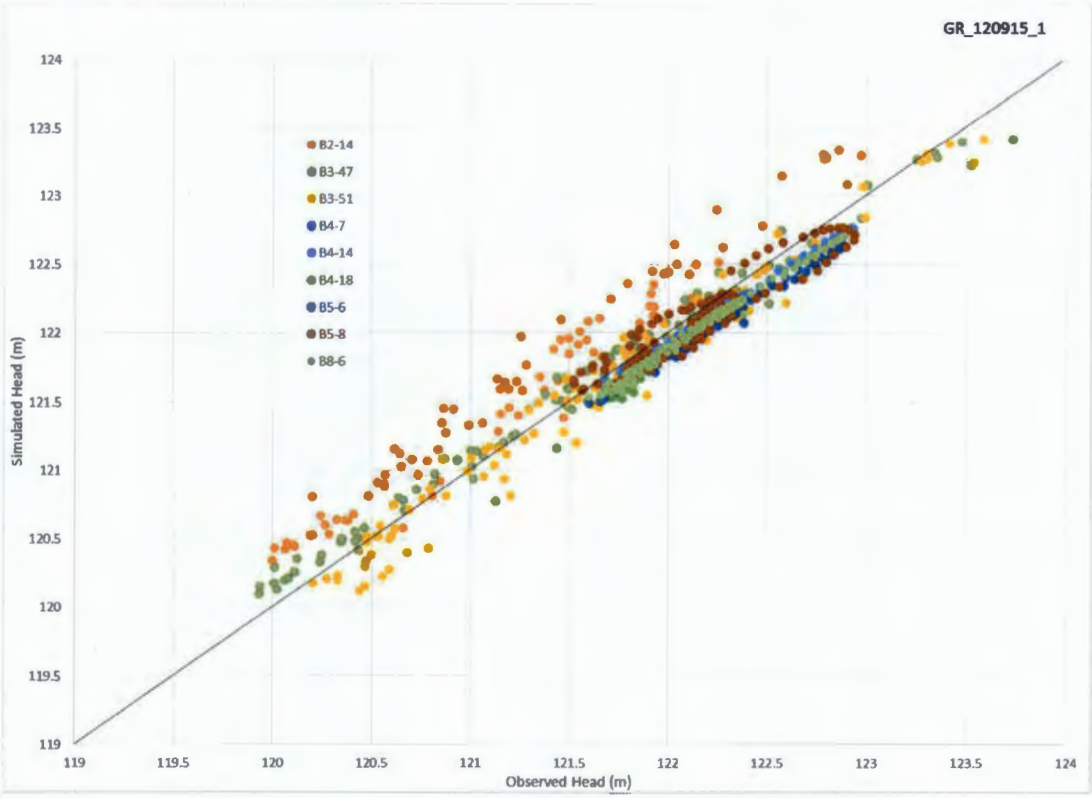

Figure 3-20 Observed versus Simulated AWLN Heads

Fitting hydraulic head alone does not guarantee that the inferred flow direction and gradient are honored. Figure 3-22 shows the observed (computed from a fitted plane) and simulated flow directions at wells 199-B4-14, B5-8, and B8-6, and Figure 3-23 shows the associated gradient magnitude. A key change to the model structure is illustrated by the results from an earlier version of the model. In model version 2g the Hanford cataclysmic channel was limited to an area in southern 100-BC roughly coincident with the depression in the surface of the RUM. The major structural change was removing the constraint that high (1,000s of m/d) Hanford hydraulic conductivity was limited to the southern area. Further changes occurred from version 4b to 7b when qualitative calibration to chromium plume migration was considered –version 4b is a superior model based on flow alone.

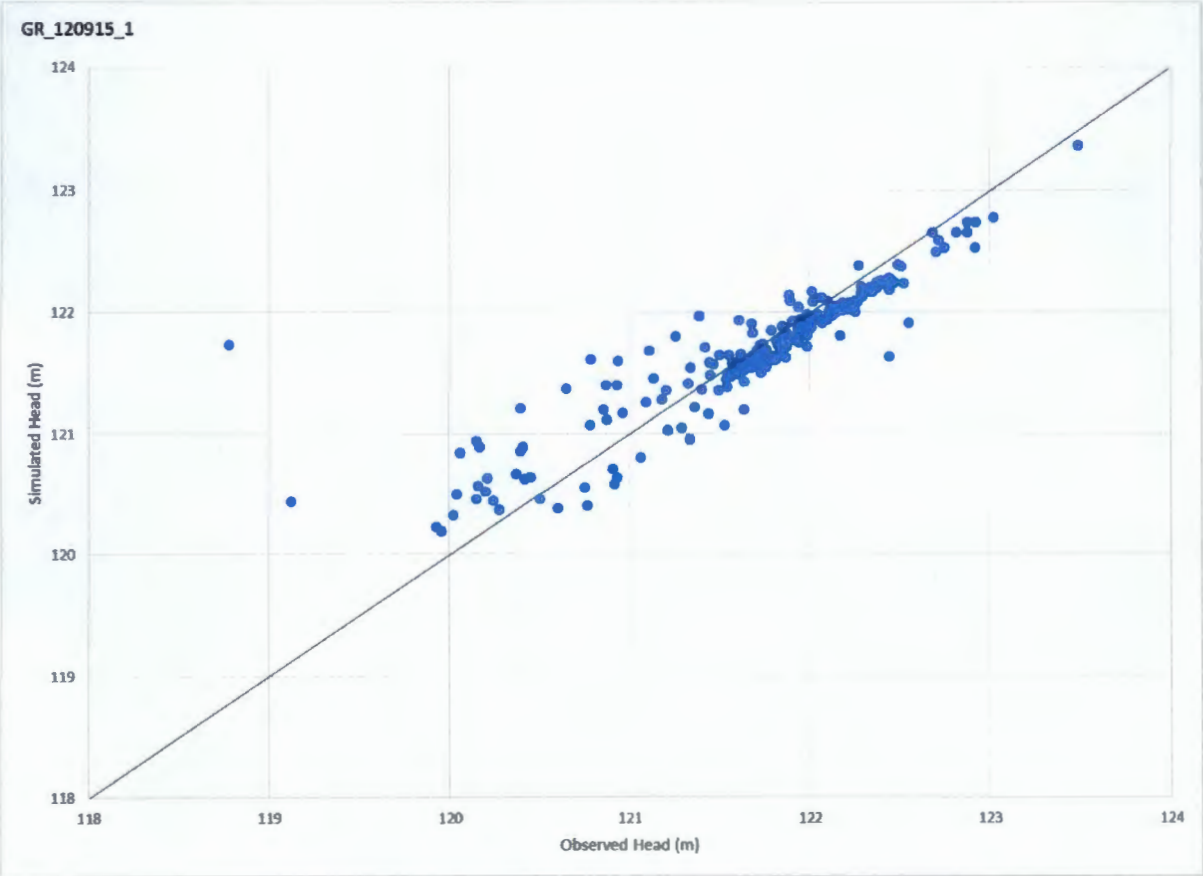

Figure 3-21 Observed versus Simulated Manually Measured Heads

In an isotropic, homogenous porous medium groundwater flow direction is orthogonal to equipotential lines. Suthersan et al. (2009) show a plume in an alluvial aquifer where the interpreted flow direction from potential is 40^0 from that actually observed via plume migration. The degraded fit to hydraulic data when plume data was included may be from structured heterogeneity such as channels.

Groundwater velocity (computed from modeled hydraulic gradient and model hydraulic conductivity) was also a calibration target. PNNL-21845 reported values of 5.1 and 3.7 m/d; corresponding simulated values were 2.8 and 2.7 m/d. The constraint provided by Hartman of 1 m/d was simulated at 0.97 m/d.

Appendix B shows the observed data and simulated hydrographs.

3.4.4 Qualitative Flow Model Evaluation

In addition to quantitative metrics a qualitative check on the flow was performed by comparing the interpreted flow field from groundwater annual reports to the simulated. Figure 3-24 andFigure 3-25 show the interpreted water table from the 2013 and 2014 annual reports and the simulated results for the same times. Agreement is qualitatively good with very low hydraulic gradient (no contours) in the south and higher hydraulic gradient to the north with flow converging on the river. The observed due east flow in the southern part of the domain is also matched.

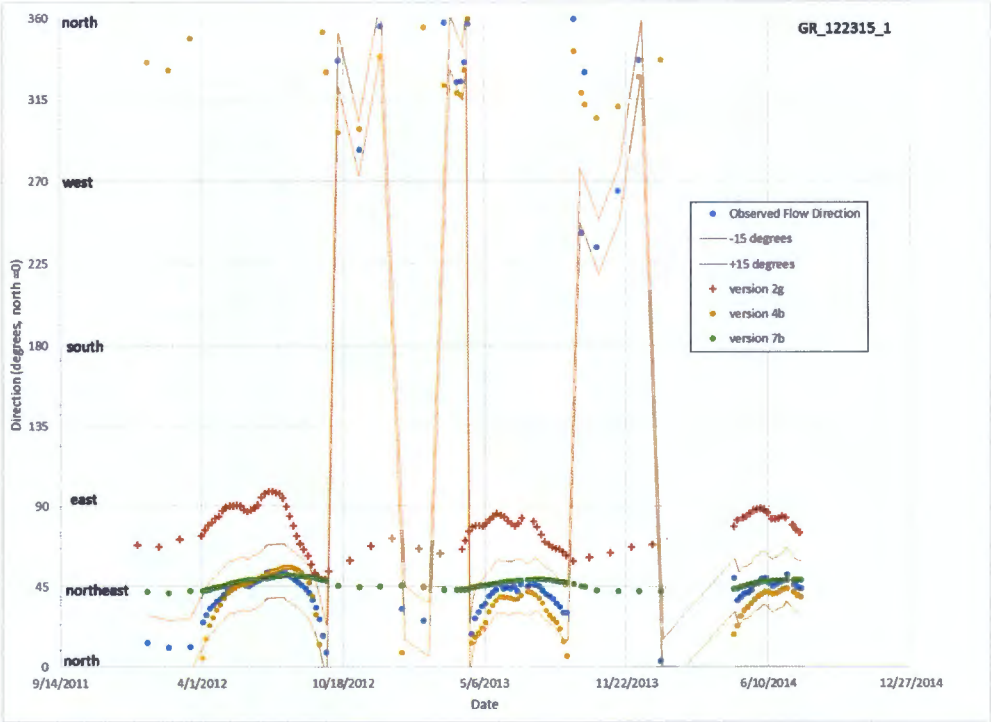

Figure 3-22. Observed and Simulated Flow Direction Over Time Computed from Wells 199-B4-14, B8-6, and B5-8

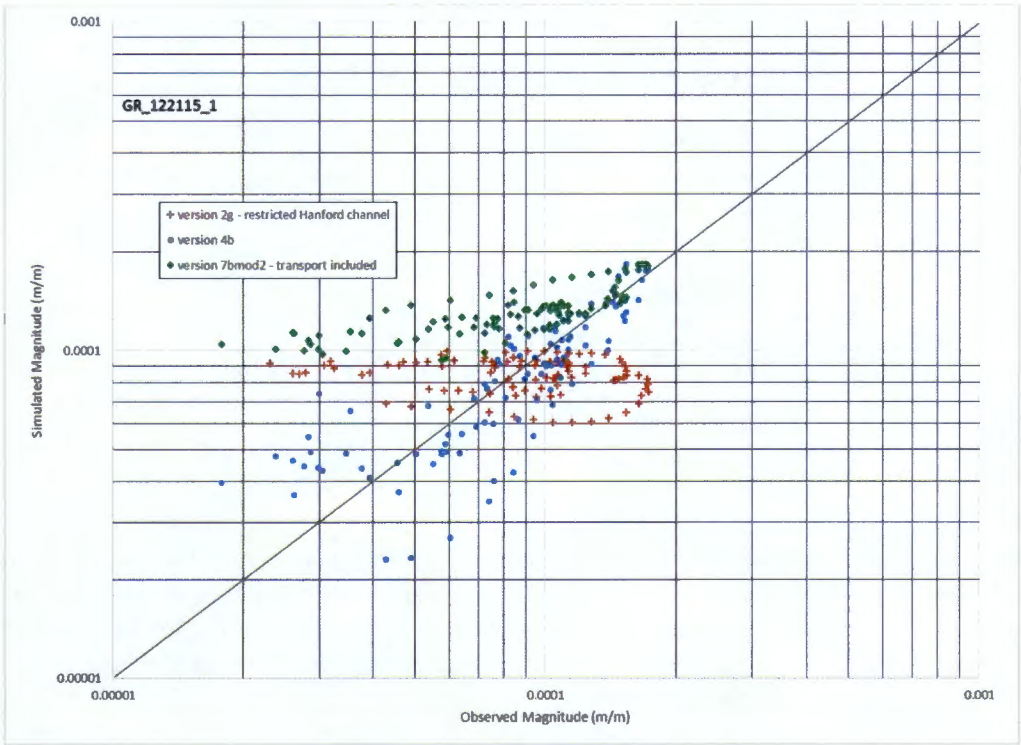

Figure 3-23. Observed Versus Simulated Hydraulic Gradient Magnitude Computed from Wells 199-B4-14, B8-6, and B5-8

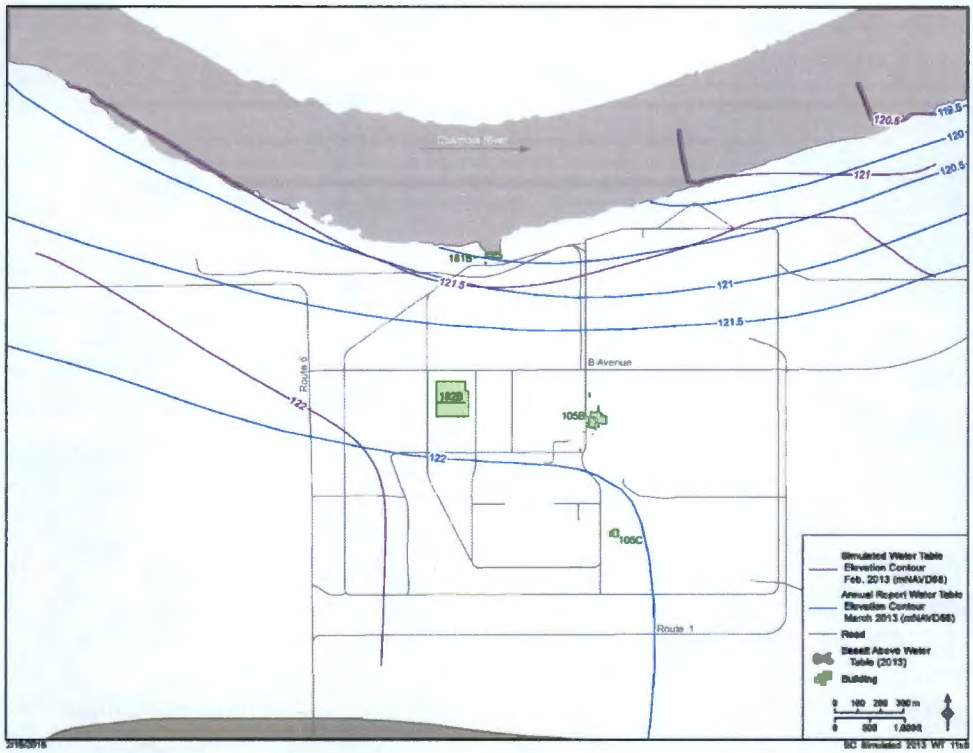

Figure 3-24. February 2013 Annual Report and Model Simulated Maps

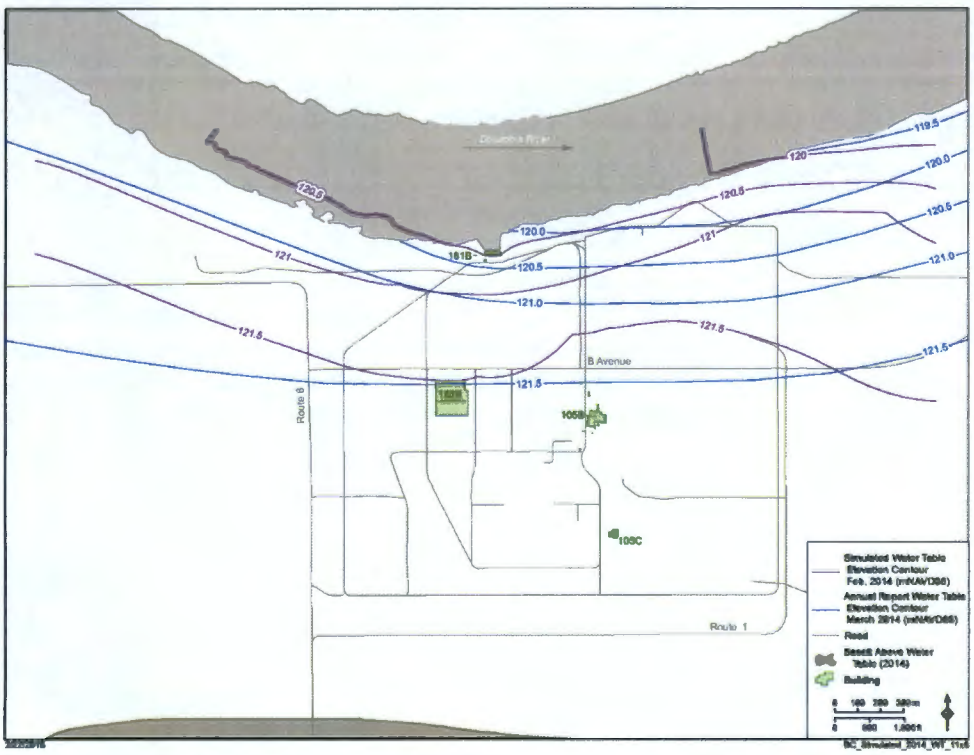

Figure 3-25. February 2014 Annual Report and Model Simulated Maps

3.4.5 Calibrated Flow Model Properties

Properties estimated as single values over some or all of the model domain are shown in Table 3-3.

Table 3-3 Single-Value Parameter Estimates

Parameter	Value
Specific yield	0.13
Specific storativity (1/m)	7.7×10^{-6}
Hanford vertical to horizontal hydraulic conductivity ratio	0.022
Ringold E vertical to horizontal hydraulic conductivity ratio	0.14
Hanford riverbed hydraulic conductivity (m/d)	419
Ringold E riverbed hydraulic conductivity (m/d)	47

Figure 3-26 through Figure 3-31 show model layer calibrated hydraulic conductivity along with the 2014 Cr(VI) plume 10, 20, and 48 µg/L contours and AWLN monitoring wells (shown regardless of layer). The area where the water table lies solely within the Ringold E is shown by lower hydraulic conductivity in layers 1 and 2. Layer 3 through 6 all had areas of high, relative to the characterization data shown in Table 2-1 and Figure 2-6, Ringold E hydraulic conductivity. The well hydrographs in these areas show good qualitative responses, and if the geologic interpretation is correct all the groundwater flow in the Hanford must pass into and through the Ringold E. This area is where the Hanford formation saturated thickness is declining (Figure 2-3) from a maximum of 30 to under 5 m. Thus, the Ringold E must have higher transmissivity to accommodate groundwater flow from the Hanford formation and still replicate groundwater potentials. Slight misidentification of the Hanford/Ringold E contact, especially if the Hanford deposits are cataclysmic flood gravels, would have a large impact on transmissivity given the approximate 2 order of magnitude difference in hydraulic conductivity.

3.5 Chromium Transport Model Calibration

3.5.1 Transport Calibration Approach and Data

The primary data used in the qualitative transport calibration are the chromium plume maps published depicting interpreted conditions each fall from 2011 to 2015. Additionally, time series of measured chromium concentrations were considered at well 199-B3-47 because persistent local chromium concentrations are inferred to be from a nearby source. The overall approach to solute-transport modeling discussed by Konikow (2010) was adopted; that is, emphasis was placed on matching major trends and locally averaged values.

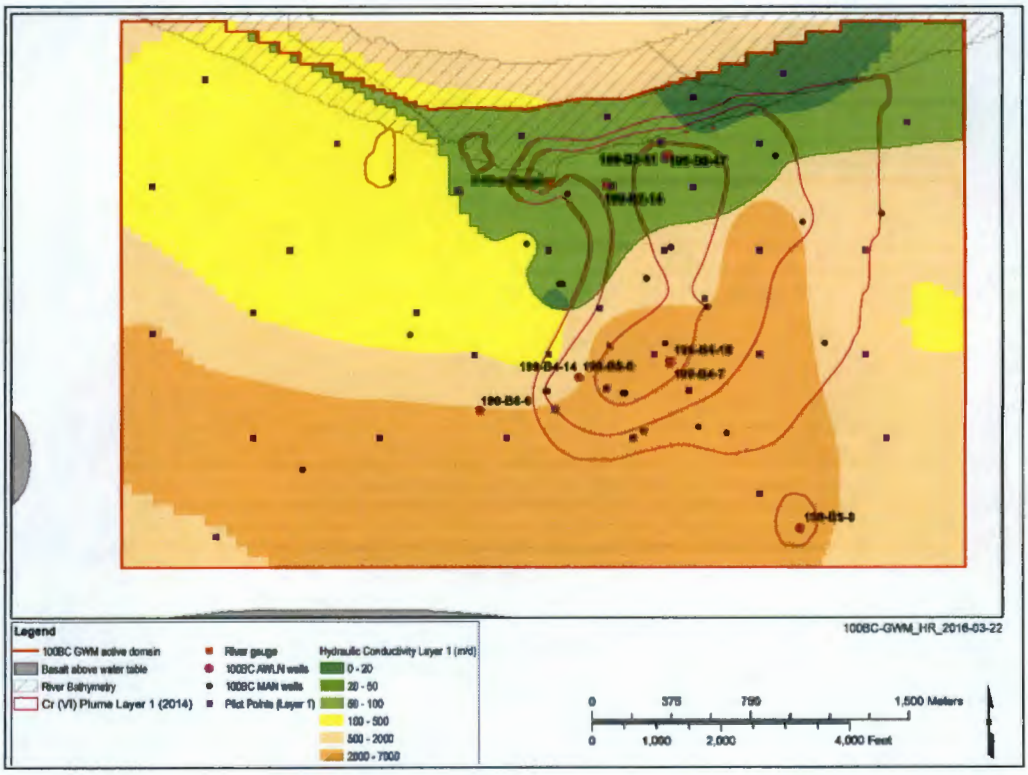

Figure 3-26 Layer 1 Hydraulic Conductivity

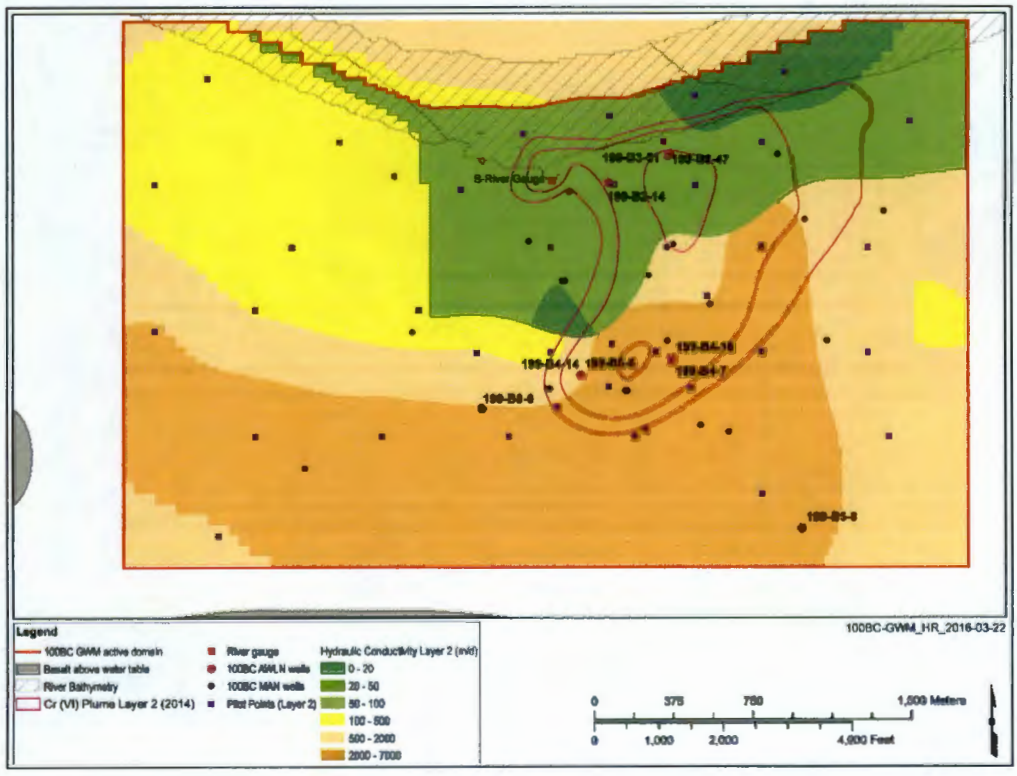

Figure 3-27 Layer 2 Hydraulic Conductivity

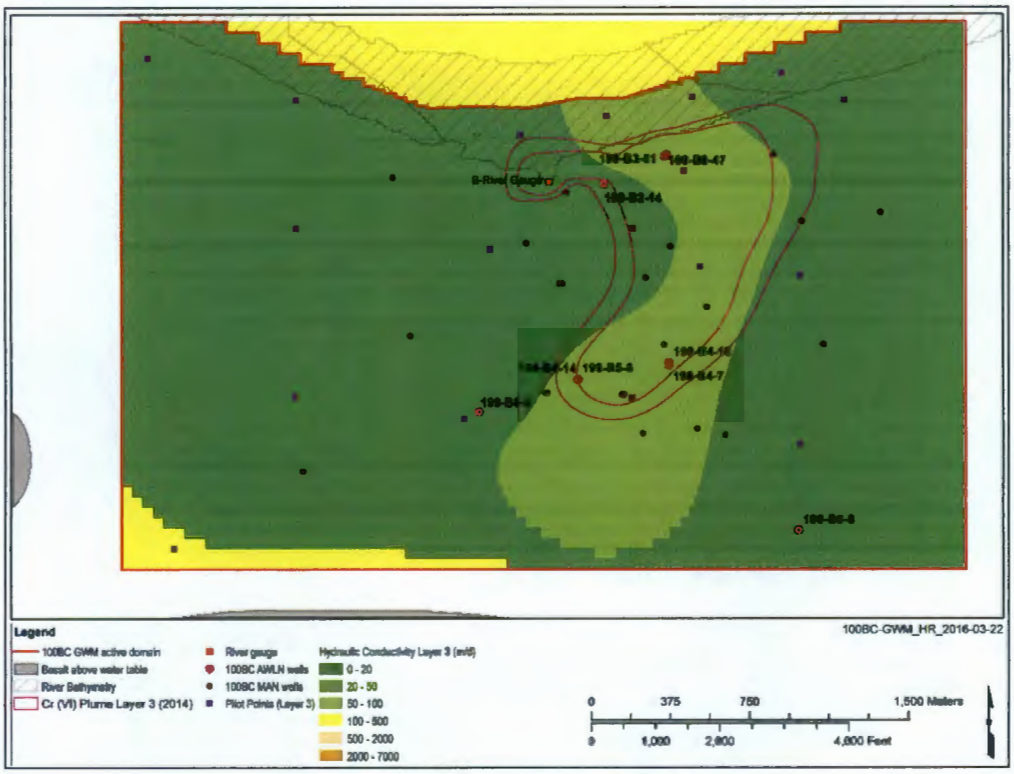

Figure 3-28 Layer 3 Hydraulic Conductivity

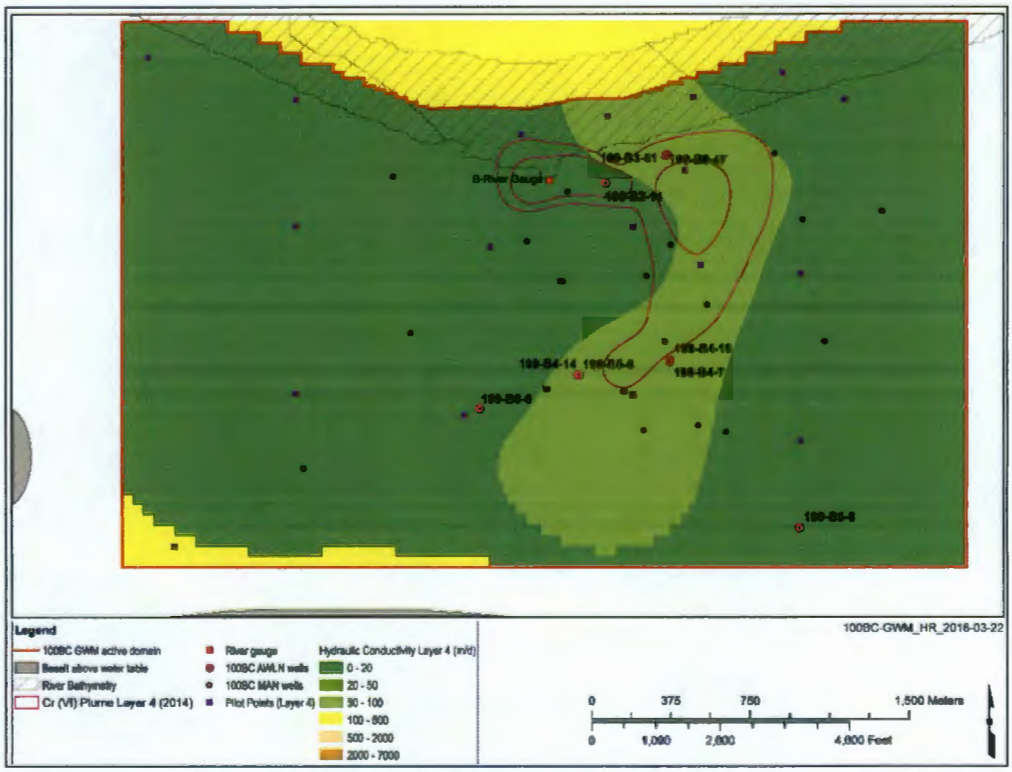

Figure 3-29 Layer 4 Hydraulic Conductivity

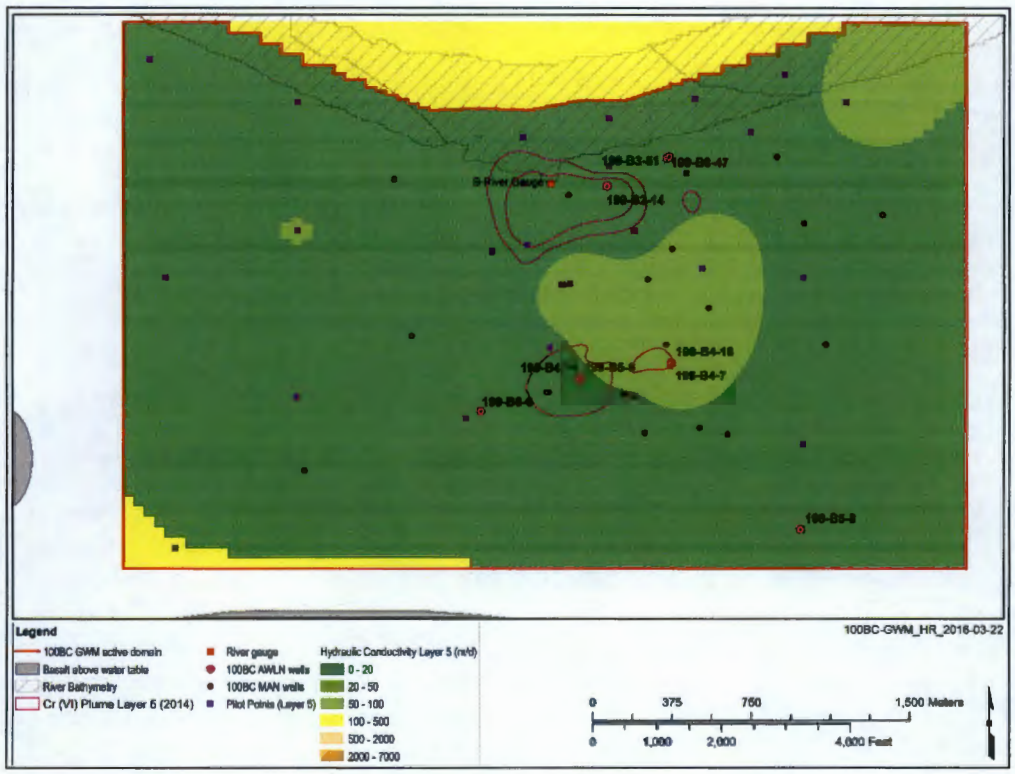

Figure 3-30 Layer 5 Hydraulic Conductivity

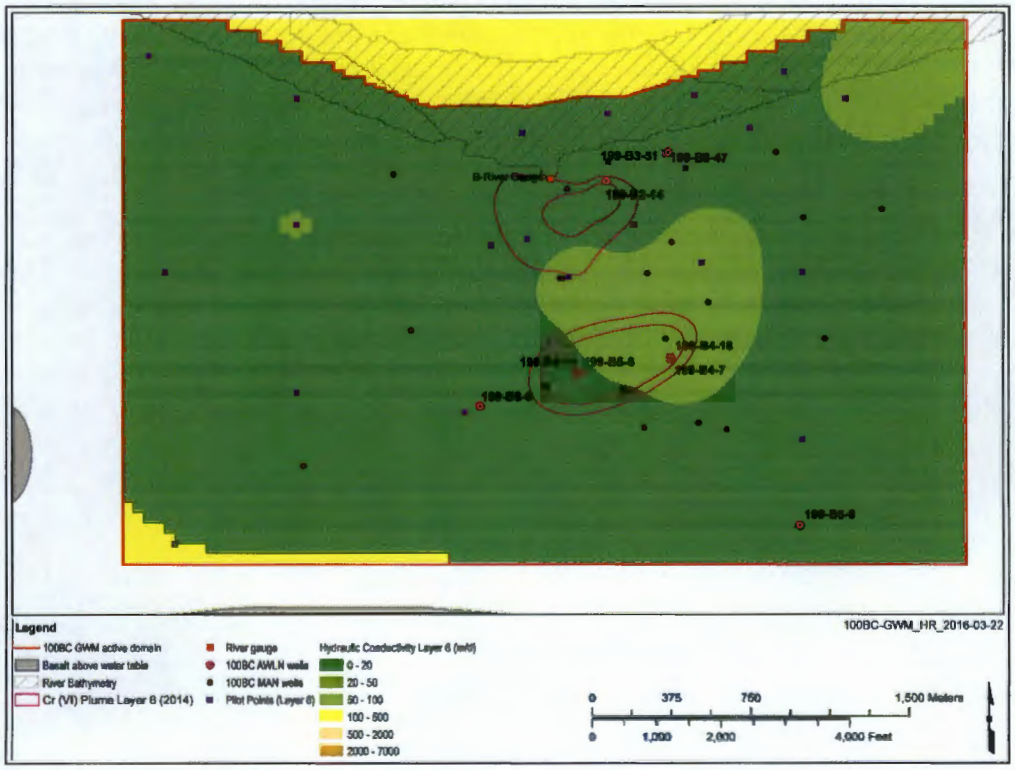

Figure 3-31 Layer 6 Hydraulic Conductivity

The simulation approach was as follows:

1. Estimate 100-C-7, 100-C-7:1, and 116-B-11 waste site 2011 mass loading by simulating a constant source from 2004 to fall 2011 and evaluating the 2011 plume. This allows accounting for hydrologic variability on plume development.
2. Estimate 100-C-7 and 100-C-7:1 late 2011-early 2012 dust control source concentration. Timing, source footprint, and source strength (mass loading) were adjusted.
3. Estimate 100-C-7 and 100-C-7:1 post excavation source strength (mass loading).
4. Implement items 1-4 in MT3DMS and the 12-year flow model.
5. Qualitatively evaluate output by comparing to annual report maps and 199-B3-47 data.
6. Repeat until sufficient qualitative match obtained.

Data used to compute estimated mass loading included Cr(VI) soil concentration, leaching rate coefficient, and flow rate. The source term is primarily conceptualized to be located in the PRZ which has much higher leaching coefficients than the saturated zone (ECF-100BC5-16-0028). A leach rate of 2 $x10^{-4}$ mg/d per 1 mg Cr(VI)/kg soil per mm/yr of flow was used for both 100-C-7:1/100-C-7 and 116-B-11 waste sites. Initial hexavalent chromium soil concentration of 15.75 and 20.5 mg/kg was used for 116-B-11 and 100-C-7:1, respectively. The value for 100-C-7:1 is within the range of 10 to 40 mg/kg observed by PNNL in the PRZ (PNNL-21845). A recharge rate of 63 mm/yr was the assumed flow rate. These parameters resulted in 11 and 1 kg/d of Cr(VI) delivered to the aquifer from 100-C-7/100-C-7:1 and 116-B-11 prior to October 2011, respectively. From October 2011 through January 2012 mass loading from 100-C-7:1/100-C-7 was increased by a factor of 9 to produce a simulated area above 48 µg/L comparable to map in the fall 2012 annual report (DOE/RL-2013-22, Rev. 0). After January 2012 the mass loading rate was reduced below the initial value to reflect source removal. At the time this work (December 2015) was conducted the plume had not clearly stabilized to reflect new conditions at 100-C-7:1/100-C-7 and residual source half of the 2011 estimate was used such that it could clearly be seen to be contributing to the plume in fall 2015 was implemented.

3.5.2 Transport Calibration Results

Figure 3-32 through Figure 3-36 show the results of Cr(VI) qualitative transport calibration.
The 100-C-7:1 and 116-B-11 waste sites were source areas. Other waste sites were considered as potential sources, but ultimately not used. Waste site 118-C-1 (105-C solid waste burial ground) was considered as a potential source creating the eastward extent of the plume, but was rejected because the waste consisted primarily of debris. The number of WIDS Cr(VI) sites is extensive, and it is possible that as the plume attenuates further other waste sites may be seen to be contributing to groundwater contamination.

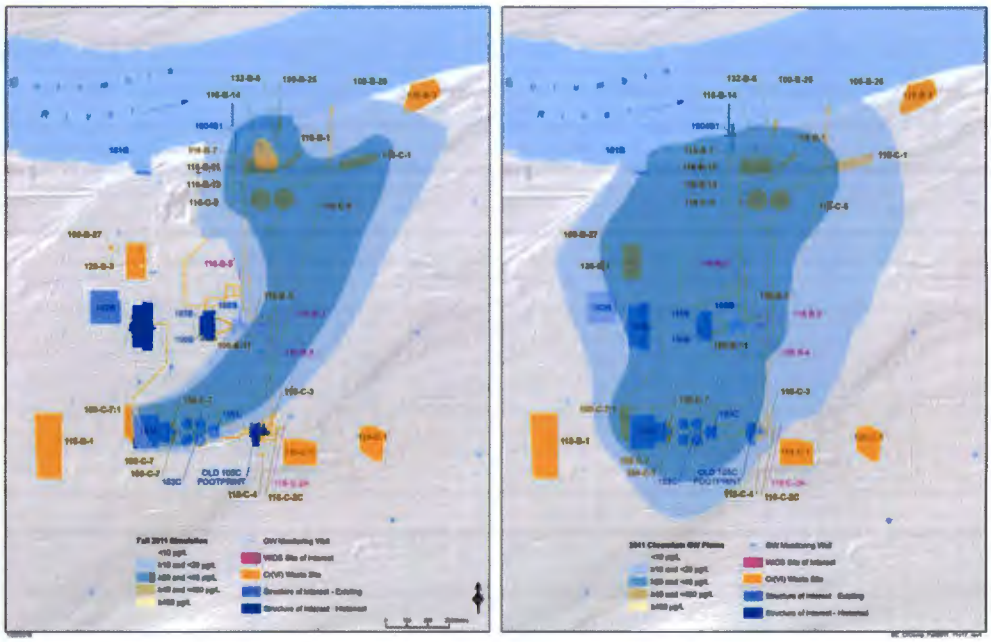

Figure 3-32. Simulated (left) and Mapped (right) Chromium Plume at the Top of the Unconfined Aquifer, Fall 2011 (DOE/RL-2010-96, Draft A)

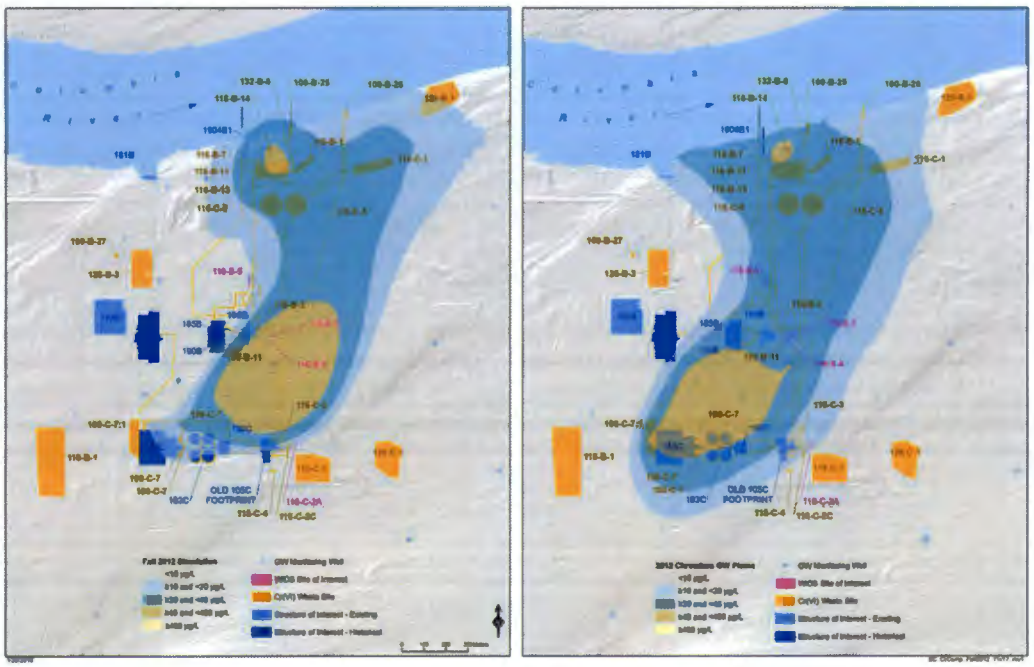

Figure 3-33. Simulated (left) and Mapped (right) Chromium Plume at the Top of the Unconfined Aquifer, Fall 2012 (DOE/RL-2013-22, Rev. 0)

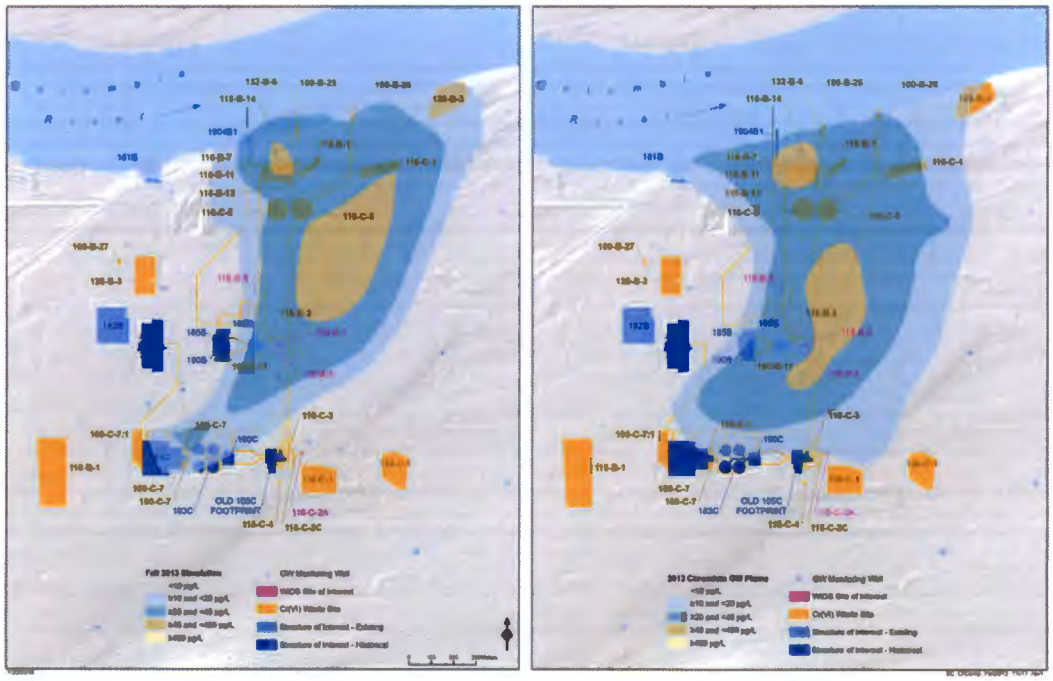

Figure 3-34. Simulated (left) and Mapped (right) Chromium Plume at the top of the Unconfined Aquifer, Fall 2013 (DOE/RL-2014-32, Rev. 0)

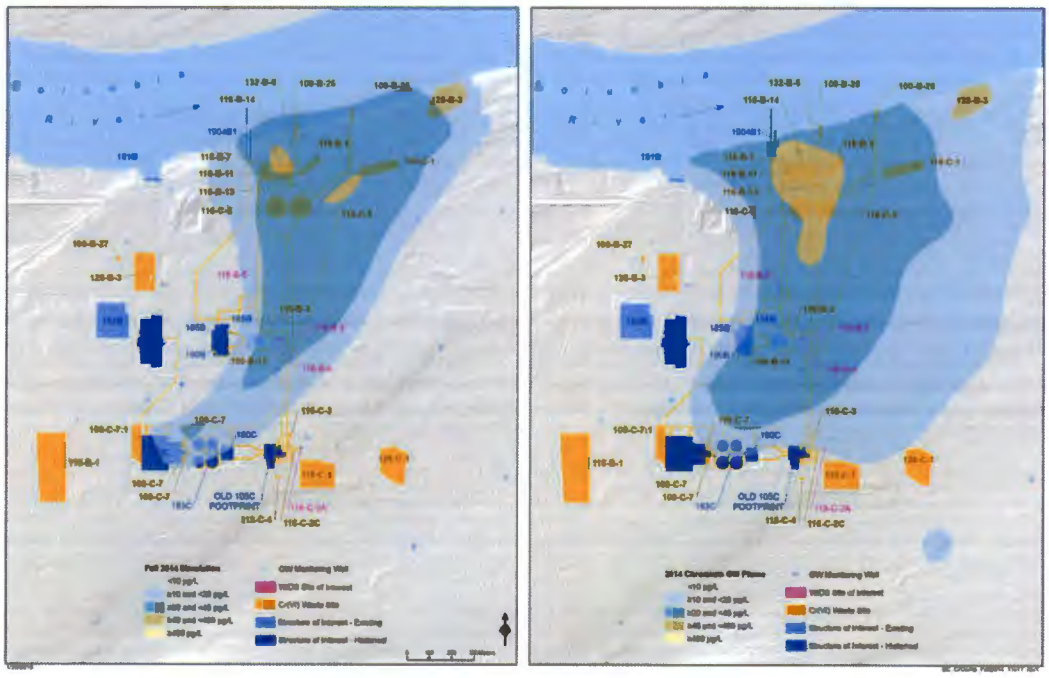

Figure 3-35. Simulated (left) and Mapped (right) Chromium Plume at the top of the Unconfined Aquifer, Fall 2014 (DOE/RL-2015-07, Rev. 0)

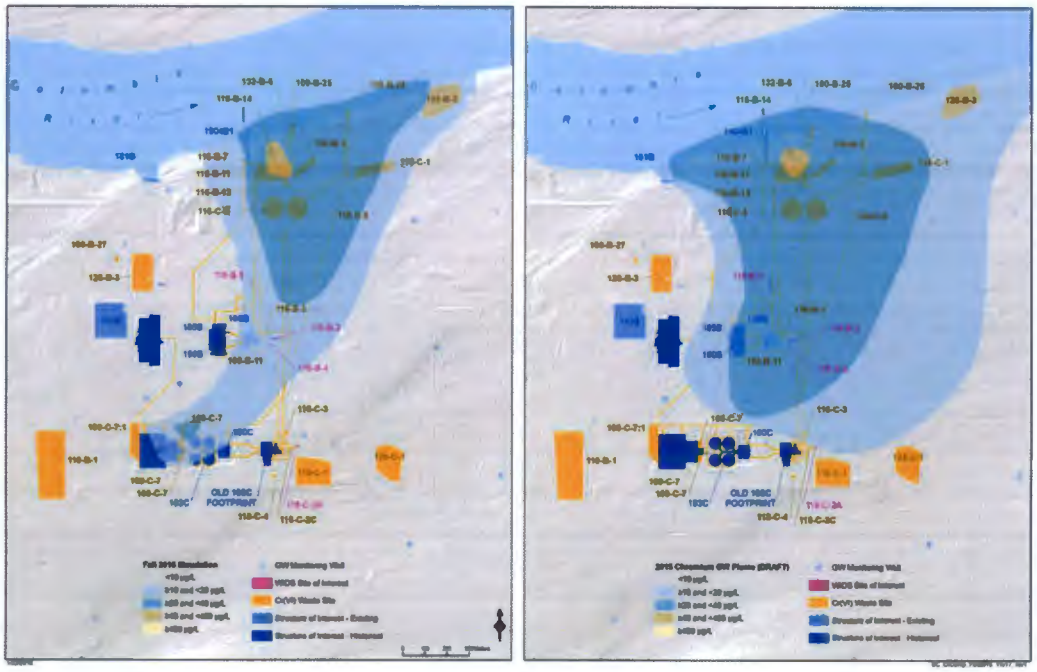

Figure 3-36 Simulated (left) and Mapped (right) Chromium Plume at the top of the Unconfined Aquifer, Fall 2015 (Mary Hartmann, personal communication, November 5, 2015)

The mass loading rate is the product of the flow rate through the PRZ, leaching rate coefficient, and soil concentration; the impact of mass loading on aquifer concentrations depends on the groundwater flow rate - all these terms have associated uncertainty. These uncertainties are confounding.

Given that the major focus of the RI/FS is on ameliorating contaminant discharge to the Columbia River further evaluation of relevant data and model behavior is important to understand potential limitations of forecasts with respect to the river. The Columbia River RI Report (WCH-380, 2010) reported areas of inferred groundwater discharge to the riverbed by mapping contrasts in temperature and specific conductance. Upwelling occurred on both sides of the river; the northern discharge is from Grant County aquifers. The deep pool by the 100-BC water intake structure had the strongest contrast indicating preferential discharge in this area. Figure 3-37 shows the simulated Cr(VI) no further action plume at the top of the unconfined aquifer along with data from WCH-380. The riverward extent of simulated Cr(VI) discharge compares well with the data, thus increasing confidence that the simulation results are properly representing the relationship between the aquifer and river.

3.6 No Further Action Cr(VI) Forecasts

The soil concentrations obtained from the post dust-control period for waste sites 100-C-7 and 100-C-7:1 were used for no further action forecasts. The soil concentration estimated for waste site 116-B-11 was not changed over time, and the value was used in the no further action forecasts. Because the no further action forecast is over a much longer period than the transport calibration the long-term reduction in the leachability of the Cr(VI) contaminated soil must be considered as described in ECF-100BC5-16-0028. The curve is given in terms of pore volume flushed ,which was converted into elapsed time in years by assuming a 63 mm/yr recharge rate, moisture content of 0.08, and a thickness of 1 m to give an estimated time to flush one pore volume of 1.3 years. The curve is shown in Figure 3-38. This factor multiplies the leaching rate coefficient of 2×10^{-4} estimated from transport calibration. This factor has immediate

consequences on computed concentrations. Concentrations of Cr(VI) at 199-B3-47 are currently on the order of 50 µg/L, and reducing the leaching rate coefficient by 10 percent after about 5 years (2020) would result in a concentration of about 45 µg/L assuming no other up gradient sources were contributing.

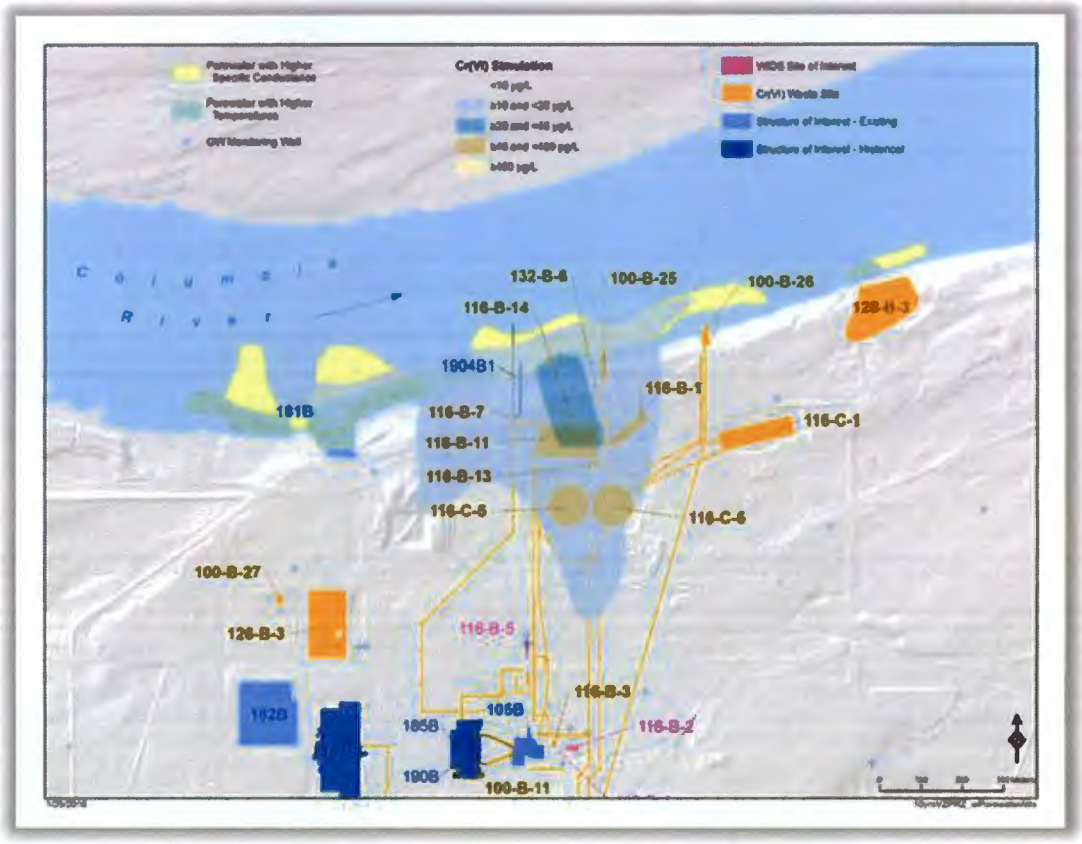

Figure 3-37. Simulated 2025 Cr(VI) Upper Unconfined Aquifer Plume and WCH-380 Porewater Data

The no further action case was simulated for 125 years beginning in January, 2015. The maximum aquifer concentration in each model layer over time is shown in Figure 3-39, and the length of shoreline with concentrations above several thresholds is shown in Figure 3-40. In both cases the overall trend is downward to lower concentrations and less river impact as the chromium source is depleted and becomes less accessible over time. The maximum aquifer concentration drops below the drinking water standard after about 15 years (calendar year 2030). The slow migration of deep Ringold contamination is reflected in model layer 6 concentrations, which despite the absence of a source have nearly the same magnitude as the upper unconfined aquifer after 80 years. The aquifer concentration decline is directly reflected in the length of impacted shoreline, only shown for 60 years (year 2075) because there is no impact at longer times. At no time is there any shoreline with concentrations greater than drinking water standard.

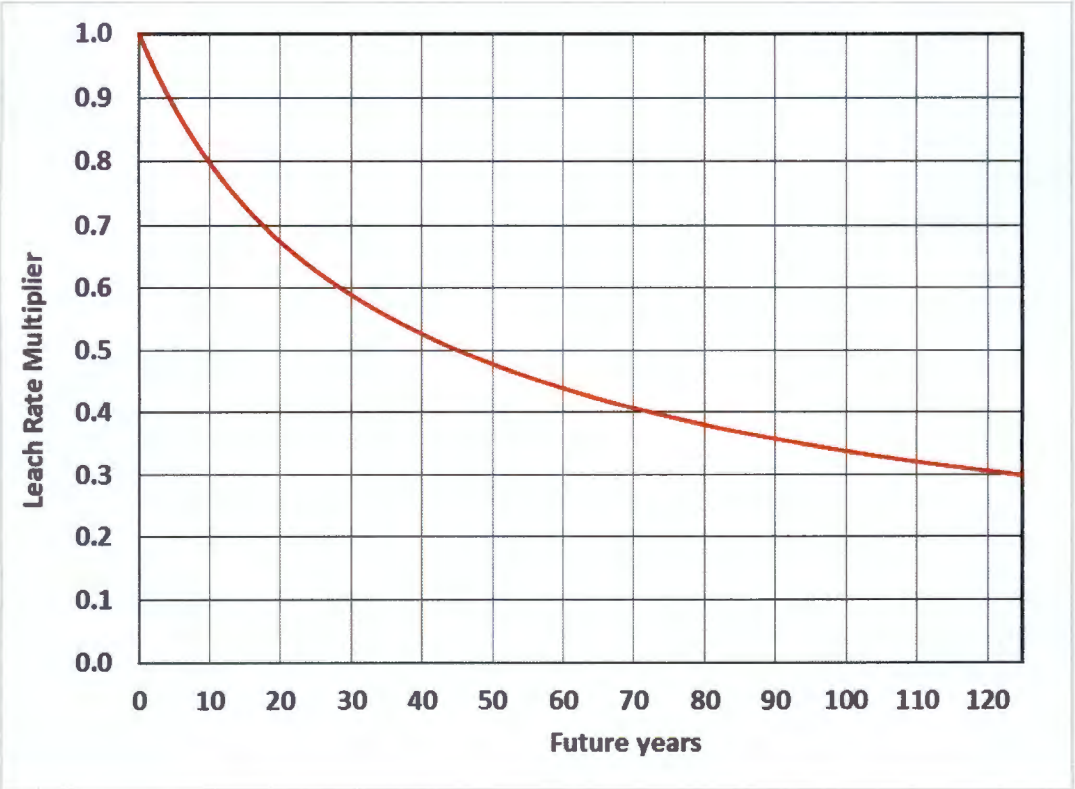

Figure 3-38. Leach Rate Constant Multiplier to Quantify the Declining Source Strength for Release of Cr(VI)

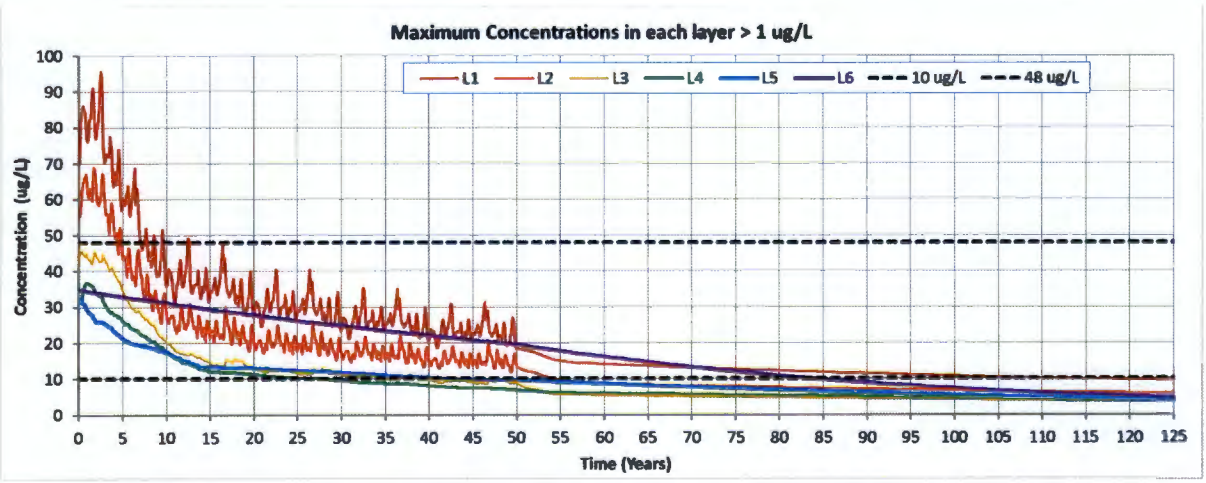

Figure 3-39. Maximum Simulated Cr(VI) Concentration by Model Layer over 125 Years - No Further Action Case

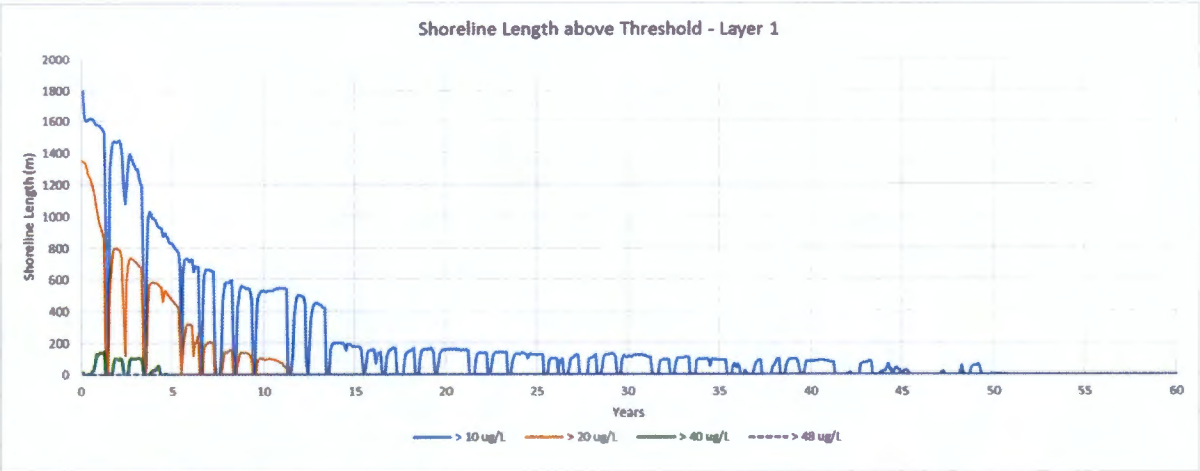

Figure 3-40. Shoreline Length above Selected Thresholds-No Further Action Case

The gradual decline forecast in plume concentrations over the next 60 years is shown in Figure 3-41 through Figure 3-44. By 2075 there is very little plume extent, and this extent continues to diminish until concentrations are below 10 ug/L everywhere after about 110 years.

Figure 3-41. Simulated 2020 Cr(VI) Plume Extents in Model Layers 1 and 6 - No Further Action Case

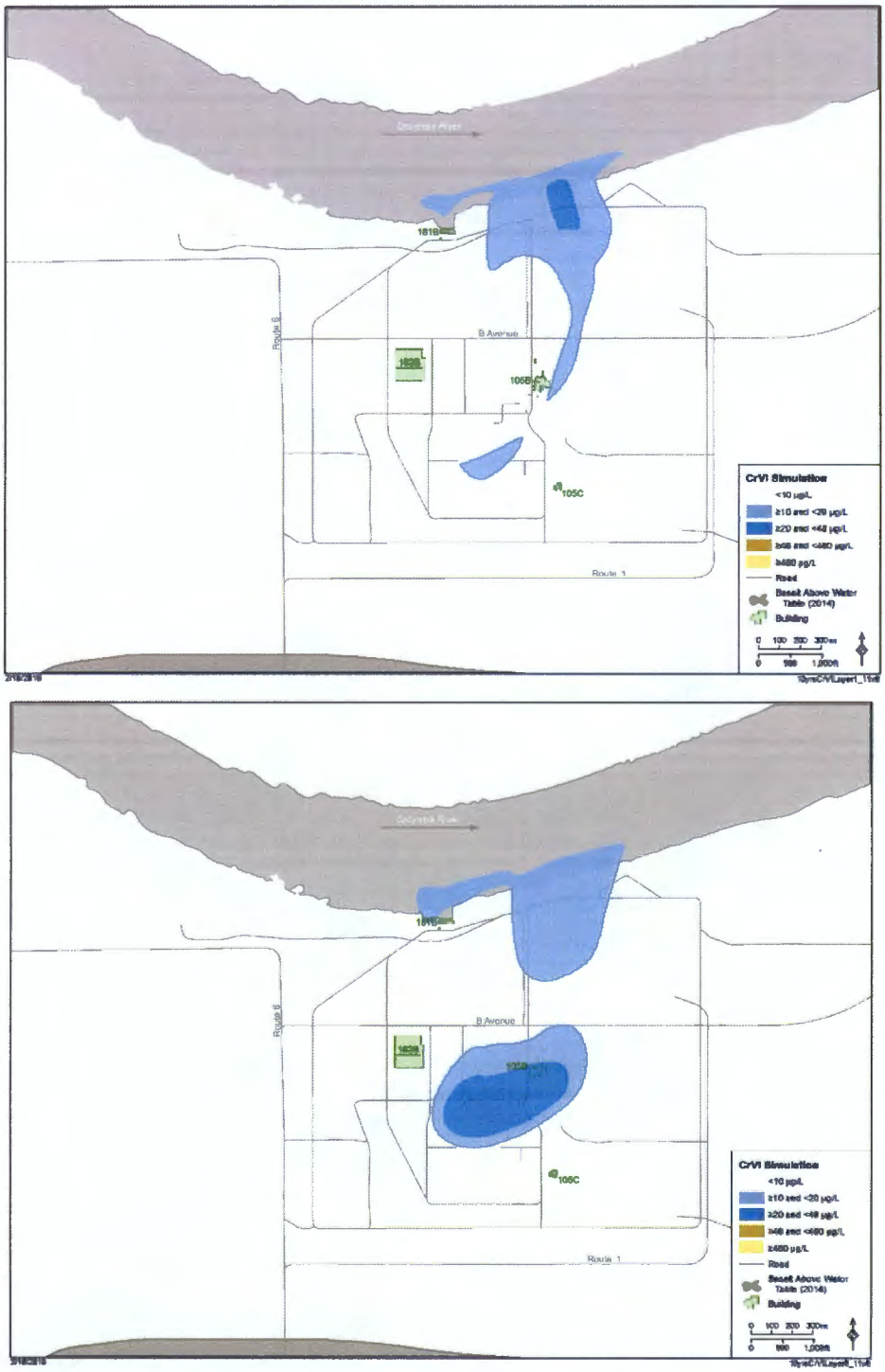

Figure 3-42. Simulated 2025 Cr(VI) Plume Extents in Model Layers 1 and 6 - No Further Action Case

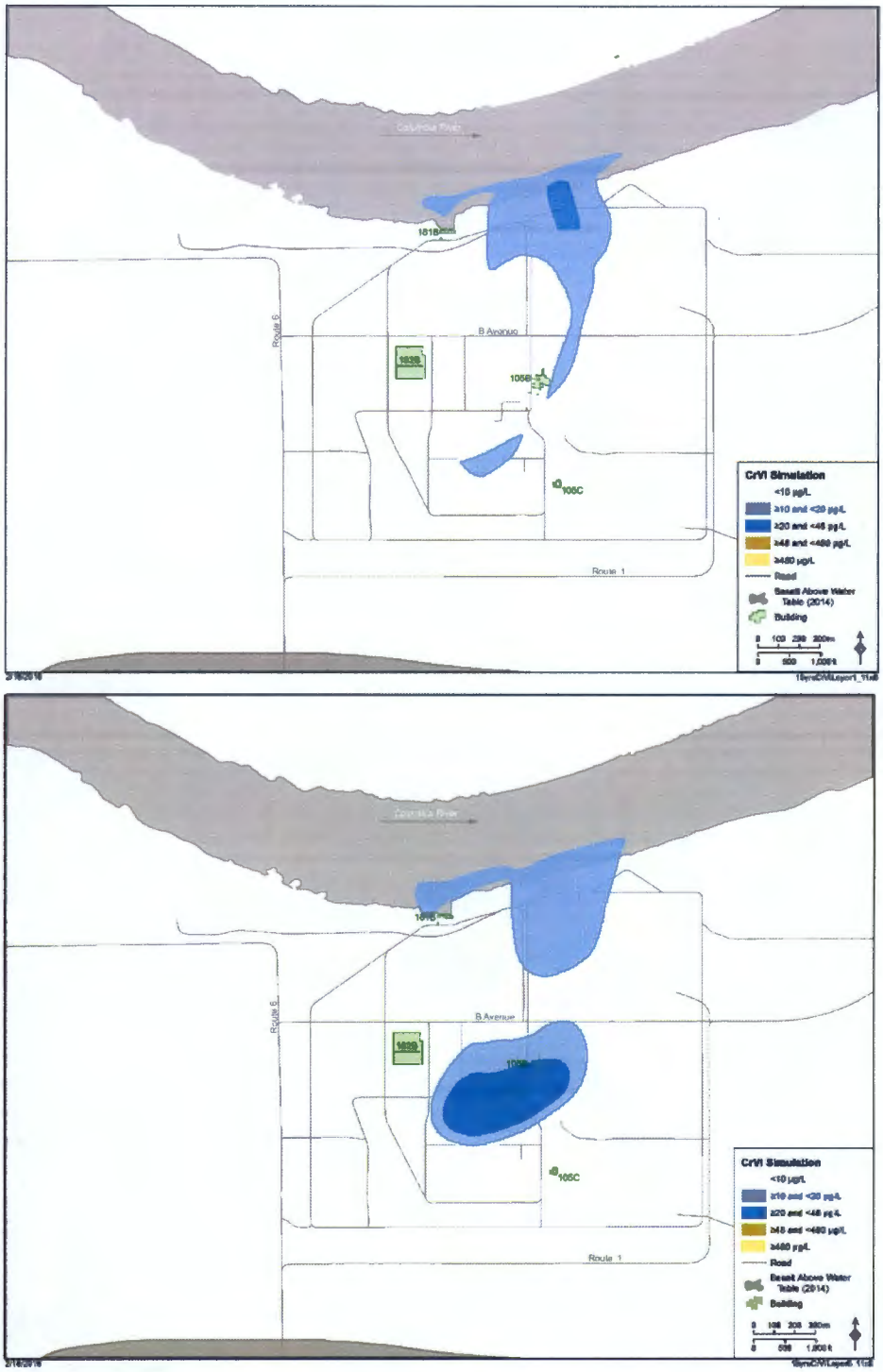

Figure 3-43. Simulated 2040 Cr(VI) Plume Extents in Model Layers 1 and 6 - No Further Action Case

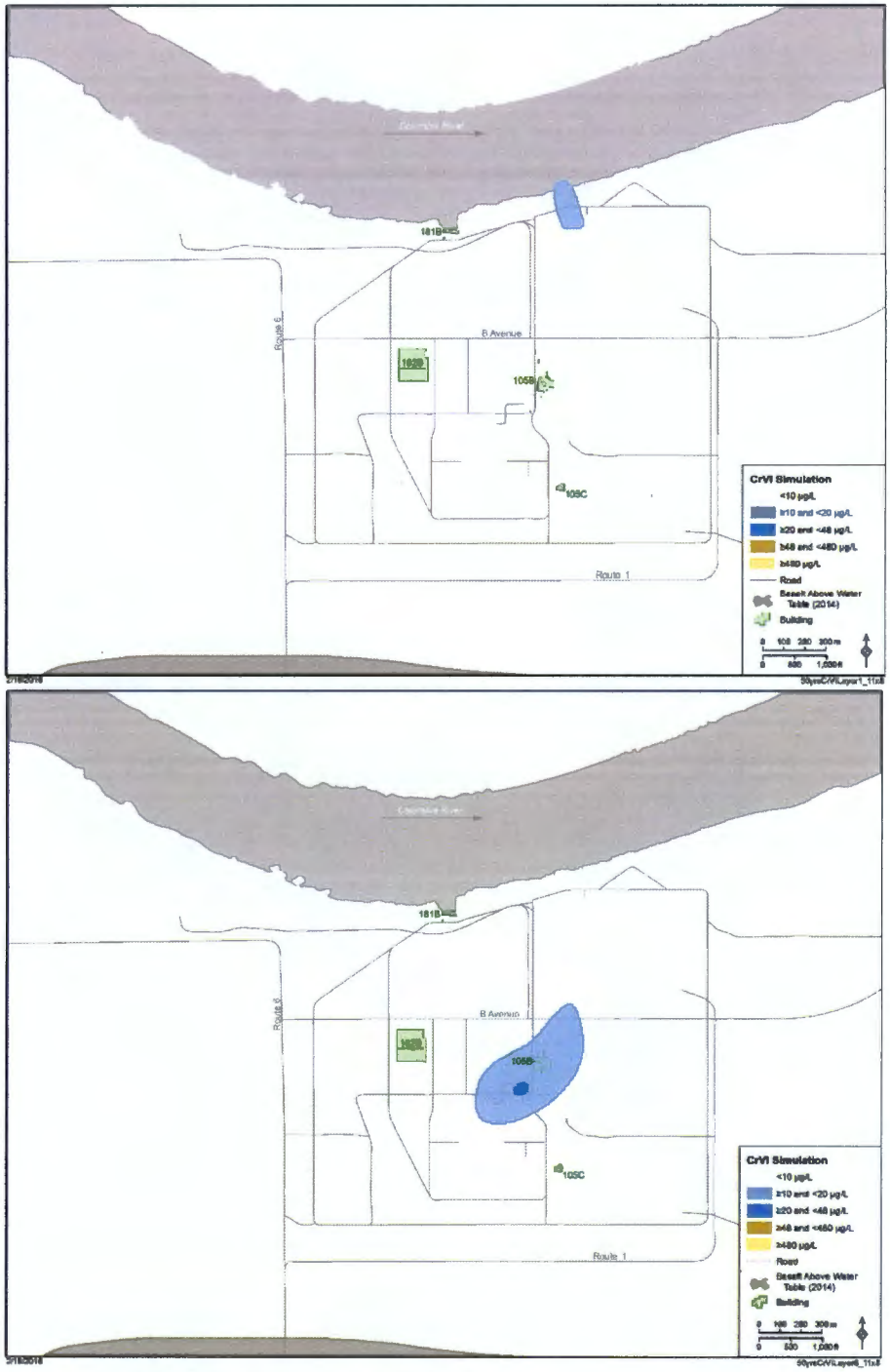

Figure 3-44. Simulated 2065 Cr(VI) Plume Extents in Model Layers 1 and 6 - No Further Action Case

4 Model Sensitivity and Uncertainty Analysis

4.1 Sensitivity Analysis

As part of its parameter estimation algorithm PEST computes first derivatives of all adjustable model parameters. Thus, sensitivity analysis was iteratively conducted during model calibration.
These derivatives are local parameter sensitivity that can also be analyzed to gain insight into important parameters near the calibrated values.

The IDENTPAR utility (part of PEST suite of software) was also used to assess model parameters. Parameters with a higher value are more informed by the calibration data. Strongly identifiable model hydraulic parameters (Figure 4-1) include specific storage (ss1), specific yield (sy1), Hanford and Ringold E formation river bed hydraulic conductivity (rivhf, rivre), and pilot points 5, 6, 7, 35, and 37 located in the 3 point problem defined by 199-B4-14, B8-6, and B5-8. All other parameters with higher identifiability values are related to the lateral general head boundary parameterization including the boundary conductance, and regression factors that relate the GHB head to Columbia River stage.

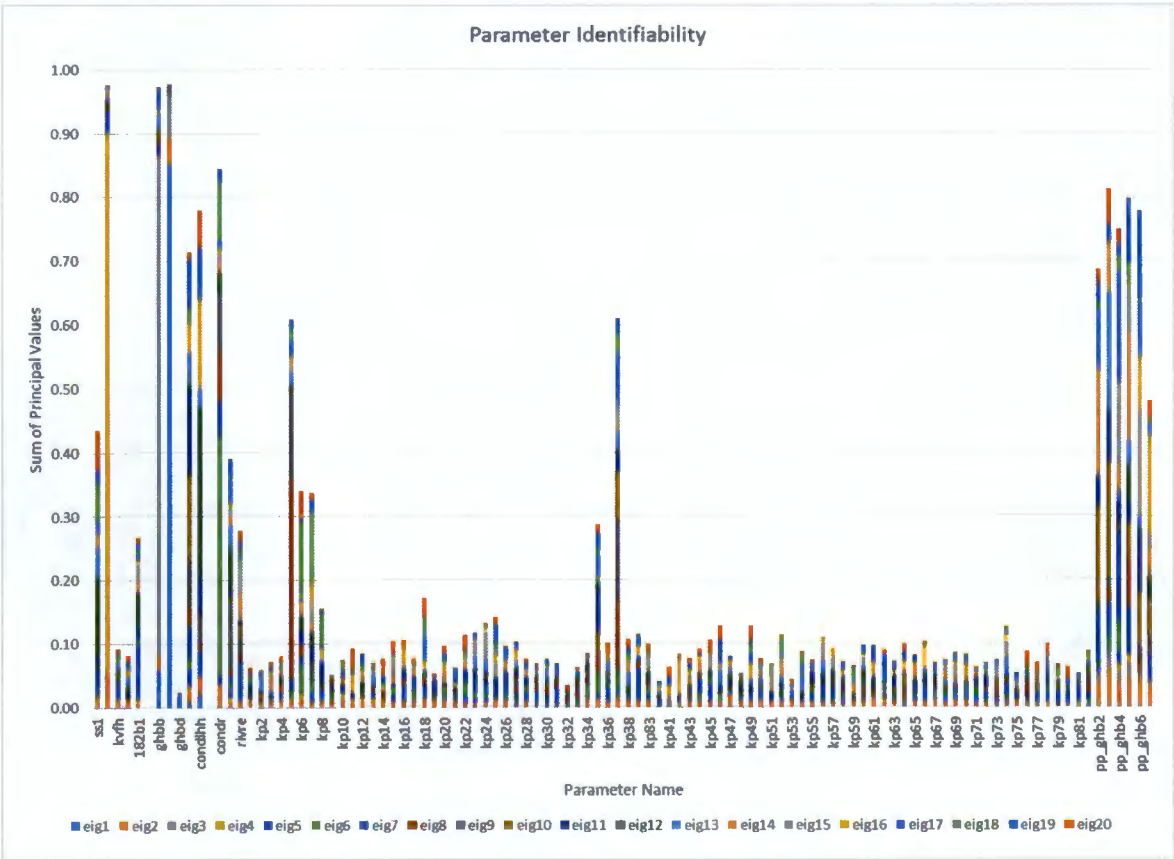

Figure 4-1. Flow Model Parameter Identifiability

The range of values for hydraulic conductivity is shown in Figure 4-2. Note the two distributions do not overlap, and are quite distinct. Comparing this figure to Figure 2-6 and Figure 2-7 shows that the lower values are comparable to observed, as are the ranges. The Ringold E has a smaller range than Hanford. Many of the Hanford values are above 1,000 m/yr, which is consistent with new geologic data showing the presence of cataclysmic flood gravels over a larger area than previously thought.

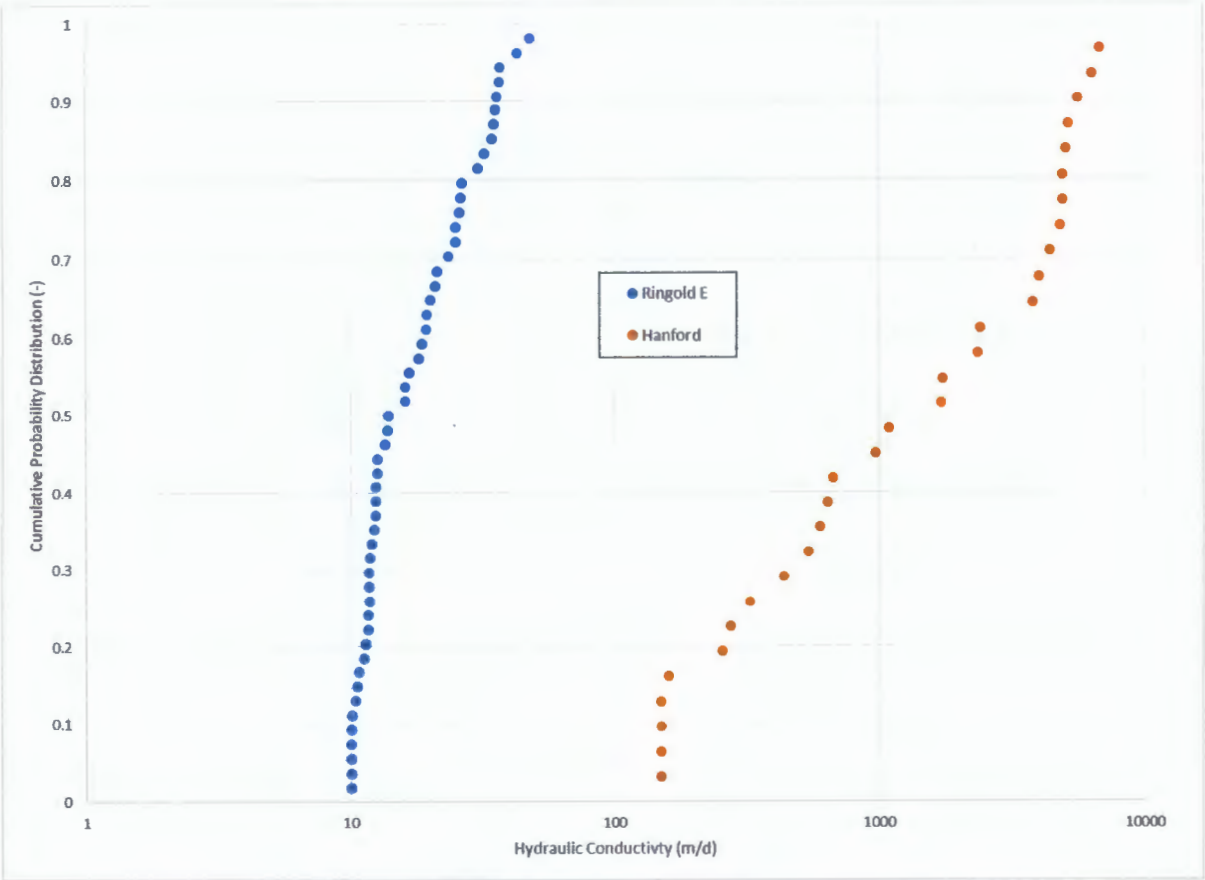

Figure 4-2. CDF of Calibrated Hanford and Ringold E Hydraulic Conductivity Pilot Points

4.2 Uncertainty Analysis

Bredehoeft (2005) suggests that selecting the proper conceptual model (that is, addressing conceptual model uncertainty) is a major problem in groundwater modeling analysis. He suggests that this can be overcome by collecting as much data as feasible using all applicable methods, and by leaving the conceptual model open to change. By using many types of groundwater data, including hydraulic head, velocity estimates, Cr(VI) concentrations associated with the 100-C-7:1 release, trends in ^{90}Sr concentrations, knowledge of source areas, and groundwater discharge patterns to the river uncertainty has been reduced, but is difficult to quantify. The broad source strengths and locations have been inferred from groundwater monitoring and historical waste-site knowledge. However, because the interval of this observation (about the last 15 years or less) is much less than the long-term forecasts required in the RI/FS process uncertainty remains.

Diffusion of solute into stagnant zones (not considering sorption) can result in significant tailing of concentrations. That is, solute is not flushed as fast as anticipated based on the properties of the formation resulting in persistent concentrations above MCL. Suthersan et al. (2009) discuss scale issues with plumes including geologic factors such as paleochannels and changes in depositional environments. Additionally, they observe that plume maps are typically interpreted using a conceptual model of transport in homogeneous media resulting in relatively smooth concentrations. Field observation has shown that most flow and contaminant flux occurs through the most permeable parts of formations. This can result in advection in some areas and diffusion in others, at greatly differing time scales. This conceptual model is

known as the dual-domain non-equilibrium model (Suthersan et al., 2013). PNNL-21845 identified local-scale heterogeneities beneath 100-C-7:1 that may lead to large-scale preferential flow paths and potentially the presence of a dual-domain effect. Because of the relatively rapid groundwater flow at 100-BC the next several years of groundwater quality data should be useful in detecting the process.

This page intentionally left blank.

5 Model Limitations

The 100-BC GWFTM was built for the specific purpose of assessing groundwater remediation options in a small area near the former B and C reactors. It was calibrated using head data from 2012 through July 2014, and further evaluated with data from 2006 through 2014. Future conditions that dramatically deviate from these may impair its accuracy. Such conditions may occur when the Columbia River Treaty between Canada and the United States is revised in 2024 – as of 2015 both countries have expressed interest in maintain, but revising the treaty (http://www.crt2014-2024review.gov/Default.aspx). The spatial parameterization technique that was used is flexible and allows for non-uniform properties, but it employs a smoothness constraint to limit extrapolation in areas with little information. As new data is collected conceptual understanding and its associated quantitative representation will change to an unknown degree. The model was also built assuming isothermal constant-density groundwater flow and transport. A qualitative transport calibration was carried out by comparing transport simulation results to annual interpretive plume maps. Any errors or data gaps in these maps will be included in the model results, and features that cannot be independently identified cannot be included in the computations.

The NRC (2007) stated that while models are useful tools, they have innate limitations including:

- Computational limitations, assumptions, and knowledge gaps.
- Used to describe important, complex, and poorly characterized problems.
- Models in the regulatory process are best seen as tools providing inputs, as opposed to "truth-generating machines".

Anderson and Lu (2003) compared a pump-and-treat system capture zone as modeled to actual system performance and found that even with some error the model contributed positively to the system design. Thus, in spite of these limitations the 100-BC GWFTM can contribute to decisions about the site.

This page intentionally left blank.

6 Model Configuration Management

The model described in this model package report is uniquely designated as the "100-BC Groundwater Flow and Transport Model" and in abbreviation form as the "100-BC GWFTM".

Version control for this model will conform to the following version numbering convention:

- 100-BC GWFTM Version #.#
  - The first version index will match the sequential calibrations of this model (first calibration = 1, second calibration =2, etc.).
  - The second version index will be used to denote a model modification, in terms of key hydraulic or structural parameters have been changed for specific purposes, without recalibration of the model. The second index is not applied to variations in model stresses (for example, pump-and-treat rate changes or modification of future recharge rate scenarios applied as a boundary condition).

For example, Model Version 1.0 is used to designate the first calibration and release of the 100-BC GWFTM. Similarly, Model Version 2.1 would refer to (as an example) the second calibration of this model, with a subsequent variation in a physical characteristic determined not to require re-calibration.

Note that individual simulations (or applications) are separately configuration controlled following the guidance provided in Appendix G of CHPRC-00189. Changes in model stresses (e.g., pump-and-treat system injection and extraction rates) are not tracked as model changes because these have no impact on model calibration; these are properly the subject of an ECF; model files for evaluation of changes in model stressed will be archived in the EMMA Application bin, indexed by ECF number.

As required by Appendix G of CHPRC-00189, all inputs and outputs for the development of this model will be committed to EMMA to maintain and preserve this configuration-managed basis of this model. Basis information (that information collected to form the basis for model input parameterization; e.g., historical pump-and-treat rates) is also stored in the EMMA for traceability purposes.

The software used to implement this model, CHPRC Build 7 of MODFLOW-2000, is configuration managed as discussed in Section 3.1. Configuration-managed software is obtained from the Hanford Site MKS Integrity™ configuration management system as required by CHPRC-00258.

6.1 Version History

Table 6-1 provides the version history of the 100-BC GWFTM.

Table 6-1 Version History of the 100-BC GWFTM

Version	Date Released	Calibration	Modification	MPR Revision
1.0	21 Mar 2016	Initial	Baseline	0

This page intentionally left blank.

7 Model Recommendations

The following are recommendations for maintaining and improving the 100-BC GWFTM:

1. Use of the AWLN data in model calibration assisted in better definition of aquifer transmissivity. More AWLN data has been collected in additional wells that could not be incorporated due to time constraints. It would be helpful to update the model with this data to improve the transmissivity distribution and resulting groundwater velocity. This would also be useful in years to come for evaluating the remedy performance.

2. An additional constraint useful for building confidence was the qualitative transport assessment using 2011 through 2015 mapped plumes. Given the groundwater velocity at 100-BC future comparisons – even quantitative combined flow and transport calibration–would help build confidence in forecasts.

3. The Columbia River Basin Treaty will be renegotiated in 2024. This will result in changes to river operation. The impact of these changes on the groundwater system and associated remedies should be evaluated as they occur in order to ensure regulatory goals are met.

This page intentionally left blank.

8 References

Aero-Metric LiDAR, 2008, RCCC-Hanford Battelle/PNNL/DOE, Digital Orthophotography & LiDAR Surveys Photogrammetric Report, prepared by Aero-metric, Seattle, Washington.

Anderson, P. and S. Lu, 2003, A Post Audit of a Model-Designed Ground Water Extraction System, Groundwater, Vol. 41, No. 2, pp. 212-218.

Avon, L., and J.D. Bredehoeft, 1989. "An analysis of trichloroethylene movement in groundwater at Castle Air Force Base, California". Journal of Hydrology, Vol. 110, p. 23-50.

Bear, J., 1972. Dynamics of Fluids in Porous Media. New York, NY: Elsevier Pub. Co.

Bear, J., and A. Verruijt, 1990. Modeling Groundwater Flow and Pollution. Reidel (Dordrecht).

CH2M Hill, 2014. Hanford Site Groundwater Monitoring Report for 2013. DOE/RL-2014-32, Rev. 0.

Chapelle, F.H., 1986. "A solute-transport simulation of brackish-water intrusion near Baltimore, Maryland". Ground Water, Vol. 24, no. 3, p. 304-311.

Chiang, C.Y., J.P. Salanitro, E.Y. Chai, J.D. Colthart, and C.L. Klein, 1989. "Aerobic biodegradation of benzene, toluene, and xylene in a sandy aquifer – Data analysis and computer modeling". Ground Water, Vol. 27, no. 6, p. 823-834.

D'Alessandro, M., F. Mousty, G. Bidoglio, J. Guimera, I. Benet, X. Sanchez-Vila, M.G. Gutierrez, and A.Y. De Llano, 1997. "Field tracer experiment in a low permeability fractured medium: Results from El Berrocal site". Journal of Contaminant Hydrology, Vol. 26, p. 189-201.

DOE/RL-95-111, 1997, *Corrective Measures Study for 100-NR-1 and 100-NR-2 Operable Units*, Rev. 0, U.S. Department of Energy, Richland Operations Office, Richland, Washington. Available at: http://www2.hanford.gov/arpir/?content=findpage&AKey=D198056722.

DOE/RL-96-17, 2009, *Remedial Design Report/Remedial Action Work Plan for the 100 Area*, Rev. 6, U.S. Department of Energy, Richland Operations Office, Richland, Washington. Available at: http://www5.hanford.gov/arpir/?content=findpage&AKey=0095436.

DOE/RL-2010-96, 2013, *Remedial Investigation/Feasiblity Study for the 100-BC-1, 100-BC-2, and 100-BC-5 Operable Units, Working Draft A*, U.S. Department of Energy, Richland Operations Office, Richland, Washington.

DOE/RL-2011-50, 2012, *Regulatory Basis and Implementation of a Graded Approach to Evaluation of Groundwater Protection*, Rev. 1, U.S. Department of Energy, Richland Operations Office, Richland, Washington. Available at: http://www5.hanford.gov/arpir/?content=findpage&AKey=0093361.

DOE/RL-2013-22, 2013, *Hanford Site Groundwater Monitoring Report for 2012, Rev. 0*, U.S. Department of Energy, Richland Operations Office, Richland, Washington.

DOE/RL-2014-32, 2014, *Hanford Site Groundwater Monitoring Report for 2013*, Rev. 0, U.S. Department of Energy, Richland Operations Office, Richland, Washington.

DOE/FL-2015-07, 2015, *Hanford Site Groundwater Monitoring Report for 2014*, Rev. 0, U.S. Department of Energy, Richland Operations Office, Richland, Washington.

Doherty, J., 2003. "Ground Water Model Calibration Using Pilot Points and Regularization." In Groundwater, v. 41 (2): pp. 170-177

Domenico, P.A., and G.A. Robbins, 1985. "The displacement of connate water from aquifers". Geol. Soc. Am. Bull., Vol. 96, p. 328-335.

ECF-Hanford-13-0020, *Process for Constructing a Three-dimensional Geological Framework Model of the Hanford Site,100 Area,* Prepared for the U.S. Department of Energy Assistant Secretary for Environmental Management, CH2M Hill Plateau Remediation Company, Richland, WA.

Engesgaard, P., K.H. Jensen, J. Molson, E.O. Frind, and H. Olsen, 1996. "Large-scale dispersion in a sand aquifer: Simulation of subsurface transport of environmental tritium". Water Resources Research, Vol. 32, no. 11, p. 3253-3266.

Ferris, J. G., 1963, "Cyclic Water-Level Fluctuations as a Basis for Determining Aquifer Transmissibility," in R. Bentall (compiler), "Methods of Determining Permeability, Transmissibility, and Drawdown," U.S. Geological Survey Water-Supply Paper 1536-I, Washington, D.C.,pp. 305-318.

Flach, G.P, S.A. Crisman, and F.J. Molz, III. 2004. Comparison of Single-Domain and Dual-Domain Subsurface Transport Models, *Groundwater*, v. 42, no. 6, pp815-828.

Flach, G.P. 2012. Relationship Between Dual-Domain Parameters and Practical Characterization Data, *Groundwater*, v. 50, no. 2, pp. 216-229.

Freeze, R.A., and J.A. Cherry, 1979, Groundwater. Englewood Cliffs, NF: Prentice Hall.

Gee, G.W., Fayer, M.J., Rockhold, M.L., Campbell, M.D., 1992, Variations in Recharge at the Hanford Site, Northwest Science, Vol. 66, No. 4, pg. 237-250.

Gee, G.W., J.M. Keller and A.L. Ward, 2005, *Measurement and Prediction of Deep Drainage from Bare Sediments at a Semiarid Site,* Vadose Zone Journal, Vol. 4, No. 1, p. 9.

Gee, G.W., M. Oostrom, M.D. Freshley, M.L. Rockhold, and J.M. Zachara, 2007, *Hanford Site Vadose Zone Studies: An Overview*, Vadose Zone Journal, Vol. 6, No. 4, pp. 899-905.

Gelhar, L.W., C. Welty, and K.R. Rehfeldt, 1992, "A critical review of data on field-scale dispersion in aquifers." Water Resources Research, Vol. 28, no. 7, p. 1955-1974.

Greenkorn, R.A., 1983,"An analytical solution for solute transport through fractured media with matrix diffusion." Journal of Hydrology, Vol. 52, p. 47-52.

Hajek, B.F., 1966, Soil Survey Hanford Project in Benton County Washington, AEC Research and Development Report, Pacific Northwest Laboratory, Richland, Washington.

Harbaugh, A. W., E. R. Banta, M. C. Hill, and M. G. McDonald, 2000, *MODFLOW 2000, The U.S. Geological Survey Modular Ground-Water Model – User Guide to Modularization Concepts and the Ground-Water Flow Process*, Open File Report 00-92, U.S. Geological Survey, Reston, Virginia. Available at: http://water.usgs.gov/nrp/gwsoftware/modflow2000/ofr00-92.pdf.

Himmelsbach, t. H. Hotzl, and P. Maloszewski, 1998,"Solute transport processes in a highly permeable fault zone of Lindau Fractured Rock Test Site (Germany)". Ground Water, Vol. 36, no. 5, p. 792-800.

IT Corporation, 1998. Report and Analysis of the BULLION Forced-Gradient Experiment. ITLV/13052-042. Las Vegas, NV.

Klein, KA. 2006. Contract No. DE-AC06-96RL13200 - Hanford Groundwater Modeling Integration. Letter to R. G. Gallagher. Richland, Washington, U.S. Department of Energy, Richland Operations Office.

Knudby, C., and J. Carrera. 2006, "On the Use of Apparent Hydraulic Diffusivity as an Indicator of Connectivity." In Journal of Hydrology, Vol. 329(3-4): pp. 377-389.

Konikow, L.F., 2010, *The Secret to Successful Solute-Transport Modeling*, Groundwater, Vol. 49, No. 2, pp. 144-159.

Lallemand-Barr, A., and P. Peaudecerf, 1978, "Recherche des relations entre les valeurs mesurs de la dispersivité macroscopique d'un millieu aquifére, ses autres caractistiques, et les conditions de mesure". Bull. Bur. Rech. Geol. Min. Fr., Sect. 3, p. 277-284.

Lavenue, A.M., and P.A. Domenico, 1986. "A preliminary assessment of the regional dispersivity of selected basalt flows at the Hanford site, Washington, U.S.A.". Journal of Hydrology, Vol. 85, p. 151-167.

Mas-Pla, J., T.-C.J. Yeh, J.F. McCarthy, and T.M. Williams, 1992. "A forced gradient tracer experiment in a coastal sandy aquifer, Georgetown site, South Carolina." Ground Water, Vol. 30, no. 6, p. 958-964.

National Research Council. 2007. Models in Environmental Regulatory Decision Making.Washington, DC: National Academy Press.

Newcomb, R. C. and S. G. Brown, 1961, *Evaluation of Bank Storage Along the Columbia River Between Richland and China Bar, Washington*, Geological Survey Water-Supply Paper 1539-I, U.S. Geological Survey, Washington, D.C.

Newcomb, R., J. Strand, and F. Frank, 1972, *Geology and Ground-Water Characteristics of the Hanford Reservation of the U.S. Atomic Energy Commission, Washington*, Professional Paper 717, U.S. Geological Survey, Washington, D.C. Available at: http://pubs.usgs.gov/pp/0717/report.pdf.

Neuman, S.P., 1990. "Universal scaling of hydraulic conductivities and dispersivities in geologic media." Water Resources Research, Vol. 26, no. 8, p. 1749-1758.

Neuman, S.P., 1995. "On advective transport in fractal permeability and velocity fields". Water Resources Research, Vol. 31, no. 6, p. 1455–1460.

Neuman, S.P., and V. Di Federico. 2003. "Multifaceted nature of hydrogeologic scaling and its interpretation". Rev. Geophys., Vol. 41, no. 3, p. 1014

PNL-10285, 1995, *Estimated Recharge Rates at the Hanford Site*, Pacific Northwest Laboratory, Richland, Washington. Available at: http://www.osti.gov/energycitations/servlets/purl/10122247-XORHkt/webviewable/10122247.pdf.

PNL-10899, 1996, *Strontium-90 Adsorption-Desorption Properties and Sediment Characterization at the 100 N-Area*, Pacific Northwest National Laboratory, Richland, Washington.

PNL-6403, 1987, *Recharge at the Hanford Site: Status Report*, Pacific Northwest Laboratory, Richland, Washington. Available at: http://www.osti.gov/bridge/servlets/purl/5539519-iBxaB8/5539519.pdf.

PNNL-6415, 2007, *Hanford Site National Environmental Policy Act (NEPA) Characterization*, Rev. 18, Pacific Northwest Laboratory, Richland, Washington. Available at: http://www.pnl.gov/main/publications/external/technical_reports/PNNL-6415Rev18.pdf.

PNL-6810, 1989, *The Field Lysimeter Test Facility (FLTF) at the Hanford Site: Installation and Initial Tests*, Pacific Northwest National Laboratory, Richland, Washington. Available at: http://www.osti.gov/bridge/servlets/purl/6518216-fj8Lhm/6518216.pdf.

PNL-7209, 1990, *Field Lysimeter Test Facility: Second Year (FY 1989) Test Results*, Pacific Northwest National Laboratory, Richland, Washington. Available at: http://www.osti.gov/bridge/servlets/purl/6973885-0GBmG8/6973885.pdf.

PNNL-13033, 1999, *Recharge Data Package for the Immobilized Low-Activity Waste 2001 Performance Assessment*, Pacific Northwest National Laboratory, Richland, Washington. Available at: http://www.pnl.gov/main/publications/external/technical_reports/13033.pdf.

PNNL-14702, 2006, *Vadose Zone Hydrogeology Data Package for Hanford Assessments*, Rev. 1, Pacific Northwest National Laboratory, Richland, Washington. Available at: http://www.pnl.gov/main/publications/external/technical_reports/PNNL-14702rev1.pdf.

PNNL-14744, 2004, *Recharge Data Package for the 2005 Integrated Disposal Facility Performance Assessment*, Pacific Northwest National Laboratory, Richland, Washington. Available at: http://www.pnl.gov/main/publications/external/technical_reports/PNNL-14744.pdf.

PNNL-16346, 2007, *Hanford Site Groundwater Monitoring for Fiscal Year 2006,* Pacific Northwest National Laboratory, Richland, Washington.

PNNL-16688, 2007, *Recharge Data Package for Hanford Single-Shell Tank Waste Management Areas*, Pacific Northwest National Laboratory, Richland, Washington. Available at: http://www.pnl.gov/main/publications/external/technical_reports/PNNL-16688.pdf.

PNNL-17841, 2008, *Compendium of Data for the Hanford Site (Fiscal Years 2004 to 2008) Applicable to Estimation of Recharge Rates*, Pacific Northwest National Laboratory, Richland, Washington. Available at: http://www.pnl.gov/main/publications/external/technical_reports/PNNL-17841.pdf.

PNNL-18732, 2009, *Field Test Report: Preliminary Aquifer Test Characterization Results for Well 299-W15-225: Supporting Phase I of the 200-ZP-1 Groundwater Operable Unit Remedial Design*, Pacific Northwest National Laboratory, Richland, Washington. Available at: http://www.pnl.gov/main/publications/external/technical_reports/PNNL-18732.pdf.

PNNL-19878, 2010, *Development of a High-Resolution Bathymetry Dataset for the Columbia River Through the Hanford Reach*, Pacific Northwest National Laboratory, Richland, Washington. Available at: http://www.pnl.gov/main/publications/external/technical_reports/PNNL-19878.pdf.

PNNL-21845, 2012, *Investigation of Hexavalent Chromium Flux to Groundwater at the 100-C-7:1 Excavation Site,* Pacific Northwest National Laboratory, Richland, Washington. Available at: http://www.pnnl.gov/main/publications/external/technical_reports/PNNL-21845.pdf.

Ptak, T., and G. Teutsch, 1994. "Forced and natural gradient tracer tests in a highly heterogeneous porous aquifer: Instrumentation and measurements." Journal of Hydrology, Vol. 159, p. 79-104.

Pickens, J.F., and G.E. Grisak, 1981a. "Scale-dependent dispersion in a stratified granular aquifer." Water Resources Research, Vol. 17, no. 4, p. 1191-1211.

Pickens, J.F., and G.E. Grisak, 1981b. "Modeling of scale-dependent dispersion in hydrogeologic systems". Water Resources Research, Vol. 17, no. 6, p. 1701-1711.

Reimus, P.W., A. Adams, M.J. Haga, A. Humphrey, T. Callahan, I. Anghel, and D. Counce, 1999. Results and Interpretation of Hydraulic and Tracer Testing in the Prow Pass Tuff at the C-Holes. Yucca Mountain Project Milestone SP32E7M4. Los Alamos, NM: Los Alamos National Laboratory.

Rivett, M.O., S. Feenstra, and J.A. Cherry, 1994. "Transport of a dissolved-phase plume from a residual solvent source in a sand aquifer". Journal of Hydrology, Vol. 159, p. 27-41.

Scheibe, T.D. and Y.-J. Chien. 2003. "An Evaluation of Conditioning Data for Solute Transport Prediction." In Groundwater, v. 41(2): 128.

Schulze-Makuch, D., 2005. "Longitudinal dispersivity data and implications for scaling behavior." Ground Water, Vol. 43, no. 3, p. 443-456.

SGW-39305, 2008, *Technical Evaluation of the Interaction of Groundwater with the Columbia River at the U.S. Department of Energy Hanford Site, 100-D Area*, Rev. 0, Fluor Hanford, Inc., Richland, Washington. Available at: http://www5.hanford.gov/arpir/?content=findpage&AKey=0812290631.

SGW-44022, 2010, *Geohydrologic Data Package in Support of 100-BC-5 Modeling*, Rev. 1, CH2M HILL Plateau Remediation Company, Richland, Washington.

SGW-48478, 2012, *Interpretation and Integration of Seismic Data in the Gable Gap*, Rev. 0, CH2M HILL Plateau Remediation Company, Richland, Washington. Available at: http://pdw.hanford.gov/arpir/index.cfm/viewDoc?accession=1104140880.

Stoller-Navarro Joint Venture (SNJV), 2006, Well ER-6-1 Tracer Test Analysis: Yucca Flat, Nevada Test Site, Nye County, Nevada. S-N/99205-084, Rev. 0.

Stoller-Navarro Joint Venture (SNJV), 2007, Phase I Contaminant Transport Parameters for the Groundwater Flow and Contaminant Transport Model of Corrective Action Unit 97: Yucca Flat/Climax Mine, Nevada Test Site, Nye County, Nevada. S-N/99205-096, Rev. 0.

Sutherson, S., C.E. Divine, and S.T. Potter, 2009, Remediating Large Plumes: Overcoming the Scale Challenge, Ground Water Monitoring & Remediation, Vol. 29, No. 1, pp. 45-50.

Suthersan, S.S., S.Potter, and Matthew Schnobrich. 2013. Groundwater Restoration: Large-Scale Benefits of Small-Scale Processes, Groundwater Monitoring & Remediation, v. 33, no 3.

U.S. Environmental Protection Agency, 2009, Guidance on the Development, Evaluation, and Application of Environmental Models, EPA/100/K-09/003. Washington, DC.

van der Kamp, G., L.D. Luba, J.A. Cherry, and H. Maathuis, 1994. "Field study of a long and very narrow contaminant plume." *Ground Water*, Vol. 32, no. 6, p. 1008-1016.

WCH-380, 2010, *Field Summary Report for Remedial Investigation of Hanford Site Releases to the Columbia River, Hanford Site, Washington: Collection of Surface Water, Pore Water, and Sediment Samples for Characterization of Groundwater Upwelling*, Rev. 1, Washington Closure Hanford, LLC, Richland, Washington. Available at: http://www.osti.gov/bridge/product.biblio.jsp?osti_id=1017505.

Zheng, C., and P. P. Wang, 1999, *MT3DMS, A Modular Three-Dimensional Multi-Species Transport Model for Simulation of Advection, Dispersion, and Chemical Reactions of Contaminants in Groundwater Systems; Documentation and User's Guide*, Report SERDP-99-1, U.S. Army Engineer Research and Development Center, Vicksburg, Mississippi. Available at: http://hydro.geo.ua.edu/mt3d/mt3dmanual.pdf.

Appendix A

Priest Rapids to B-Gauge Correlation

This page intentionally left blank.

Executive Summary

Following the procedures outlined in "Columbia River Stage Correlation for the Hanford Area" (ECF-Hanford-13-0028 Revision 0), a regression relationship was developed suitable for determining approximate water surface elevations at the B-River gauge site (adjacent to the 100-BC area) using water levels recorded at the USGS gauge on the Columbia River downstream from Priest Rapids dam (USGS Gauge #12472800). All analyses were performed using Matlab, with a customized script ("Hanford_SW_B.m") created for this project.

It is concluded that the following regression equation best allows for predictions of B-River water surface elevations based on water surface elevations measured at the USGS gauge:

$$WSE_{B-River,t+lag} = 0.84742(WSE_{USGS,t}) + 15.107$$

Where "WSE" is the water surface elevation (UNITS: meters), "t" is the instant in time, and "lag" is the time lag between the USGS gauge and the B-River gauge (1.2 hrs.). The time lag was interpolated from data presented in ECF-Hanford-13-0028 Revision 0, was assumed constant irrespective of streamflow, and not verified for this analysis. Separating available data into high-flow and low-flow periods for regression was also investigated, but separate regression equations for such periods did not yield any significant increase in accuracy compared to measured water surface elevations.

It is suspected that B-River water surface elevations recorded after 2010-11-01 are likely to be referenced to the NGVD29 vertical datum rather than to the reported NAVD88 datum. This assertion was theorized based on our analysis of available data, and could not be independently verified or refuted.

Regression Analysis–Input Data

To develop the regression relationship, all available streamflow records were obtained for USGS gauge #12472800. On 6/25/2015, data was downloaded from the USGS' Instantaneous Data Archive (http://ida.water.usgs.gov/ida/available_records.cfm?sn=12472800). Data was downloaded at for the period from 1987-10-01 to 2007-10-01, with the time interval of 15 minutes. This dataset (referred to as "Dataset 1") contained only recorded stream flows, and not associated gauge heights. To determine gauge heights from the streamflow

data the most-recent stage-flow rating curve for USGS gauge #12472800, was used as downloaded from http://waterdata.usgs.gov/wa/nwis/current?type=ratings on 6/25/2015. Data from 2007-10-01 to 2015-06-25 was downloaded from the USGS NWIS website on 6/25/2015 (http://waterdata.usgs.gov/nwis/uv?site_no=12472800). This dataset contained both recorded gauge heights and corresponding streamflow values, and hence no further processing was needed using the available rating curve data.

The data was adjusted to correct for time-offsets due to daylight savings time. Specifically the USGS had classified each water level with a time attribute: either "PST" for "Pacific Standard Time or "PDT" for "Pacific Daylight Time." To correct for daylight savings affects, 1-hour was subtracted from all data with the "PDT" attribute. In the resulting dataset, INTERA then removed the duplicate data and utilized the flow and gauge height values that originally had the "PST" attribute.

To convert the gauge height data to water surface elevations, the elevation of the gauge datum was added to each gauge height value. Per the "Station Notes" on the USGS NWIS site, the datum for USGS gauge #12472800 is 390 ft. above the NAVD 1929 datum. To convert from the NAVD 1929 datum to the standard NAVD88 datum, 3.49 ft was added. Finally water surface elevations were converted from units of "Feet" to "Meters" by dividing the NAVD88 datum (in feet) by 3.2808 ft./m. The water surface elevation at gauge #12472800 is therefore calculated from the following equation:

$$WSE(m) = \frac{(H + 390 + 3.49)ft}{3.2808\frac{ft}{m}}$$

Water level data at the B-river gauge location was provided. This data was already referenced to the NAVD88 datum, provided with units of "Meters," and corrected for daylight savings time. Data was available from 2000-01-26 to 2014-07-31, with data generally available at 1-hr intervals.

Figure A-1 shows the water elevation data for the USGS gauge and the B-river gauge for the period of the B-river gauge data. As shown in Figure A-1, all B-river gauge elevations prior to 2004 were collected infrequently compare to those recorded after 2004.

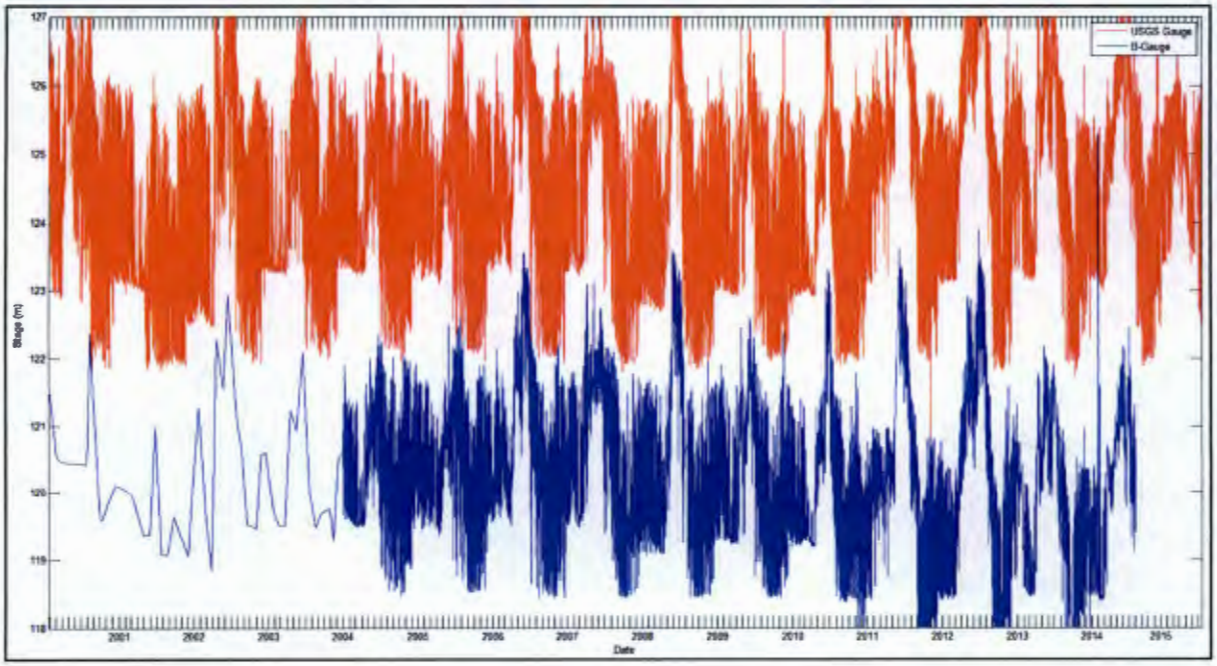

Figure A-1. Time-History of Water Levels at the USGS Gauge Below Priest Rapids Dam & at the B-River Gauge Location

Regression Analysis – Calculation Methodology

To develop a regression equation between the USGS gauge and the B-river gauge, it is necessary to compare water surface elevations at each location at times when the same "parcel" of water is passing each gauge location. As water flows downstream from the USGS gauge location to the B-river gauge location, water passing the B-river gauge location must have passed the USGS gauge location at an earlier time. To properly time-reference the water level comparison, it is necessary to apply a time-lag to the water level data at the B-river gauge. Specifically, the time of the B-river gauge measurement was reduced so as to approximately match the time the water would have been passing the USGS gauge location. A similar approach was utilized in "Columbia River Stage Correlation for the Hanford Area" (ECF-Hanford-13-0028 Revision 0). To determine the approximate time lag, linear interpolation was performed between the time lag for the K-River gauge (from ECF-Hanford-13-0028 Revision 0) and the USGS gauge, based on the relative location of the B-River gauge between the USGS gauge and the K-River gauge. No calculations were performed to assess the validity of this lag calculation approach. The B-River gauge time lag was calculated as follows:

$$L_B = L_K\left(\frac{D_{USGS} - D_B}{D_{USGS} - D_K}\right) = (1.5\ hrs)\left(\frac{394.5mi - 384.1mi}{394.5mi - 381.5mi}\right) = 1.2\ hrs$$

To apply the time lag, the time of the B-river gauge measurement was uniformly **REDUCED** by 1.2 hrs., without consideration of how streamflow might alter the travel time of water parcels moving between the USGS and B-River gauge locations.

Comparisons of elevations between the USGS and time-lagged B-river gauge were then made at the times of the time-lagged B-river gauge measurements. If the time-lagged B-river gauge measurement occurred at a time in-between those of the USGS gauge measurement, then a USGS water level was determined by simple linear interpolation between successive USGS gauge measurements. Initial comparisons between 88,332 measurements are shown in Figure A-2. As shown, there are two distinct "diagonal bands" of data which indicate generally high correlation of water levels between the USGS gauge and the B-Gauge. Through trial-and-error, it was identified that the first "diagonal band" consists of data prior to November 1, 2010 (Shown as black "x"s in Figure A-2). The second "diagonal band" (shown as red "o"s in Figure A-2) consists of data collected on and after November 1, 2010.

The existence of two distinct "diagonal bands" of highly-collated data suggests that a datum shift occurred in one of the datasets around the November 1, 2010 timeframe. Inquiries were made into any maintenance or installation records available from the B-River gauge data, and failed to identify any reasons for this apparent shift. Analysis of USGS records from the NWIS system also did not provide insight into the cause of this apparent shift. As shown in Figure A-3, which is a close-up view of the data from Figure A-2, the datum shift amounts to approximately a 1.2 m increase in USGS stage (green lines), or a 1.0 m decrease in B-River stage (orange lines). The 1.0 m decrease in B-River gauge water elevations is of similar magnitude to the increase in elevation resulting from the conversion of the USGS gauge datum from NGVD29 to NAVD88. Therefore it is possible that the B-River gauge data recorded AFTER November 1, 2010 may not have been properly adjusted to the NAVD88 datum; no evidence was found to refute or confirm this suggestion.

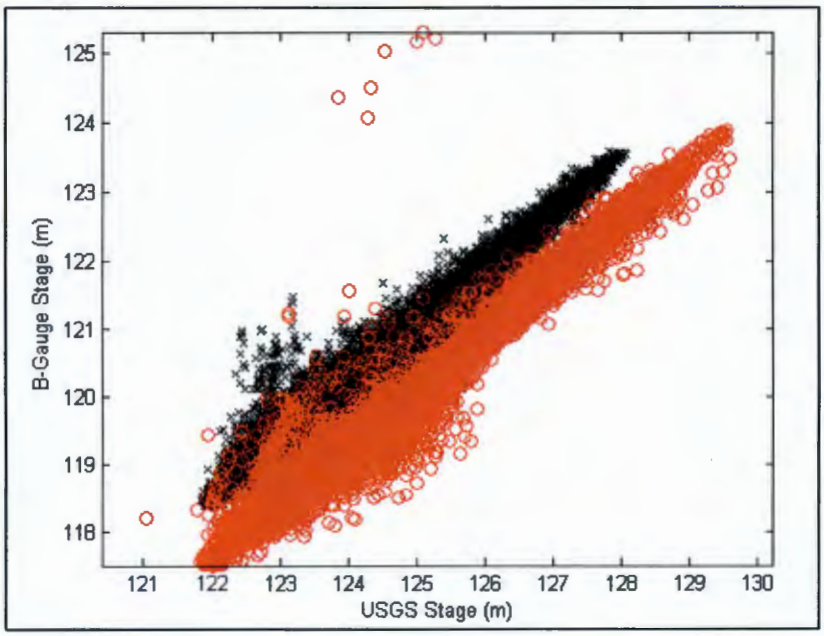

Figure A-2. Initial comparison between USGS stage and B-Gauge stage, showing two distinct diagonal bands of highly correlated data. Data prior to 2010-11-01 is shown with black "x"s, and data after 2010-11-01 is shown with red "o"'s.

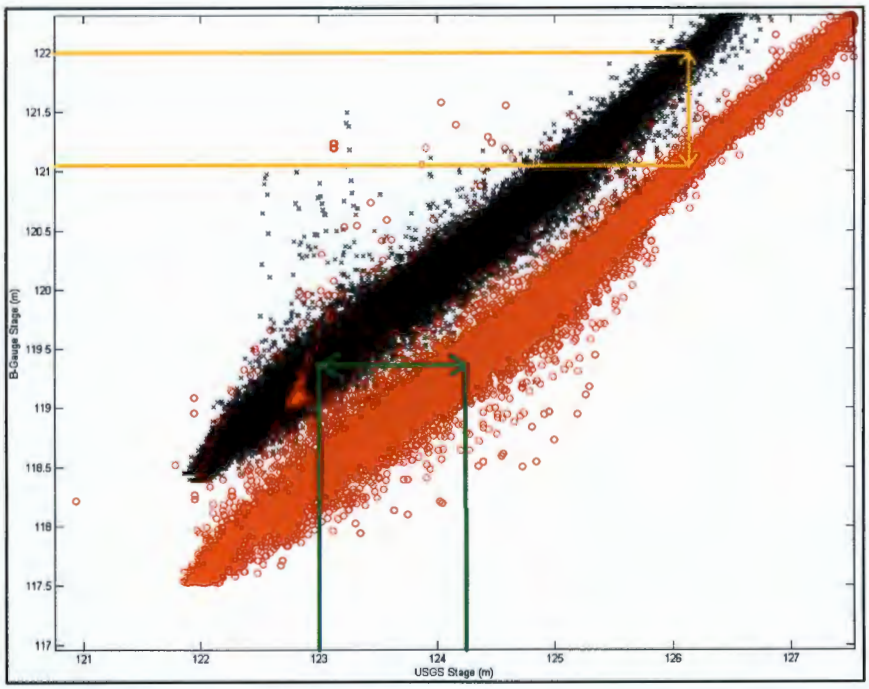

Figure A-3. Zoomed-In view of Figure A-2, showing the initial comparison between USGS stage and B-Gauge stage, showing two distinct diagonal bands of highly correlated data. Data prior to 2010-11-01 is shown with black "x"s, and data after 2010-11-01 is shown with red "o"'s. There appears to be an approximate horizontal shift of 1.2 m in USGS stage after 2010-11-01 (Green lines), or a decrease of approximately 1-m in B-gauge stage after 2010-11-01 (orange lines).

It is assumed that the B-River gauge measurements were improperly referenced to the NAVD88 datum after November 1, 2010. To adjust the datum, 3.49 ft. (1.06 m) was added to the reported B-River water surface elevation for all data collected after November 1, 2010. The resulting data comparison and linear regression equation are presented in Figure A-4.

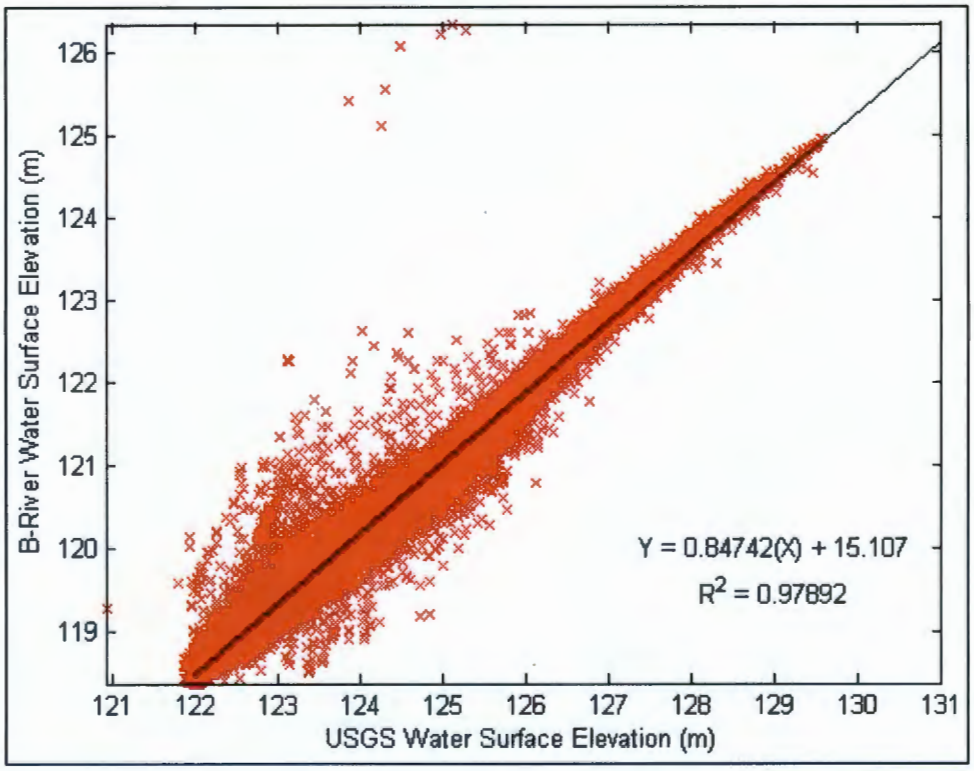

Figure A-4. Final Comparison Between USGS Stage and B-Gauge Stage

From Figure A-4, the regression equation correlating B-River water surface elevations to USGS gauged water surface elevations is:

$$WSE_{B-River,t+lag} = 0.84742(WSE_{USGS,t}) + 15.107$$

Where "WSE" is the water surface elevation (UNITS: meters), "t" is the instant in time, and "lag" is the time lag between the USGS gauge and the B-River gauge (1.2 hrs.). The correlation between the datasets is extremely good, with an R^2 value of 0.97892. Higher correlation would be achieve upon filtering out the anomalously high water level readings from the B-River gauge dataset; these anomalies are the readings exceeding 125 m at the B-River location. It is notable that there is a fairly large range of spread of measured data about the correlation equation shown in Figure A-4 (black line).

Figure A-5 presents a close-up view of Figure A-4 at the lower end of the data spectrum, where it is evident that for a given measured USGS gauge elevation, there can be a range of corresponding measured B-River elevations, with the range approaching 0.7 m. As shown in Figure A-4, this range diminishes as water levels at the USGS gauge increase.

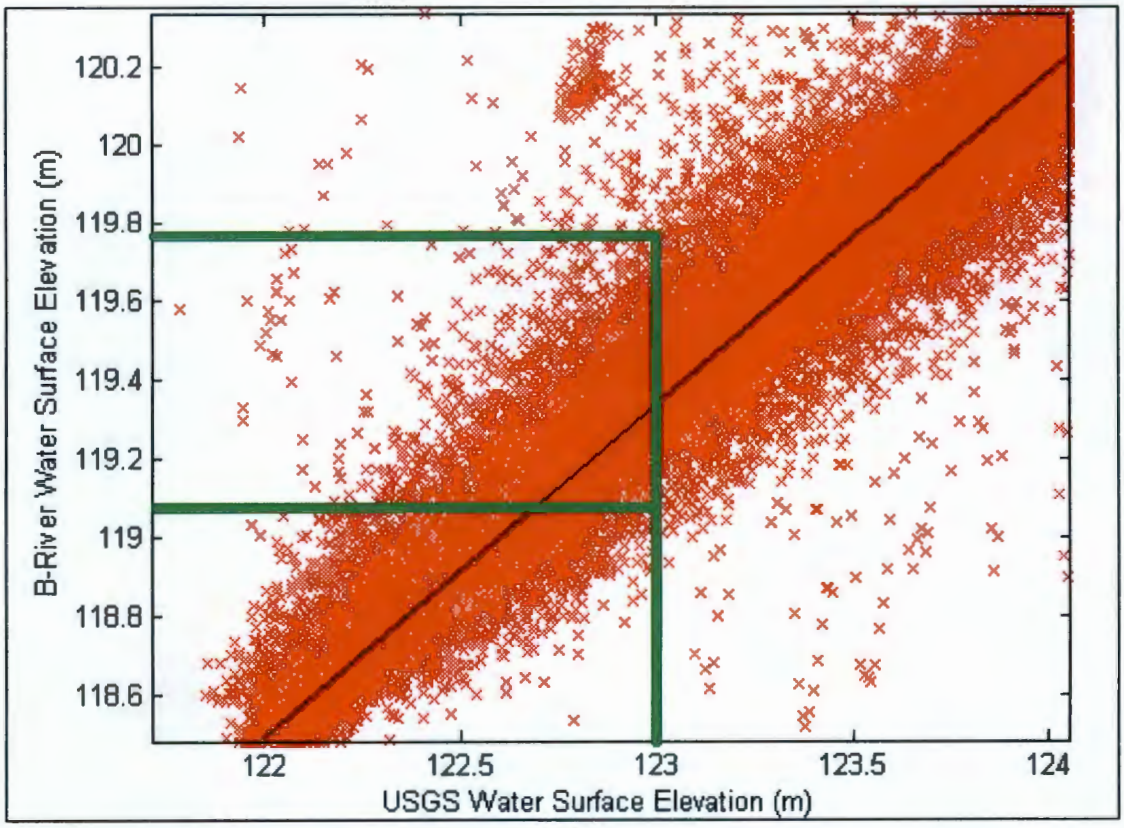

Figure A-5. Zoomed-In Comparison between USGS and B-Gauge Water Surface Elevations, Showing a Range in Measured B-River Water Surface Elevations for a given USGS Elevation

Figures A-6 and A-7 present comparisons of measured and computed water surface elevations at the B-River location for two randomly selected 1-week periods. As shown in Figure A-6, for the period from 2012-09-06 to 2012-09-13, water levels in the Columbia River were low, and the computed levels tended to under-predict the measured levels when troughs of hydropower release waves passed the B-gauge location. The wave peaks, however, were will captured by the regression. This suggests that the regression analysis does not adequately take into account the physical dispersion of the release wave as it travels downstream from Priest Rapids Dam. Figure A-7 shows water surface elevations in May of 2013, when stream flow was high. In this situation, the computed

water levels were systematically slightly lower than the measured water levels, yet follows the same temporal wave patterns. This result suggests that increased regression accuracy could possibly be achieved by separating periods of high and low flow, and thus developing separate regression equations for each scenario. To test this analysis, separate regression equations were generated for data from when the USGS water surface elevation was above and below 126 m. (Figure A-8). As shown, the R^2 value for higher flow periods is actually slightly lower than that obtained when all data is included in a single regression equation. The R^2 value for lower flow periods is also lower than that obtained when all data is included in a single regression equation. The regression time-series generated from higher flow data did slightly increase the general agreement with measured B-River gauge water surface elevations (Figure A-9), but not significantly enough to justify using separate equations for high and low flow periods.

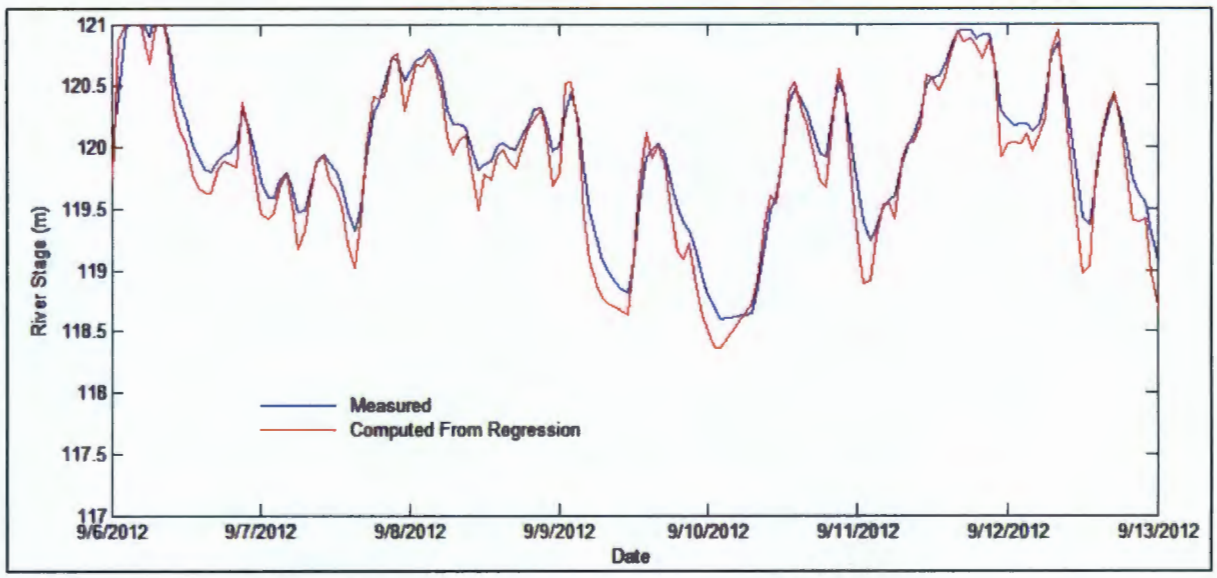

Figure A-6. Measured and Computed Water Surface Time-Histories for the B-River Gauge Location in September 2012 (a low-flow period)

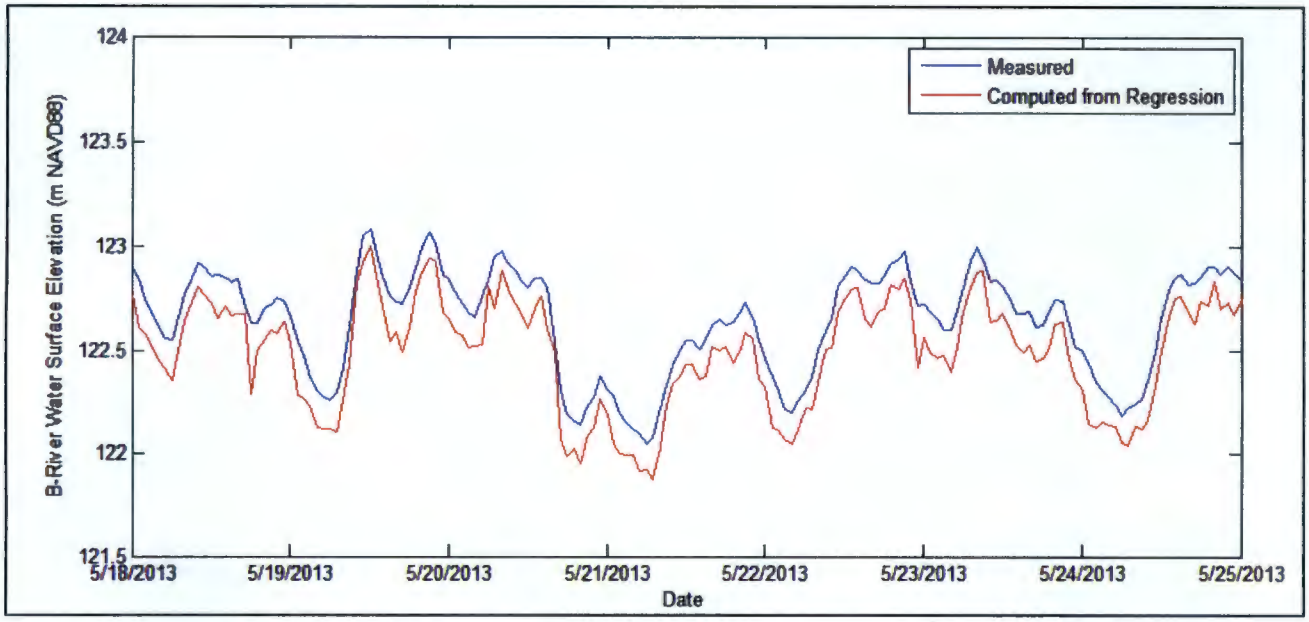

Figure A-7. Measured and Computed Water Surface Time-Histories for the B-River Gauge Location in May 2013 (a high-flow period)

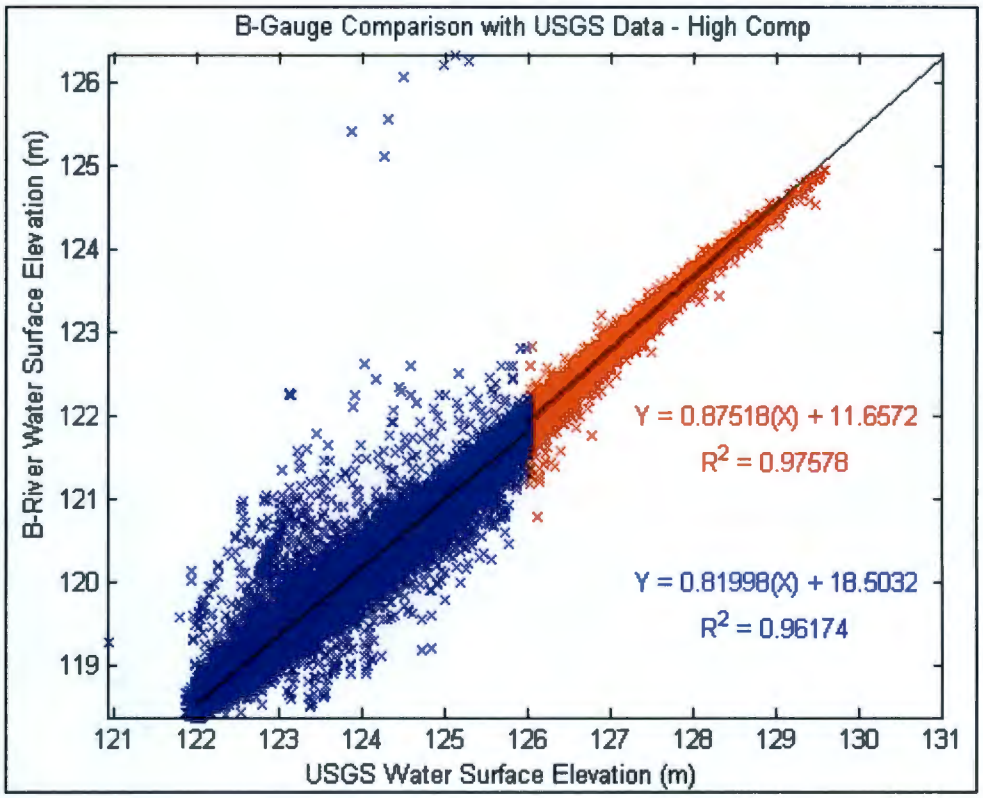

Figure A-8. Developing Separate Regression Equations for High and Low Flow Periods - USGS and B-River Water Surface Elevations

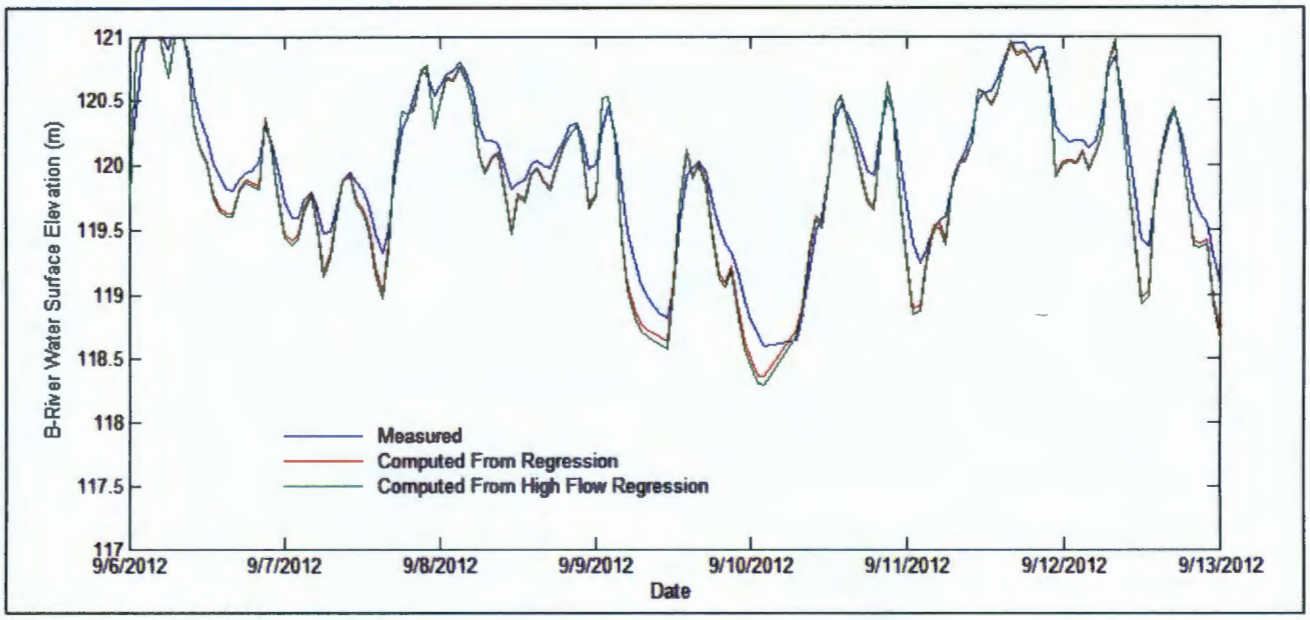

Figure A-9. Measured and Computed Water Surface Time-Histories for the B-River Gauge Location in May 2013 (a high-flow period). Use of the High Flow Regression Equation did not Significantly Improve Agreement with Measured Values

Appendix B

Observed Data and Simulated Hydrographs

This page intentionally left blank.

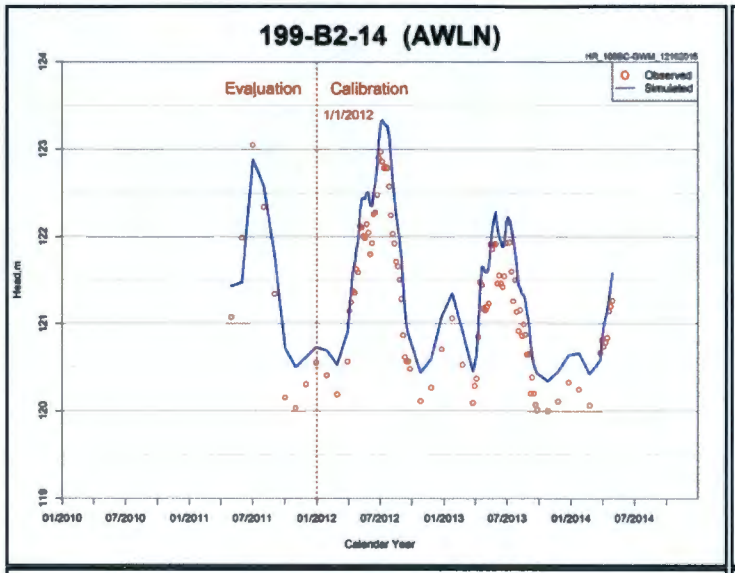
199-B2-14 (AWLN)
Evaluation
Calibration
1/1/2012
Observed
Simulated
Head,m
Calendar Year

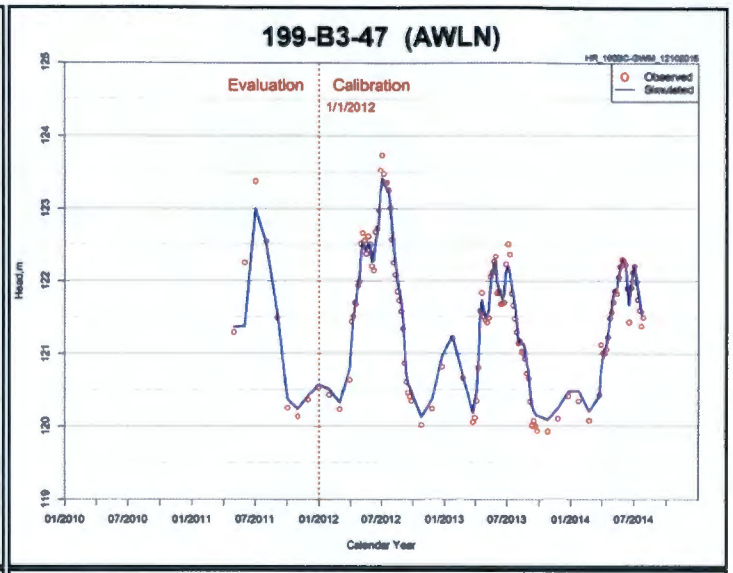
199-B3-47 (AWLN)
Evaluation
Calibration
1/1/2012
Observed
Simulated
Head,m
Calendar Year

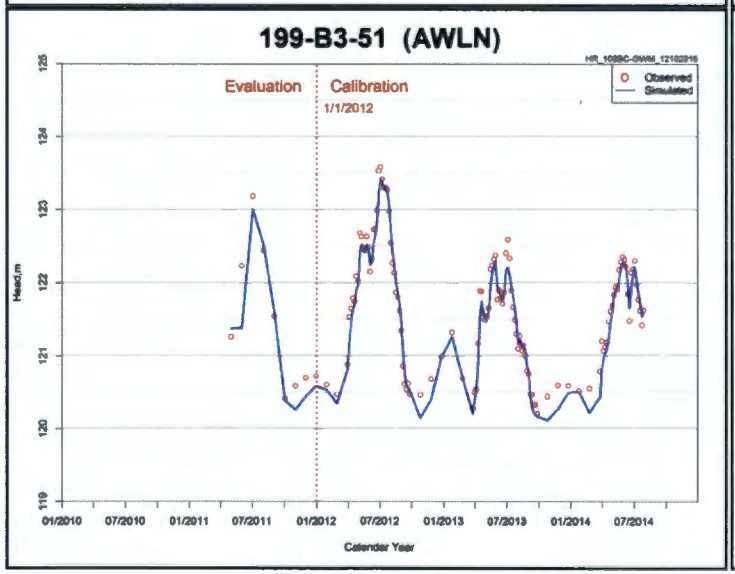
199-B3-51 (AWLN)
Evaluation
Calibration
1/1/2012
Observed
Simulated
Head,m
Calendar Year

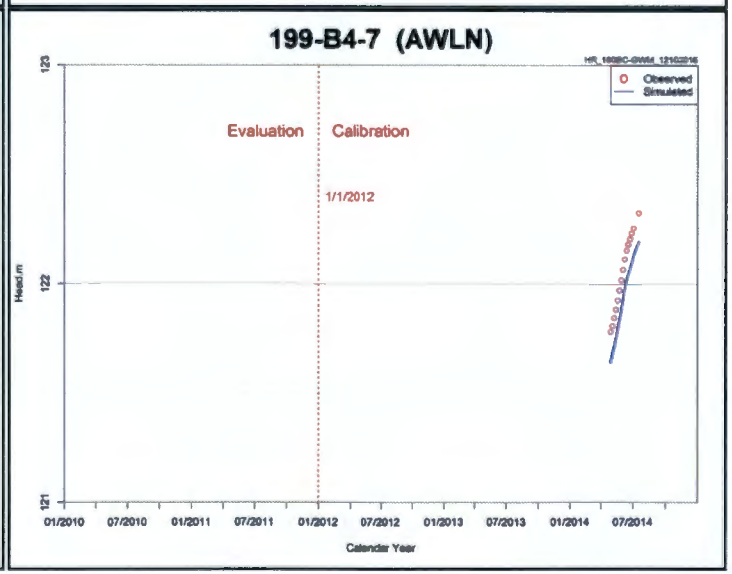
199-B4-7 (AWLN)
Evaluation
Calibration
1/1/2012
Observed
Simulated
Head,m
Calendar Year

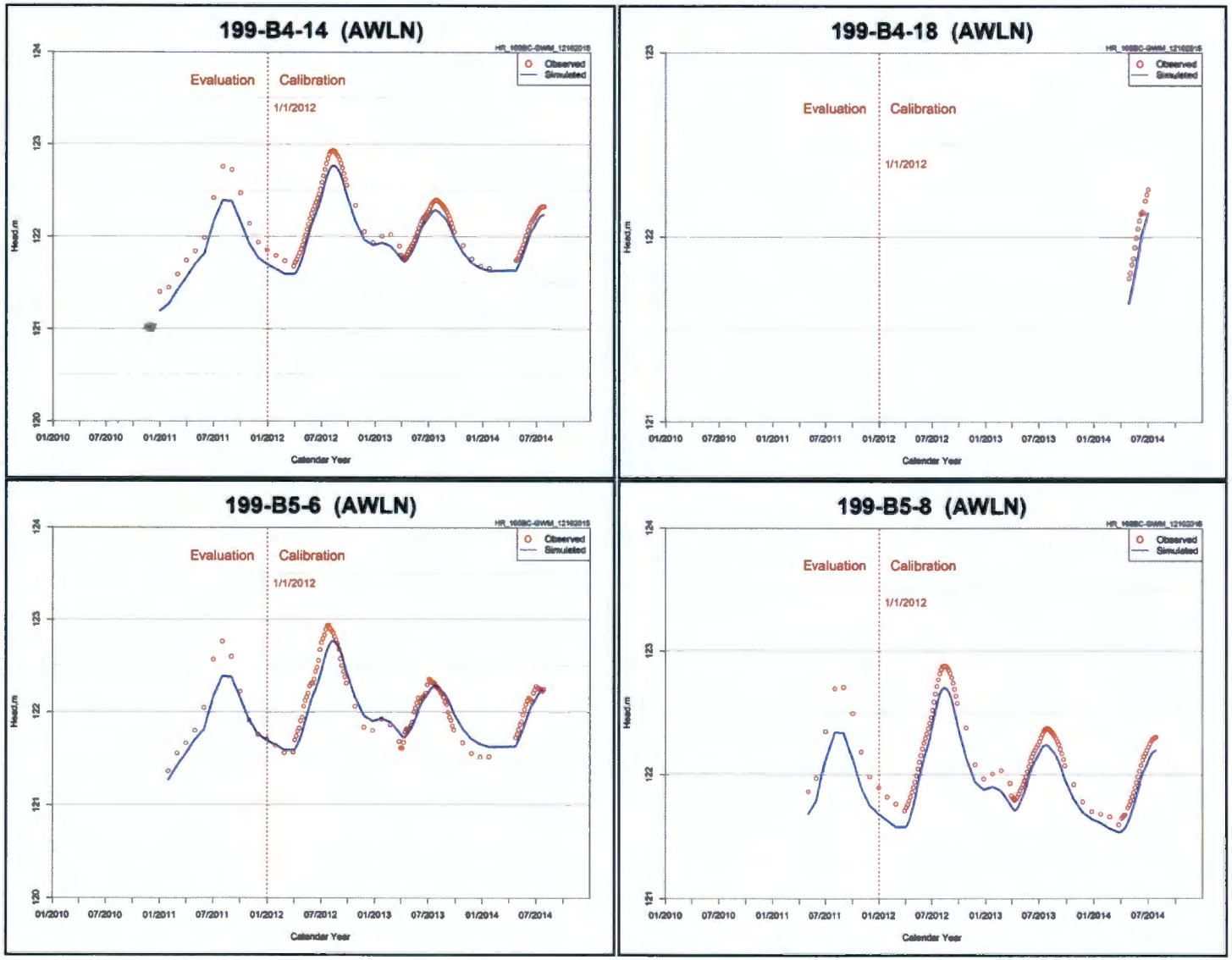
199-B4-14 (AWLN)
199-B4-18 (AWLN)
199-B5-6 (AWLN)
199-B5-8 (AWLN)
Evaluation
Calibration
1/1/2012
Observed
Simulated
Head,m
Calendar Year
01/2010
07/2010
01/2011
07/2011
01/2012
07/2012
01/2013
07/2013
01/2014
07/2014

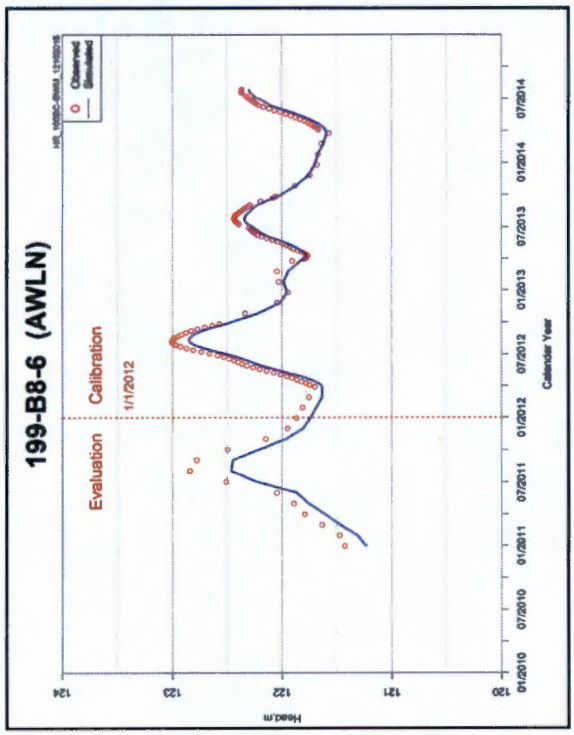
199-B8-6 (AWLN)
Evaluation
Calibration
1/1/2012
Observed
Simulated
Head,m
124
123
122
121
120
01/2010
07/2010
01/2011
07/2011
01/2012
07/2012
01/2013
07/2013
01/2014
07/2014
Calendar Year

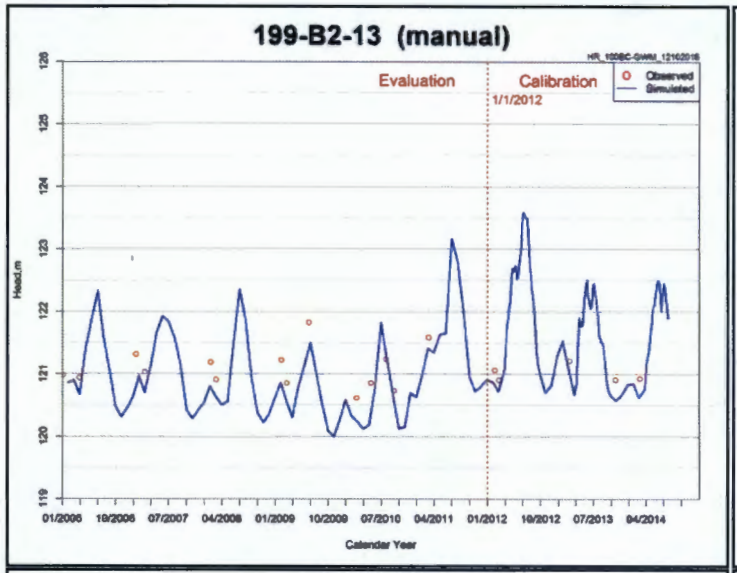
199-B2-13 (manual)
Evaluation
Calibration
1/1/2012
Observed
Simulated
Head,m
Calendar Year

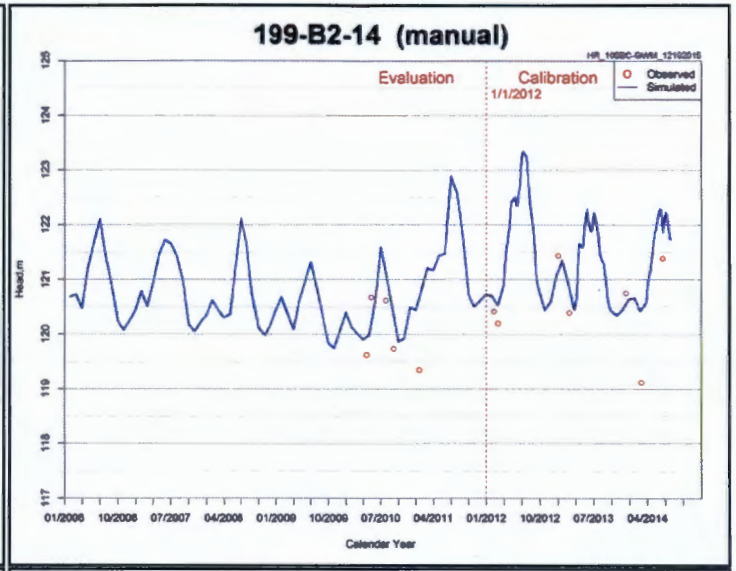
199-B2-14 (manual)
Evaluation
Calibration
1/1/2012
Observed
Simulated
Head,m
Calendar Year

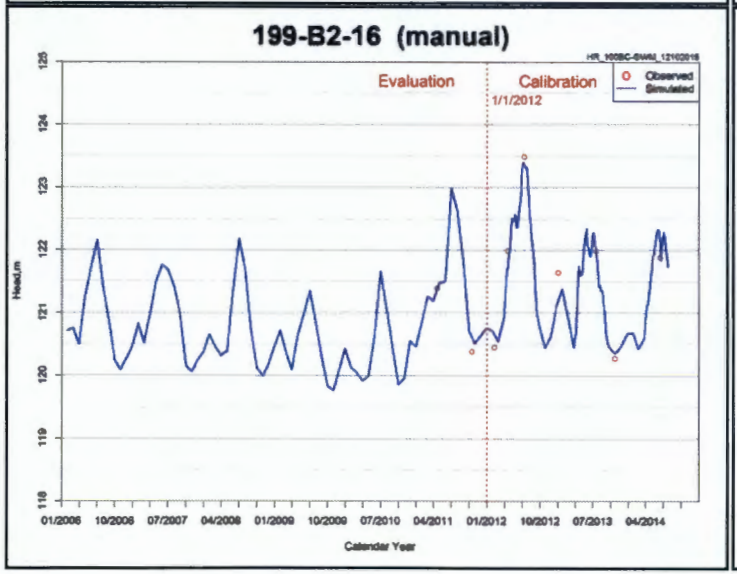
199-B2-16 (manual)
Evaluation
Calibration
1/1/2012
Observed
Simulated
Head,m
Calendar Year

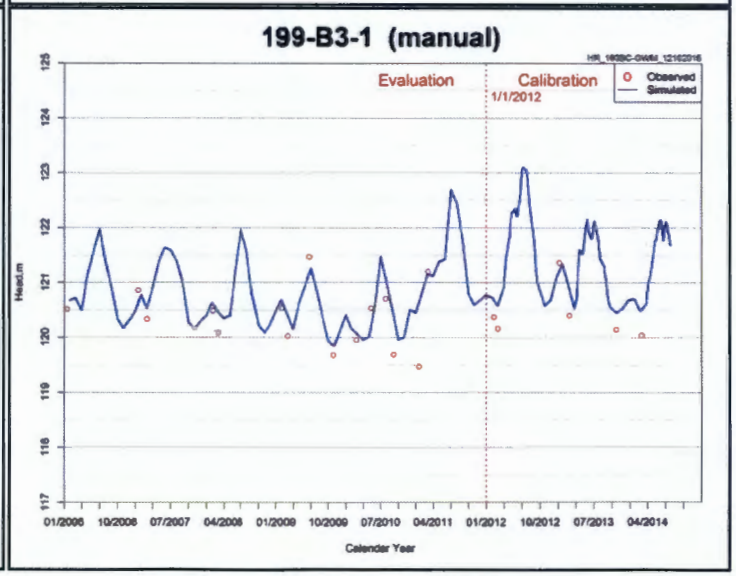
199-B3-1 (manual)
Evaluation
Calibration
1/1/2012
Observed
Simulated
Head,m
Calendar Year

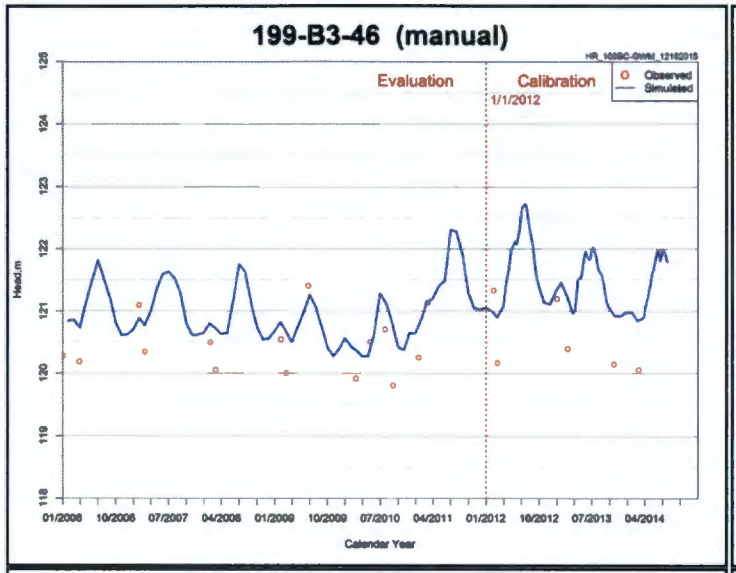
199-B3-46 (manual)
Evaluation
Calibration
1/1/2012
Observed
Simulated
Head,m
Calendar Year

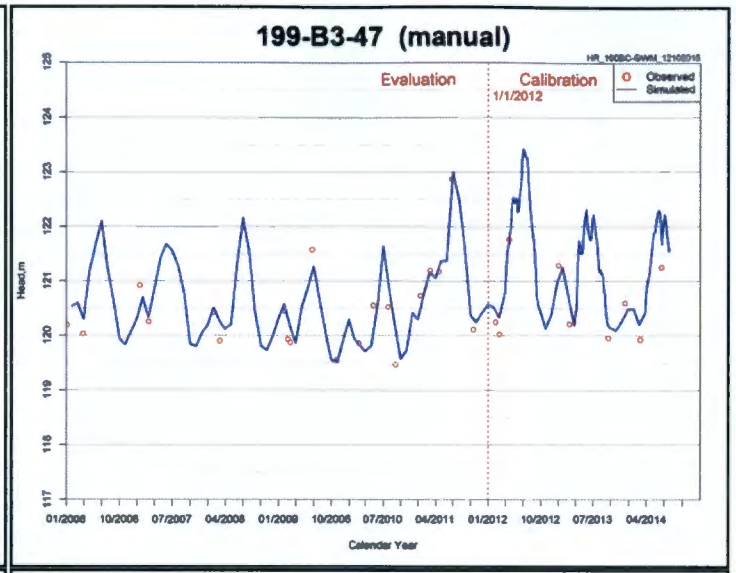
199-B3-47 (manual)
Evaluation
Calibration
1/1/2012
Observed
Simulated
Head,m
Calendar Year

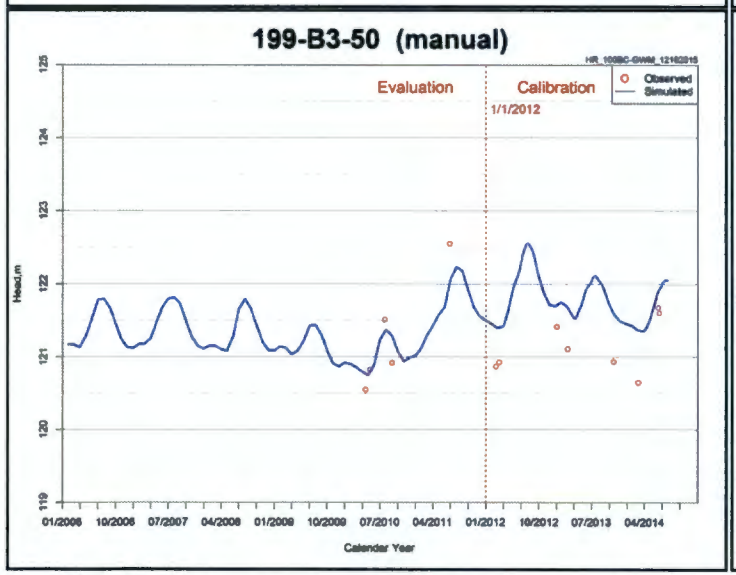
199-B3-50 (manual)
Evaluation
Calibration
1/1/2012
Observed
Simulated
Head,m
Calendar Year

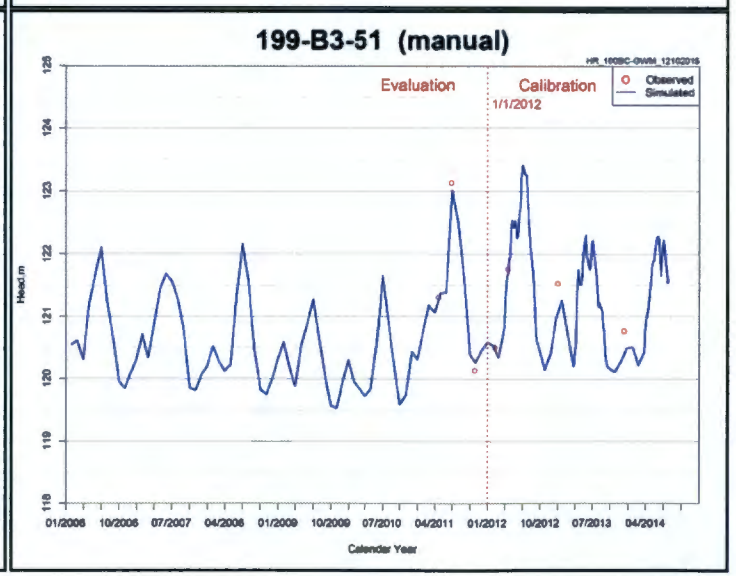
199-B3-51 (manual)
Evaluation
Calibration
1/1/2012
Observed
Simulated
Head,m
Calendar Year

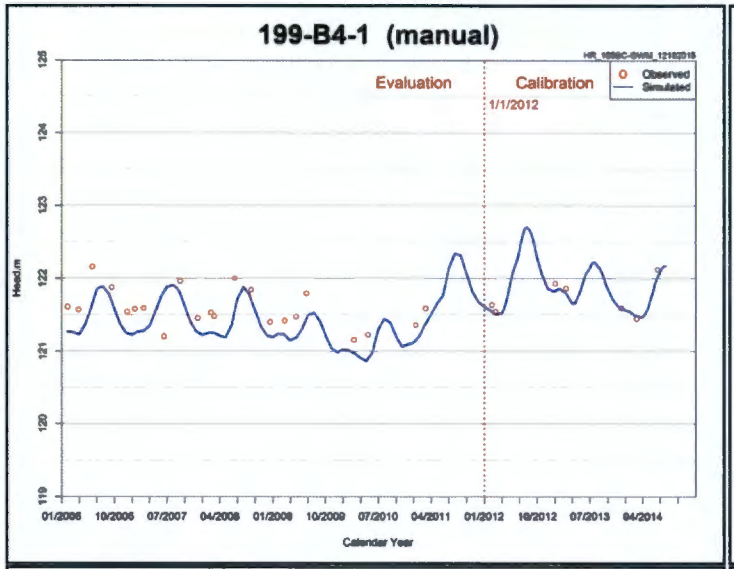
199-B4-1 (manual)
Evaluation
Calibration
1/1/2012
Observed
Simulated
Head,m
125
124
123
122
121
120
119
01/2006
10/2006
07/2007
04/2008
01/2009
10/2009
07/2010
04/2011
01/2012
10/2012
07/2013
04/2014
Calendar Year

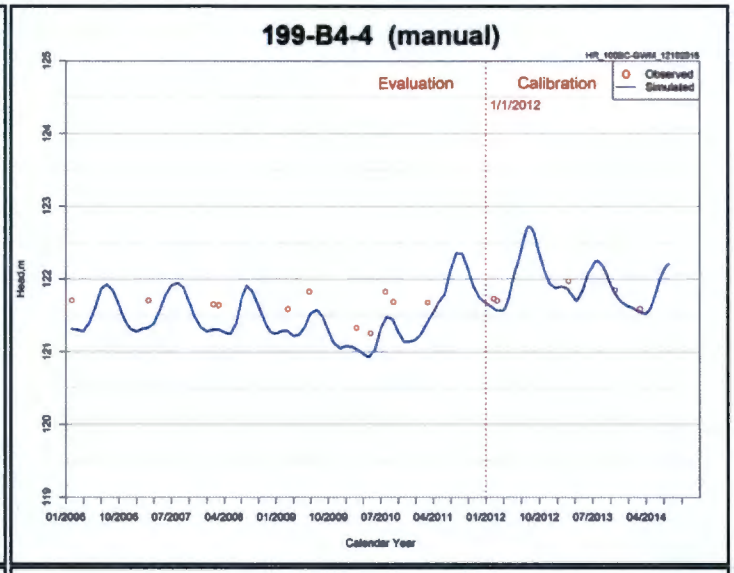
199-B4-4 (manual)
Evaluation
Calibration
1/1/2012
Observed
Simulated
Head,m
125
124
123
122
121
120
119
01/2006
10/2006
07/2007
04/2008
01/2009
10/2009
07/2010
04/2011
01/2012
10/2012
07/2013
04/2014
Calendar Year

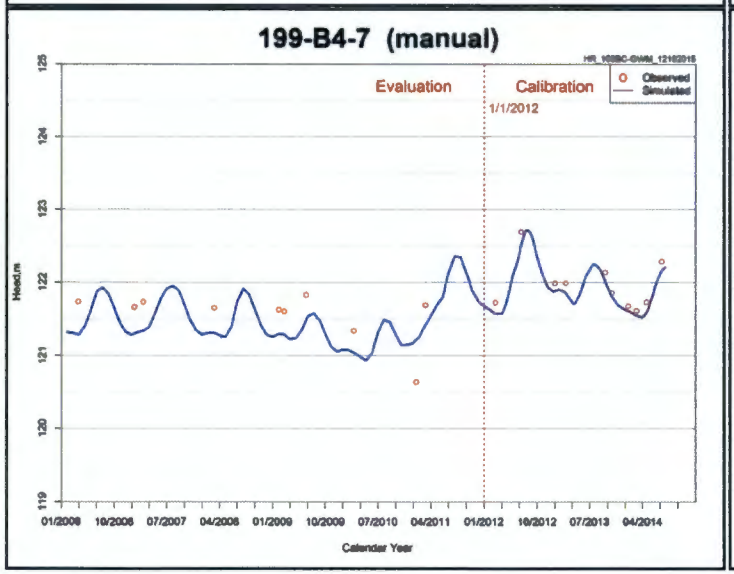
199-B4-7 (manual)
Evaluation
Calibration
1/1/2012
Observed
Simulated
Head,m
125
124
123
122
121
120
119
01/2006
10/2006
07/2007
04/2008
01/2009
10/2009
07/2010
04/2011
01/2012
10/2012
07/2013
04/2014
Calendar Year

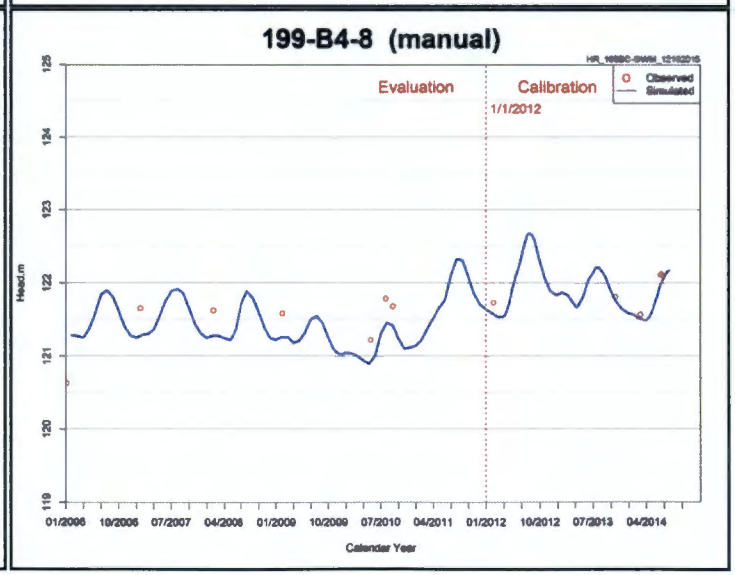
199-B4-8 (manual)
Evaluation
Calibration
1/1/2012
Observed
Simulated
Head,m
125
124
123
122
121
120
119
01/2006
10/2006
07/2007
04/2008
01/2009
10/2009
07/2010
04/2011
01/2012
10/2012
07/2013
04/2014
Calendar Year

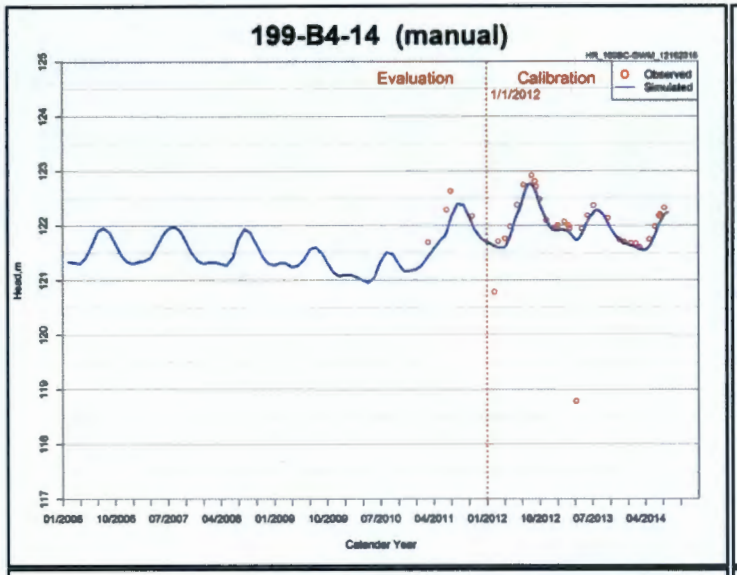
199-B4-14 (manual)
Evaluation
Calibration
1/1/2012
Observed
Simulated
Head,m
Calendar Year

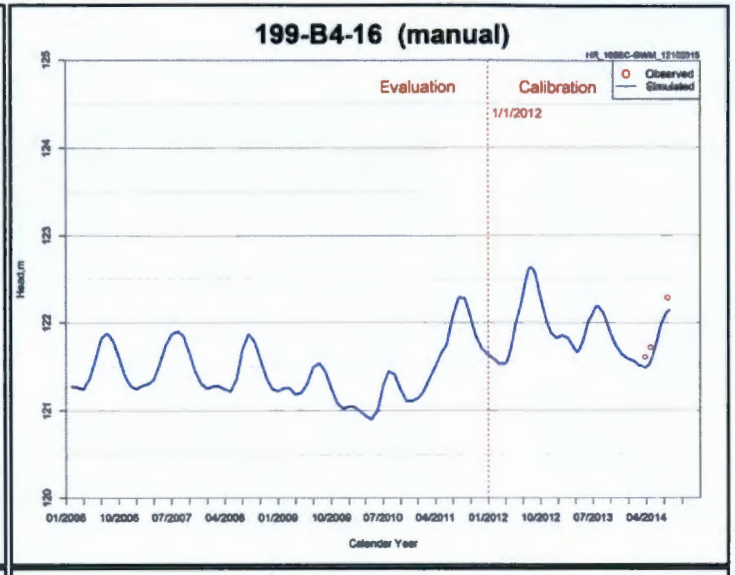
199-B4-16 (manual)
Evaluation
Calibration
1/1/2012
Observed
Simulated
Head,m
Calendar Year

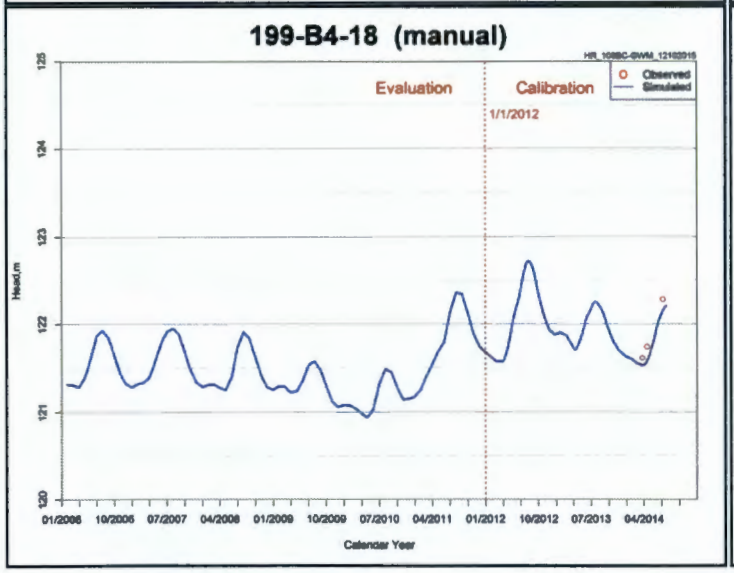
199-B4-18 (manual)
Evaluation
Calibration
1/1/2012
Observed
Simulated
Head,m
Calendar Year

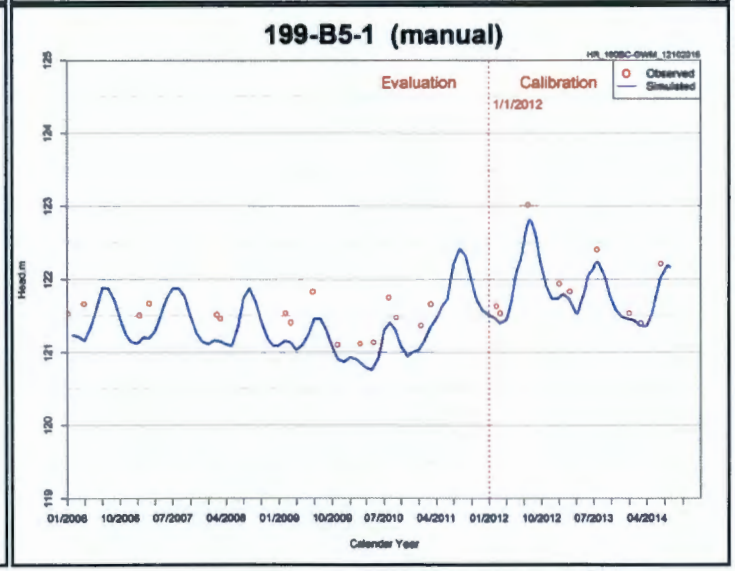
199-B5-1 (manual)
Evaluation
Calibration
1/1/2012
Observed
Simulated
Head,m
Calendar Year

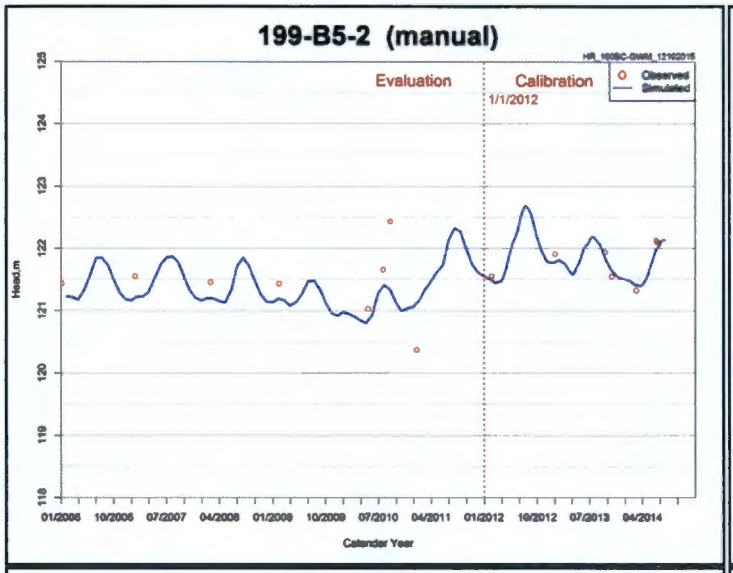
199-B5-2 (manual)
Evaluation
Calibration
1/1/2012
Observed
Simulated
Head,m
Calendar Year

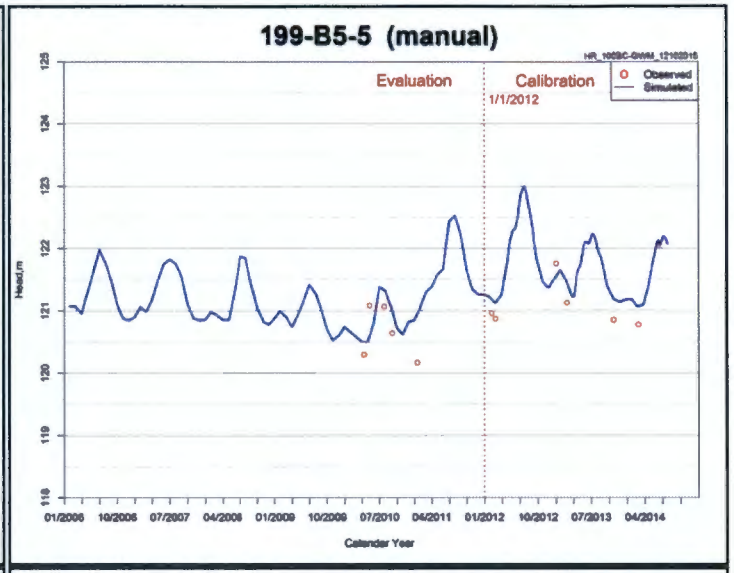
199-B5-5 (manual)
Evaluation
Calibration
1/1/2012
Observed
Simulated
Head,m
Calendar Year

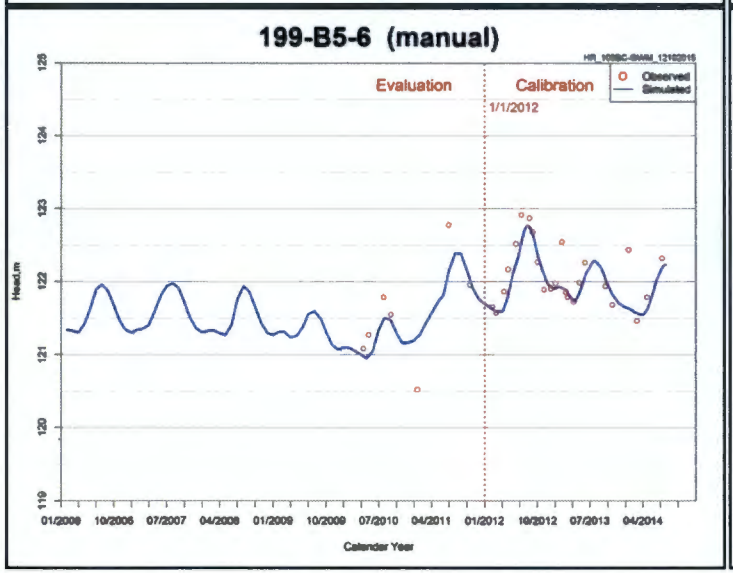
199-B5-6 (manual)
Evaluation
Calibration
1/1/2012
Observed
Simulated
Head,m
Calendar Year

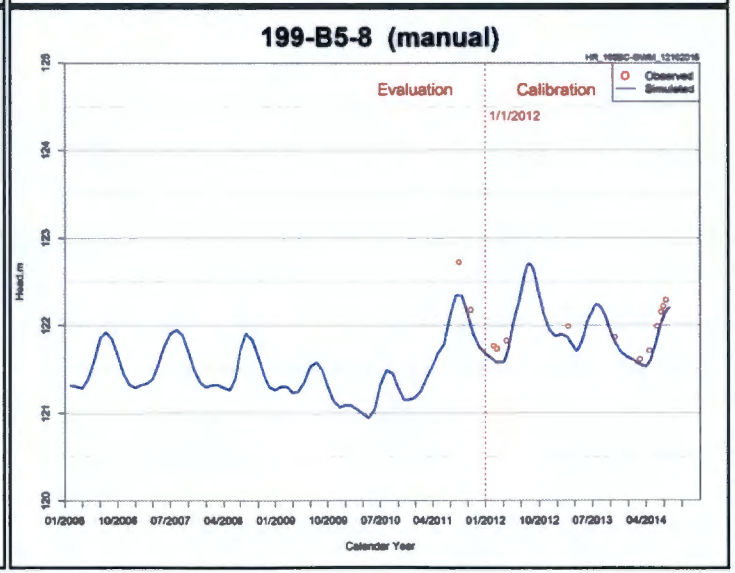
199-B5-8 (manual)
Evaluation
Calibration
1/1/2012
Observed
Simulated
Head,m
Calendar Year

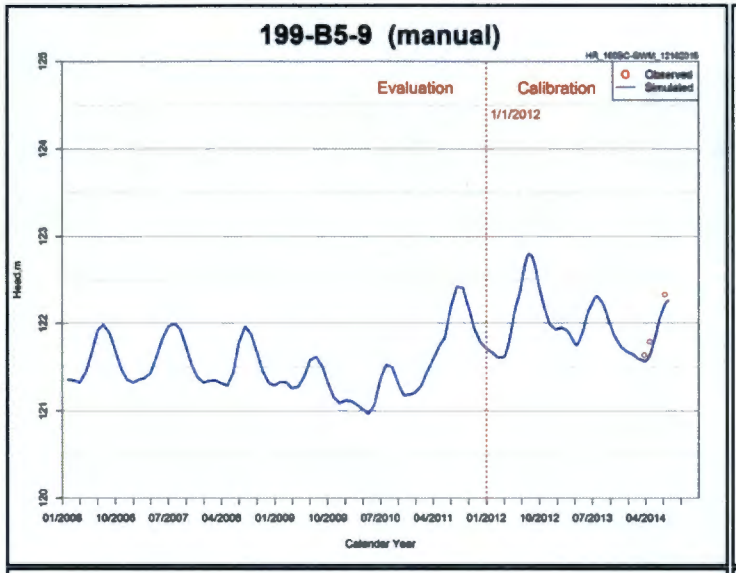
199-B5-9 (manual)
Evaluation
Calibration
1/1/2012
Observed
Simulated
Head,m
Calender Year

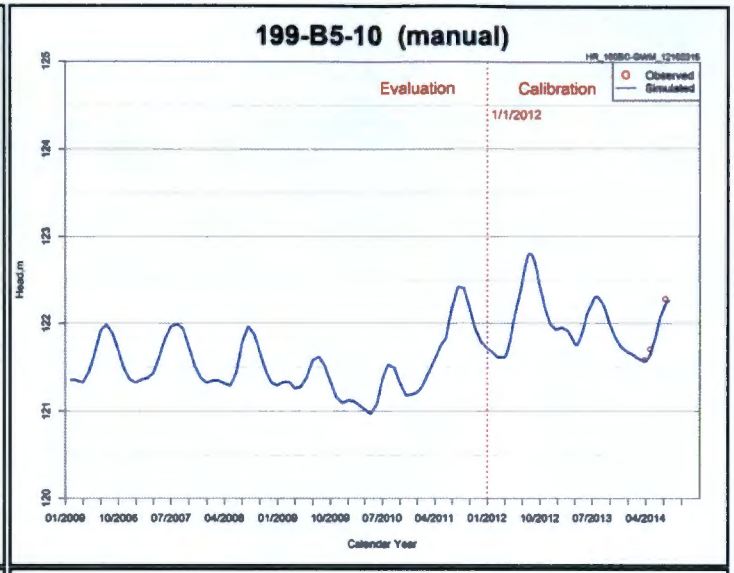
199-B5-10 (manual)
Evaluation
Calibration
1/1/2012
Observed
Simulated
Head,m
Calender Year

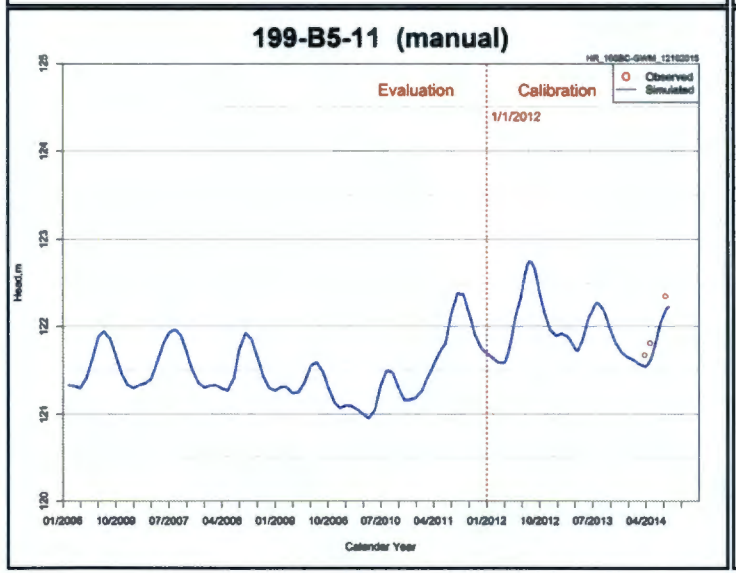
199-B5-11 (manual)
Evaluation
Calibration
1/1/2012
Observed
Simulated
Head,m
Calender Year

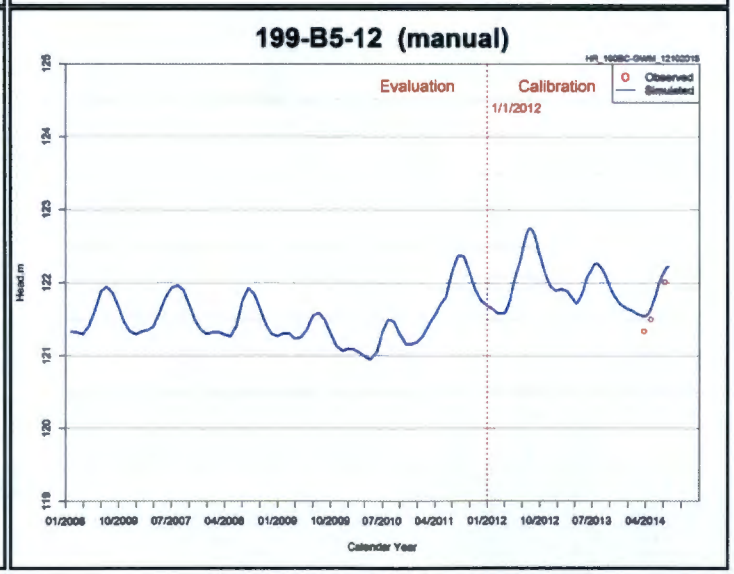
199-B5-12 (manual)
Evaluation
Calibration
1/1/2012
Observed
Simulated
Head,m
Calender Year

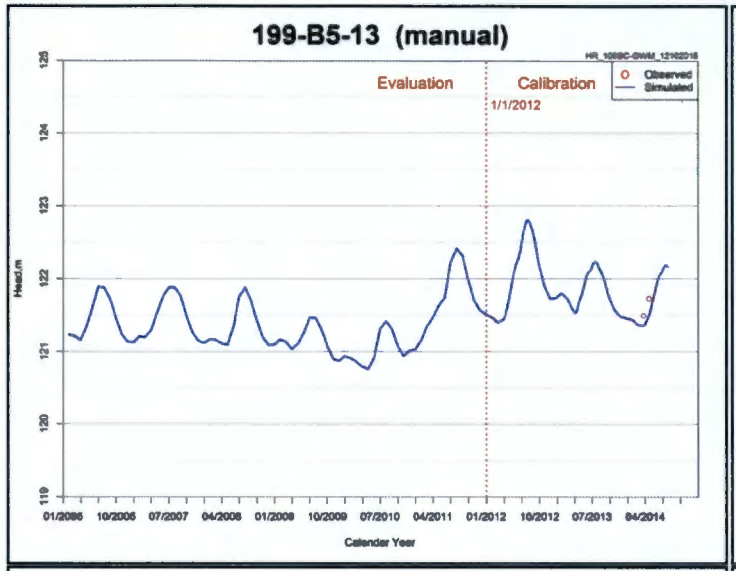
199-B5-13 (manual)
Evaluation
Calibration
1/1/2012
Observed
Simulated
Head,m
Calendar Year

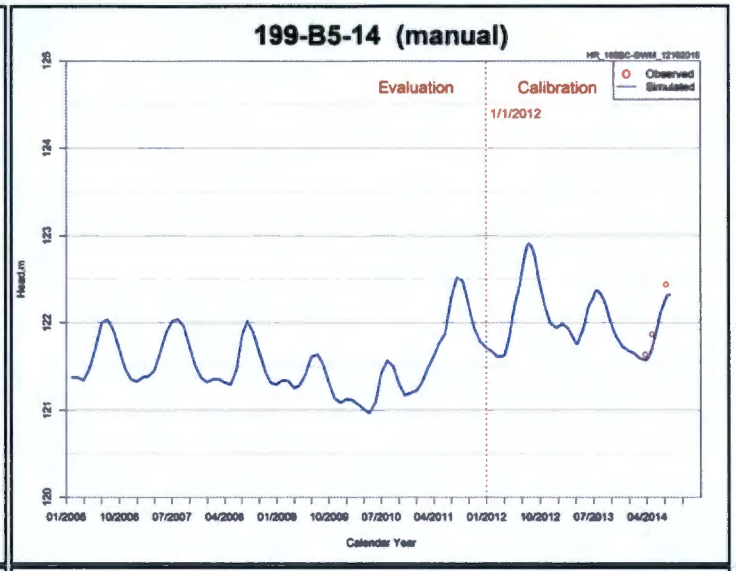
199-B5-14 (manual)
Evaluation
Calibration
1/1/2012
Observed
Simulated
Head,m
Calendar Year

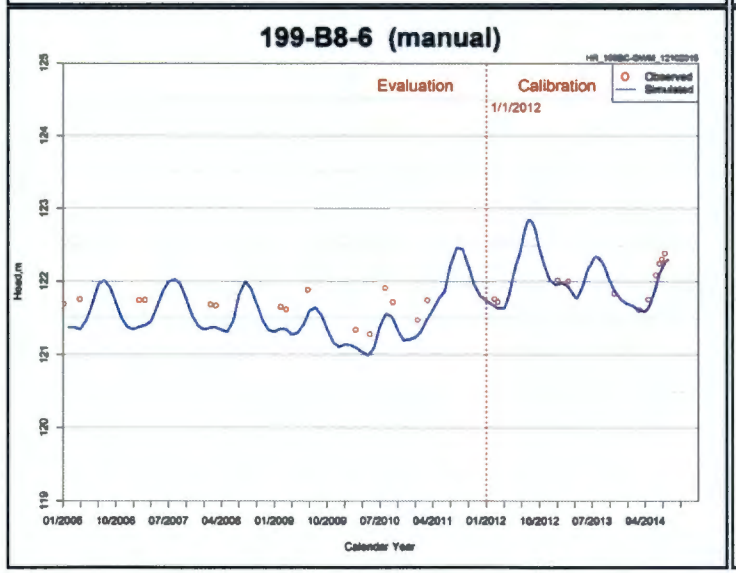
199-B8-6 (manual)
Evaluation
Calibration
1/1/2012
Observed
Simulated
Head,m
Calendar Year

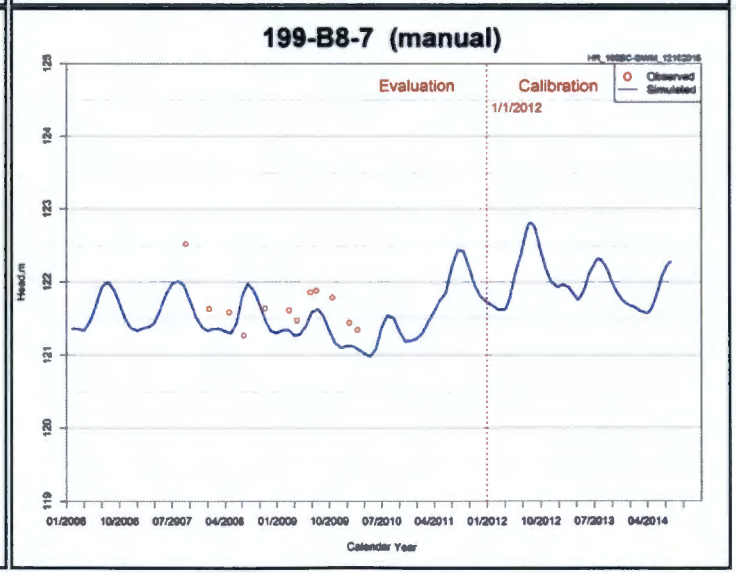
199-B8-7 (manual)
Evaluation
Calibration
1/1/2012
Observed
Simulated
Head,m
Calendar Year

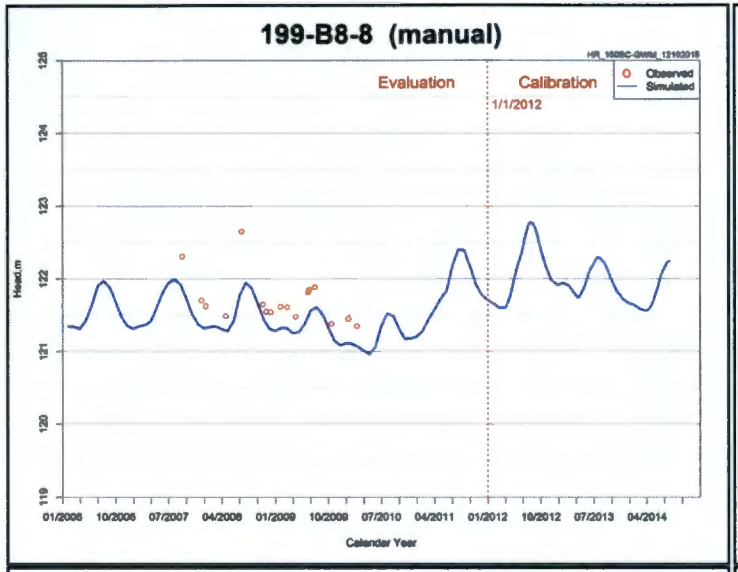
199-B8-8 (manual)
Evaluation
Calibration
1/1/2012
Observed
Simulated
Head,m
125
124
123
122
121
120
119
01/2006
10/2006
07/2007
04/2008
01/2009
10/2009
07/2010
04/2011
01/2012
10/2012
07/2013
04/2014
Calendar Year

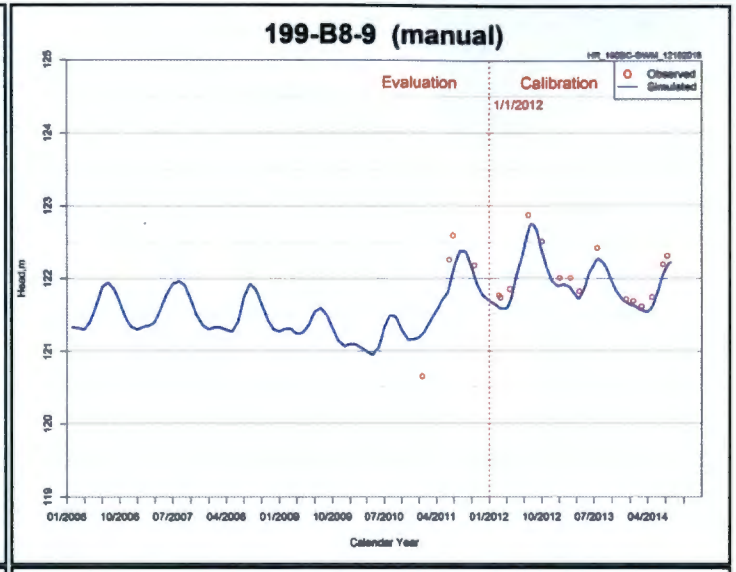
199-B8-9 (manual)
Evaluation
Calibration
1/1/2012
Observed
Simulated
Head,m
125
124
123
122
121
120
119
01/2006
10/2006
07/2007
04/2008
01/2009
10/2009
07/2010
04/2011
01/2012
10/2012
07/2013
04/2014
Calendar Year

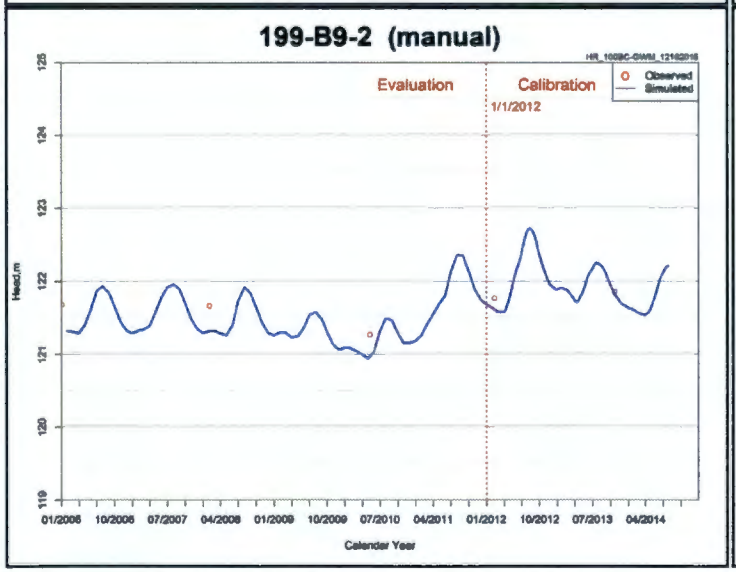
199-B9-2 (manual)
Evaluation
Calibration
1/1/2012
Observed
Simulated
Head,m
125
124
123
122
121
120
119
01/2006
10/2006
07/2007
04/2008
01/2009
10/2009
07/2010
04/2011
01/2012
10/2012
07/2013
04/2014
Calendar Year

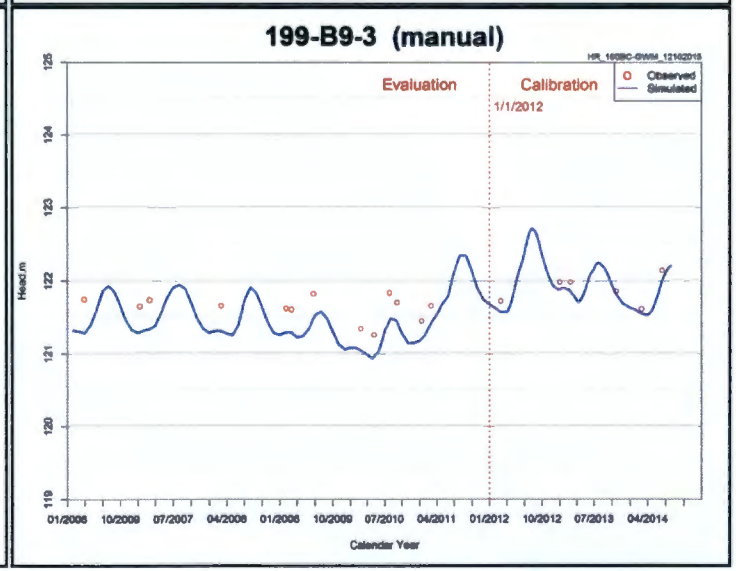
199-B9-3 (manual)
Evaluation
Calibration
1/1/2012
Observed
Simulated
Head,m
125
124
123
122
121
120
119
01/2006
10/2006
07/2007
04/2008
01/2009
10/2009
07/2010
04/2011
01/2012
10/2012
07/2013
04/2014
Calendar Year

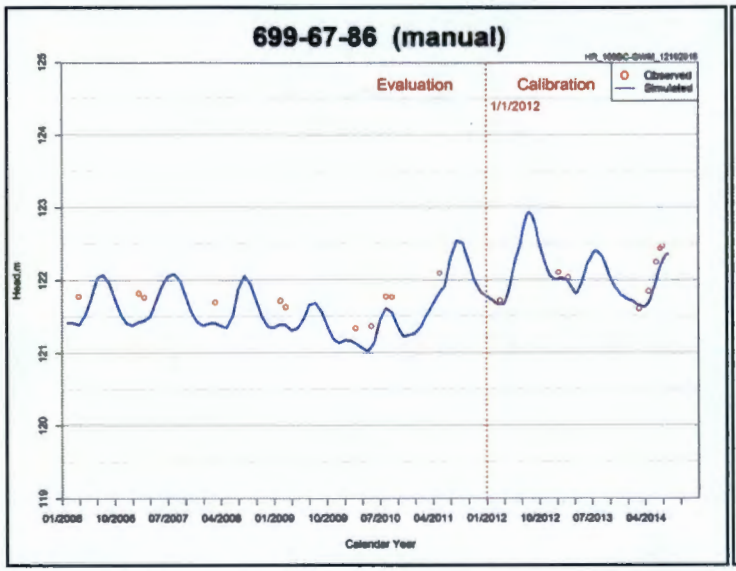
699-67-86 (manual)
Evaluation
Calibration
1/1/2012
Observed
Simulated
Head,m
125
124
123
122
121
120
119
01/2006
10/2006
07/2007
04/2008
01/2009
10/2009
07/2010
04/2011
01/2012
10/2012
07/2013
04/2014
Calendar Year

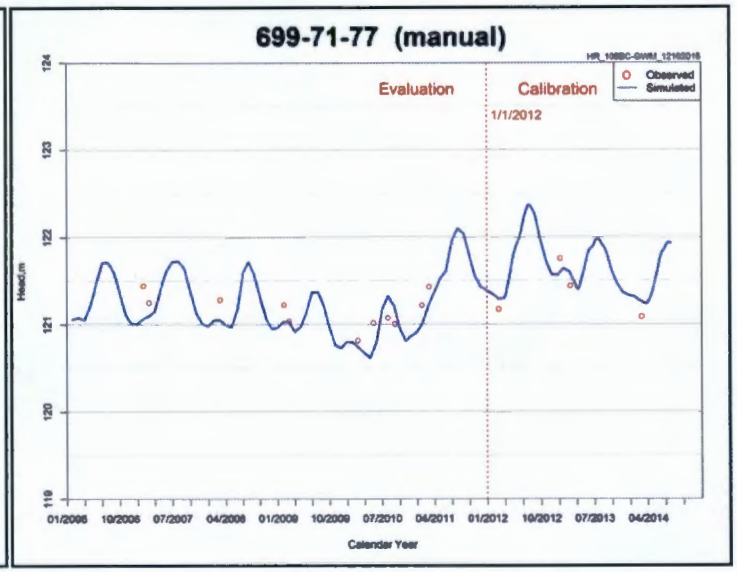
699-71-77 (manual)
Evaluation
Calibration
1/1/2012
Observed
Simulated
Head,m
124
123
122
121
120
119
01/2006
10/2006
07/2007
04/2008
01/2009
10/2009
07/2010
04/2011
01/2012
10/2012
07/2013
04/2014
Calendar Year